BEHAVIOUR OF SQUARE HIGH STRENGTH CONCRETE COLUMNS UNDER LOAD REVERSALS

by

Wojciech Lipien

A thesis submitted to
the Faculty of Graduate Studies and Research
in partial fulfilment of the requirements
for the degree of
Master of Applied Science
in Civil Engineering *

Department of Civil Engineering
Faculty of Engineering
University of Ottawa
Ottawa, Ontario

November, 1995

* The M.A.Sc of Civil Engineering Program is a Joint Program with Carleton University
Administered by the Ottawa-Carleton Institute for Civil Engineering

ISBN 0-612-15643-5

UNIVERSITÉ D'OTTAWA
UNIVERSITY OF OTTAWA

Abstract

Strength of concrete used in construction industry has steadily increased over the years. High strength concretes, with strengths of up to 130 MPa, have been used in columns of a number of multistorey buildings. High-strength concrete offers economic advantages and superior performance. However, strength and deformability of concrete are known to be inversely proportional. Therefore, engineers are concerned with brittleness of high-strength concrete when used in structural applications. Deformability of high-strength concrete columns becomes especially important in seismic resistant design where inelastic deformations of columns are expected, especially at the first storey level.

Strength and deformation characteristics of confined high-strength concrete columns were investigated in this investigation. The emphasis was placed on experimental research since little test data was available on full size columns with concrete strengths of up to 100 MPa. Ten square columns were designed, prepared and tested. Properties of columns were selected to allow assessment of the importance of confinement parameters for high-strength concrete columns and their effects on structural performance. The test parameters included the volumetric ratio, strength, spacing and arrangement of transverse reinforcement, concrete strength and the level of axial compression. The specimens were tested under constant axial compression and incrementally increasing lateral deformation reversals, simulating seismic action.

The experimental data indicate that high-strength concrete columns can be confined to behave in a ductile manner. The volumetric ratio of confinement reinforcement required for high-strength concrete columns is higher than that required for normal-strength concrete columns, although the spacing requirement does not appear to be a function of concrete strength. Columns confined with higher grade lateral reinforcement require lower volumetric ratios of confinement steel. The arrangement of lateral reinforcement plays an important role on improving deformability. Columns confined with well distributed longitudinal reinforcement, laterally supported by transverse reinforcement show improved deformability. The volumetric ratio and spacing limitations for these columns need not be as stringent as those required for less favourable steel

arrangements. The effect of axial compression is to reduce column ductility. Therefore, high-strength concrete columns, when expected to resist high axial compression, must be designed following more stringent confinement requirements.

An analytical investigation was also conducted to assess the applicability of conventional analyses techniques used for normal-strength concrete columns to those made with high-strength concrete. The applicability of a recently developed confinement model, based on test data under concentric compression, was verified against experimental data obtained in this investigation. The results indicate that the confinement model can be employed to columns under combined bending and axial load. Furthermore, moment-curvature relationships obtained by plane section analysis, moment-rotation and force-displacement relationships obtained by integration of curvatures and consideration of column plastic hinging region, as usually done for columns with normal-strength concrete, produce fairly accurate representation of experimentally observed force-deformation relationships.

Acknowledgement

The author of this thesis wishes to express his sincere gratitude to Dr. M. Saatcioglu for his guidance, advice and financial support throughout this research project.

I would also like to thank the technical staff of the Civil Engineering Department, and especially Mr. Mongi Grira, for their assistance during the experimental part of this project.

Finally, thanks are due to my fellow students whose help in casting the specimens was indispensable and greatly appreciated.

Contents

Abstract i
Acknowledgement iii
Notations xiv

1 Introduction 1

1.1 General 1
1.2 Objective and Scope 2
1.3 Previous Research 3

2 Experimental Program 10

2.1 General 10
2.2 Test Specimens 10
2.3 Column Design 12
2.4 Properties of Concrete 13
2.5 Properties of Longitudinal Rerinforcement 14
2.6 Properties of Transverse Reinforcement 14
2.7 Preparation of Formwork and Casting 15
2.8 Test Setup 15
2.9 Instrumentation 18
2.10 Test Procedure 20

3 Observed Behaviour and Test Results 46

3.1 General 46
3.2 Observed Behaviour and Force - Displacement Relationship 46

4. Analysis of Test Data 110

4.1 General 110
4.2 Effects of Test Parameters 110
4.2.1 Effect of Concrete Strength 111
4.2.2 Effect of Volumetric Ratio of Transverse Reinforcement 111
4.2.3 Effect of Yield Strength of Transverse Reinforcement 112
4.2.4 Effect of Tie Spacing 113
4.2.5 Effect of Tie Arrangement 114
4.2.6 Effect of Axial Compression 114
4.3 Analytical Research 115
4.3.1 Computation of Force-Displacement Relationship 115
4.3.2 Computation of Column Strength 118

5. Summary and Conclusions 139

5.1 Summary 139
5.2 Conclusions 140

Appendix A 144

List of Figures

1. Reinforcement Arrangement for a Typical Specimen 24

2. Concrete Stress-Strain Relationship for Specimens RS-2 and RS-4 25

3. Concrete Stress-Strain Relationship for Specimens RS-3 through RS-10 26

4. Longitudinal Reinforcement Stress-Strain Relationship 27

5. Transverse Renforcement Arrangements 28

6. Reinforcement Cages - Top View 29

7. Reinforcement Cages 30

8. Transverse Reinforcement Stress-Strain Relationship for Specimens RS-1, RS-5 and RS-7 through RS-10 31

9. Transverse Reinforcement Stress-Strain Relationship for Specimens RS-2 and RS-6 32

10. Transverse Reinforcement Stress-Strain Relationship for Specimens bRS-3 and RS-4 33

11. Overall View of the Actuators Used 34

12 Schematic View of the Test Setup 35

13. View of the Test Setup 36

14. View of the Components of the Vertical Loading System 37

15. View of the Loading Beam 38

16. View of the Foundation 39

17. Preparation of the Foundation 40

18. Locations of Strain Gauges on Transverse Reinforcement for Specimens RS -1 through RS-6, and Specimen RS-8 41

19. Locations of Strain Gauges on Transverse Reinforcement for Specimens RS-7, RS-9 and RS-10 42

20. View of the Test Setup and Column Specimen Prior to Testing 43

21. Lateral Displacement History 45

22. Extent of Damage at Different Load Stages Specimen RS-1 60

23. Force Displacement - Relationship Excluding P-Δ Effect Specimen RS-1 61

24. Force Displacement - Relationship Including P-Δ Effect Specimen RS-1 62

25. Base Moment - Total Rotation Relationship in the Hinge Region Specimen RS-1 63

26. Base Moment - Slip Rotation Relationship Specimen RS-1 64

27. Extent of Damage at Different Load Stages Specimen RS-2 65

28. Force Displacement - Relationship Excluding P-Δ Effect Specimen RS-2 66

29. Force Displacement - Relationship Including P-Δ Effect Specimen RS-2 67

30. Base Moment - Total Rotation Relationship in the Hinge Region Specimen RS-2 68

31. Base Moment - Slip Rotation Relationship Specimen RS-2 69

32. Extent of Damage at Different Load Stages Specimen RS-3 70

33. Force Displacement - Relationship Excluding P-Δ Effect

Specimen RS-3 71

34. Force Displacement - Relationship Including P-Δ Effect
Specimen RS-3 72

35. Base Moment - Total Rotation Relationship in the Hinge Region
Specimen RS-3 73

36. Base Moment - Slip Rotation Relationship
Specimen RS-3 74

37. Extent of Damage at Different Load Stages Specimen RS-4 75

38. Force Displacement - Relationship Excluding P-Δ Effect
Specimen RS-4 76

39. Force Displacement - Relationship Including P-Δ Effect
Specimen RS-4 77

40. Base Moment - Total Rotation Relationship in the Hinge Region
Specimen RS-4 78

41. Base Moment - Slip Rotation Relationship
Specimen RS-4 79

42. Extent of Damage at Different Load Stages Specimen RS-5 80

43. Force Displacement - Relationship Excluding P-Δ Effect
Specimen RS-5 81

44. Force Displacement - Relationship Including P-Δ Effect
Specimen RS-5 82

45. Base Moment - Total Rotation Relationship in the Hinge Region
Specimen RS-5 83

46. Base Moment - Slip Rotation Relationship
Specimen RS-5 84

47. Extent of Damage at Different Load Stages Specimen RS-6 85

48. Force Displacement - Relationship Excluding P-Δ Effect
Specimen RS-6 86

49. Force Displacement - Relationship Including P-Δ Effect
Specimen RS-6 87

50. Base Moment - Total Rotation Relationship in the Hinge Region Specimen RS-6 88

51. Base Moment - Slip Rotation Relationship Specimen RS-6 89

52. Extent of Damage at Different Load Stages Specimen RS-7 90

53. Force Displacement - Relationship Excluding P-Δ Effect Specimen RS-7 91

54. Force Displacement - Relationship Including P-Δ Effect Specimen RS-7 92

55. Base Moment - Total Rotation Relationship in the Hinge Region Specimen RS-7 93

56. Base Moment - Slip Rotation Relationship Specimen RS-7 94

57. Extent of Damage at Different Load Stages Specimen RS-8 95

58. Force Displacement - Relationship Excluding P-Δ Effect Specimen RS-8 96

59. Force Displacement - Relationship Including P-Δ Effect Specimen RS-8 97

60. Base Moment - Total Rotation Relationship in the Hinge Region Specimen RS-8 98

61. Base Moment - Slip Rotation Relationship Specimen RS-8 99

62. Extent of Damage at Different Load Stages Specimen RS-9 100

63. Force Displacement - Relationship Excluding P-Δ Effect Specimen RS-9 101

64. Force Displacement - Relationship Including P-Δ Effect Specimen RS-9 102

65. Base Moment - Total Rotation Relationship in the Hinge Region Specimen RS-9 103

66. Base Moment - Slip Rotation Relationship

Specimen RS-9 104

67. Extent of Damage at Different Load Stages Specimen RS-10 105

68. Force Displacement - Relationship Excluding P-Δ Effect Specimen RS-10 106

69. Force Displacement - Relationship Including P-Δ Effect Specimen RS-10 107

70. Base Moment - Total Rotation Relationship in the Hinge Region Specimen RS-10 108

71. Base Moment - Slip Rotation Relationship Specimen RS-10 109

72. Normalized Force-Displacement Relationship Envelopes Excluding P-Δ Effect (Specimens RS-1 and RS-9) 120

73. Normalized Force-Displacement Relationship Envelopes Excluding P-Δ Effect (Specimens RS-5 and RS-8) 121

74. Normalized Force-Displacement Relationship Envelopes Excluding P-Δ Effect (Specimens RS-1 and RS-2) 122

75. Normalized Force-Displacement Relationship Envelopes Excluding P-Δ Effect (Specimens RS-6 and RS-8) 123

76. Normalized Force-Displacement Relationship Envelopes Excluding P-Δ Effect (Specimens RS-3 and RS-4) 124

77. Normalized Force-Displacement Relationship Envelopes Excluding P-Δ Effect (Specimens RS-7 and RS-9) 125

78. Normalized Force-Displacement Relationship Envelopes Excluding P-Δ Effect (Specimens RS-9 and RS-10) 126

79 (a) Pressure Distribution Resulting from Different Reinforcement Arrangements 127

79 (b) Stress Strain Relationship for Confined Concrete 127

80. Progressing of Plastic Hinge 128

81. Strain and Bond Stress in Anchored Reinforcement 129

82. Analytical and Experimental Force-Column Tip Displacement

Relationship Excluding P-Δ Effect (Specimen RS-1) 130

83. Analytical and Experimental Force-Column Tip Displacement Relationship Excluding P-Δ Effect (Specimen RS-2) 131

84. Analytical and Experimental Force-Column Tip Displacement Relationship Excluding P-Δ Effect (Specimen RS-3) 132

85. Analytical and Experimental Force-Column Tip Displacement Relationship Excluding P-Δ Effect (Specimen RS-4) 133

86. Analytical and Experimental Force-Column Tip Displacement Relationship Excluding P-Δ Effect (Specimen RS-5) 134

87. Analytical and Experimental Force-Column Tip Displacement Relationship Excluding P-Δ Effect (Specimen RS-6) 135

88. Analytical and Experimental Force-Column Tip Displacement Relationship Excluding P-Δ Effect (Specimen RS-7) 136

89. Analytical and Experimental Force-Column Tip Displacement Relationship Excluding P-Δ Effect (Specimen RS-8) 137

90. Analytical and Experimental Force-Column Tip Displacement Relationship Excluding P-Δ Effect (Specimen RS-9) 138

91. Analytical and Experimental Force-Column Tip Displacement Relationship Excluding P-Δ Effect (Specimen RS-10) 139

A.1 Longitudinal Bar Strains Measured in Specimen RS-1 144

A.2 Transverse Reinforcement Strains Measured in Specimen RS-1 145

A.3 Longitudinal Bar Strains Measured in Specimen RS-2 149

A.4 Transverse Reinforcement Strains Measured in Specimen RS-2 150

A.5 Longitudinal Bar Strains Measured in Specimen RS-3 151

A.6 Transverse Reinforcement Strains Measured in Specimen RS-3 152

A.7 Longitudinal Bar Strains Measured in Specimen RS-4 154

A.8 Transverse Reinforcement Strains Measured in Specimen RS-4 155

A.9 Longitudinal Bar Strains Measured in Specimen RS-5 157

A.10 Transverse Reinforcement Strains Measured in Specimen RS-5 158

A.11 Longitudinal Bar Strains Measured in Specimen RS-6 161

A.12 Transverse Reinforcement Strains Measured in Specimen RS-6 162

A.13 Transverse Reinforcement Strains Measured in Specimen RS-7 164

A.14 Longitudinal Bar Strains Measured in Specimen RS-8 167

A.15 Transverse Reinforcement Strains Measured in Specimen RS-8 168

A.16 Longitudinal Bar Strains Measured in Specimen RS-9 172

A.17 Transverse Reinforcement Strains Measured in Specimen RS-9 173

A.18 Longitudinal Bar Strains Measured in Specimen RS-10 177

A.19 Transverse Reinforcement Strains Measured in Specimen RS-10 178

List of Tables

Table 1 Properties of Test Specimens 24

Table 2 Mix Designes..... 25

Table 3 Concrete Strength Development 26

Table 4 Maximum Horizontal Forces 119

Notations

f'_c = Ultimate strength of plain concrete obtained from standard cylinder test

f'_{cc} = Confined concrete compressive strength in member

f'_{co} = Unconfined concrete compressive strength in member

ε_{01} = Strain corresponding to peak stress of unconfined concrete

ε_1 = Strain corresponding to peak stress of confined concrete

ε_{085} = Strain corresponding 85% of peak stress of unconfined concrete on the descending branch

ε_{85} = Strain corresponding 85% of peak stress of confined concrete on the descending branch

ρ_t, ρ_s = Volumetric ratio of transverse reinforcement

P_0 = Nominal concentric column capacity

u_f = Frictional bond stress between concrete and reinforcing steel

Chapter 1

Introduction

1.1 General

Concrete strength used in practice has been increasing gradually over the years. Recently, high-strength concretes (HSC) of up to 130 MPa strength were used in construction industry. HSC offers economy and superior performance when used in columns of multistorey buildings. Increased strength results in smaller member sizes while maintaining a relatively high lateral stiffness. Furthermore, it allows the use of uniform column sections with variations in concrete strength over the height of building. This results in savings in formwork cost. Additional benefits can also be realized through improved performance relative to durability and corrosion resistance.

While HSC appears to be a superior material as compared to normal-strength concrete, ductility of concrete is known to be inversely proportional to its strength. Therefore, HSC usually exhibits brittle behaviour and explosive failure under compression. Lack of ductility is a source of concern among structural engineers, especially in seismic applications where deformability of columns are relied up on during strong earthquakes to dissipate seismic energy. One potential solution to

the problem of brittle material behaviour is to provide lateral confinement by hoops and cross ties. The research project reported in this thesis was undertaken to address issues related to deformability of HSC columns under simulated seismic loading, when confined with hoops and cross ties.

HSC is defined in this research program as concrete with strengths in excess of those used in developing the majority of current design provisions outlined in building codes. This implies that concretes with a strength range of 40 MPa to 130 MPa are referred to as high-strength concrete.

1.2 Objective and Scope

The primary objective of the research project is to investigate strength and deformation characteristics of confined HSC columns under simulated seismic loading. The objective includes the assessment of confinement parameters for HSC columns and their effects on column performance. The experimental and analytical research conducted in this project is intended to generate much needed experimental data and design information for HSC columns in seismically active regions.

The scope consists of experimental and analytical investigations, and includes the following tasks:

- Review of previous research on experimental investigation of HSC columns under reversed cyclic loading.

- Design of 10 large-scale column specimens, with due considerations given to the appropriate parameters of confinement.

- Design and construction of experimental set-up suitable for testing large capacity HSC columns under constant axial compression and incrementally increasing lateral deformation reversals.

- Construction and instrumentation of test columns.

- Conducting tests of 10 full-size HSC columns using a computer controlled MTS loading system and recording data by means of two data acquisition systems.

- Evaluation of test data, and investigation of test parameters.

- Analytical computation of inelastic force-displacement relationships using a confined concrete model for HSC, and comparison with those obtained experimentally.

- Generation of design information for confinement reinforcement of HSC columns.

- Preparation of a thesis and presentation of results.

1.3 Previous Research

HSC is a relatively new material that gained its broad popularity only in recent years. Therefore, there has not been much research conducted on different aspects of HSC. The limited research reported in the literature on performance of HSC columns under simulated seismic loading is reviewed and presented in this chapter.

Thomsen and Wallace [1] reported in 1994 the results of column tests performed on twelve specimens. The objective of the study was to evaluate effects of different parameters on behaviour of columns subjected to axial and lateral loads. The specimens had identical height of 19 inches and identical sectional dimensions of 6 in x 6 in. The same longitudinal bar arrangement was used in all columns, comprising of eight-No. 3 Grade 60 (60 ksi) bars placed uniformly along the perimeter. Two different grades of steel (115 ksi and 185 ksi) and four different spacings of transverse reinforcement were used. Specimens were subjected to constant axial compression equal to 0.0, 0.1 and 0.2 of the gross concentric capacity of section. The authors reported stable hysteretic behaviour and excellent ductility during testing. Strength decay of specimens was unnoticeable at drift levels of 2% or less, and buckling of longitudinal reinforcement did not occur until after the drift level of 4%. It was concluded that higher strength transverse steel did not significantly improve the ductility of columns in the drift range of 2% or less.

Azizinami et al. [2] reported the results of 2/3-scale column specimens with square cross sections. Each column had a cross section of 12 in x 12 in and a height of 8 ft. The columns were reinforced with 2.44 % longitudinal reinforcement. The volumetric ratio of transverse reinforcement ranged between 2.36% and 3.82%. All columns had an identical arrangement of longitudinal reinforcement, consisting of three bars at each face. Yield strength of longitudinal reinforcement was 60 ksi. Two different yield strengths of transverse reinforcement were used, consisting of Grades 60 and 120 ksi. Spacing of transverse reinforcement was either 1-5/8 in or 2-5/8. Concrete compressive strength ranged between 3910 psi and 15050 psi. Axial forces applied were $0.2P_o$, $0.3P_o$ or $0.4P_o$. The experiments showed that all specimens exhibited good energy-dissipation characteristics. It was concluded that an increase in f'_c did not result in reduction of column displacement ductility ratio. On the other hand a

reduction in tie spacing resulted in an increase in displacement capacity. An increase in axial compression resulted in reduction of displacement capacity, although for HSC this reduction was smaller than that for normal-strength concrete. The use of high-strength transverse reinforcement was ineffective at an axial load level of $0.2P_0$. The ductility improved with volumetric ratio of transverse reinforcement and deteriorated with axial compression.

Sakai and Otani [3] and **Sakai et al** [9] reported the results of column tests performed on HSC with a shear span-to-depth-ratio of 2. The specimens had a clear height of 1000 mm and cross-sectional dimensions of 250 mm x 250 mm. Concrete strength used was identical in all specimens and was equal to 100 MPa. Three different yield strengths and two different arrangements of transverse reinforcement were used. Longitudinal reinforcement comprised of either 12 bars with four crossties or no crossties at all (seven specimens), or 4 bars with no crossties (one specimen). The columns were subjected to axial stress ratio of 0.35 times the compressive strength of concrete except for one column which had a compressive stress level of $0.5f'_c$. Higher ductility was obtained in specimens with interior hoops and high-strength transverse reinforcement. Ductility was also improved when closer hoop spacing was used.

An experimental study was performed by **Bing, Park, and Tanaka** [4] on five reinforced concrete columns with concrete strength of 100 MPa, to assess the suitability of New Zealand concrete design code to HSC columns. The researchers pointed out the pronounced effects of spalling of cover concrete and lack of efficiency of confinement reinforcement on ductility. It was concluded that the observed ductility of columns was not satisfactory.

Research performed by **Kato** [5] comprised of eight column specimens designed to

fail in three different modes; flexure, shear and bond splitting. The shear-span-to-depth ratio was 2.0 for six specimens, and 1.5 for the remaining two specimens. The level of axial load ranged between 0.20 and 0.45 of the cross-sectional area multiplied by concrete strength. Concrete strength used ranged between 65 MPa and 80 MPa. The main objective of the study was to establish methods for evaluating deformation capacities of columns exhibiting different modes of failure. In addition, the effects of arrangement, strength and diameter of longitudinal reinforcement, configuration and strength of shear reinforcement, level of axial force and shear-span-to-depth ratio were investigated. The importance of the effect of slippage of reinforcement on deformation capacities was underlined.

Shear strength of reinforced concrete columns was investigated by **Kuramoto and Minami [6]**. Six columns were tested with shear-span-to-depth ratio of 1.50. Strength of concrete and longitudinal reinforcement were 120 MPa and 700 MPa, respectively. The main objectives were the investigation of axial compression and quantity and strength of shear reinforcement. It was concluded that columns with higher strength transverse reinforcement had lower shear capacities and stiffnesses after cracking than those with lower strength reinforcement. The ultimate shear capacity was found to decrease with increase in axial compression and decrease in transverse steel stress. It was also reported that the diagonal tension capacity of columns increased with increasing axial compression.

Kabeyasava et al. [7] tested two columns with 70 MPa concrete, with either 620 MPa or 1000 MPa reinforcement. Both specimens had a 250 mm square cross-section and a 1000 mm height. The columns were subjected to triaxial loading accompanied by either a constant or a variable axial force. The level of constant axial force was 0.367 of the cross-sectional area multiplied by concrete strength. The variable force varied between 0.1 and 0.6 of the cross-sectional area multiplied by concrete strength. It was

observed that the column under variable axial force showed better ductility characteristics with reduced strength.

Kabeyasawa et al [19] reported tests of HSC columns under axial compression and lateral load reversals. Three specimens with concrete strengths of 80 MPa were tested. Shear-span-to-depth ratio for all columns was equal to 2.0. Strengths of longitudinal and transverse reinforcement were 880 MPa and 1360 MPa, respectively. The level of axial stress varied between $0.35f'_c$ and $0.52f'_c$. The specimens showed stable behaviour up to 2% lateral drift. It was reported that column deformability decreased with increasing axial compression, which otherwise improved with increased ratio of longitudinal reinforcement.

Shear behaviour of five HSC columns was investigated by **Hibi et al [8]**. The strength of concrete used varied between 91 MPa and 100 MPa. Two different strengths of longitudinal reinforcement were used consisting of grades 432 MPa and 725 MPa. The strength of hoop reinforcement was either 812 or 127 MPa. The level of axial stress ranged between $0.30f'_c$ and $0.44f'_c$. Two different arrangements of reinforcement were used consisting of 4 and 5 bars at each face. The shear-span-to-depth ratio for all columns was 1.5. Those columns that were subjected to $0.30f'_c$ axial stress showed ductile behaviour. Columns under higher axial compression of $0.45f'_c$ failed due to shear. The results emphasized the importance of axial compression on shear capacity and deformability of columns.

Muguruma et al [11] tested eight columns with concrete compressive strength of 86 and 116 MPa. Strength of transverse reinforcement was either 328 MPa or 792 MPa. The level of axial compression ranged between 0.254 to 0.629 of the capacity of columns based on gross sectional area ($A_g f'_c$).The volumetric ratio of transverse reinforcement for all specimens was 1.61%. Hoop spacing was 35 mm. It was reported

that the use of high-strength transverse reinforcement allowed development of large ductilities. It was also reported that the efficiency of lateral confinement in improving ductility was reduced with increase in concrete compressive strength.

Chung et al. [12] reported the results of 23 reinforced concrete column specimens with concrete strengths ranging between 16 MPa and 94 MPa. All the specimens were subjected to axial loads bending moments and shear forces. Main variables of the experiments included concrete strength, level of axial force (from 0.1 to 0.4 of cross sectional area multiplied by concrete strength), transverse reinforcement ratio and number of cycles imposed at each deflection level. It was concluded that columns with concrete strengths greater than 50 MPa had to be subjected to low levels of axial compression to develop ductile behaviour. Analytically computed values of maximum and yield moments, based on the stress-strain relationship of concrete and steel agreed very well with those obtained experimentally. It was also concluded that higher percentage of shear reinforcement resulted in improved ductility.

The effectiveness of confinement using high-strength transverse reinforcement was studied by **Muguruma et al. [13]**. Four columns with concrete compressive strength of 130 MPa and transverse steel strength of 408 MPa and 873 MPa were tested under simulated seismic loading. All columns had 500 mm height and 200 mm square cross sections. Two different levels of axial compression were applied consisting of 0.343 and 0.473 of $f'_c A_g$. Hoop spacing was 35 mm in all columns. It was concluded that in spite of the very high strength of concrete used, it was possible to achieve ductile behaviour of columns with the use of high-strength transverse reinforcement.

Watanabe et al [14] investigated the suitability of HSC for use in high rise buildings in seismically active regions. Three columns with 60 MPa concrete were subjected to axial load and lateral load reversals. One of the columns was subjected to tensile force

while the other column was tested under biaxial bending. Level of axial compression was either $0.20f'_c$ or $0.18f'_c$. Lateral reinforcement consisted of high-strength steel of 1300 MPa. The columns behaved in a ductile manner with no visible damage up to $2\Delta_y$ displacement level and showed 14% strength decay at $4\Delta_y$. Biaxial bending did not reduce ductility. The researchers concluded that the use of high-strength transverse reinforcement was desirable to improve the efficiency of confinement.

Chapter 2

Experimental Program

2.1 General

Full-size HSC columns were designed, prepared and tested under simulated seismic loading. This chapter describes the properties of columns and materials used, as well as test setup and test procedure. The observed behaviour of columns and test results are discussed in Chapter 3.

2.2 Test Specimens

Ten full-scale column specimens, representing part of a first story column between the footing and point of inflection, were designed, built and tested. Each specimen consisted of column and footing portions. The column cross-section was 250 mm square and the column height was 1640 mm measured from the column-footing interface to the point of inflection where the lateral load was applied. This height included 1360 mm of concrete column and 280 mm of steel loading assembly near the inflection point where the column was subjected to little bending and hence remained elastic. This height of column was chosen to represent a realistic shear

span, representative of most columns used in practice. Typical cross-section of a column specimen is shown in Fig.1. The shear span selected promoted flexural behaviour under load reversals. Design strengths of concrete used were 60 MPa for two specimens, and 100 MPa for the remaining eight. The actual cylinder strengths obtained at the time of testing were 64 MPa and 104 MPa, respectively. The concrete strength used and the cross-sectional dimension considered allowed the application of up to approximately 28% of concentric capacity with the capacity of the loading system utilized.

Two longitudinal reinforcement ratios were used; 2.56% for the eight bar arrangement, and 3.80% for the twelve bar arrangement. The longitudinal bars were extended into the footing which had a depth of 340 mm. They all had 180 mm long hooks in the footing. This met the development length requirements of CSA Standard A23.3-M84 [15]. Clear concrete cover in all columns was 10 mm, measured from the face of the column to the outer surface of the perimeter hoop. Three different grades (400 MPa, 570 MPa, 1000 MPa) and five different spacings (45 mm, 47 mm, 50 mm, 62.5 mm, 100 mm) of steel were used for transverse reinforcement. These arrangements of reinforcement and material properties allowed the investigation of different parameters of confinement on column behaviour. Table 1 provides a summary of column properties.

Each column had four Grade 800 MPa, 19 mm diameter bolts embedded in concrete, vertically protruding from the column top section. They were used to connect the loading beam to the column. The crossties were eliminated within the top 300 mm portion of columns to avoid difficulties in placing bolts during casting.

The footing for each specimen was heavily reinforced. They had four holes, two

on each side of the column, which allowed the column to be fully fixed to the laboratory strong floor by means of 800 MPa, 38 mm steel threaded rods.

2.3 Column Design

The columns were designed using expected material strengths and reinforcement arrangements that would allow the investigation of confinement parameters. An important consideration in the test program was to use realistic size HSC columns, representative of those used or likely to be used in practice, with full sizes or near-full size dimensions, to eliminate potential size effects. The choice of cross-sectional dimension was dictated by four parameters; the capacity of the test equipment, strength of concrete, level of axial load, and realistic column size. As a result, 250 mm x 250 mm square cross section was selected for all columns. The column height was selected to be 1640 mm. This resulted in a shear span-to-depth ratio of 6.56, which is typical of most columns in practice.

The design strengths of concrete were 60 MPa and 100 MPa. The 60 MPa strength was representative of the lower end of the strength range usually associated with high-strength concretes. The 100 MPa strength was close to the high end of the strength range, approaching 130 MPa which is usually regarded as the maximum possible strength that can be attained with conventional materials of concrete. It was also recognized that concrete would become more brittle with increasing strength. This was kept in mind in determining the confinement steel requirements in columns. The design variables considered in the experimental program included strength of concrete, yield strength of transverse reinforcement, spacing of transverse reinforcement, volumetric ratio of transverse reinforcement, arrangement of longitudinal reinforcement and level of axial load. The columns were designed such that companion columns could be compared to assess the significance of

these design variables. Figure 1 and Table 1 summarize the characteristics of columns designed for the experimental program.

The longitudinal reinforcement consisted of No-15 bars with hooks at their footing ends. Each hook had a 180 mm extension, conforming to CSA Standard A23.3-M84 [15], as well as ACI-318-89 [16]. The development length of longitudinal reinforcement was computed to be approximately 360 mm. Transverse reinforcement was continued approximately 3 to 4 spacing distance down into the footing.

2.4 Properties of Concrete

Four different batches of concrete were used in preparing the specimens. The first batch was used for casting footings of specimens RS-1 and RS-2. The second batch was used for column portions of specimens RS-1 and RS-2. The third and fourth batches were used to cast the footings and columns of specimens RS-3 through RS-10, respectively. Table 2 includes mix designs used for each batch. Several control cylinders were cast from each batch to monitor strength gain. Strength gain with time was established by testing at least three randomly chosen cylinders. First three cylinders from each batch were tested after 24 hours, followed by tests at 3, 7; 14, 21, and 28 days. Additional cylinders were tested during the period in which column tests were performed. The results are shown in Table 3. Cylinders with concrete age of up to 7 days were capped with sulphur compound. Cylinders with older concretes were ground at the ends to ensure uniform application of load. Stress-strain relationships of concrete, during the period of column testing, are shown in Figs. 2 and 3. Attempts were made to obtain post peak portions of these relationships. Strain measurements were taken by two strain gauges with 20 mm gauge length, glued on opposite sides of

cylinders. The average strain was used to plot the stress-strain curves.

2.5 Properties of Longitudinal Reinforcement

No-15 bars with hooks were ordered from a local supplier to be used as longitudinal reinforcement. The length of each bar from the end to the hook was 1720 mm, and the length of the hook was 180 mm. All the bars were deformed with 16 mm nominal diameter. Three randomly selected coupons were tested to establish the yield strength of steel. The average yield strength obtained was 419 MPa. Strain measurements were taken using an extensometer with a gage length of 50 mm. The stress-strain relationship for longitudinal bars is shown in Fig. 4.

2.6 Properties of Transverse Reinforcement

Three different types of reinforcing steel were used as lateral reinforcement. Type I hoops and cross-ties consisted of Grade 400, No-10 deformed reinforcement, and were used in Columns RS-3 and RS-4. Type II transverse reinforcement consisted of smooth wires with 6.35 mm diameter, and was used in columns RS-2 and RS-6. The remaining six columns (RS-1, RS-5, RS-7, RS-8, RS-9, and RS-10) had Type III transverse reinforcement consisting of high-strength smooth wire with 7.5 mm diameter. Type I and Type II lateral reinforcement were prepared and delivered by a local supplier. Type III reinforcement was supplied by STELCO and the hoops and cross ties were manufactured in the structures laboratory of the University of Ottawa. This was done by first cutting pieces of wire from the coil of steel that was supplied and then by straightening them before they were bent into hoops and cross-ties by a custom made jig. The configuration of transverse reinforcement used in all

specimens is shown in Fig.5. Reinforcement cages used are illustrated in Figs. 6 and 7.

Three randomly chosen coupons were tested from each type of steel to establish the stress strain-relationship. The average of three tests was plotted in Figs. 8 through 10.

2.7 Preparation of Formwork and Casting

The column formwork was prepared in the laboratory using plywood. The formwork was treated by form oil prior to casting. Fig. 6 illustrates reinforcement cages in the formwork prior to casting.

Eight specimens, with a design concrete strength of 100 MPa, were cast from two batches of concrete supplied by a local ready mix concrete company. The concrete was prepared in the plant based on specified mix designs. Additional superplasticizer was added in the laboratory to achieve the desired workability. The remaining two specimens, with a design concrete strength of 60 MPa, were cast using two other batches of concrete mixed in the laboratory. The slump for all batches was about 200 mm. Control cylinders were cast from all batches and were tested to monitor the strength gain up to the day of column testing.

2.8 Test Setup

The columns were tested under constant axial compression, accompanied by lateral deformation reversals. This necessitated a loading system that could be controlled separately in vertical and horizontal directions. The details of the loading system

are described below.

Lateral Load System

Horizontal deformation reversals were applied by means of a 1000 kN capacity MTS hydraulic actuator. The maximum stroke of the actuator was 500 mm which allowed maximum horizontal displacement of ± 250 mm relative to the neutral position. The actual stroke and load during testing were monitored and recorded by two independent data acquisition systems. One was part of the MTS control system and the other was a Siemetric Data Acquisition System. The latter system was also used to record the strains in reinforcement and displacements of columns through strain gauges and LVDT's, respectively. The detailed configuration of data recording sensors is described in Sec. 2.9, under "Instrumentation."

The required hydraulic pressure was supplied by a 33 GPM pump. The same pump also supplied oil to the vertical load system. The pressure was controlled through an MTS servo-valve to apply the required load. Two multidirectional swivels were placed at the ends of each actuator. This allowed lining up of actuators with directions of loads, eliminating the risk of damage to an actuator due to accidental eccentricities and/or force components that may be developed perpendicular to its axis. Geometric dimensions of a typical actuator are illustrated in Fig 11.

The horizontal actuator was supported by a mecano set that consisted of a pair of A-frames bolted on three pairs of C-channels. The channels were secured to the laboratory strong floor by means of 1800 mm long, 64 mm diameter Grade 400 MPa bolts. The maximum force applied by the horizontal actuator during testing was estimated to be below 300 kN. This was significantly below the capacity of the support system. The actuator was connected to the support through a 50 mm

thick, Grade 180 MPa steel plate, which was bolted to the A-frames. The other end of the actuator was connected to the loading beam placed on each specimen. The details of the loading beam are described in the next section. Both ends of the actuator were bolted using Grade 8 high-strength bolts with 38 mm diameter, 400 mm length. The details of the horizontal load system are shown in Fig. 12 and 13.

Vertical Load System

The main elements of the vertical load system consist of a loading beam, foundation, and two MTS actuators. The actuators were placed one on either side of the column, to apply constant axial compression during testing. These actuators were identical to that used for horizontal loading. Fig. 14 illustrates the vertical load system.

The axial load was transferred to the column through a loading beam. The loading beam is shown in Fig. 15 and consisted of two parts. The upper part was a built-up box section which was attached to the vertical actuators by means of 400 mm long, 38 mm diameter Grade 8 bolts. The bottom part was a built-up I section, stiffened in the direction of horizontal load by means of steel plates that were welded to form stiffeners. The bottom piece of the loading beam also served as a spacer to accommodate the vertical actuator length. The bottom and top pieces of the loading beam were connected together by eight 25 mm diameter, 100 mm long Grade 8 bolts.

The loading beam was manufactured by welding 44W weldable steel plates with 300 MPa (44 ksi) yield strength. Four holes were drilled in the bottom flange of the loading beam to secure the beam to the column specimen through bolts that had been cast in concrete at the top of each specimen.

A rigid foundation was prepared as part of the vertical load assembly to support the bottom ends of vertical actuators. The foundation consisted of a composite structure which included steel plates welded to C-channels and reinforced concrete beams. Figs. 16 and 17 illustrate the overall view of the foundation. The steel plates, with 75 mm thickness and 280 MPa yield strength, served as a base for the actuators, and were used to connect the actuators to the foundation. Eight of the holes used to connect the actuators were of countersink type. This allowed hiding the bolt heads in the plate so that the plate could lay flat on the floor. Four additional holes were drilled, each with 75 mm diameter, to bolt the foundation to the laboratory strong floor. Bolts used for this purpose were Grade 400 MPa, 1800 mm long and 64 mm diameter.

The reinforced concrete portion of the foundation increased the overall stiffness and provided even support for the footing of the specimen. It contained four nuts to accommodate 32 mm threaded rods to pretension the footing to the foundation. These rods were approximately 900 mm mm long and were made out of Grade 7 high-strength steel. The rods were not cast in the foundation so that they could be replaced if damaged.

Lateral Restraining Frames

A pair of frames were used, one on either side of specimen to provide lateral bracing in the horizontal plane. This was found necessary to maintain the stability of columns at or after failure. The frames were secured to the laboratory strong floor and were tied together at the top by means of hollow steel box sections.

2.9 Instrumentation

The specimens were instrumented to measure lateral displacements, rotations of

the hinging region, strains in reinforcement, as well as horizontal and vertical loads. The data were recorded by both Sciemetric Data Acquisition System and MTS controller.

Lateral displacements were measured at three different locations using two different types of LVDTs. Deflection at the level of horizontal force was measured using a temposonic LVDT which was connected directly to the MTS data acquisition system. Stroke capacity of this LVDT was ± 250 mm and the output gave displacement in mm. Two LVDT's were placed on both sides of the column to measure column tip deflection, each with a 150 mm stroke capacity. These LVDT's were calibrated before use and gave readings in mV.

The rotations in the hinging region was measured by means of four 50 mm stroke LVDTs placed vertically. These LVDTs were attached to hangers mounted on threaded rods which had been cast in column core to allow reading beyond the spalling of cover concrete. Two of these LVDTs were placed with a gauge length of 250 mm, one on each side of the column, measuring vertical displacements of the column hinging region relative to footing. These were 100 mm away from the face of the column on each side so that the distance between these two readings in the horizontal plane was equal to the column width (250 mm) plus twice this distance (2x100 mm). The difference between these readings and the distance between the readings gave total rotation of the hinging region, consisting of rotations due to flexure and anchorage slip. Additional two LVDTs were placed with a gauge length of 30 mm to measure the rotation due to anchorage slip. These readings gave the crack width at column footing interface. However, they also picked up flexural rotations within the bottom 30 mm segment of column because they were mounted 30 mm above the base. These LVDTs were also placed 100 mm away from the column face. Location of rotational and

displacement LVDT's is shown in Fig. 18 and 19.

A light steel frame was built around the column to attach displacement LVDTs. The frame was attached to column footing, leading to displacement readings relative to the footing.

Steel strains were measured on longitudinal and transverse reinforcement by electrical resistance strain gauges. Four strain gauges were placed on longitudinal reinforcement in each column. Three of them were located on one longitudinal bar, one at column footing interface, another one at 125 mm above and the third one at 125mm below the interface. These gauges were monitored during testing to establish the strain profile and yield penetration into the footing. The fourth strain gauge was placed on the opposite bar subjected to stresses of opposite sign at column footing interface.

The number of strain gauges on transverse reinforcement varied among the specimens. The locations of strain gauges on transverse reinforcement are shown in Fig.20.

2.10 Test Procedure

The first step in test procedure involved positioning of column in the middle of the foundation that had been secured to the laboratory strong floor. The column footing was then bolted to the foundation by high strength threaded rods. The loading beam was placed on the column with the bottom flange holes matching with the top column bolts. The horizontal actuator was positioned and connected to the web of the top beam. The vertical actuators were then connected to the bottom flange of the loading beam.

The first step in testing was to apply the axial load. The lateral displacement history, shown in Fig. 21 was followed to apply deformation reversals. Three initial cycles were applied within the elastic range, followed by incementally increasing displacement cycles corresponding to $1\Delta y$, $2\Delta y$, $3\Delta y$ etc. Three deformation cycles were applied at each level of displacement. The value of displacement corresponding to $1\Delta y$ was determined visually during testing as displacement at which a significant change occurred in the slope of the force-displacement relationship, signifying yielding. Deformation cycles were applied slowly. Each test was completed within approximately three hours. Testing continued until a 50% or higher drop was observed in lateral load resistance.

Table 1 - Properties of Test Specimens

COL.#	COMP. STRENGTH OF CONCRETE f'c [MPa]	ARRANG. OF LONGITUD. BARS ϕ=15mm fy=420MPa	DIAMETER OF TRANSV. REINFORC. [mm]	SPACING OF TRANSV. REINFORC. [mm]	VOLUM. RATIO FOR CORE CONCRETE SECTION FOR TR. REINF. ρ_s	VOLUM. RATIO OF TRANS. REINF. REQUIRED BY ACI $(\rho_s)_{ACI}$	YIELD STRENGTH OF TRANSV. REINF. fy [MPa]	$\frac{\rho_s f_y}{f'_c}$
RS-1	64	12 BAR	7.5	62.5	2.54	1.3	1000	42.3
RS-2	64	12 BAR	6.35	45	2.54	2.2	575	22.82
RS-3	104	8 BAR	2(11.3)	100	5.58	5.14	420	22.53
RS-4	104	8 BAR	11.3	50	5.58	5.14	420	22.53
RS-5	104	8 BAR	7.5	62.5	1.9	2.1	1000	18.26
RS-6	104	8 BAR	2(6.35)	50	3.56	3.6	575	19.68
RS-7	104	8 BAR	7.5	47	2.54	2.1	1000	24.32
RS-8	104	8 BAR	2(7.5)	62.5	3.8	2.1	1000	36.53
RS-9	104	12 BAR	7.5	62.5	2.54	2.1	1000	24.42
RS-10	104	12 BAR	7.5	62.5	2.54	2.1	1000	24.42

Table 2 - Mix Designes

SPECIMEN	CEMENT (10 % SF) [kG]	SAND [kG]	AGGREG. [kG]	SUPERPL. [L]	WATER* [kG]	RETARDER [L]
RS-1, RS-2 Footings and Columns	550	726	1130	12	160	0
RS-3 through RS-10 Footings and Columns	555	726	1122	20	111	1.6

* includes water in superplasticizer and moisture in sand

Table3 - Concrete Strength Development

AGE [DAYS]	BATCH# I [MPa]	BATCH# II
1	29	-
3	54	-
7	67	52
14	85	57
21	90	61
28	98	64

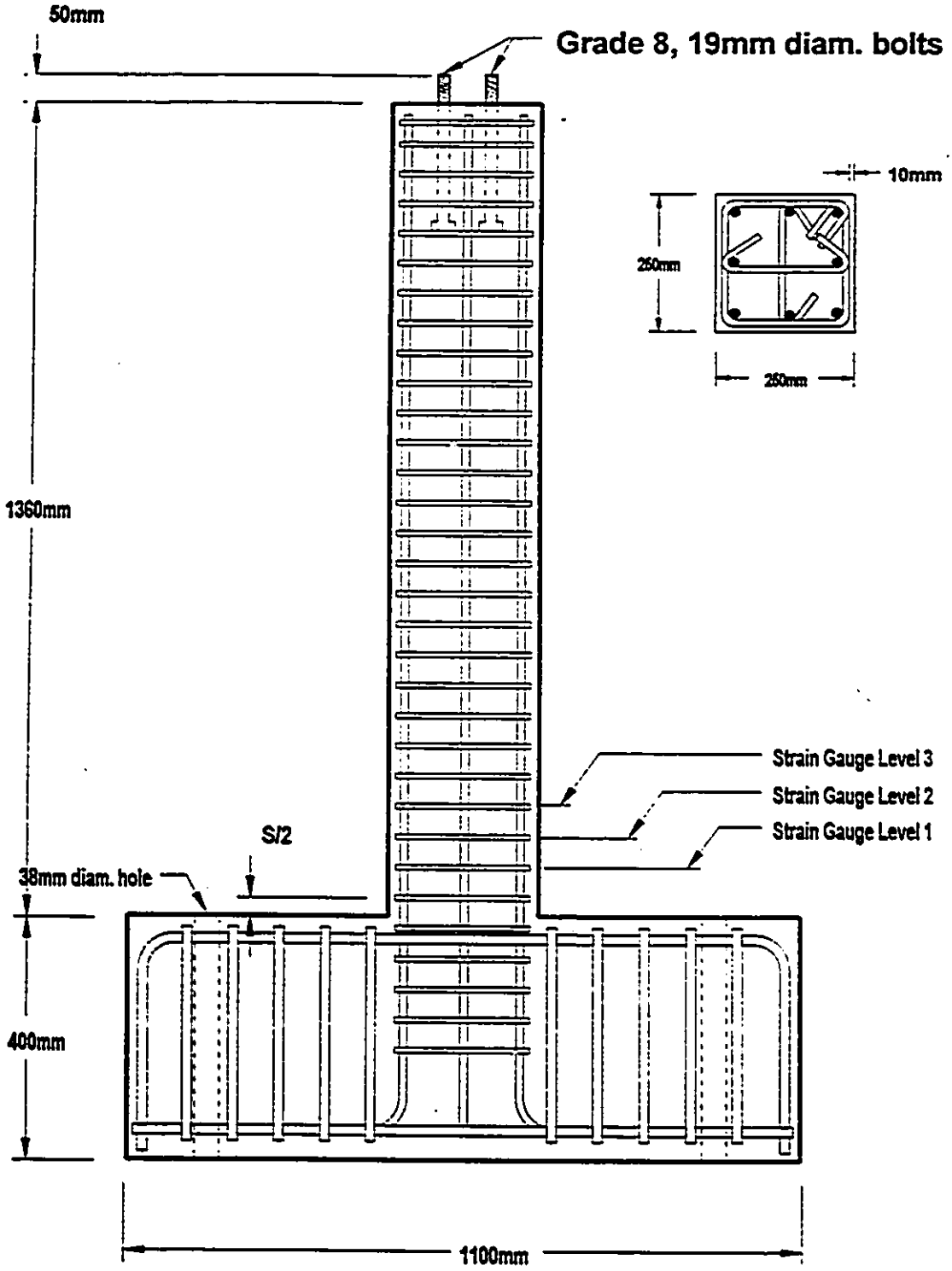

Reinforcement Arrangement for a Typical Specimen

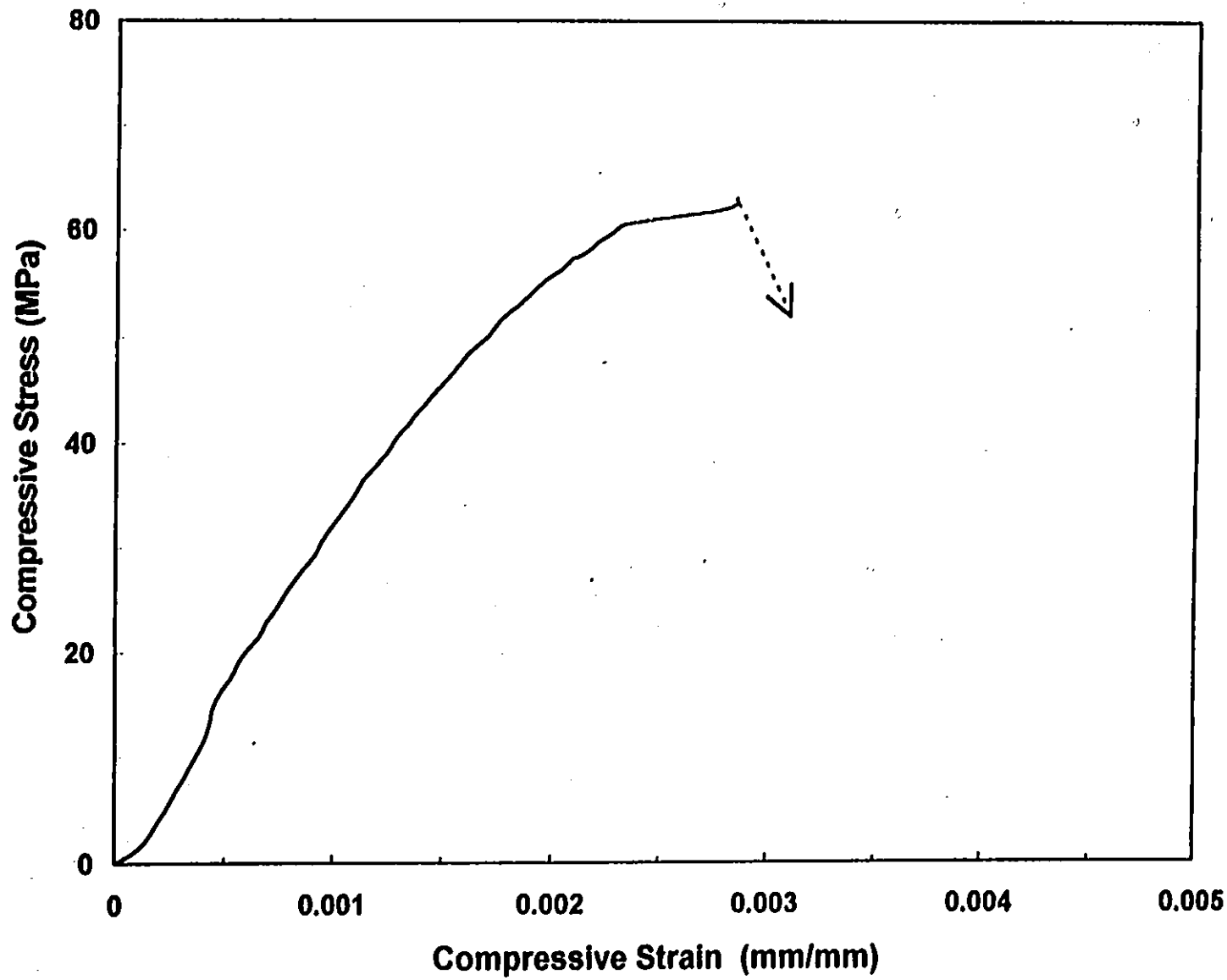

Fig. 2 Concrete Stress-Strain Relationship for Specimens RS-1 and RS-2

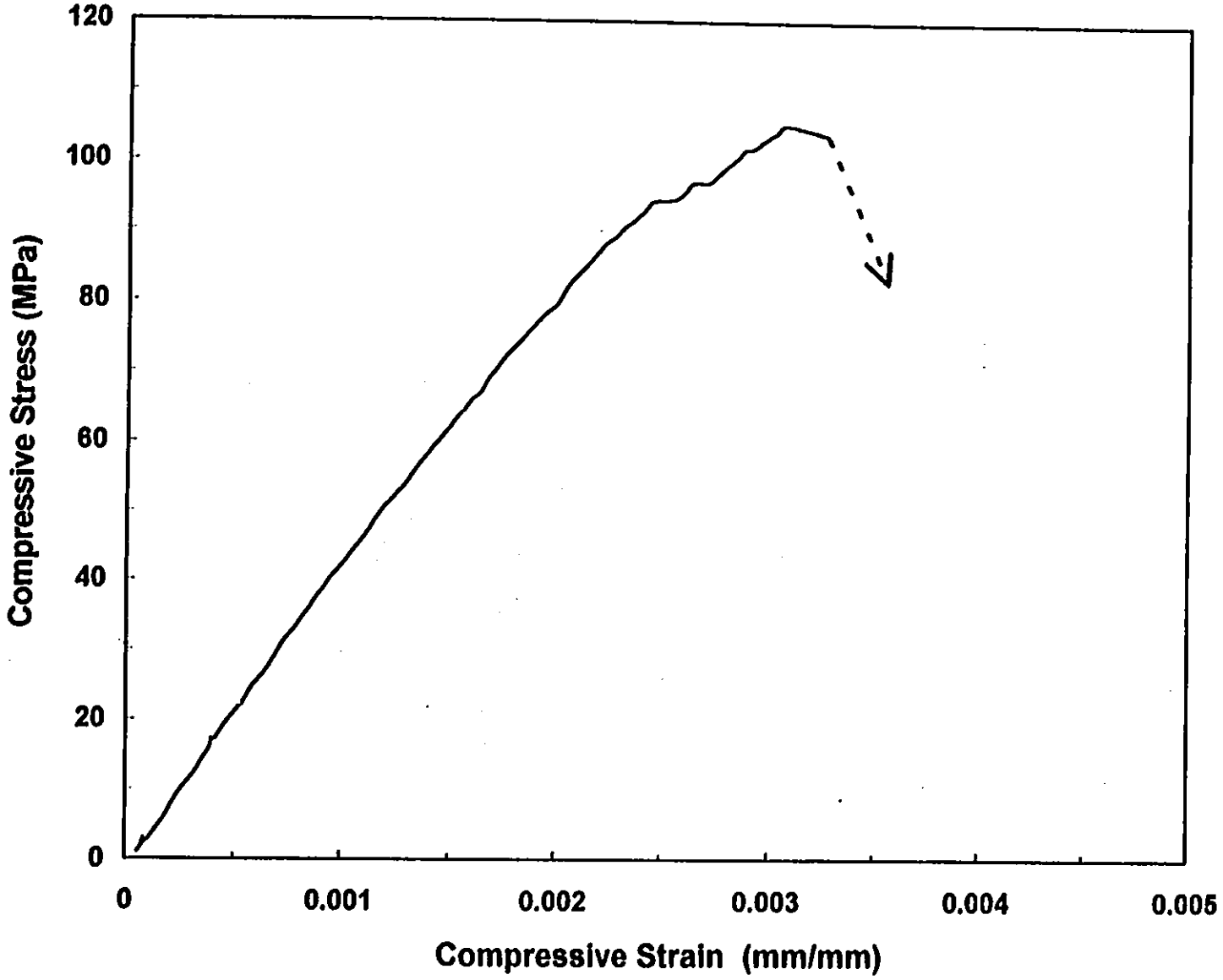

Fig. 3 Concrete Stress-Strain Relationship for Specimens RS-3 through RS-10.

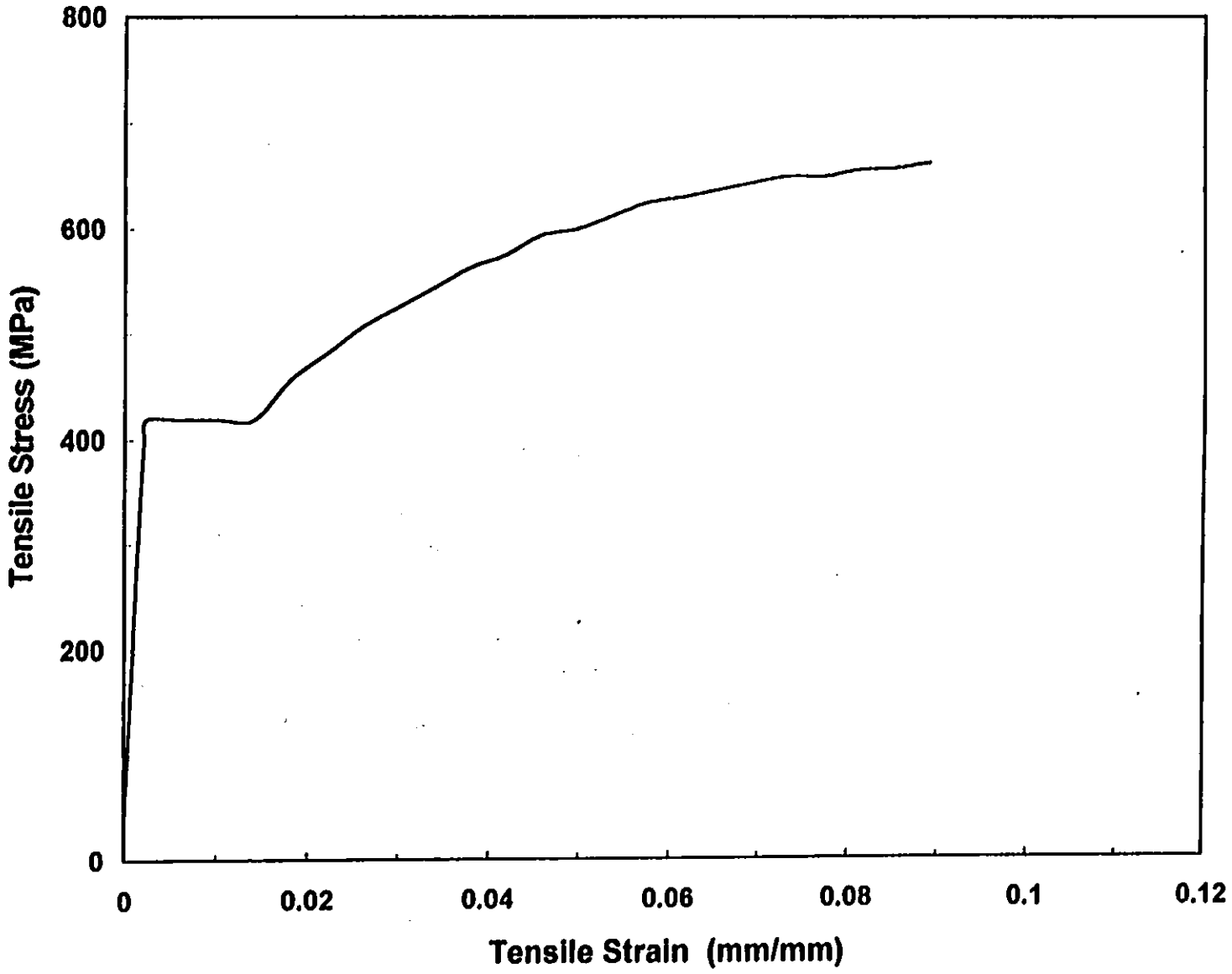

Fig. 4 Longitudinal Reinforcement Stress Strain Relationship.

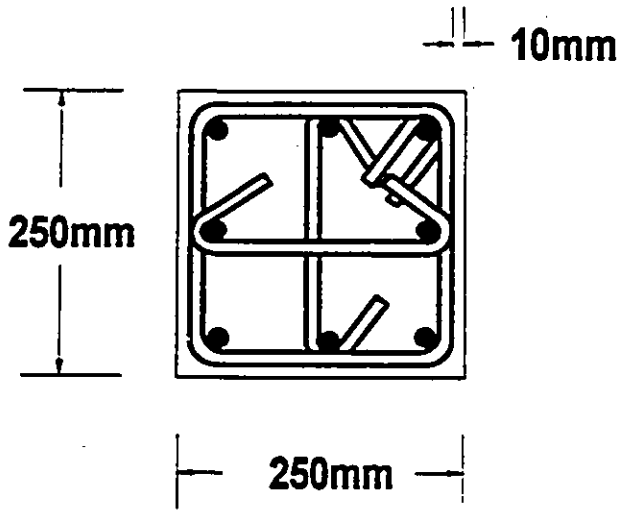

8 Bar Arrangement (col.#: 3 - 8)

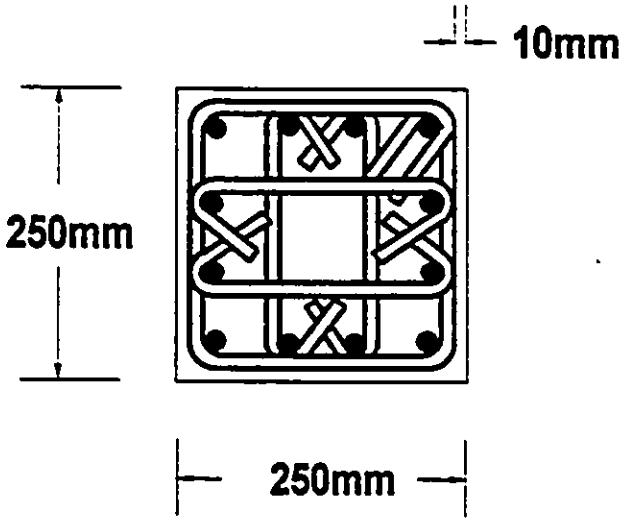

12 Bar Arrangement (col.#: 1, 2, 9, 10)

Fig. 5 TRANSVERSE REINFORCEMENT ARRANGEMENTS

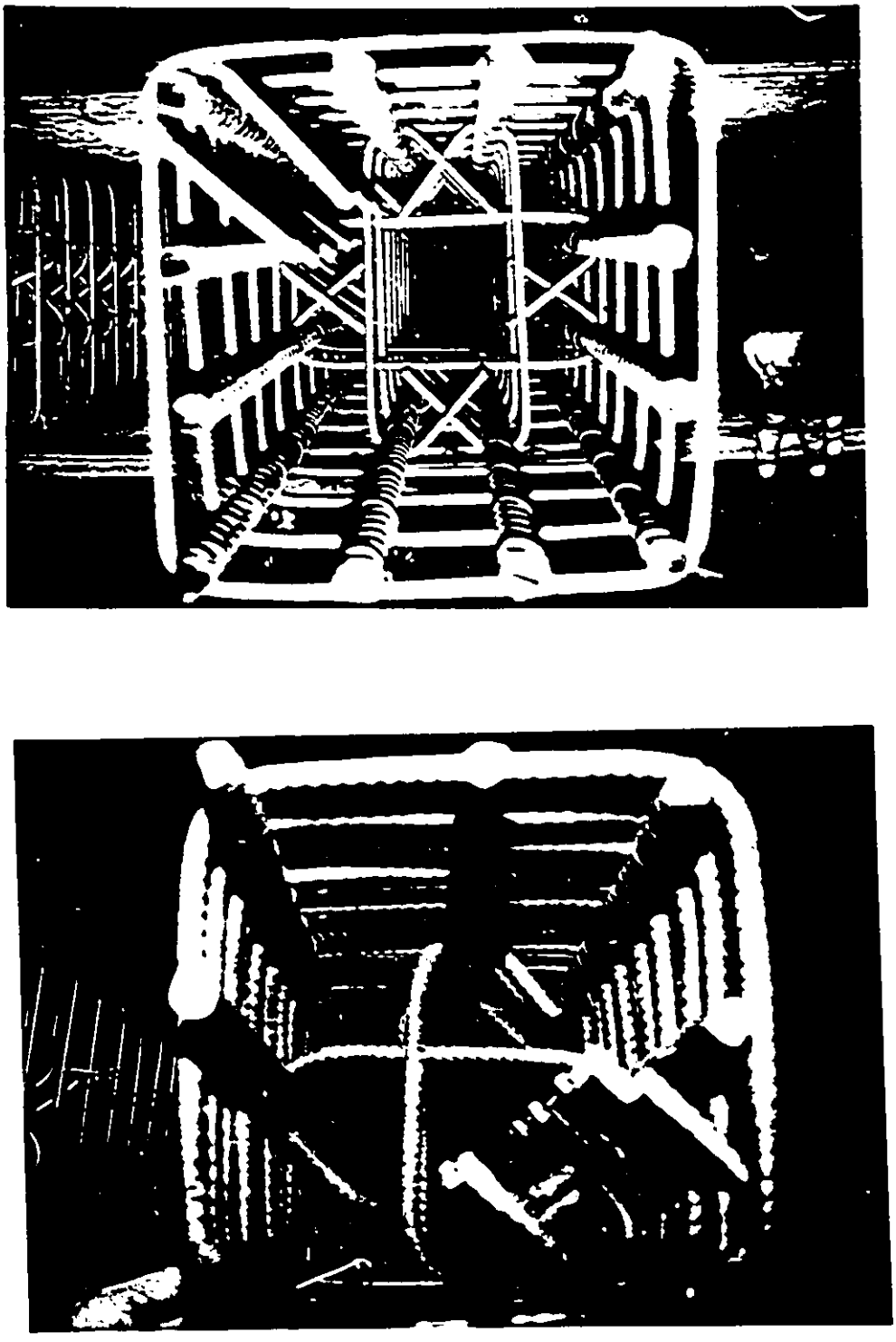

Fig. 6 Reinforcement Cages - Top View

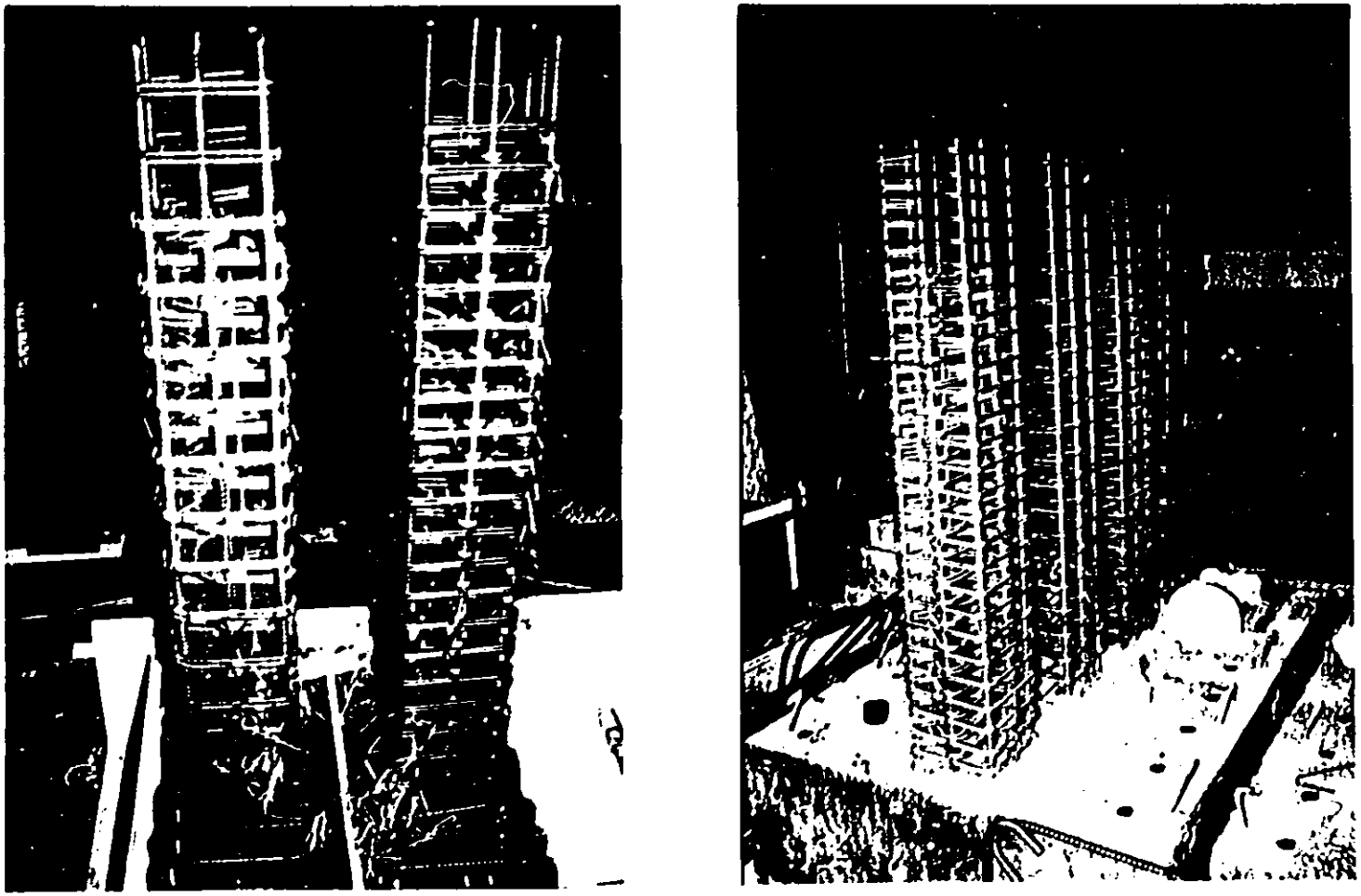

Fig. 7 Reinforcement Cages

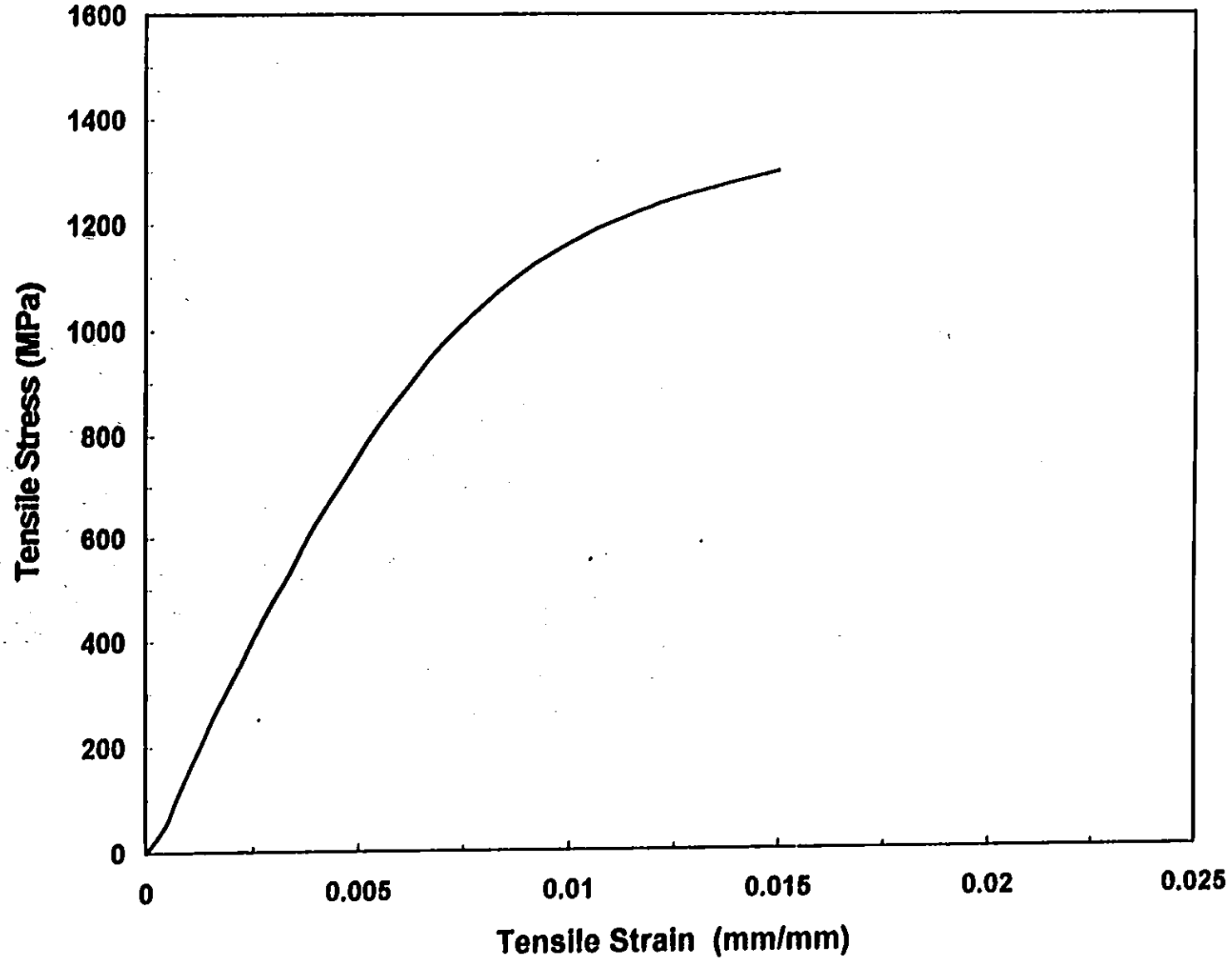

Fig. 8 Transverse Reinforcement Stress-Strain Relationship for Specimens RS-1, RS-5 and RS-7 through RS-10

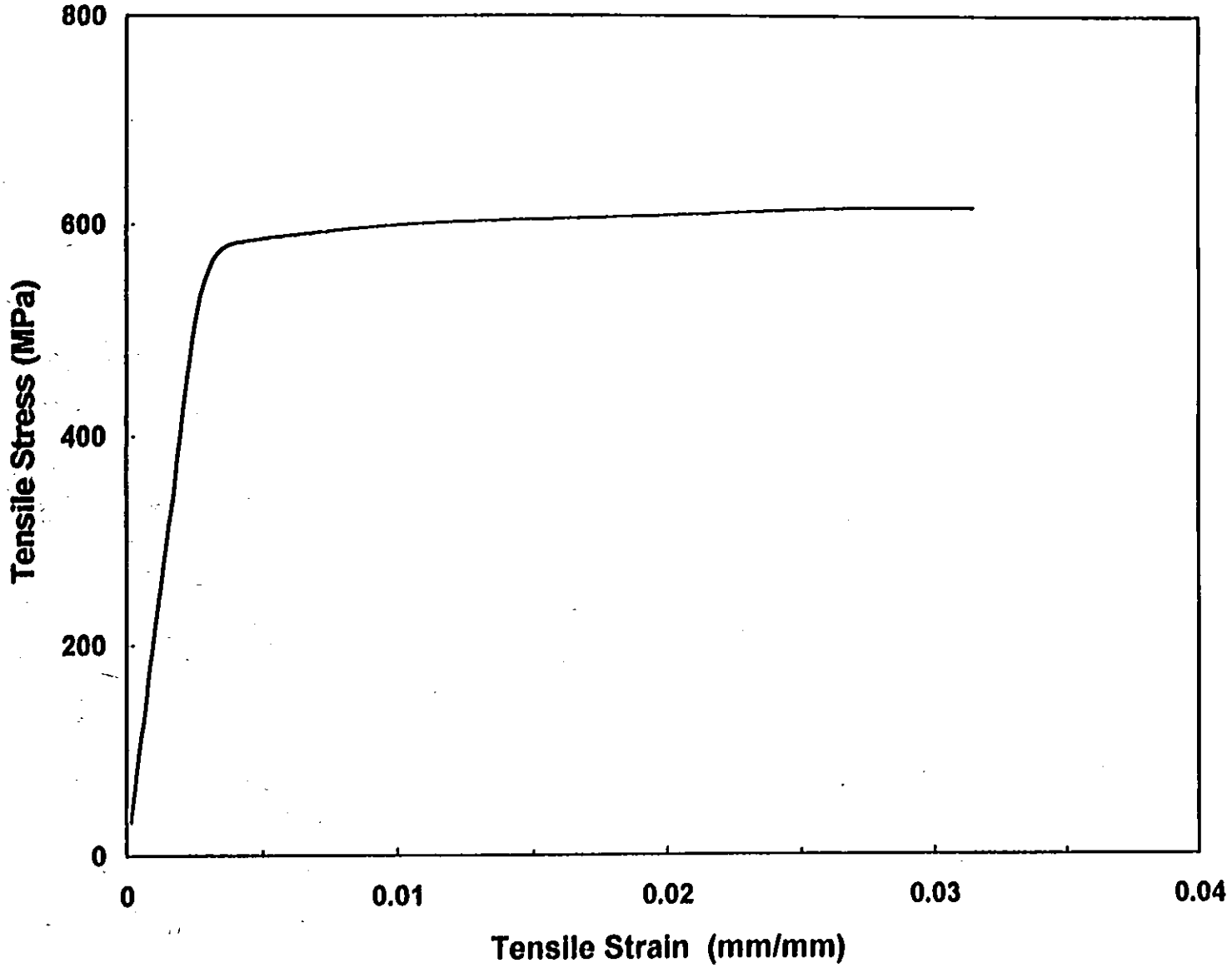

Fig. 9 Transverse Reinforcement Stress-Strain Relationship for Specimens RS-2 and RS-6

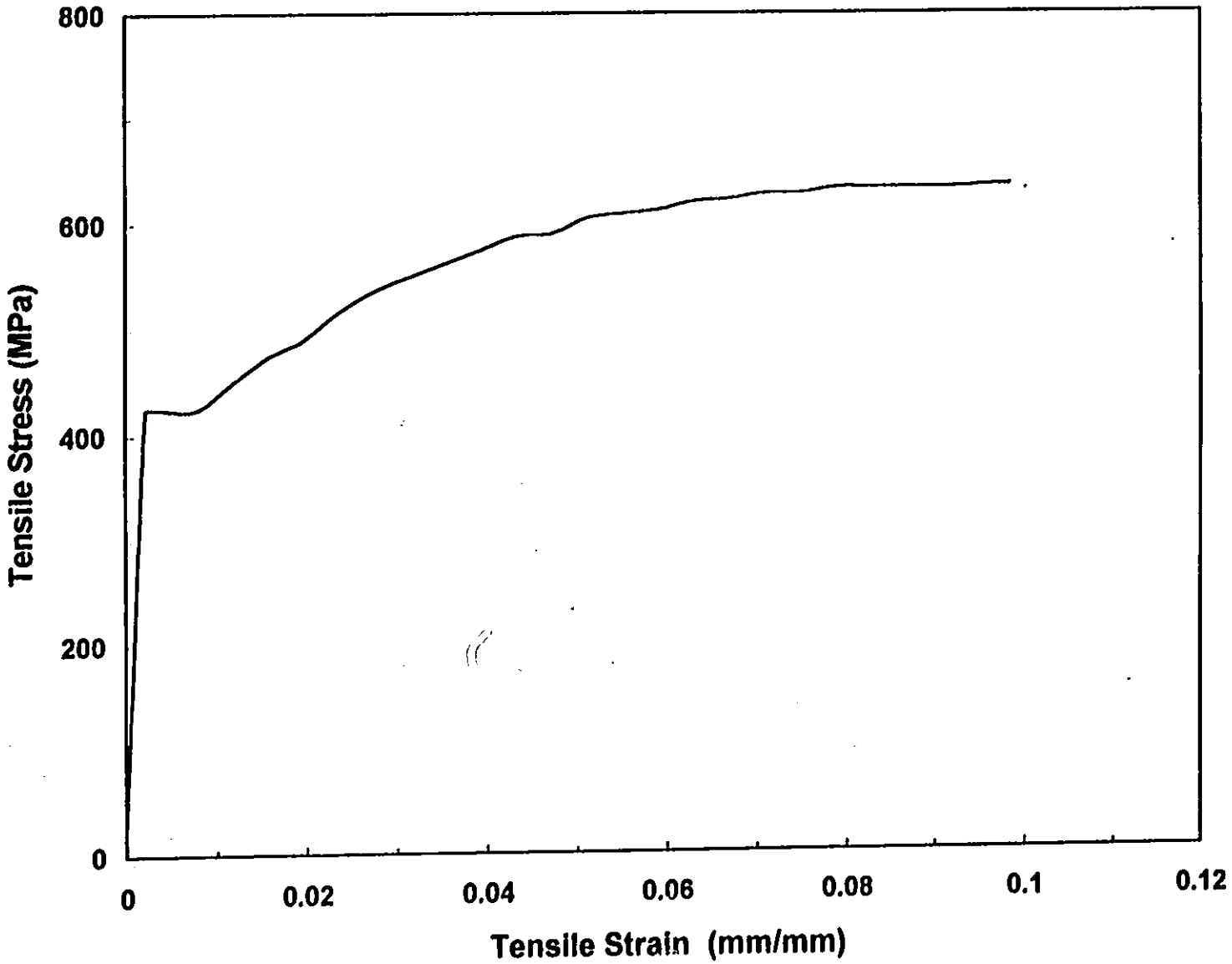

Fig. 10 Transverse Reinforcement Stress-Strain Relationship for Specimens RS-3 and RS-4

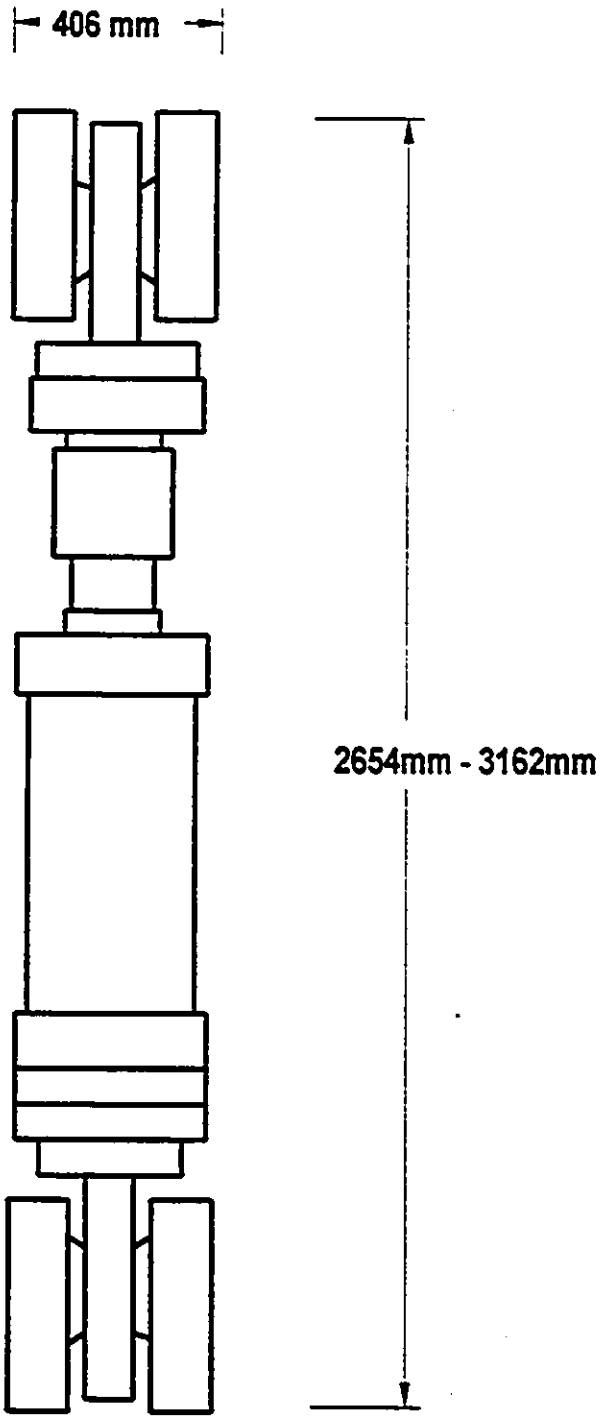

Fig.11 Overall View of the Actuators Used

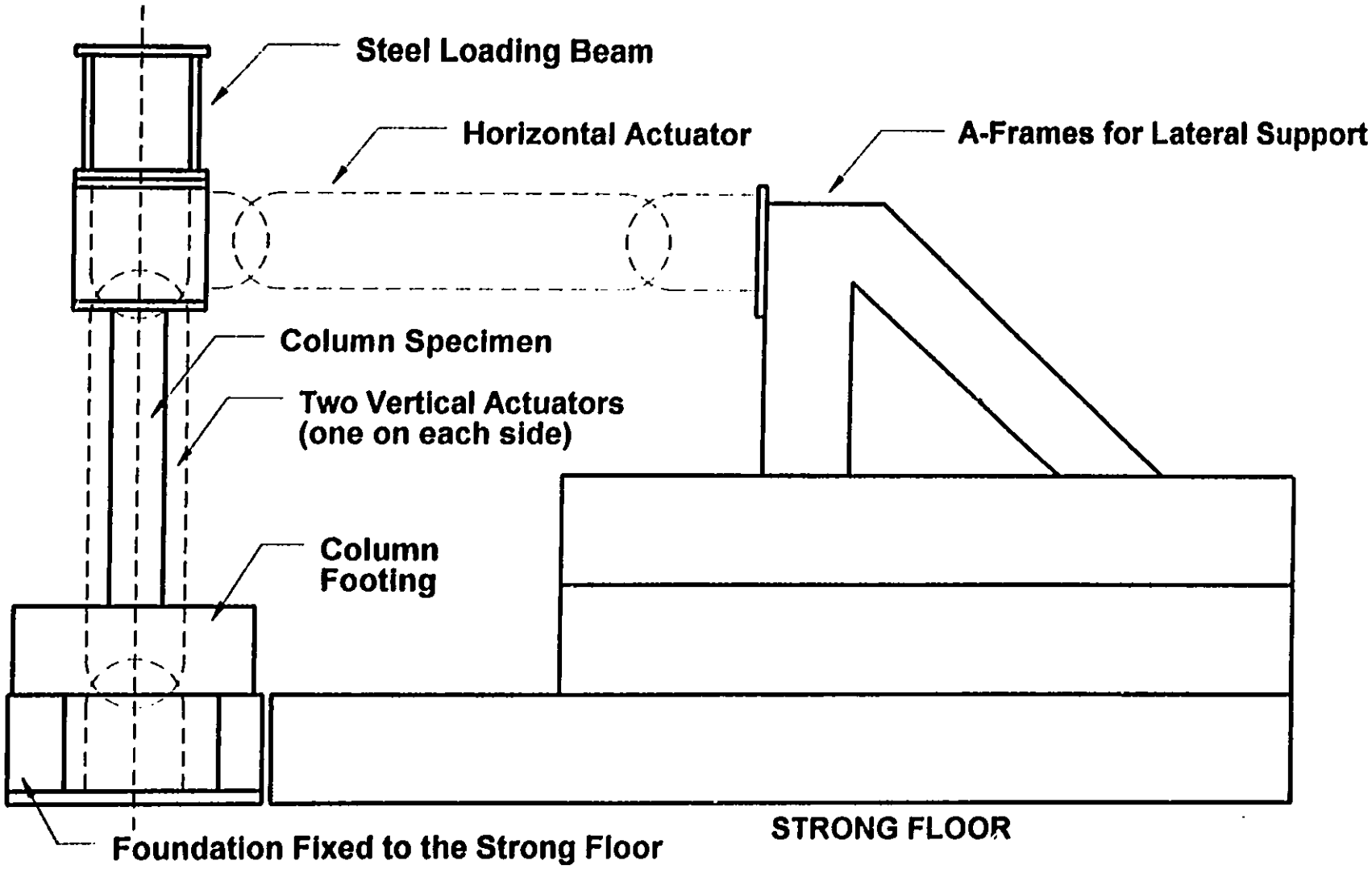

Fig.12 Schematic View of the Test Setup

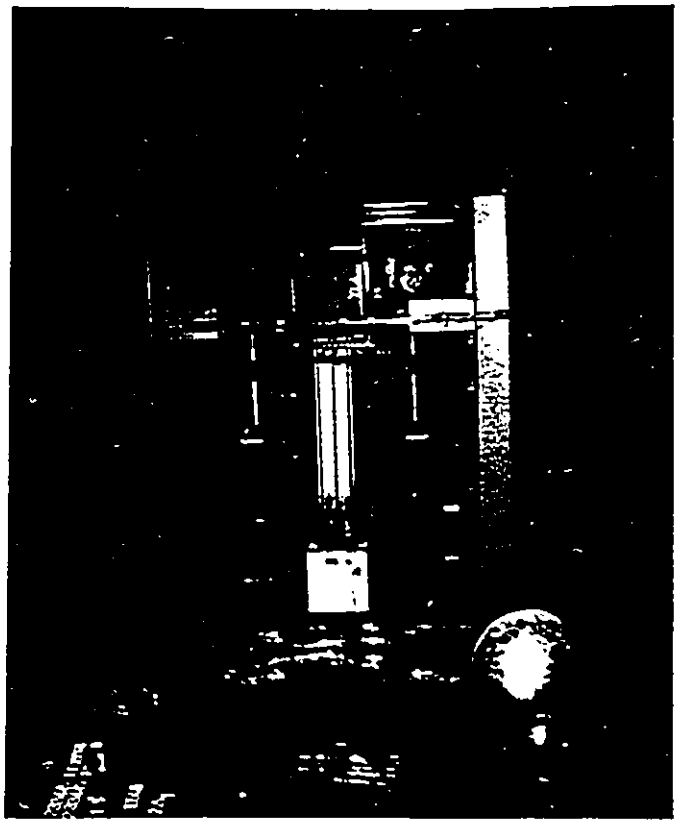

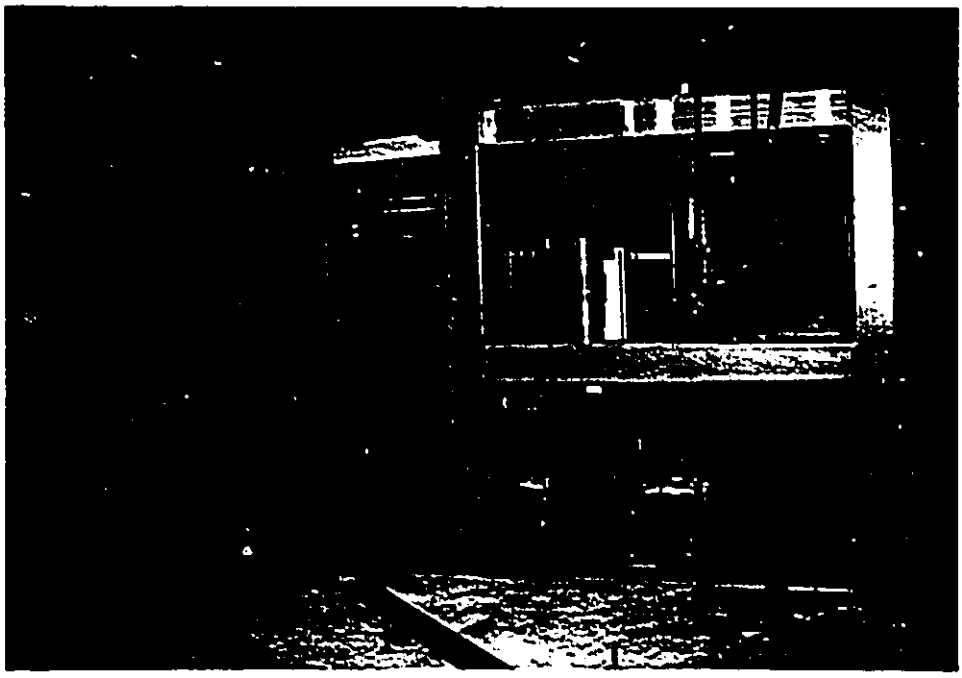

Fig. 13 View of the Test Setup

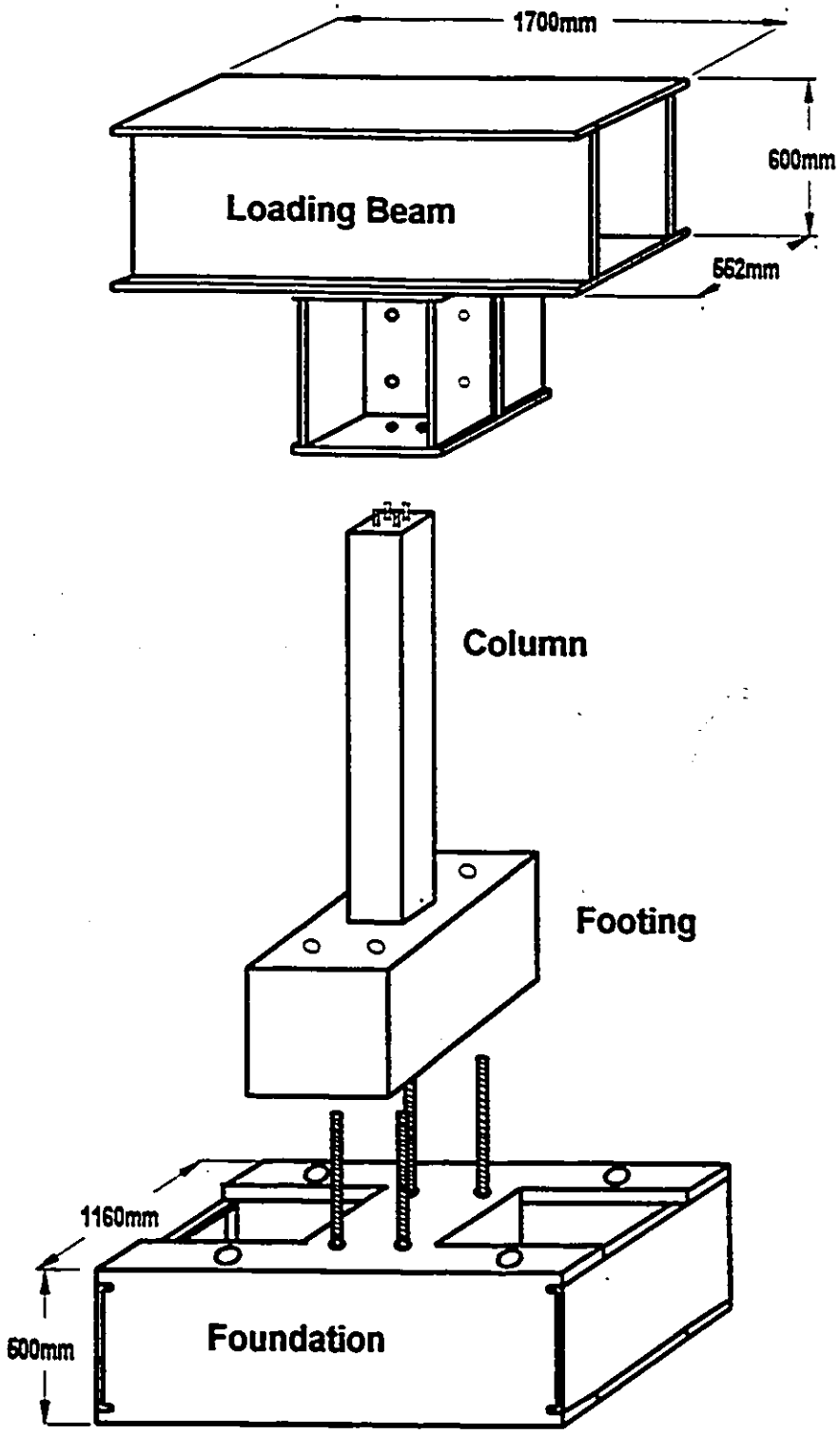

Fig. 14 View of the Components of the Vertical Loading System

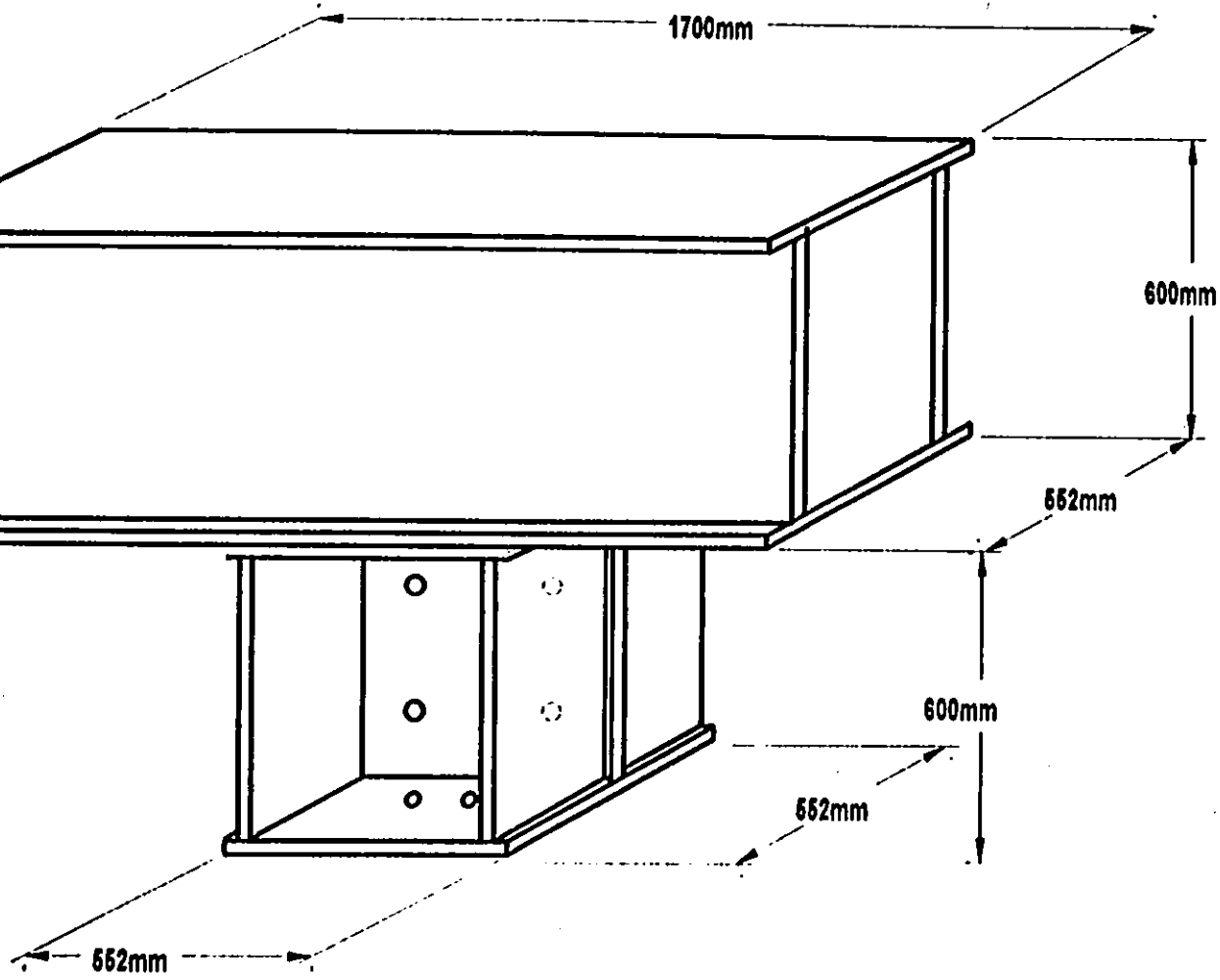

Fig. 15 View of the Loading Beam

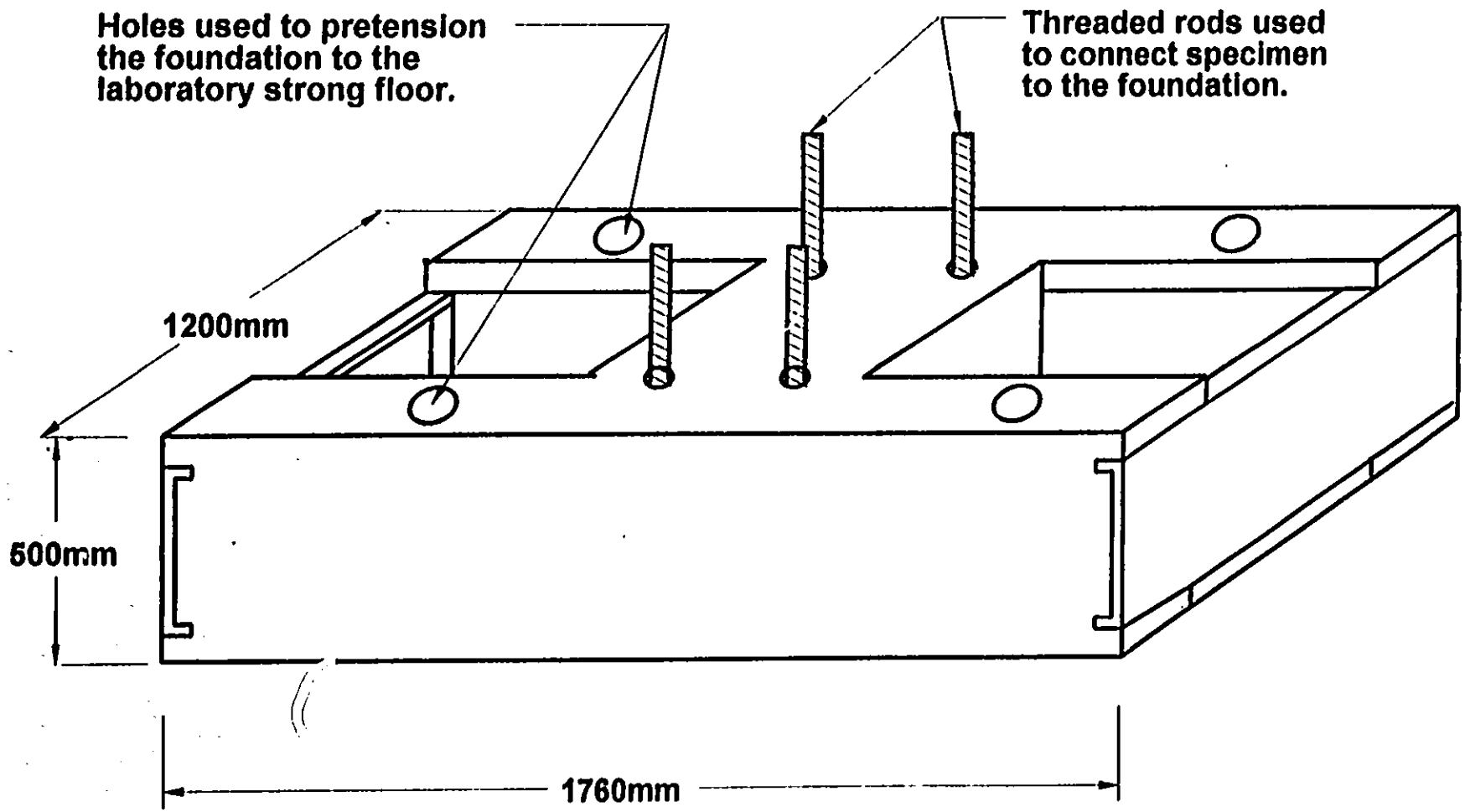

Fig. 16 View of the Foundation

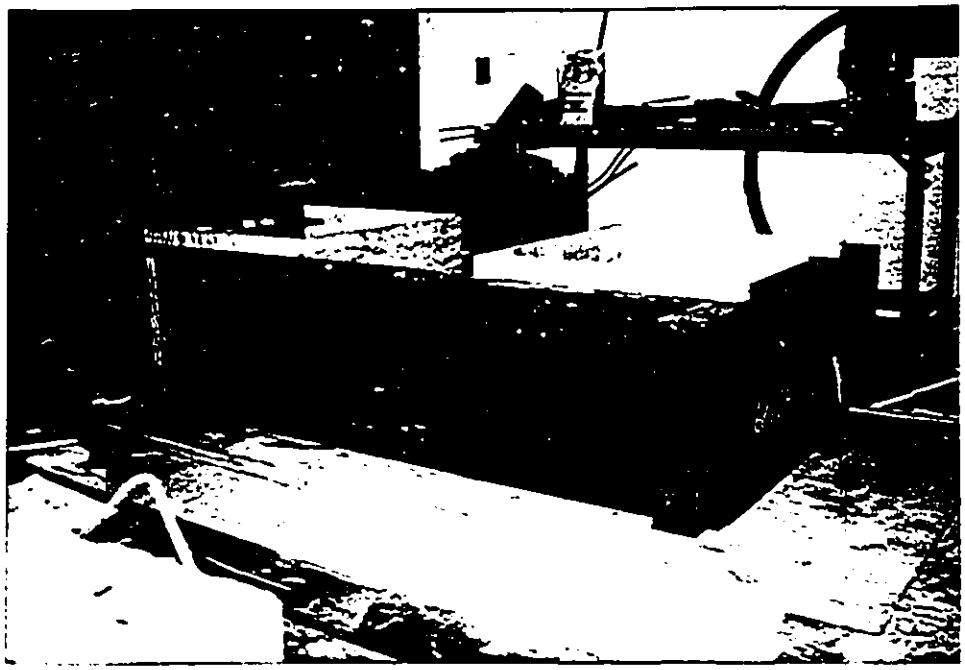

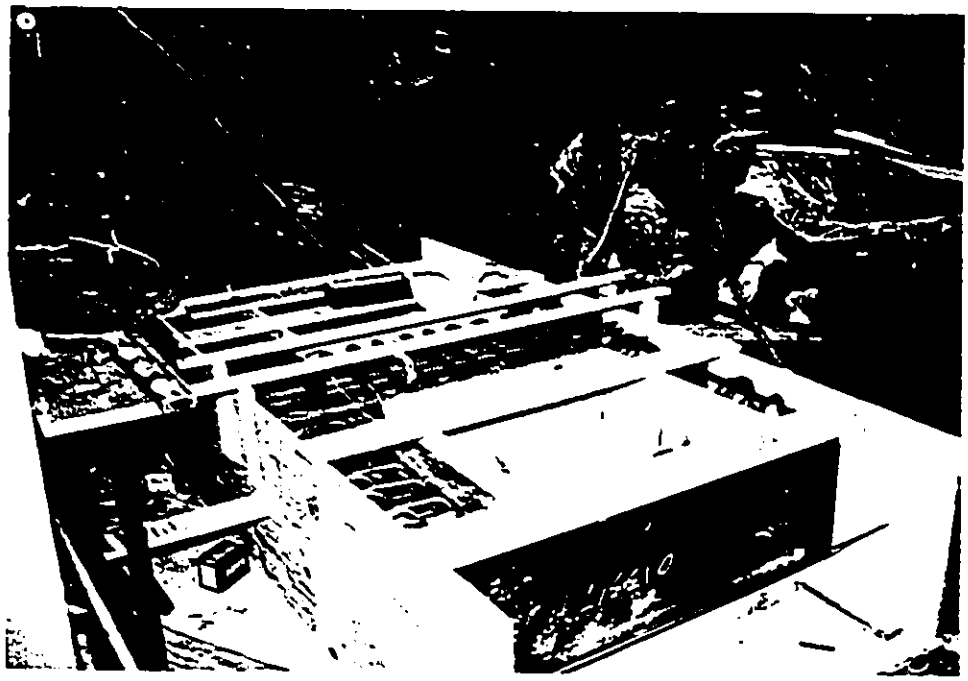

Fig. 17 Preparation of the Foundation

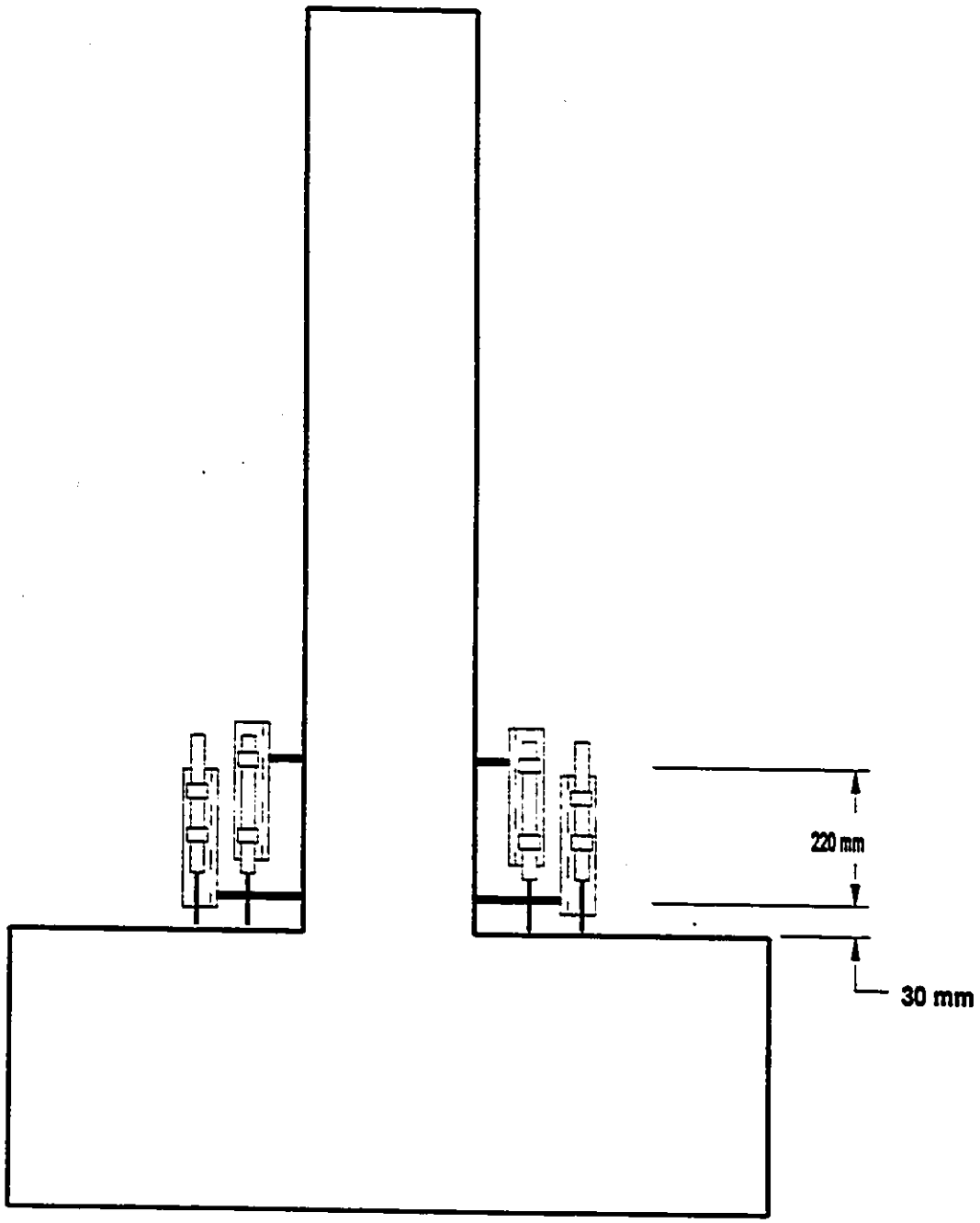

Fig. 18 Locations of LVDTs Used to Measure Rotations

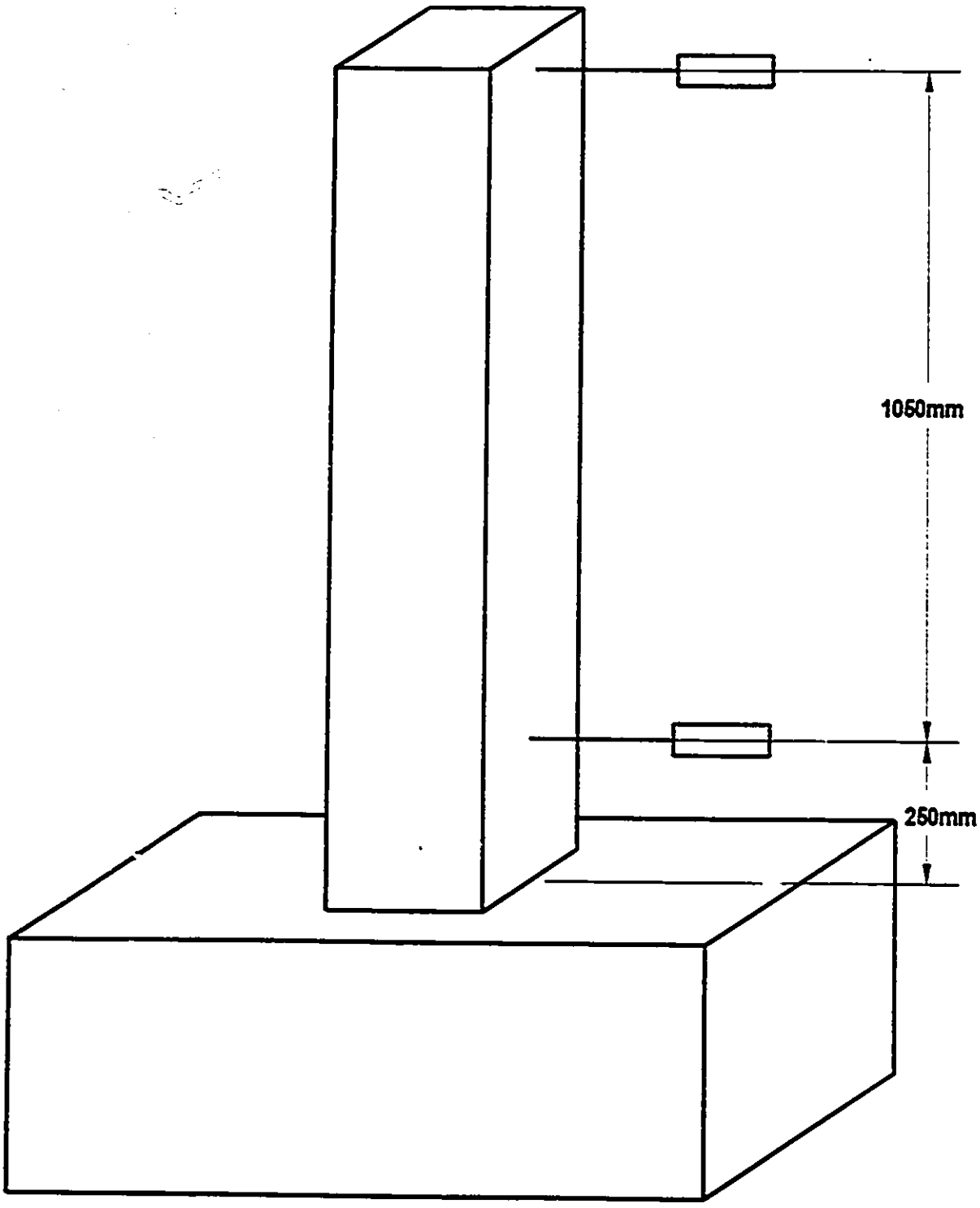

Fig. 19 Horizontal LVDT Locations

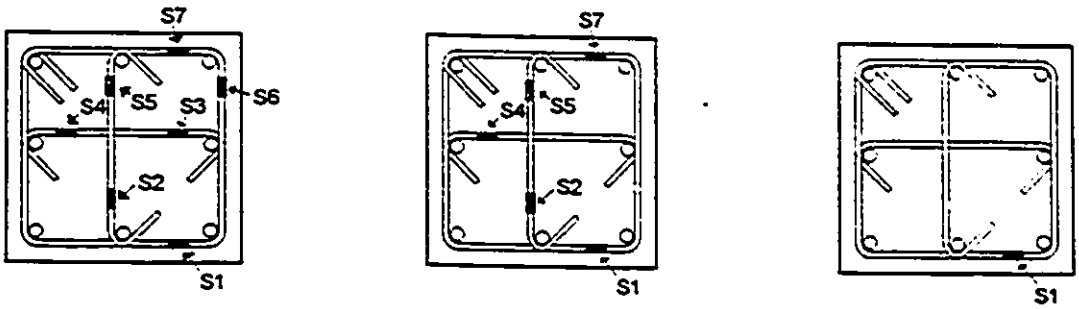

LEVEL 1 LEVEL 2 LEVEL 3

Columns #: RS-1, RS-3, RS-4, RS-5, RS-6, RS-8

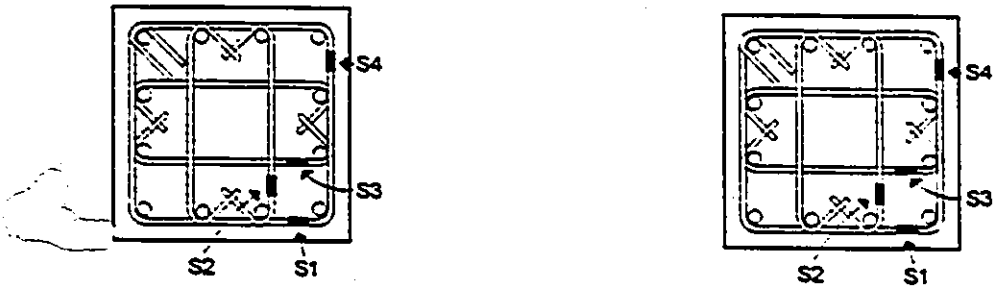

LEVEL 1 LEVEL 2

Columns #: RS-2

Fig. 20 Locations of Strain Gauges on Transverse Reinforcement.

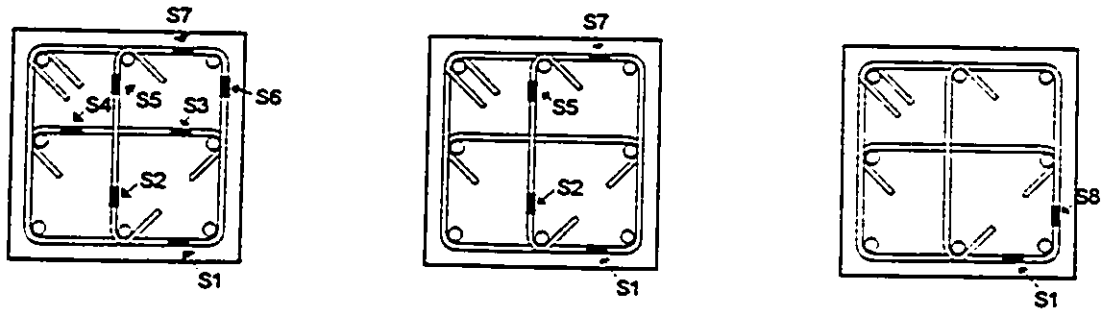

LEVEL 1 LEVEL 2 LEVEL 3

Column #: RS-7

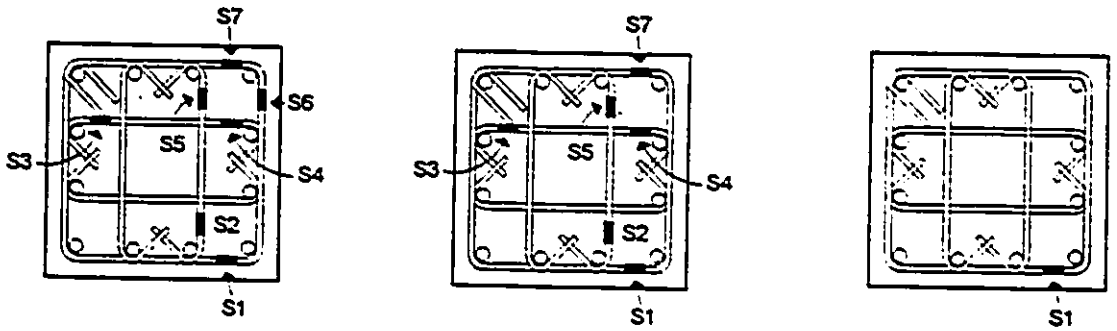

LEVEL 1 LEVEL 2 LEVEL 3

Columns #: RS-9, RS-10

Fig. 20 Locations of Strain Gauges on Transverse Reinforcement - Continued

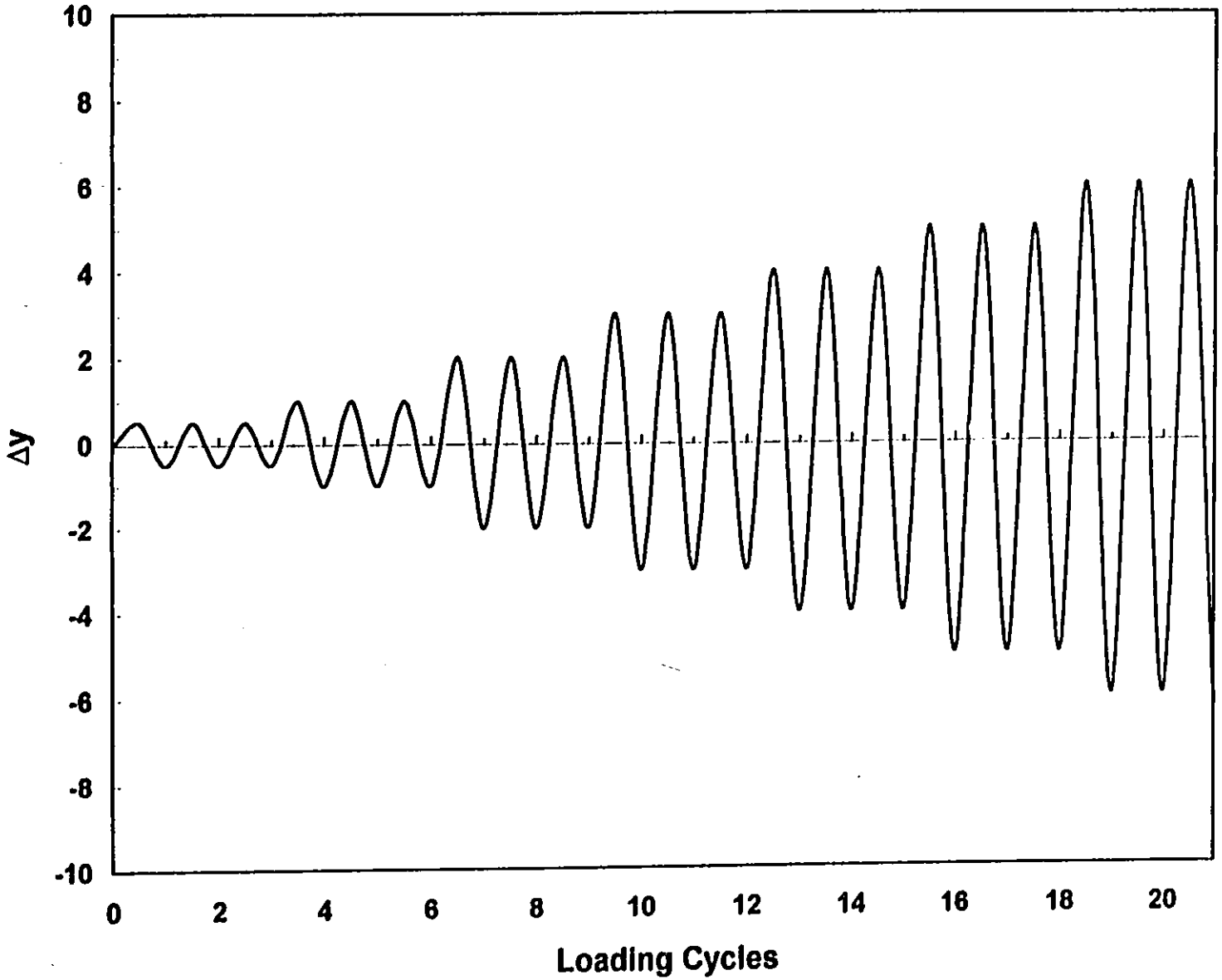

Fig. 21 Horizontal Loading Path Applied

Chapter 3

Observed Behaviour and Test Results

3.1 General

The observed behaviour of each column during testing is discussed in the following sections. Recorded data, in the form of force-displacement hysteretic relationships are also presented, illustrating strength and deformation characteristics of columns. Hysteretic moment rotation relationships of column hinging regions and reinforcement strain data are also discussed. Evaluation of test data and the effects of test variables, including analytical computations are presented in Chapter 4.

3.2 Observed Behaviour and Force-Displacement Relationships

Specimen RS-1

Column RS-1 was one of the two columns with 64 MPa concrete. It was confined by a 12-bar arrangement and 1000 MPa transverse reinforcement, closely spaced.

All the physical properties of this column are summarized in Fig. 22.

Fig. 22 also illustrates the progression of damage observed during testing. The yield displacement was determined during testing to be Δ_y = 25 mm. Some hairline cracks were observed during displacement cycles of $1\Delta_y$. The only visible damage observed at this load stage was the crushing of cover concrete on the south side, near one of the corners, close to the base. None of the strain gauges on transverse reinforcement developed the yield strain. Transverse strains on ties at level 3 were slightly higher than those at level 1, indicating higher lateral expansion of concrete in regions above the base than near the base.

Propagation of cracks was observed during the cycles of $2\Delta_y$. The existing cracks became wider and diagonal cracks were noticed on the east and west faces of column. Cover concrete started spalling near the base and more extensive damage of the hinging region was observed. Strains in longitudinal reinforcement at 125 mm above the base reached 1.25% in compression. Strains in tension were not available because of the damage to the strain gauge. Strains in longitudinal reinforcement at 125mm below the column base, inside the footing, approached the yield strain. The maximum transverse strains recorded in transverse reinforcement was 0.1%.

Increased flexural and diagonal cracks were observed during cycles of $3\Delta_y$. The damage in the hinging region was severe and spalling of the whole hinging region cover was observed on the south and north sides. The strain gauge on longitudinal reinforcement at 125 mm below the base showed development of 0.2% strain, indicating yield penetration into the footing. The maximum transverse reinforcement strain recorded at this load level was 0.25%.

More damage was observed at $4\Delta_y$ displacement cycles. Cover concrete on the east and west sides were completely spalled off, exposing longitudinal and transverse reinforcement. Hinging of the column near the base was visibly noticeable. Slight increase in strains of longitudinal reinforcement was observed at 125mm below the base.

$5\Delta_y$ was the highest level of displacement applied to this specimen. The longitudinal bars buckled and the column experienced a sudden reduction in load resistance. Complete force-displacement hysteretic relationships, recorded during testing, are shown in Figs. 23 and 24 for cases without and with P-Δ effects, respectively. The relationship that excludes P-Δ effects indicates that the column capacity never dropped below 80% of the maximum load. When P-Δ effect is included, the drift capacity observed at 20% strength decay becomes + %.

Hysteretic base moment-total hinging region rotation, and base moment-anchorage slip rotation relationships are shown in Figs. 25 and 26, respectively. It should be noted that the anchorage slip rotation includes a portion of flexural rotation within the bottom 30 mm of column due to the manner in which it was recorded. The results indicate that approximately 1/3 of the total rotation recorded is caused by anchorage slip, while the remaining 2/3 is caused by flexure. This observation is consistent with strain readings recorded in longitudinal reinforcement inside the footing, which indicate significant yield penetration into the footing giving rise to extension of reinforcement and corresponding column rotation. The strain gauge data is presented in Appendix A.

Specimen RS-2

Column RS-2 was companion to RS-1. It had the same characteristics as RS-1 except for the strength of steel and spacing of transverse reinforcement. All the

physical properties of this column are summarized in Fig. 27.

Fig. 27 also shows column RS-2 at selected stages of loading. First flexural cracks became visible during deformation cycles at Δ_y. The yield displacement Δ_y was determined to be 25 mm. No other damage was noticeable at this deformation level. Strains in longitudinal bars reached yielding at column-footing interface. Maximum recorded strain in transverse reinforcement was 0.05%.

More flexural cracks and widening of existing cracks were observed during cycles at $2\Delta_y$. Diagonal cracks were also noticed on east and west faces of column. Concrete at bottom corners crushed and some spalling of the cover on the south and north sides occurred. Maximum strain in transverse reinforcement reached 0.2%. Severe spalling of cover concrete was observed during $3\Delta_y$ cycles within the hinging region. This can be seen in Fig 27. New flexural and diagonal cracks occurred further along the column height. Longitudinal bar strain at 125mm below the column footing interface reached 0.2% in tension and 0.15% in compression.

The damage in the hinge region increased at $4\Delta_y$. More cover spalling occurred especially on east and west faces of column. New horizontal and diagonal cracks were noticed, and strains in longitudinal and transverse reinforcement increased. The column failed at $5\Delta_y$ following extensive damage to the hinging region, coupled with buckling of longitudinal reinforcement. Complete force-displacement hysteretic relationships, recorded during testing, are shown in Figs.28 and 29 for cases without and with P-Δ effects, respectively. The relationship that excludes P-Δ effects indicates that column capacity never dropped to 80% of the maximum load. When P-Δ effects are included, the relationship indicates a drift capacity of 4 % at 20 % strength decay.

Hysteretic base moment-total hinging region rotation, and base moment-anchorage slip rotation relationships for column RS-2 are shown in Figs. 30 and 31, respectively. The results indicate that approximately 1/4 of the total rotation recorded is caused by anchorage slip, while the remaining 3/4 is caused by flexure. This observation is consistent with strain readings recorded for the longitudinal column reinforcement inside the footing, which indicated yield penetration into the footing and corresponding extension of reinforcement and rotation. The strain gauge data is presented in Appendix A.

Specimen RS-3

Specimen RS-3 was manufactured using 104 MPa concrete. In spite of the wide tie spacing of 100 mm and the 8-bar arrangement with 419 MPa strength transverse reinforcement it contained a high volumetric ratio of 5.58 % transverse reinforcement. The physical properties of column RS-3 are summarized in Fig.32.

Fig. 32 also illustrates the column at selected load stages. Several hairline cracks were visible during cycles at yield displacement (Δ_y) which was established to be 20 mm. Concrete started spalling near the base in compression corners. Longitudinal bar strains were 0.14 % in tension and 0.5 % in compression. The maximum strain recorded in transverse reinforcement was 0.05%. Few additional cracks were observed during the cycles at $2\Delta_y$. Additional flexural and diagonal cracks formed during deformation cycles at $3\Delta_y$. The spalling of cover concrete was observed especially on north and south faces, and partly on the other two faces, exposing reinforcement. Column failure occurred at $4\Delta_y$. The capacity reduced very significantly when the core concrete crushed and the longitudinal bars buckled at $4\Delta_y$. Complete force-displacement hysteretic relationships, recorded during testing, are shown in Figs. 33 and 34 for cases without and with P-Δ effects, respectively. The relationship that excludes P-Δ effects indicates that

column capacity never dropped to 80% of the capacity. When P-Δ effects are included however, the drift capacity is observed to be 2.5% at 20% strength decay.

Hysteretic base moment-total hinging region rotation and base moment-anchorage slip rotation relationships for the column are shown in Figs. 35 and 36, respectively. The last 8 cycles of anchorage slip data were recorded incorrectly and hence were not included in the plot shown in Fig. 36. The results indicate that rotations due to anchorage slip formed only a negligible fraction of total rotation. This observation is consistent with strain readings recorded for the longitudinal column reinforcement inside the footing which does not indicate any significant yield penetration into the footing. The strain gauge data is presented in Appendix A.

Specimen RS-4

Column RS-4 was identical to RS-3 except for tie spacing. The physical properties of RS-4 are summarized in Fig. 37. The same figure also shows the extent of damage observed at selected stages of loading.

The yield displacement (Δ_y) was established to be 20 mm. Several flexural cracks were observed at $1\Delta_y$ on south and north sides of column close to the base. Cover concrete started spalling off near the corners of the hinging region. Strains in longitudinal reinforcement reached 0.18 % in tension and 0.22 % in compression. The maximum transverse strain recorded at this load stage was 0.1 %. The spalling of concrete continued during cycles at $2\Delta_y$, exposing transverse and longitudinal reinforcement. It became visible that concrete cover on the south side of specimen was thinner than that on the opposite side. This resulted in some difference in capacity in two opposite directions. Additional flexural and diagonal

cracks formed and the existing crack widths became wider at $2\Delta_y$. One of the strain gauges on transverse reinforcement indicated yielding of lateral steel at this load stage. Concrete cracking and cover spalling increased during cycles of $3\Delta_y$. More yielding of transverse reinforcement was observed at $4\Delta_y$. The column showed a gradual strength decay and failed after sustaining deformation cycles at $5\ \Delta_y$.

Complete force-displacement hysteretic relationships, recorded during testing, are shown in Figs. 38 and 39 for cases without and with P-Δ effects, respectively. These relationships indicate a drift capacity of 6 % and 3 % at 20 % strength decay when P-Δ effects were ignored and considered, respectively. Hysteretic base moment-total hinging region rotation, and base moment-anchorage slip rotation relationships for column RS-4 are shown in Figs. 40 and 41, respectively. The results indicate that approximately 1/8 of the total rotation recorded was caused by anchorage slip, while the remaining 7/8 was caused by flexure. The strain gauge data is presented in Appendix A.

Specimen RS - 5

Specimen RS-5 had 104 MPa concrete and 1000 MPa transverse reinforcement. The column was confined with the least amount of transverse reinforcement, giving a volumetric ratio of 1.9 %. The physical properties of RS-5 are summarized in Fig. 42. The same figure also shows the extent of damage observed at selected stages of loading.

Several flexural cracks were noticed on south and north sides of column at $1\Delta_y$. Concrete started spalling off at three corners close to the base. No other damage was visible. Strains in longitudinal bars reached 0.01% in tension and 0.15% in compression. Maximum transverse reinforcement strain recorded was 0.04%. The

area of spalled concrete increased drastically during the cycles of $2\Delta_y$, exposing transverse and longitudinal reinforcement. Additional flexural cracks on north and south sides and diagonal cracks on east and west sides of column were observed.

More flexural and diagonal cracks were observed during the first cycle of $3\Delta_y$. The transverse reinforcement developed 0.3 % strain. More spalling of cover concrete was observed on north and south sides, although the damage did not seem to propagate further away from the base. Spalling of the side covers occurred during this load stage forming a clear hinging area near the base. The column failed during the third cycle of $3\Delta_y$.

Complete force-displacement hysteretic relationships, recorded during testing, are shown in Figs. 43 and 44 for cases without and with P-Δ effects, respectively. These relationships indicate a drift capacity of 4 % and 2 % at 20 % strength decay when the P-Δ effects were ignored and considered, respectively. Hysteretic base moment-total hinging region rotation and base moment-anchorage slip rotation relationships for the column are shown in Figs. 45 and 46, respectively. The results indicate that approximately 1/8 of the total rotation recorded was caused by anchorage slip, while the remaining 7/8 was caused by flexure. The strain gauge data is presented in Appendix A.

Specimen RS-6

Specimen RS-6 was made out of 104 MPa concrete. It was confined by transverse reinforcement of 575 MPa strength. The physical properties of column are summarized in Fig. 47. The same figure also illustrates the progression of damage observed during testing.

The yield displacement (Δ_y) was established as 25mm. Several flexural cracks

were visible during the cycles of $1\Delta_y$. Maximum tensile and compressive strains in longitudinal reinforcement were 0.4% and 0.8%, respectively. Transverse reinforcement strains were close to zero suggesting little lateral expansion of concrete at this load stage. Damage to concrete occurred at $2\Delta y$ in the hinging region of column near the base. Crushing and spalling of concrete were localized in the hinging region. Large pieces of concrete spalled off on the south side whereas the damage was limited to the corners of the column on the north side. The transverse steel strains exceeded 0.2%. Strength degradation started during the cycles at the next displacement level which led to the failure of the column. The maximum strain recorded in transverse reinforcement was 0.25%.

Complete force-displacement hysteretic relationships, recorded during the test, are shown in Figs. 48 and 49 for cases without and with P-Δ effects, respectively. These relationships indicate a drift capacity of 6 % and 3 % at 20 % strength decay when P-Δ effects were ignored and considered, respectively. Hysteretic base moment-total hinging region rotation, and base moment-anchorage slip rotation relationships are shown in Figs. 50 and 51, respectively. The results indicate that approximately 1/6 of the total rotation recorded was caused by anchorage slip while the remaining 5/6 was caused by flexure. The strain gauge data is presented in Appendix A.

Specimen RS-7

Specimen RS-7 was made out of 104 MPa concrete with 1000 MPa transverse reinforcement. The physical properties of the column are summarized in Fig. 52. The same figure also illustrates observed damage at selected load stages.

The yield displacement (Δ_y) was established to be 25 mm. Damage at $1\Delta_y$ was limited to some flexural cracking. The transverse reinforcement showed little

strains and remained in the elastic range. More flexural cracking was observed at $2\Delta_y$ with little spalling of cover concrete. The transverse reinforcement developed 0.3% strain at this load stage. Large pieces of concrete spalled off at $3\Delta_y$ and the column started experiencing gradual strength decay. The column developed a sudden loss of strength and was not able to sustain the second cycle at $4\Delta_y$.

Complete force-displacement hysteretic relationships, recorded during the test, are shown in Figs. 53 and 54 for cases without and with P-Δ effects, respectively. The relationship that excludes P-Δ effects indicates that column capacity never dropped to 80% of strength. When P-Δ effects were included the drift capacity was 3% at 20% strength decay.

Hysteretic base moment-total hinging region rotation, and base moment-anchorage slip rotation relationships are shown in Figs. 55 and 56, respectively. The results indicate that approximately 1/8 of the total rotation recorded was caused by anchorage slip while the remaining 7/8 was caused by flexure. The strain gauge data is presented in Appendix A.

Specimen RS-8

Specimen RS-8 was companion to RS-7 and had identical properties except for the volumetric ratio and spacing of transverse reinforcement. The properties of the column are summarized in Fig. 57. The same figure also illustrates observed damage during selected stages of loading.

The yield displacement (Δ_y) was established to be 25 mm. Some flexural cracking and limited spalling of cover concrete were observed during cycles at $1\Delta_y$. The maximum tensile and compressive strains recorded in longitudinal reinforcement were 0.46% and 0.57%, respectively. The transverse steel strain was equal to

0.1%. Increased damage was observed at $2\Delta_y$. A large piece of cover concrete broke off from the column approximately 300mm from the base. The concrete damage was essentially limited to the bottom portion of column near the base. Additional flexural cracking was also observed at this load stage. The column exhibited gradual strength decay during cycles of $2\Delta_y$.

The damage observed at $3\Delta_y$ was extensive. The formation of the hinge was clearly visible. Number of diagonal cracks increased and concrete cover spalled off along the sides of the column, exposing reinforcement. The maximum strain in transverse reinforcement was in the range of 0.25%. Additional spalling was observed at $4\Delta_y$. This was especially visible on east and west sides of the column where large amounts of concrete cover spalled off, exposing longitudinal and transverse reinforcement.

Complete force-displacement hysteretic relationships, recorded during the test, are shown in Figs. 58 and 59 for cases without and with P-Δ effects, respectively. The relationship that excludes P-Δ effects indicates that column capacity never dropped to 80% of its strength. When P-Δ effects were included the drift capacity was 3% at 20% strength decay.

Hysteretic base moment-total hinging region rotation, and base moment-anchorage slip rotation relationships are shown in Figs. 60 and 61, respectively. The results indicate that approximately 1/8 of the total rotation recorded was caused by anchorage slip, while the remaining 7/8 was caused by flexure. The strain gauge data is presented in Appendix A.

Specimen RS-9

Specimen RS-9 was companion to RS-10 and had identical properties. The

properties of the column are summarized in Fig. 62. The same figure also illustrates observed damage during selected stages of loading.

The yield displacement (Δ_y) was established to be 25 mm. Some flexural cracking and limited spalling of cover concrete were observed during cycles at $1\Delta_y$. The maximum tensile and compressive strains recorded in longitudinal reinforcement were 0.45 % and 0.88 %, respectively. The transverse steel strain was equal to 0.12 %.

A large piece of concrete spalled off at $2\Delta_y$ exposing reinforcement. Existing flexural cracks widened and new cracked were developed. Significant reduction in stiffness occurred during second and third cycle. The column exhibited gradual strength decay during cycles of $2\Delta_y$. Formation of plastic hinge was clearly visible.

The damage observed at $3\Delta_y$ was extensive. The hinge became more visible. Number of diagonal cracks increased and concrete cover spalled off along the sides of the column, exposing reinforcement. Core concrete started crushing and falling off the column. The maximum strain in transverse reinforcement was in the range of 0.33 %. Additional spalling was observed at $4\Delta_y$. Severe damage occurred to the core. This caused sudden and significant drop in capacity during the last cycle.

Complete force-displacement hysteretic relationships, recorded during the test, are shown in Figs. 63 and 64 for cases without and with P-Δ effects, respectively. These relationships indicate a drift capacity of 6 % and 3 % at 20 % strength decay when the P-Δ effects were ignored and considered, respectively. Hysteretic base moment-total hinging region rotation, and base moment-anchorage slip rotation relationships are shown in Figs. 65 and 66, respectively. The results

indicate that approximately 1/8 of the total rotation recorded was caused by anchorage slip, while the remaining 7/8 was caused by flexure. The strain gauge data is presented in Appendix A.

Specimen RS-10

Column RS-10 was used to investigate the effect of axial load on ductility. It was subjected to 14% of P_o, which was half of the load applied to the companion specimen, RS-9. It was confined by a 12-bar arrangement and 1000 MPa transverse reinforcement, closely spaced. All the physical properties of this column are summarized in Fig. 67.

Fig. 67 also illustrates the progression of damage observed during testing. The yield displacement was determined during testing to be Δ_y= 25 mm. Some hairline cracks were observed during displacement cycles at $1\Delta_y$. There was no visible damage observed at this load stage. The maximum tensile and compressive strains recorded in longitudinal reinforcement were 0.67 % and 1 %, respectively. The transverse steel strain was equal to 0.07 %.

Propagation of cracks was observed during the cycles of $2\Delta_y$. Crushing of concrete was observed near column base at this load stage. A few horizontal cracks appeared on both sides of the specimen.

Diagonal cracks became visible during cycles of $3\Delta_y$. Big pieces of concrete cover spalled of on south and north sides of column. The damage propagated to west and east sides of column. Formation of the hinge was clearly visible. The strain gauge on longitudinal reinforcement at 125 mm below the base showed development of 0.3 % strain, indicating yield penetration into the footing.

More damage was observed at $4\Delta_y$ displacement cycles. Cover concrete all around the hinging region was completely spalled off, exposing longitudinal and transverse reinforcement. Hinging of the column near the base was visibly noticeable. Slight increase in strains of longitudinal reinforcement was observed at 125mm below the base.

More damage was observed in the core concrete at $5\Delta_y$. There was no additional spalling of cover concrete beyond the hinge. $6\Delta_y$ was the highest level of displacement applied to this specimen. The longitudinal bars buckled and the column experienced a sudden reduction in load resistance. Complete force-displacement hysteretic relationships, recorded during testing, are shown in Figs. 68 and 69 for cases without and with P-Δ effects, respectively. These relationships indicate a drift capacity of 8 % and 4 % at 20 % strength decay when the P-Δ effects were ignored and considered, respectively.

Hysteretic base moment-total hinging region rotation and base moment-anchorage slip rotation relationships for the column are shown in Figs. 70 and 71, respectively. The results indicate that approximately 1/3 of the total rotation recorded was caused by anchorage slip, while the remaining 2/3 was caused by flexure. This observation is consistent with strain readings recorded for the longitudinal column reinforcement inside the footing which indicated a significant yield penetration into the footing that gave rise to the extension of reinforcement and corresponding column rotation. The strain gauge data is presented in Appendix A.

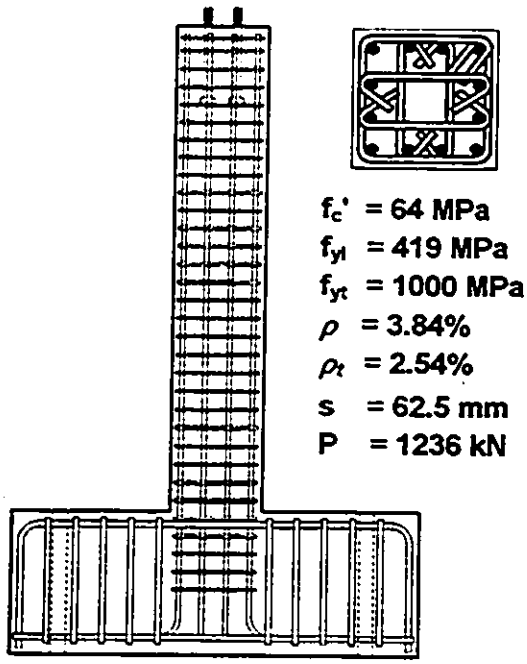

a) 1 Δy

b) 3 Δy

c) 5 Δy

Fig. 22 Extent of Damage at Different Load Stages Specimen RS-1

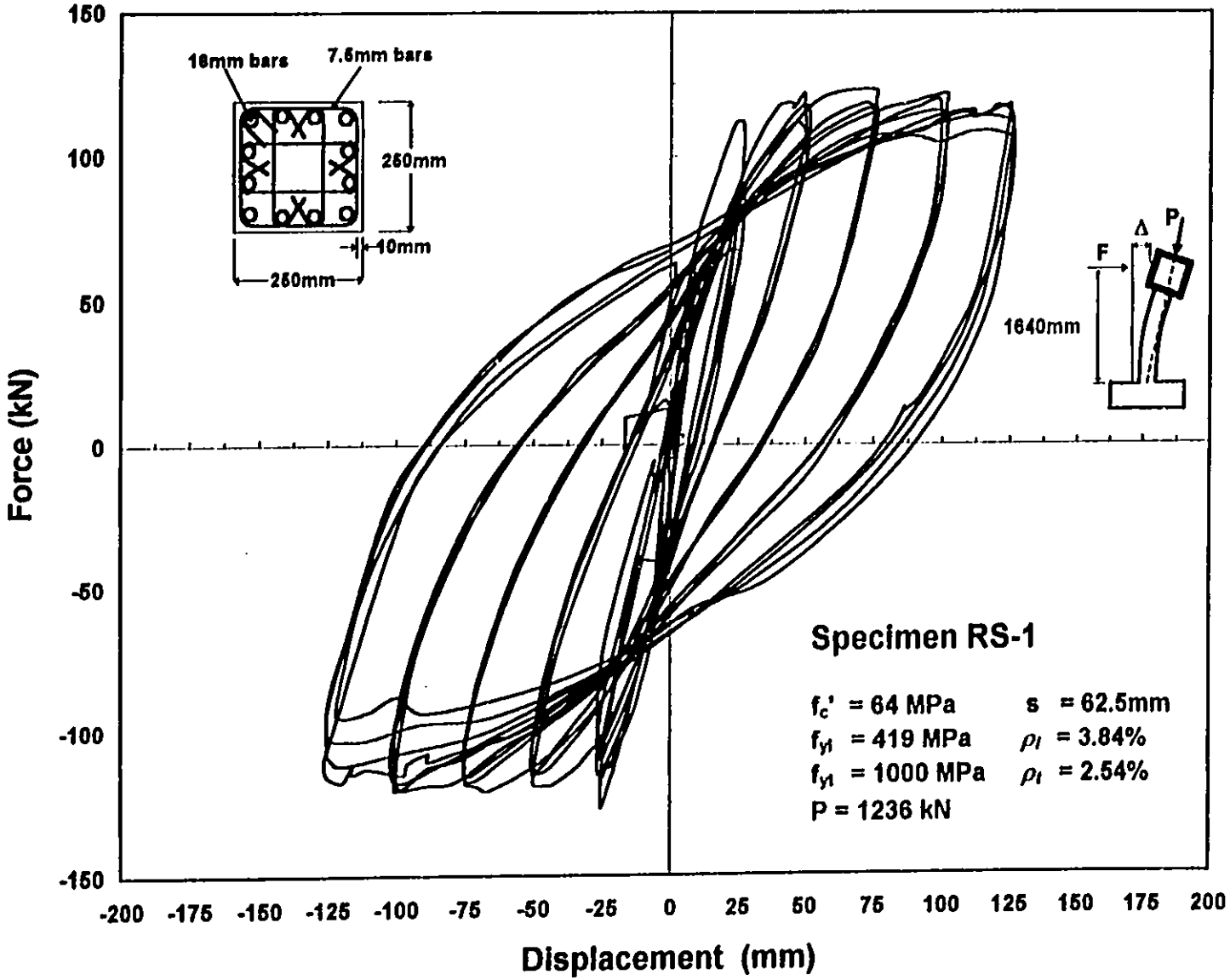

Fig. 23 Force - Displacement Relationship Excluding P-Δ Effect

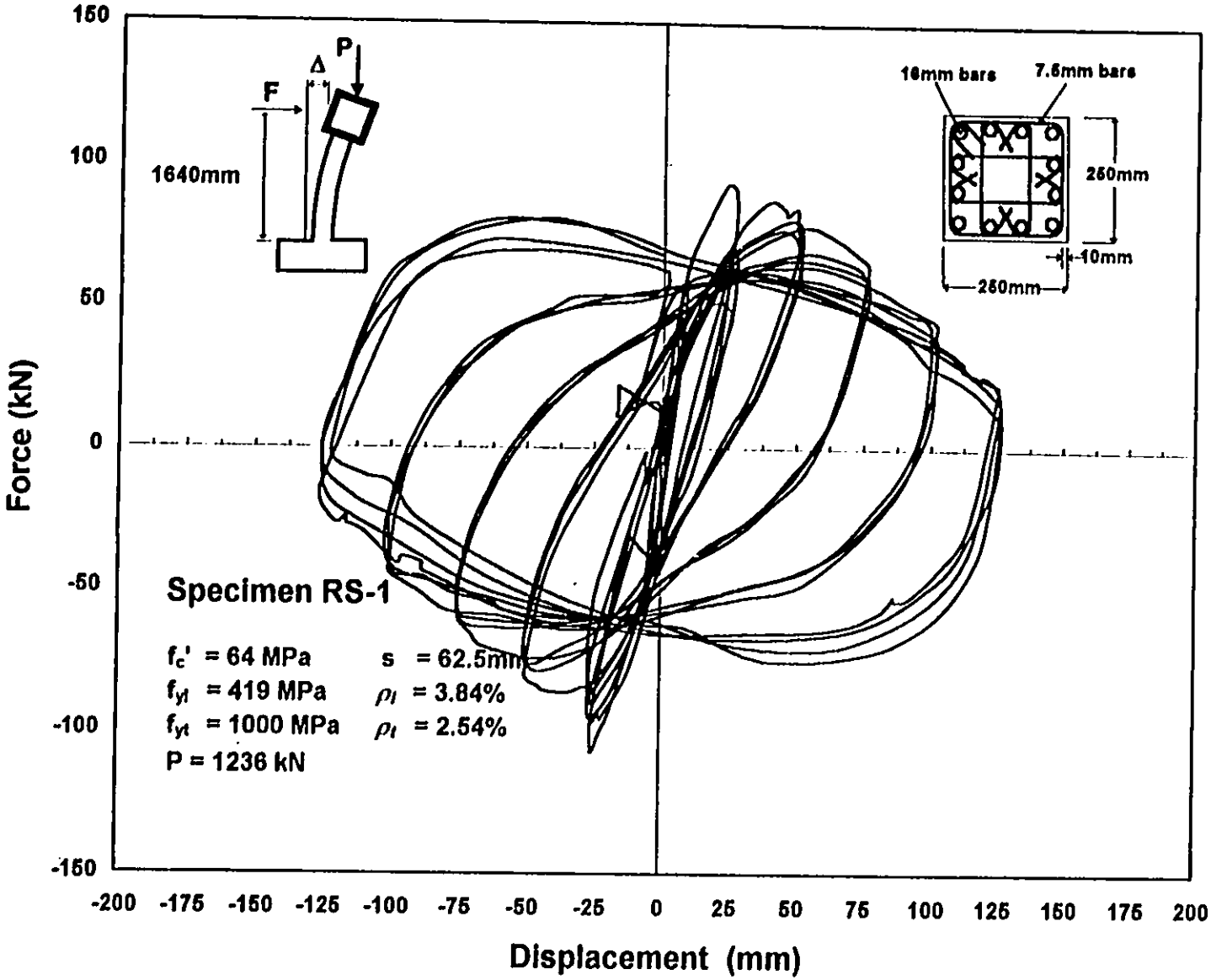

Fig. 24 Force - Displacement Relationship Including P-Δ Effect

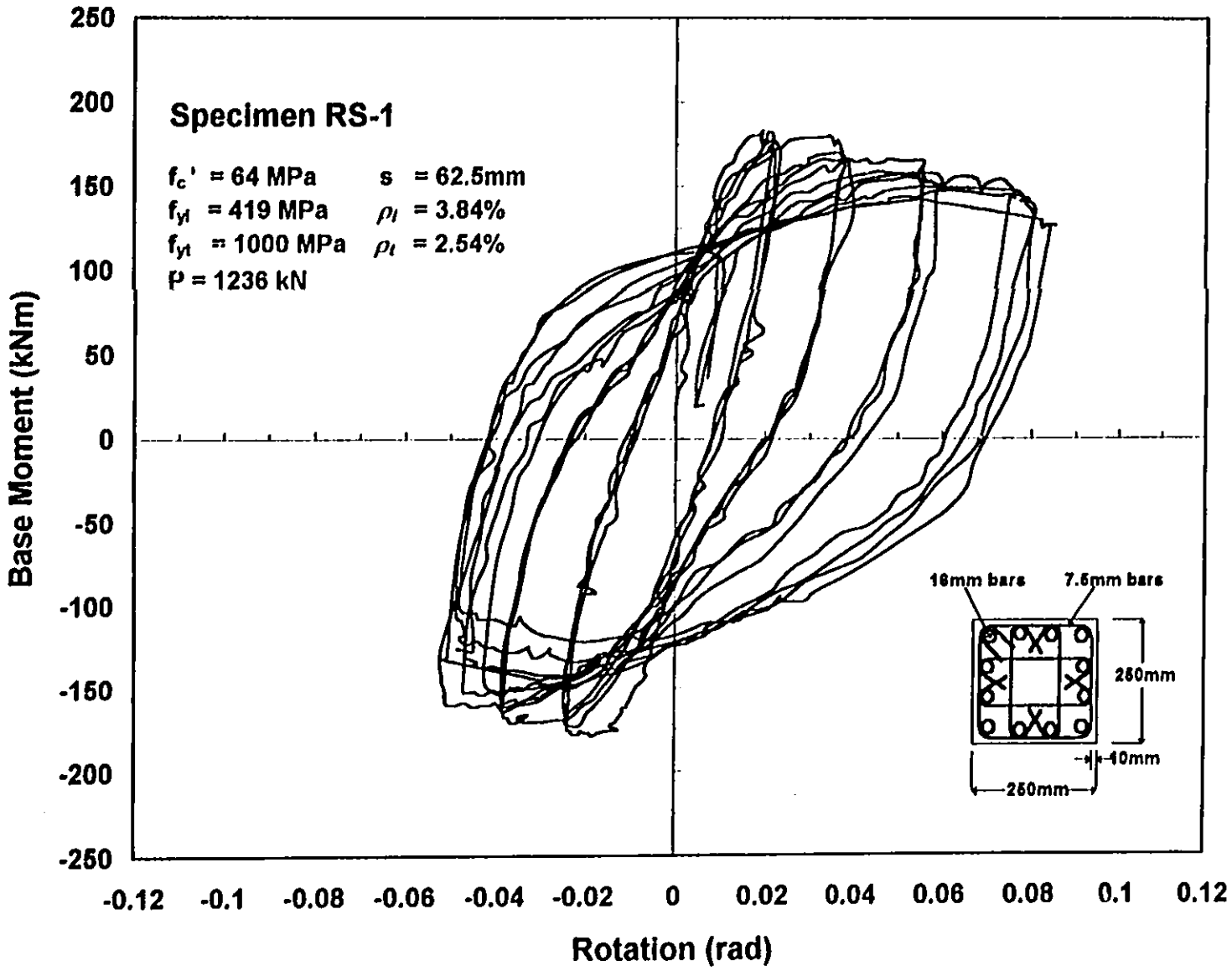

Fig. 25 Base Moment - Total Rotation Relationship in the Hinge Region

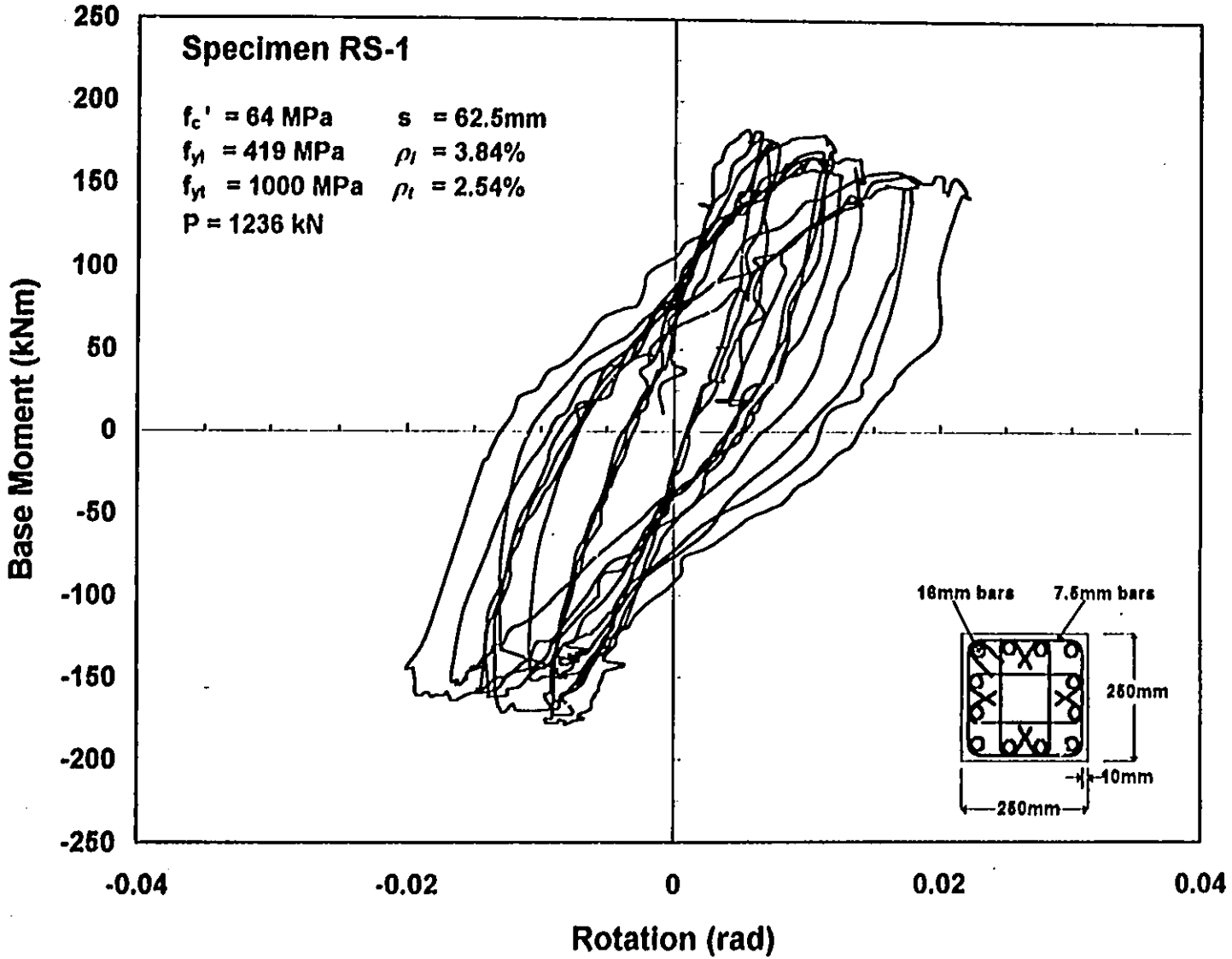

Fig. 26 Base Moment - Slip Rotation Relationship

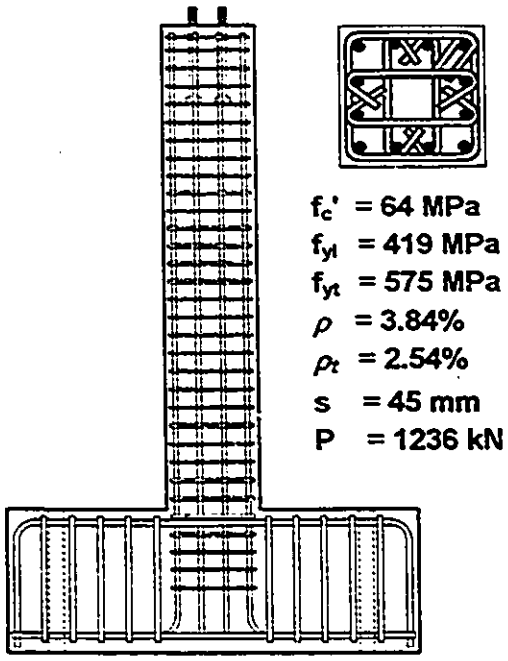

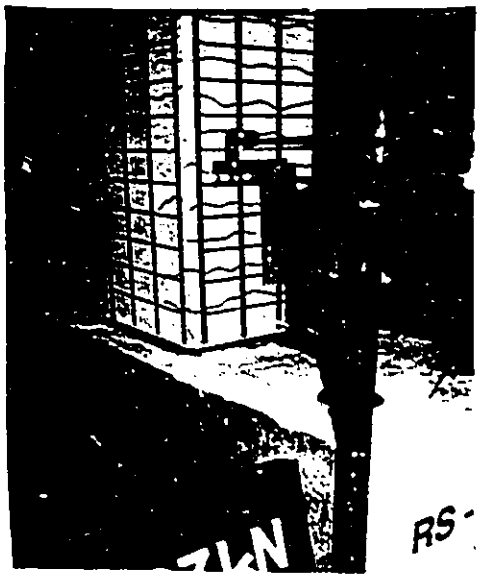

a) 1 Δy

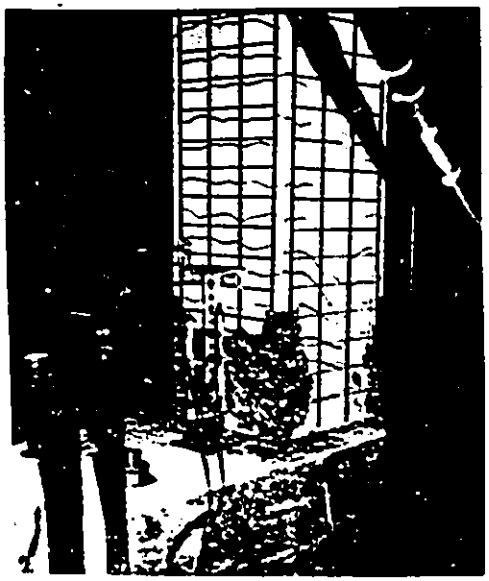

b) 3 Δy

c) 5 Δy

Fig. 27 Extent of Damage at Different Load Stages Specimen RS-2

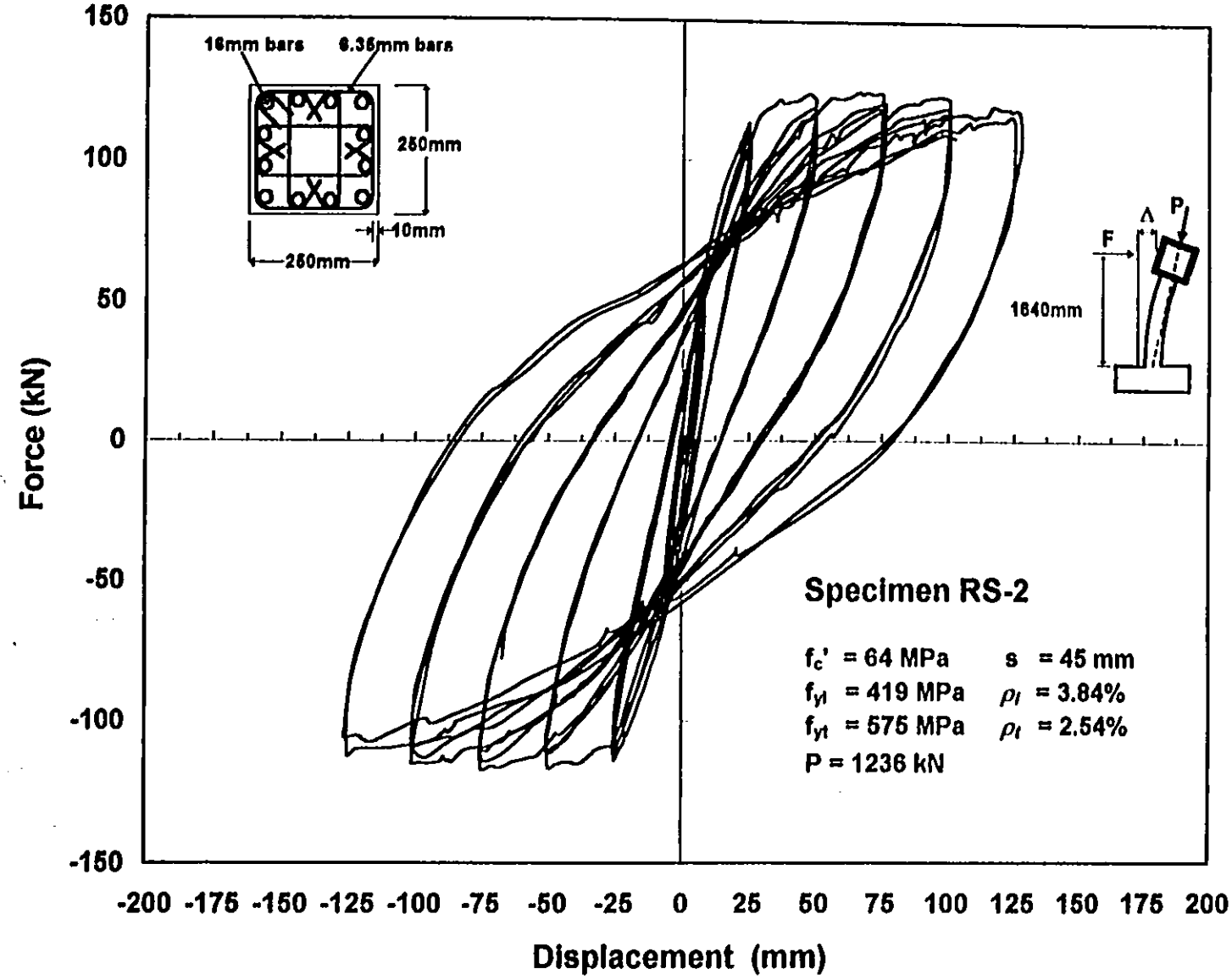

Fig. 28 Force - Displacement Relationship Excluding PΔ Effect

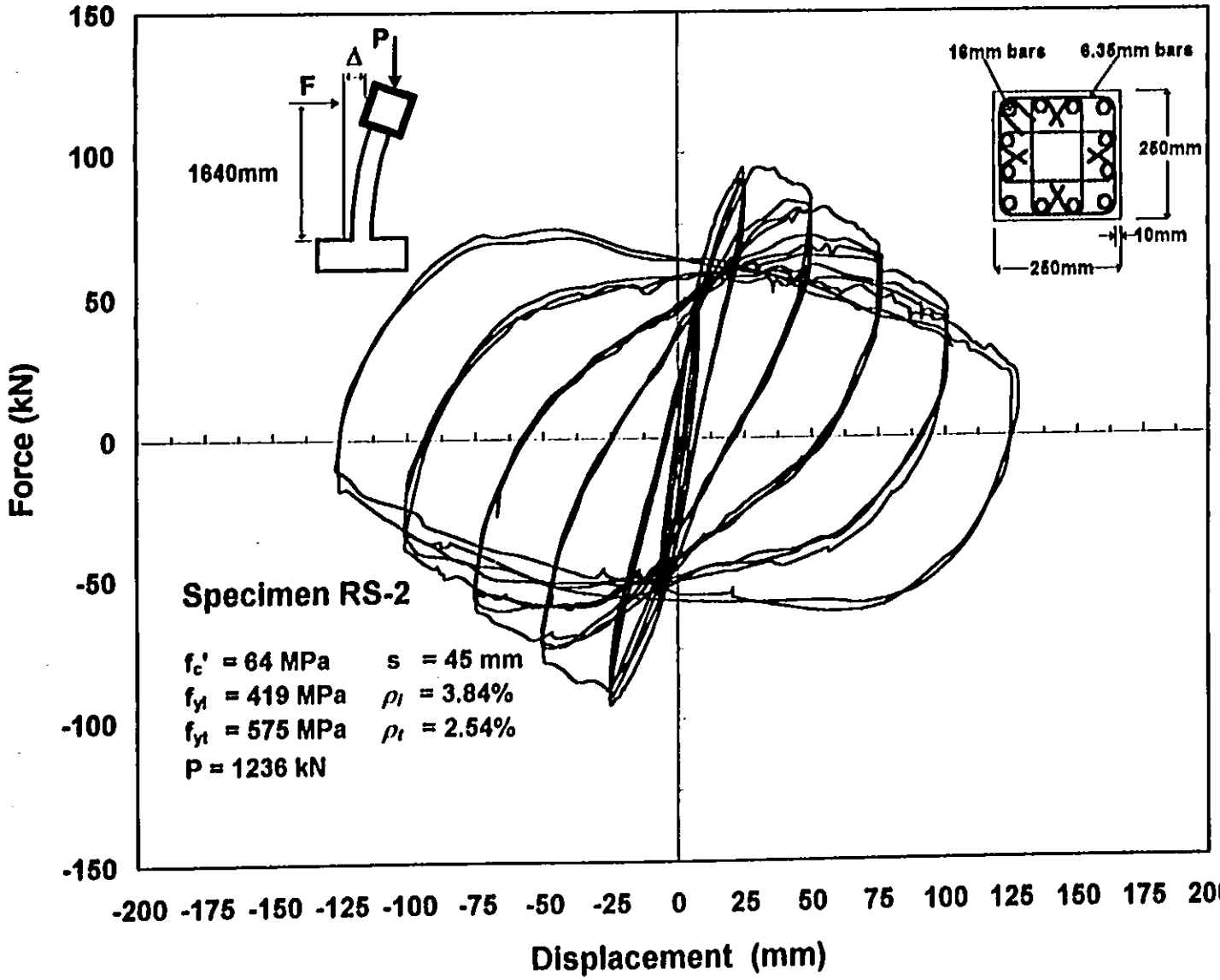

Fig. 29 Force - Displacement Relationship Including PΔ Effect

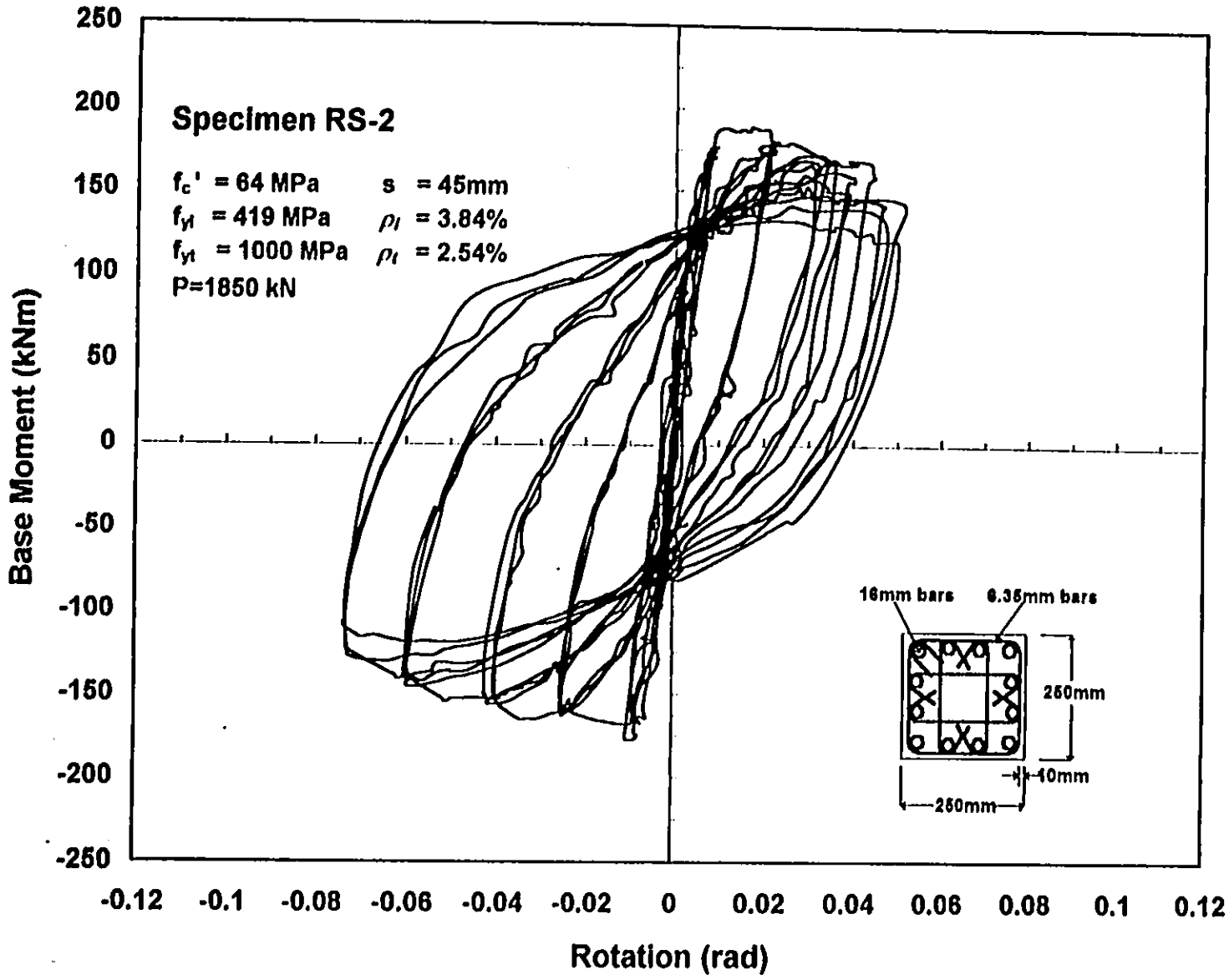

Fig. 30 Base Moment - Total Rotation Relationship in the Hinge Region

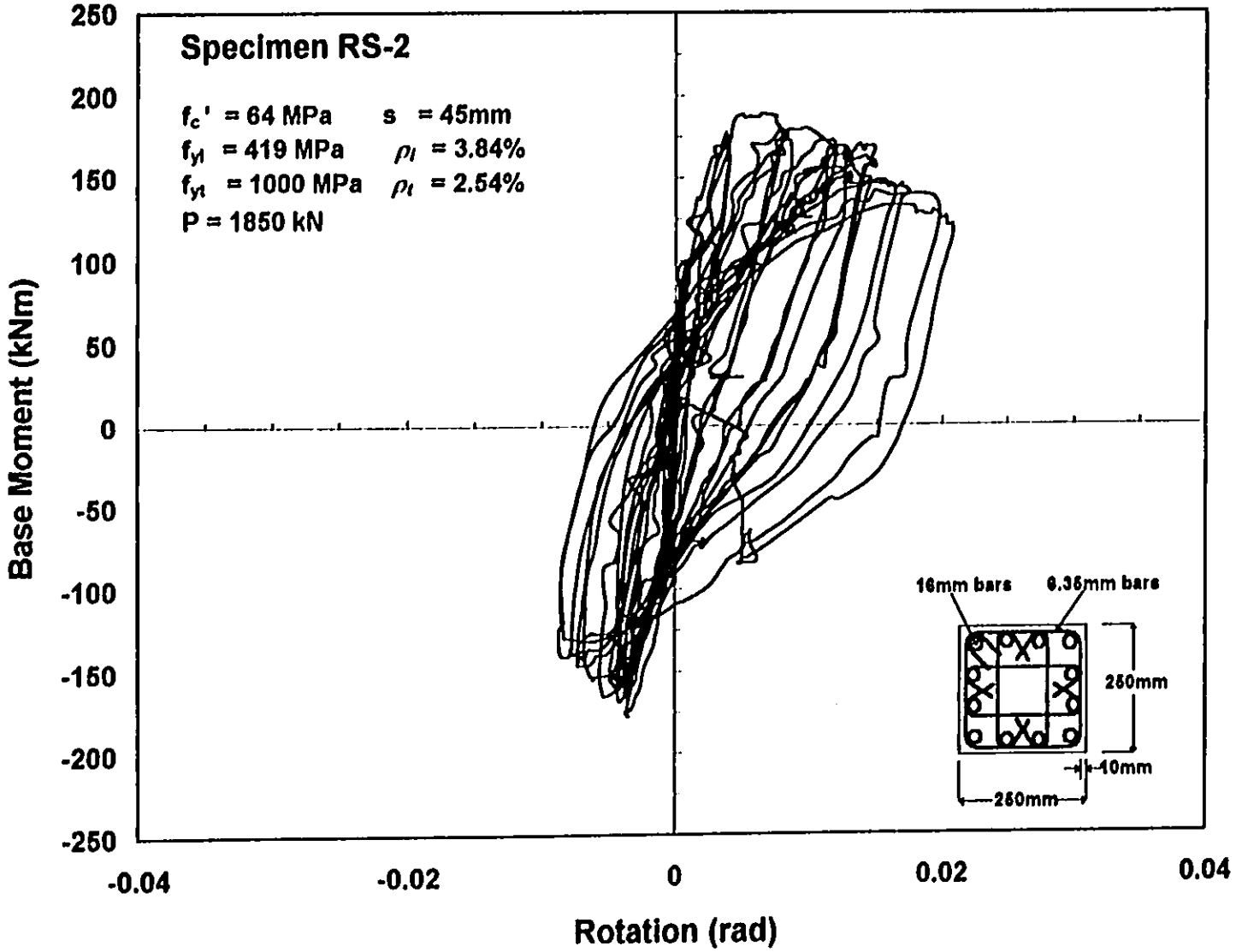

Fig. 31 Base Moment - Slip Rotation Relationship

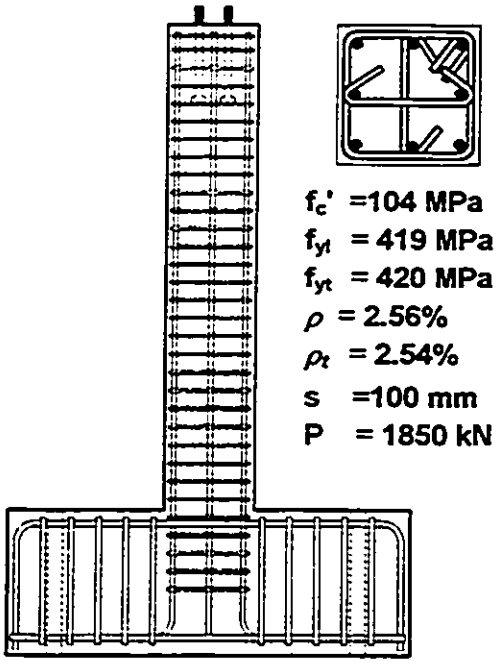

a) 2 Δy

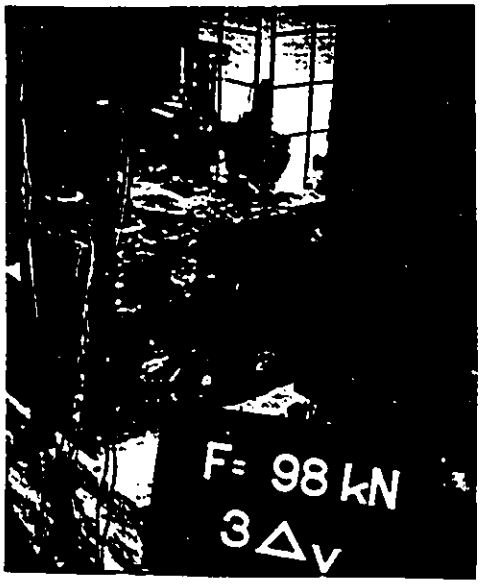

b) 3 Δy

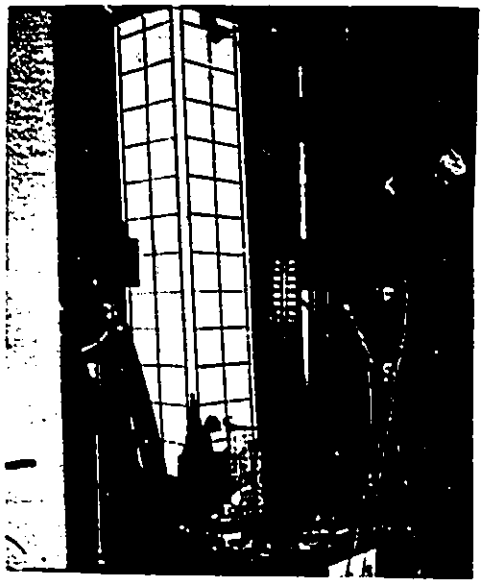

c) 4 Δy

Fig. 32 Extent of Damage at Different Load Stages Specimen RS-3

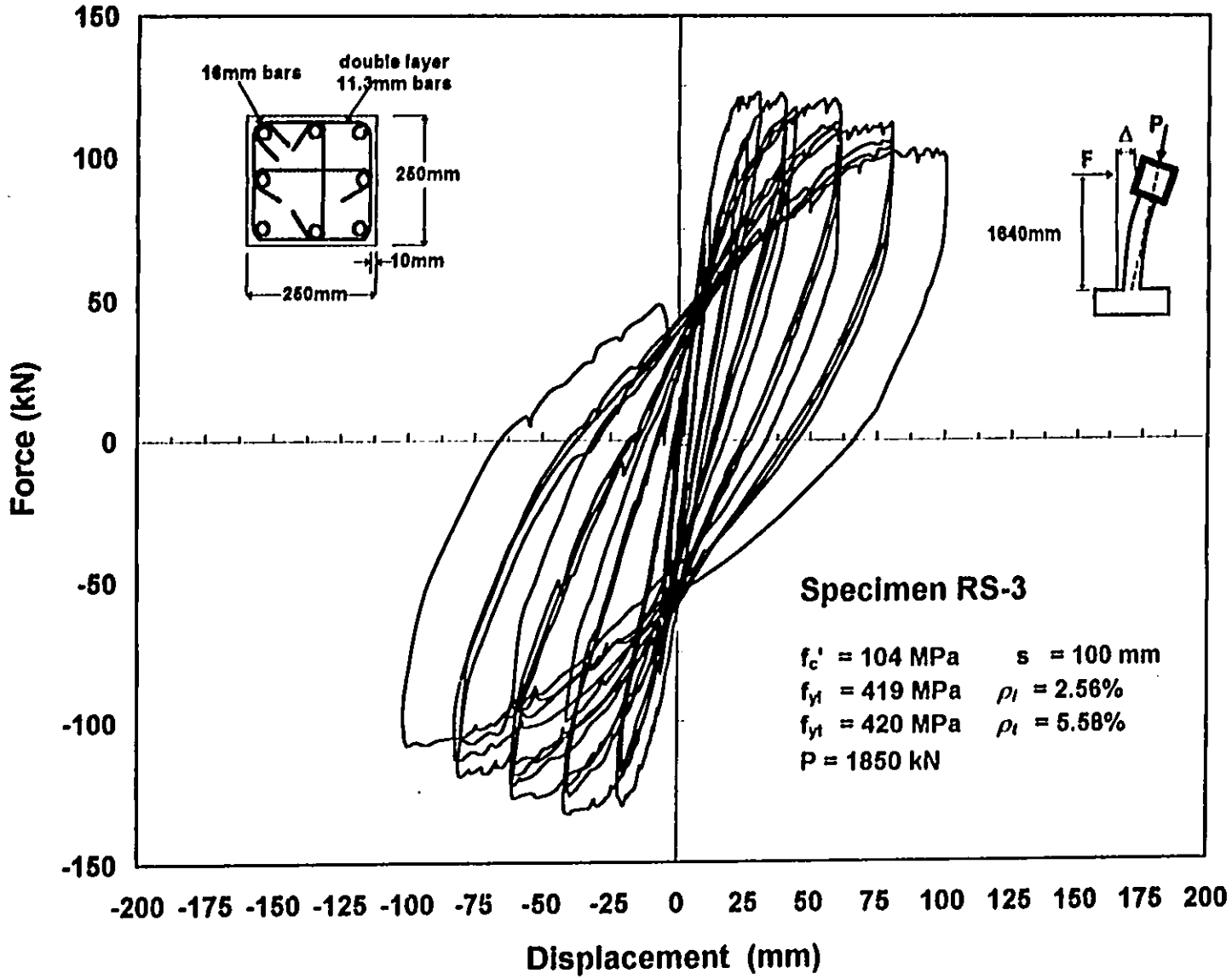

Fig. 33 Force - Displacement Relationship
Excluding PΔ Effect

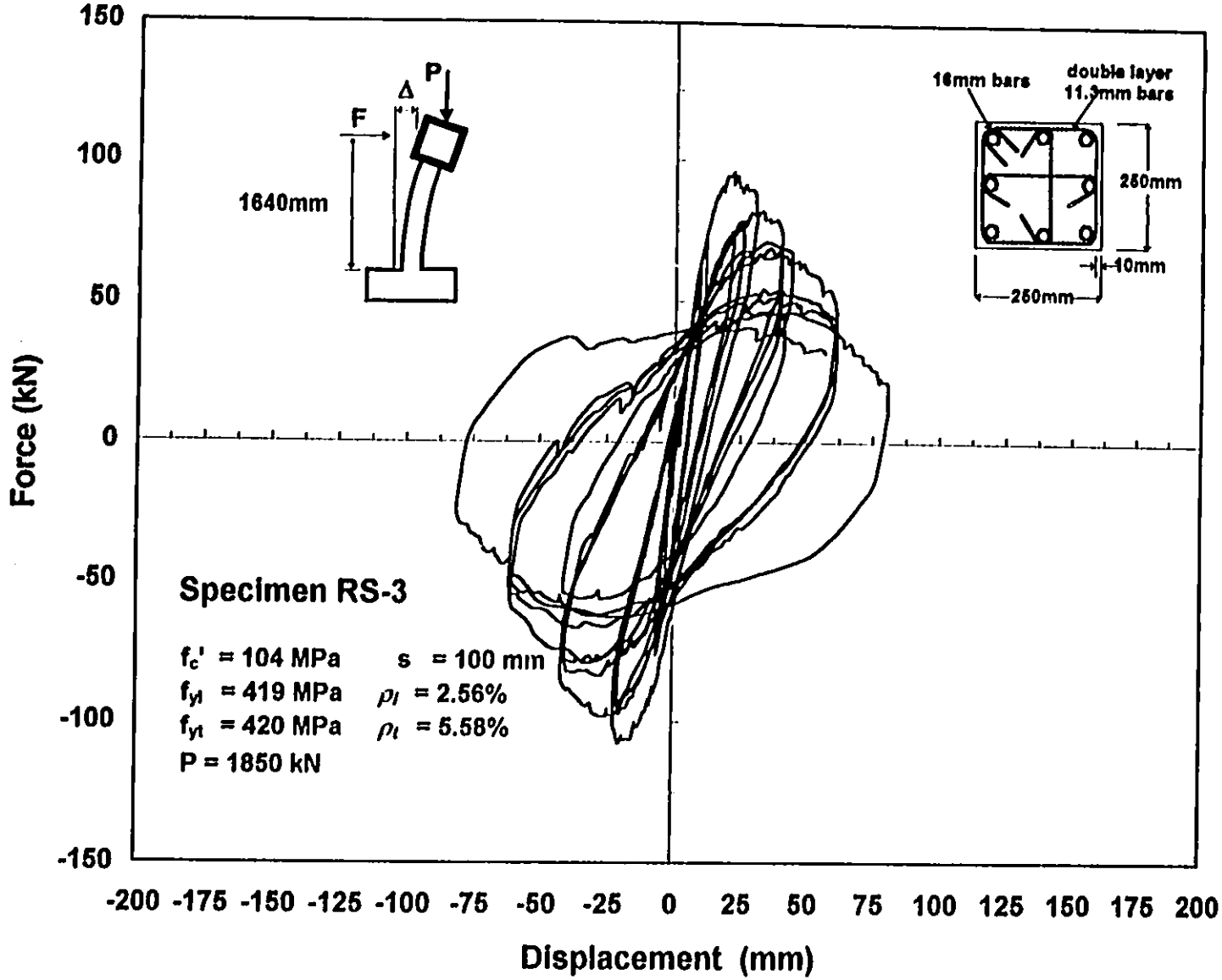

Fig. 34 Force - Displacement Relationship Including PΔ Effect

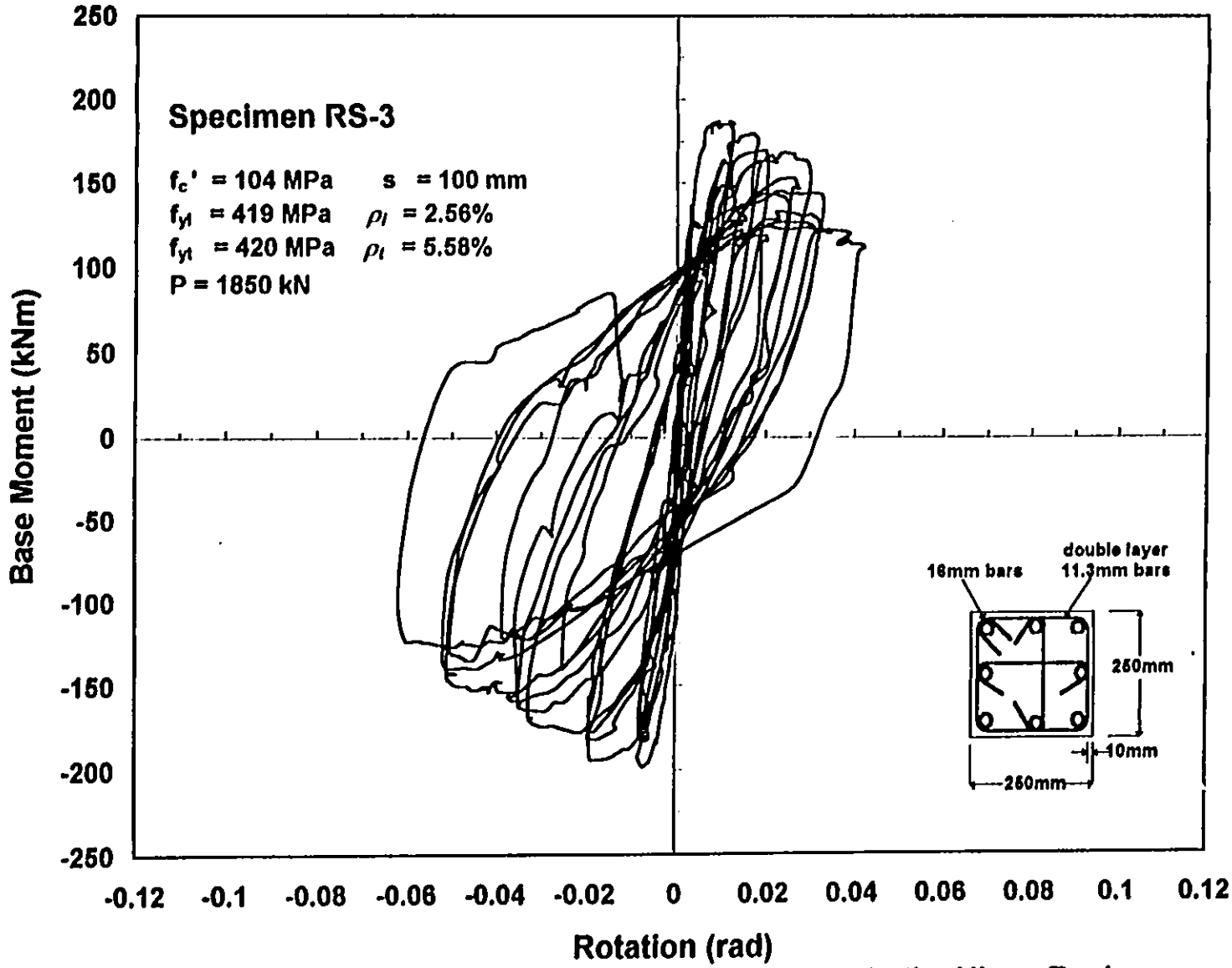

Fig. 35 Base Moment - Total Rotation Relationship in the Hinge Region

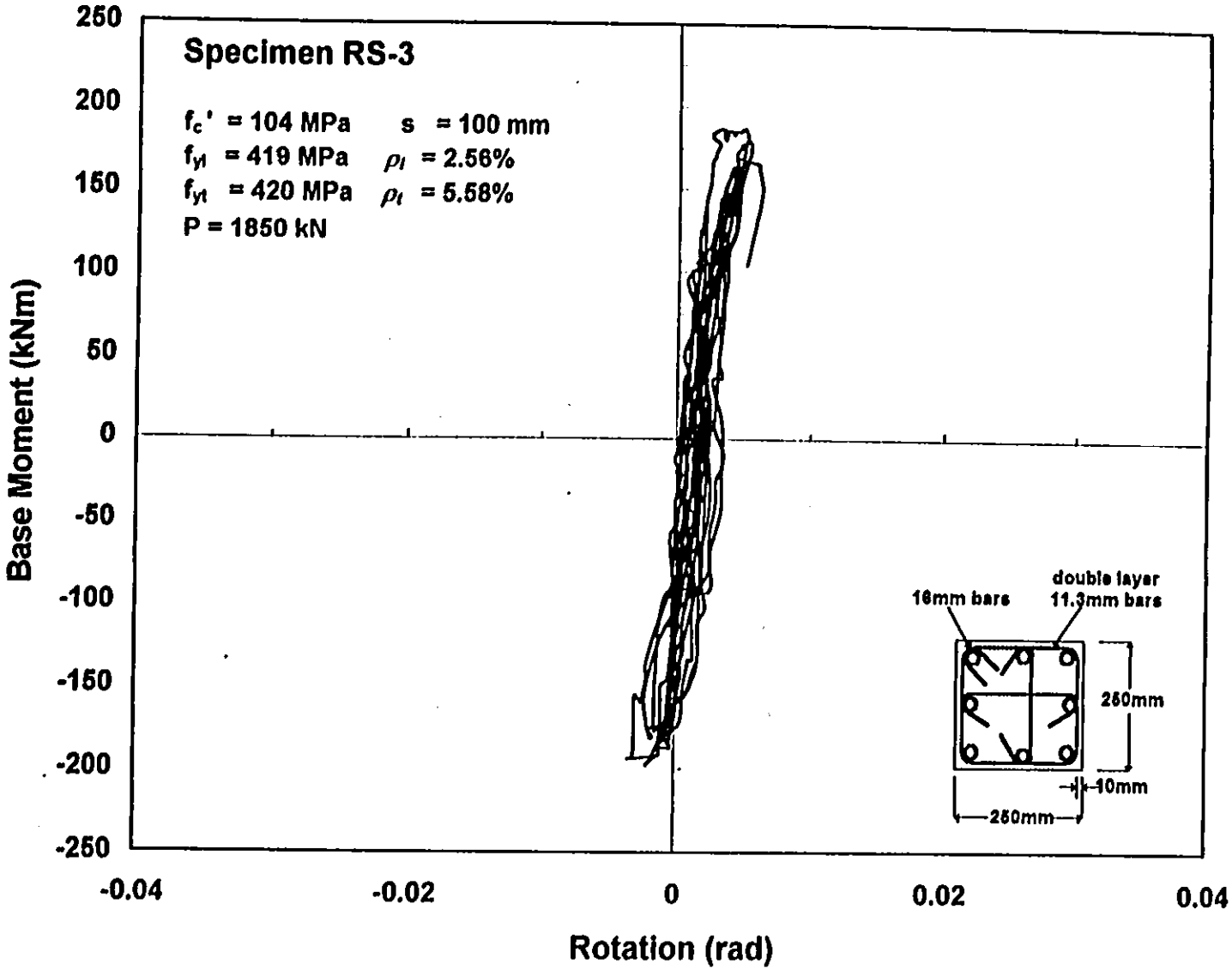

Fig. 36 Analytical and Experimental Moment - Anchorage Slip Rotation Relationships

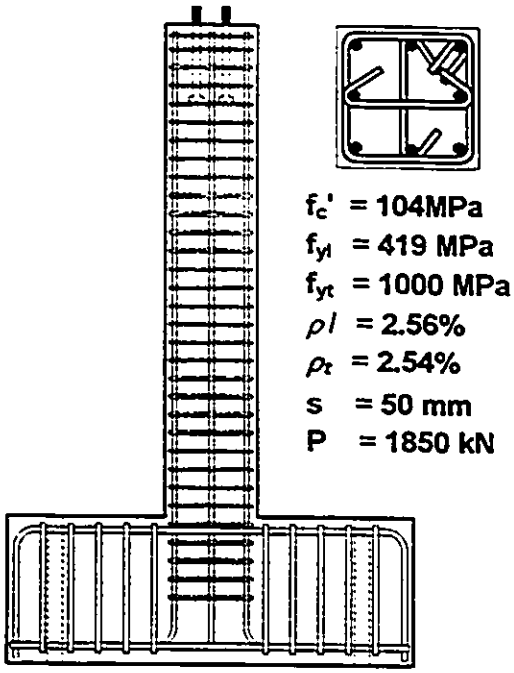

f_c' = 104MPa
f_{yl} = 419 MPa
f_{yt} = 1000 MPa
ρl = 2.56%
ρ_t = 2.54%
s = 50 mm
P = 1850 kN

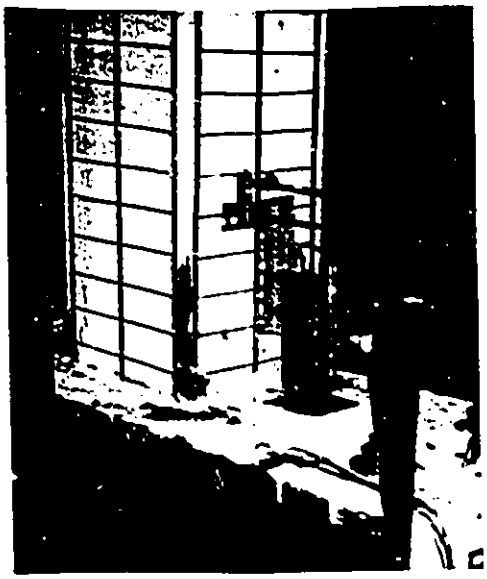

a) 1 Δy

b) 3 Δy

c) 5 Δy

Fig. 37 Extent of Damage at Different Load Stages Specimen RS-4

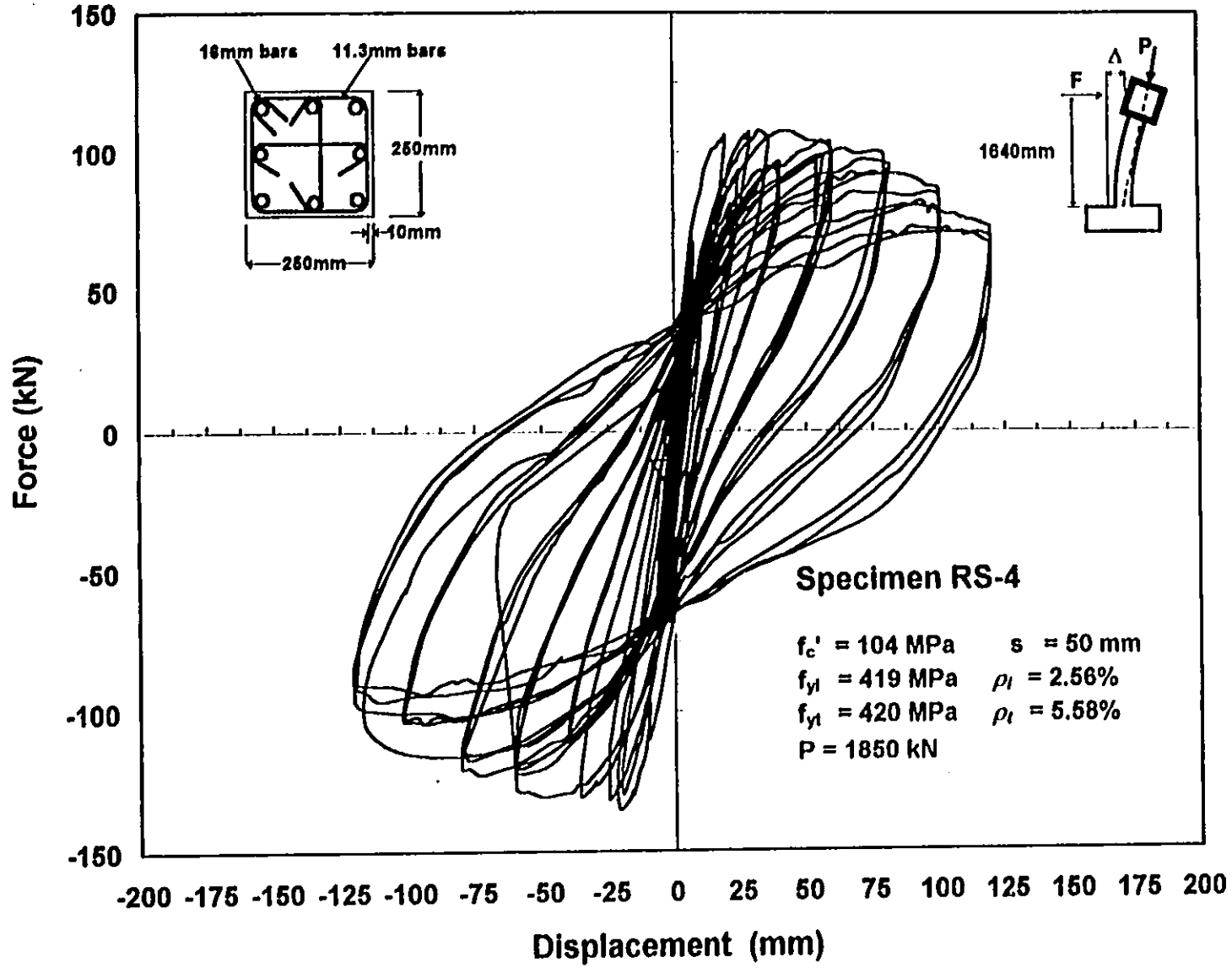

Fig. 38 Force - Displacement Relationship Excluding PΔ Effect

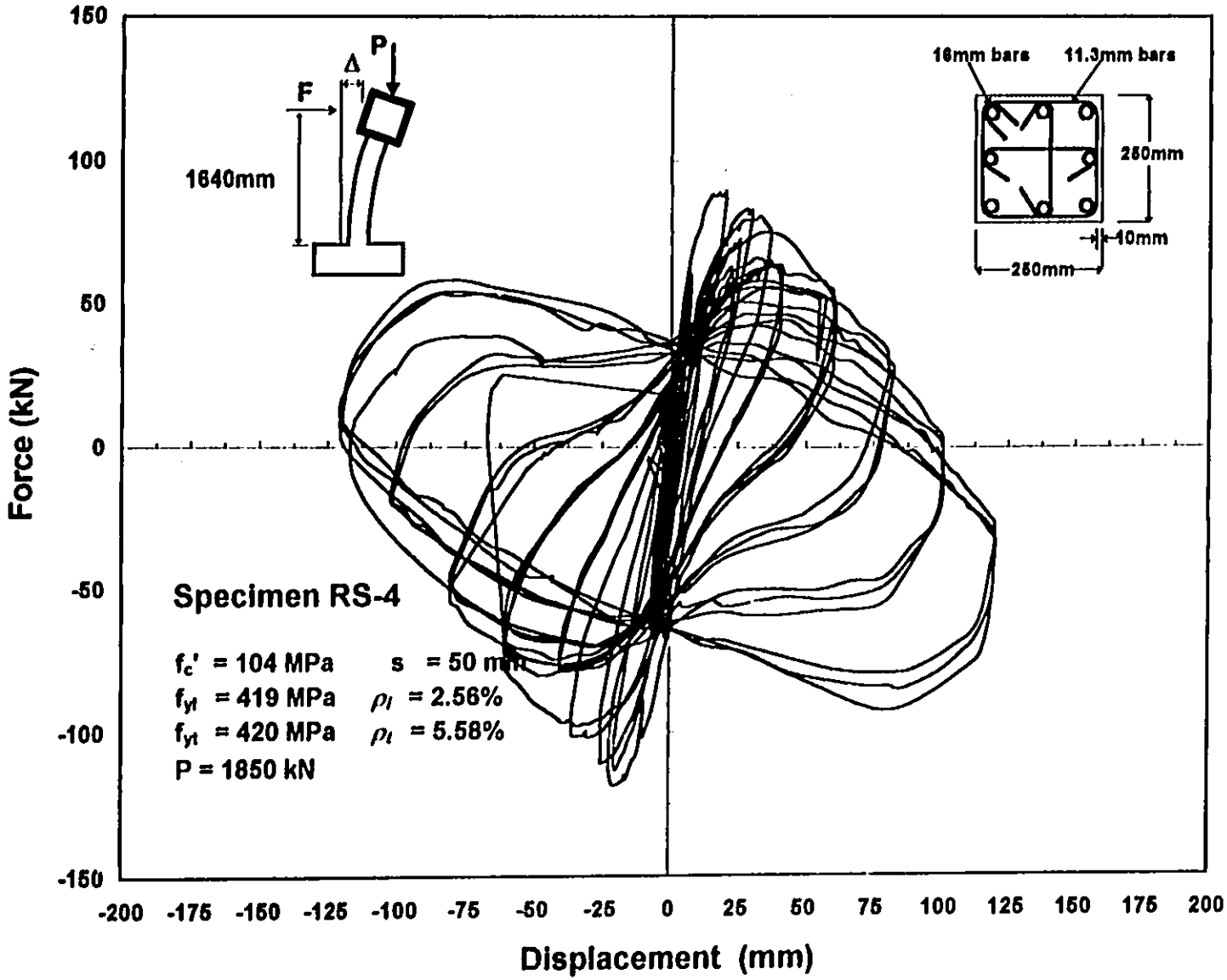

Fig. 39 Force - Displacement Relationship Including PΔ Effect

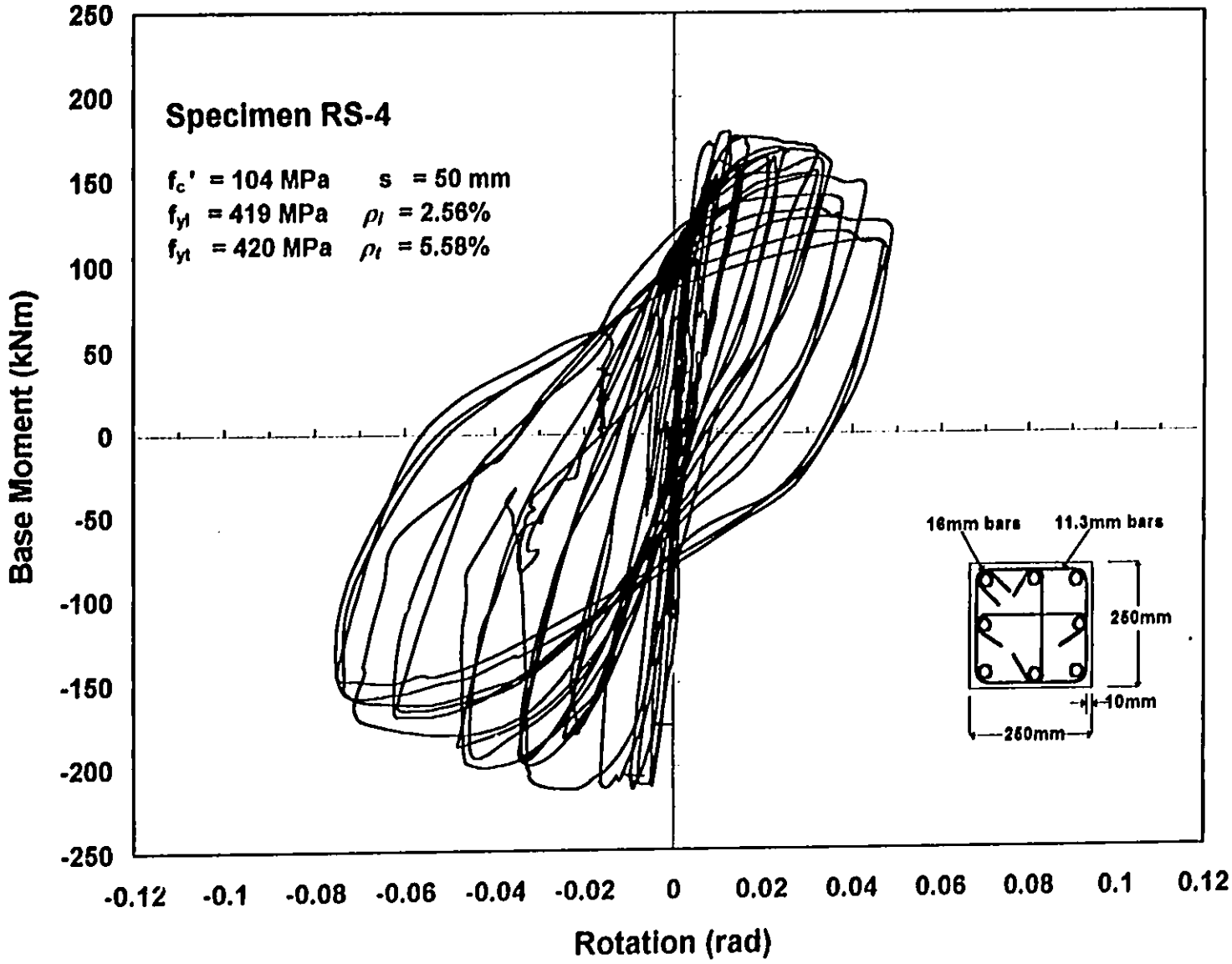

Fig. 40 Base Moment - Total Rotation Relationship in the Hinge Region

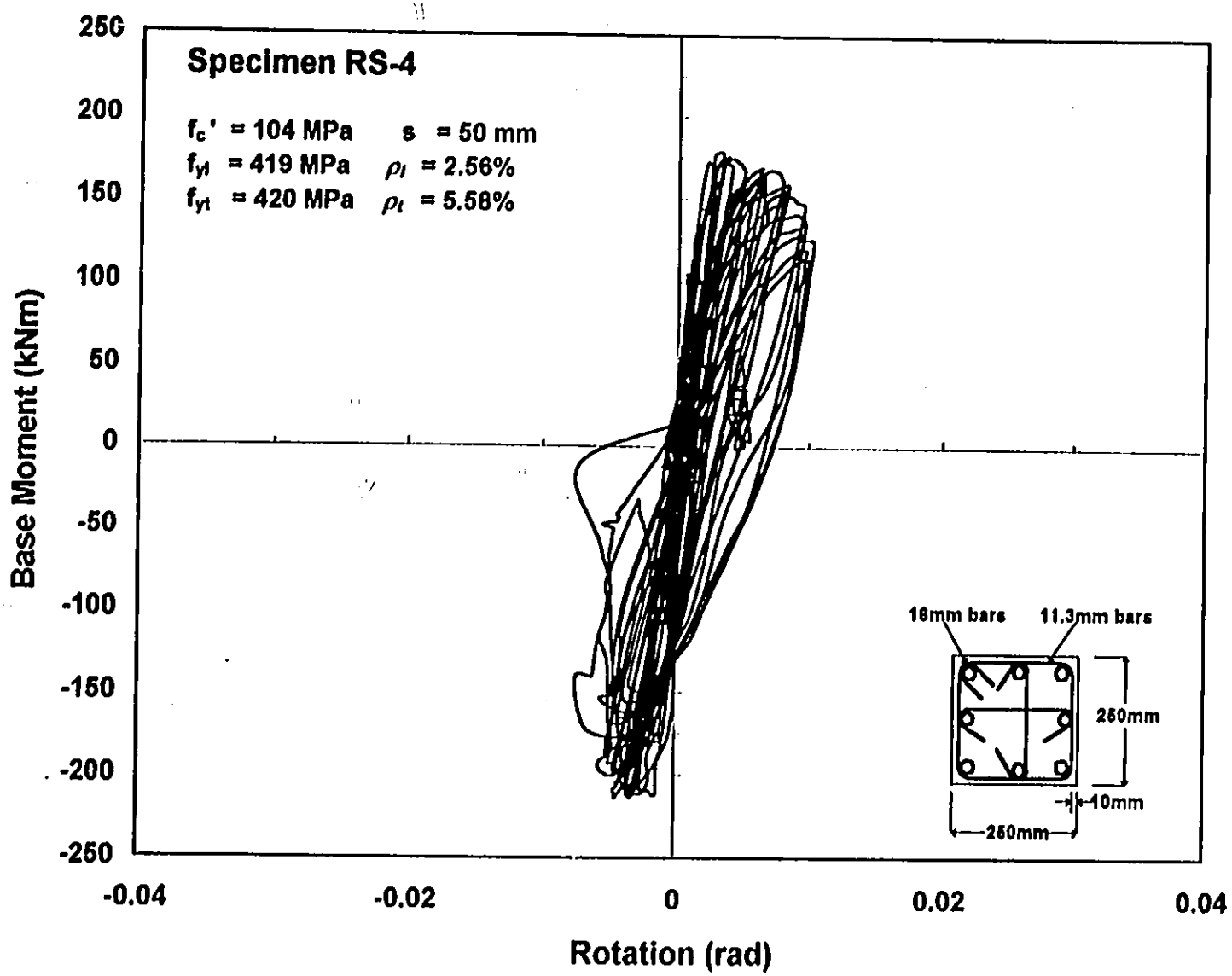

Fig. 41 Base Moment - Slip Rotation Relationship

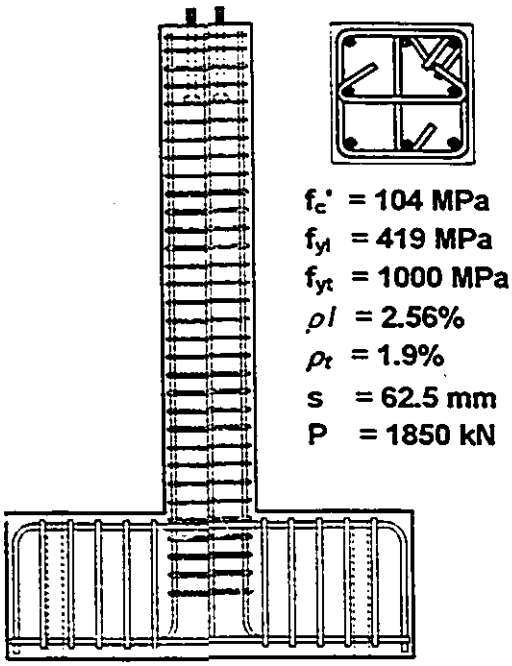

a) 1 Δy

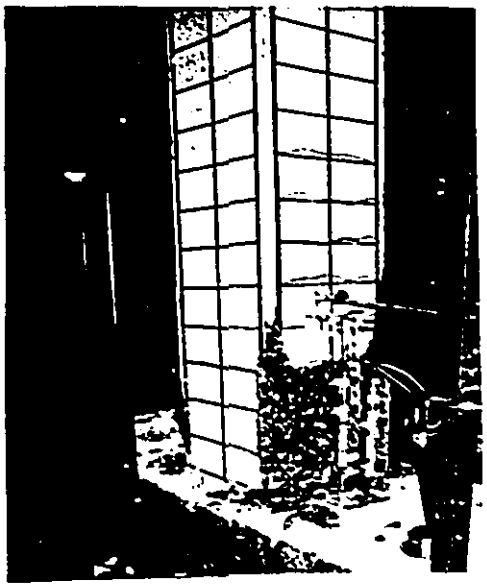

b) 2 Δy

c) 3 Δy

Fig. 42 Extent of Damage at Different Load Stages Specimen RS-5

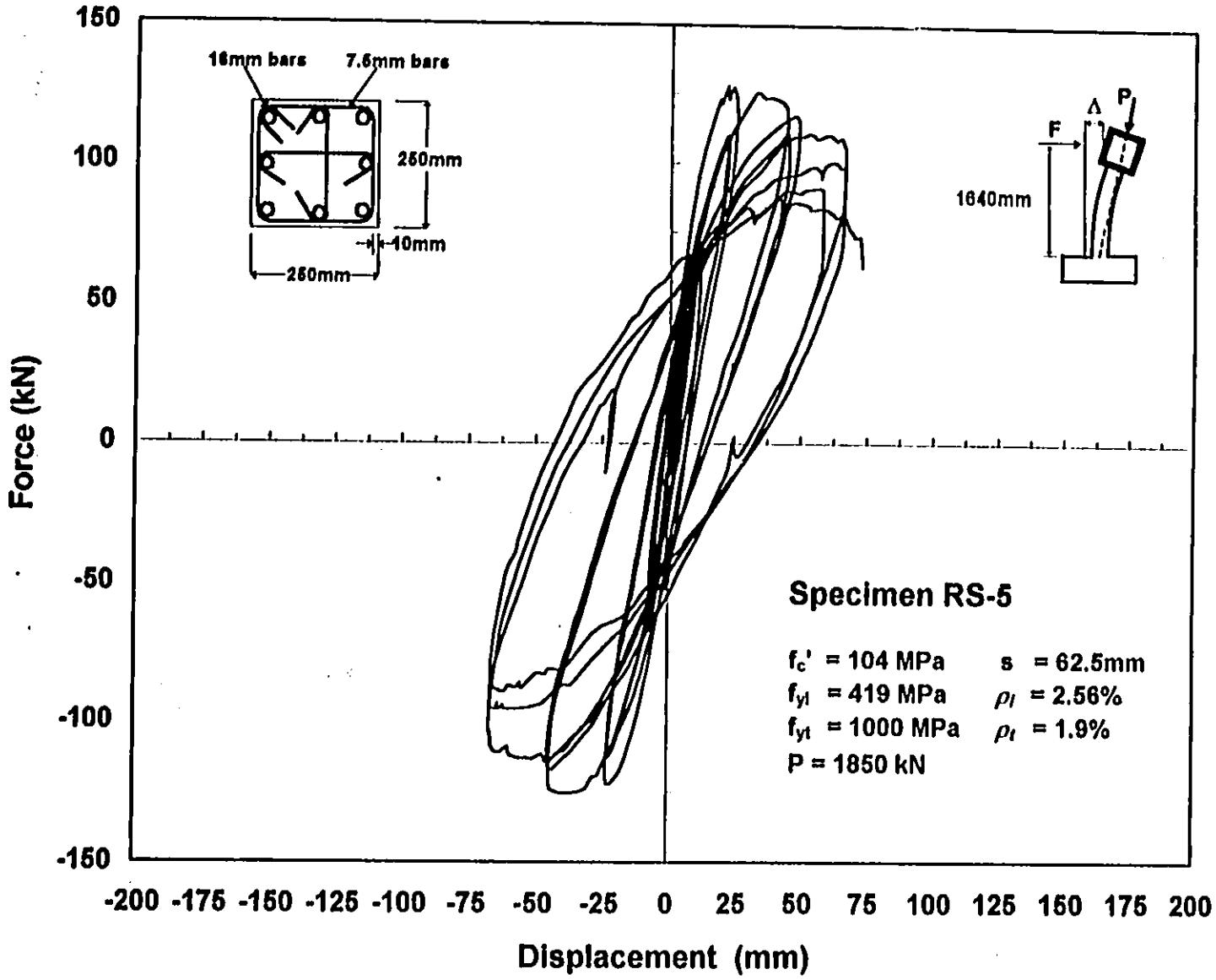

Fig. 43 Force - Displacement Relationship
Excluding PΔ Effect

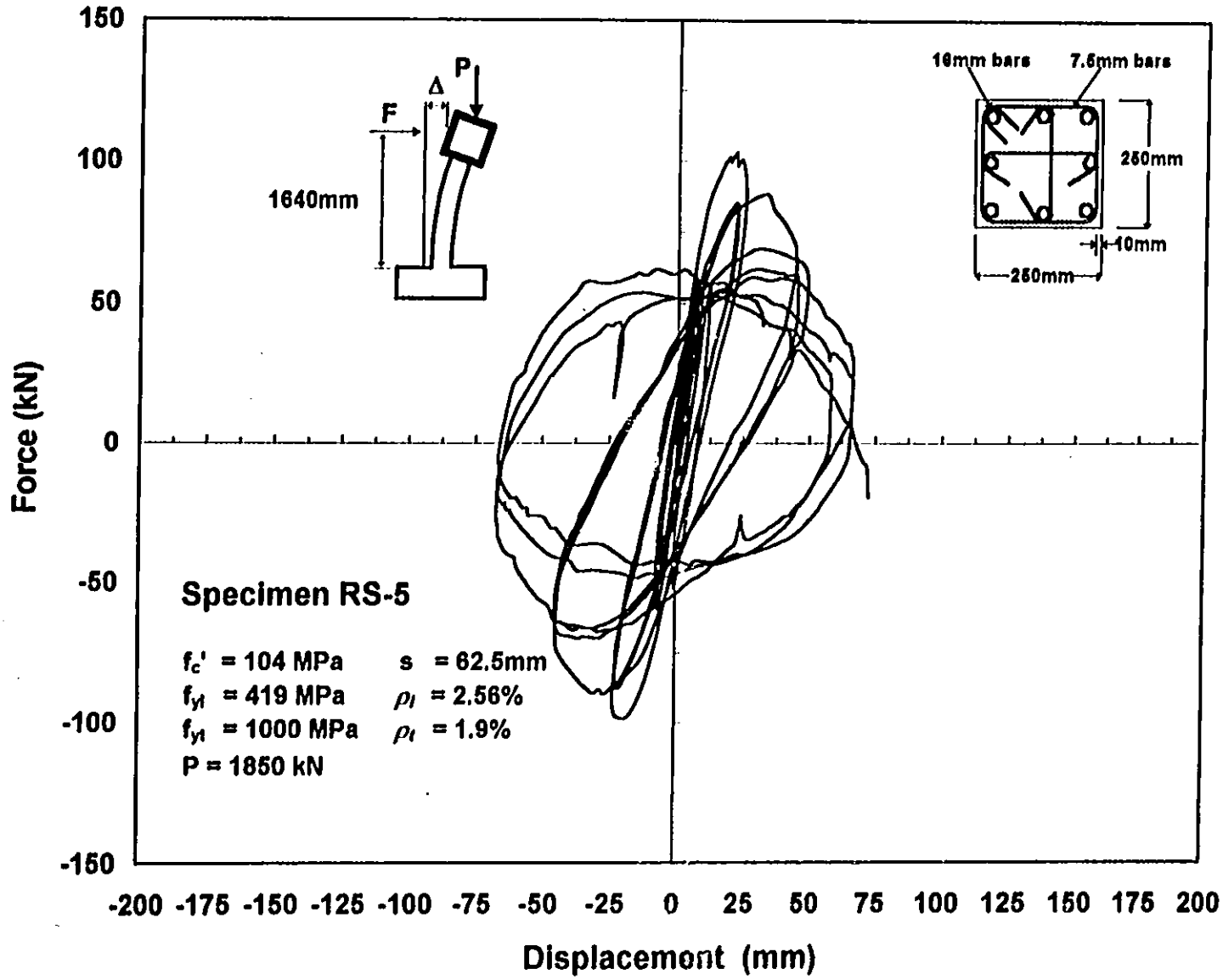

Fig. 44 Force - Displacement Relationship Including PΔ Effect

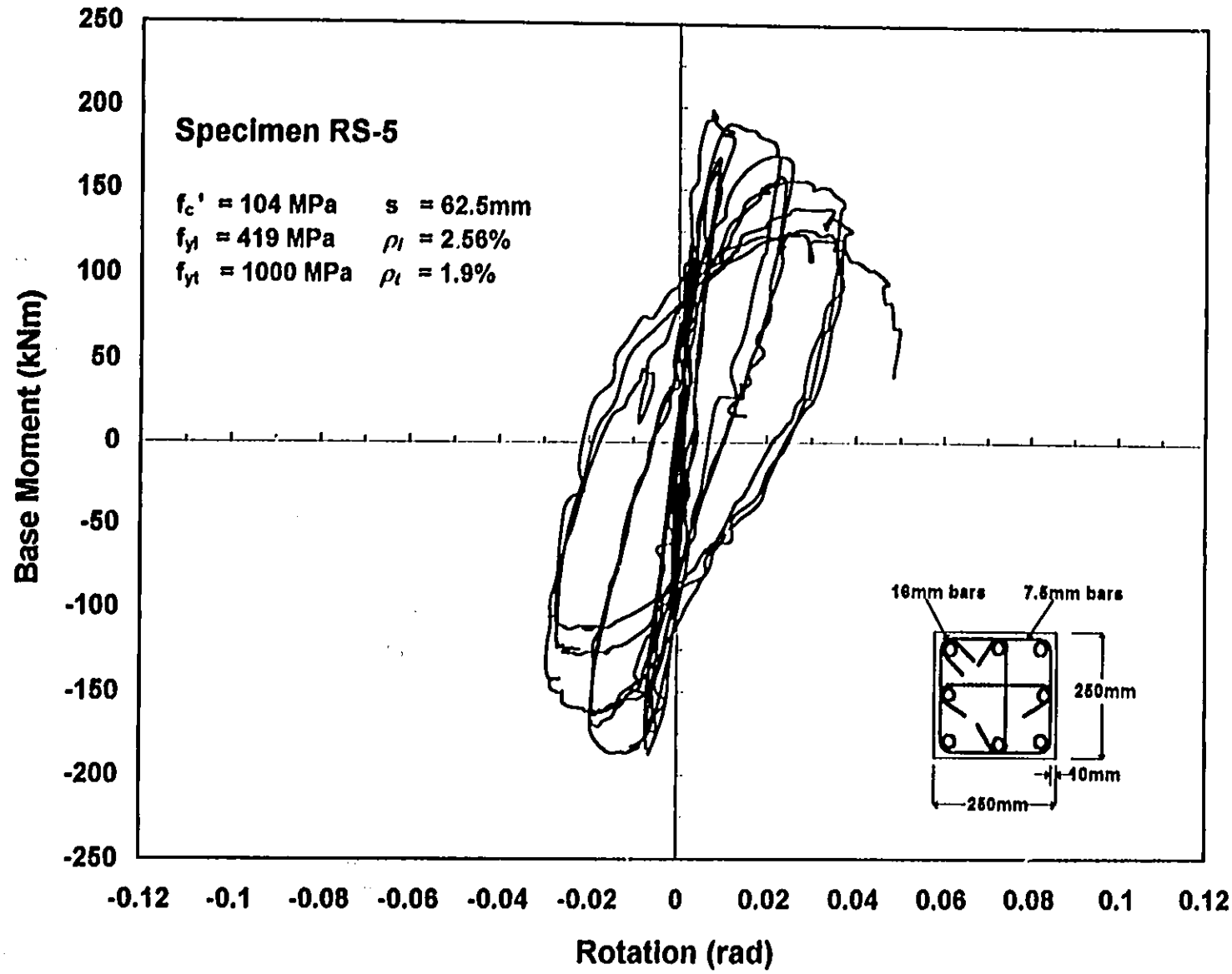

Fig. 45 Base Moment - Total Rotation Relationship in the Hinge Region

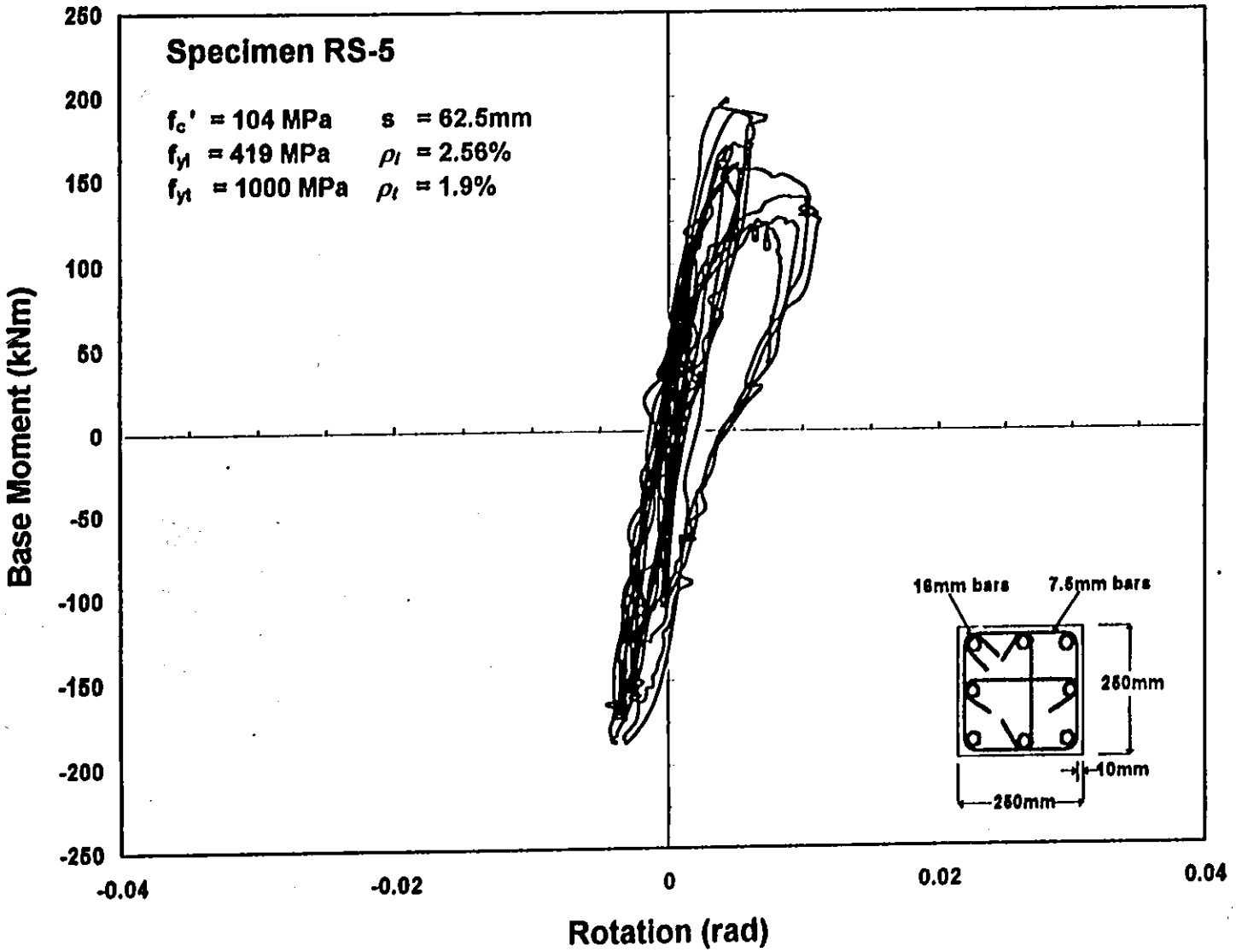

Fig. 46 Base Moment - Slip Rotation Relationship

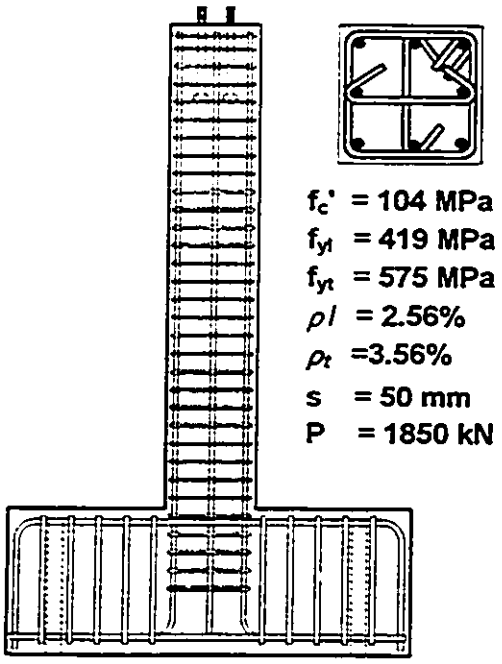

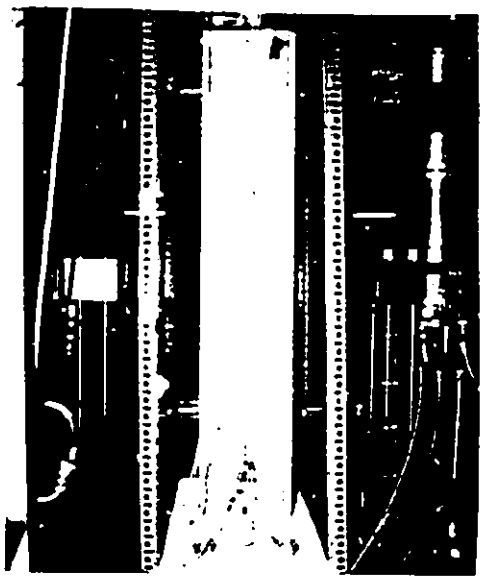

a) 1 Δy

b) 2 Δy

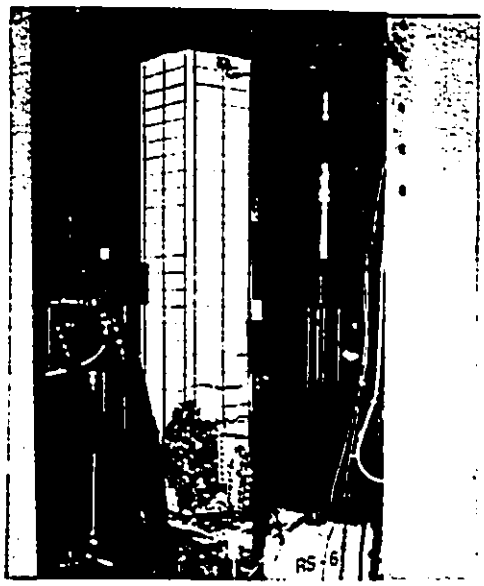

c) 3 Δy

Fig. 47 Extent of Damage at Different Load Stages Specimen RS-6

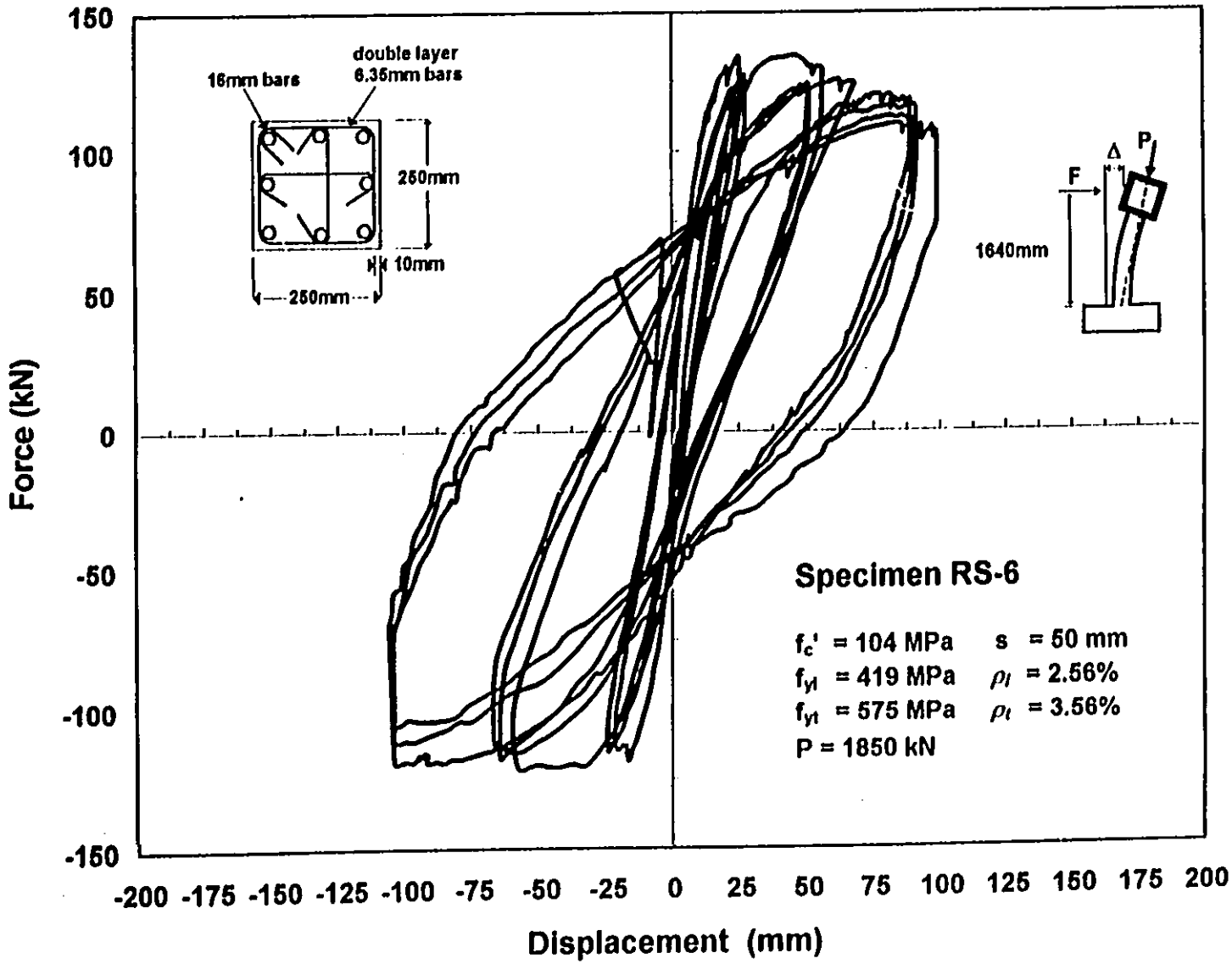

Fig. 48 Force - Displacement Relationship
Excluding P-Δ Effect

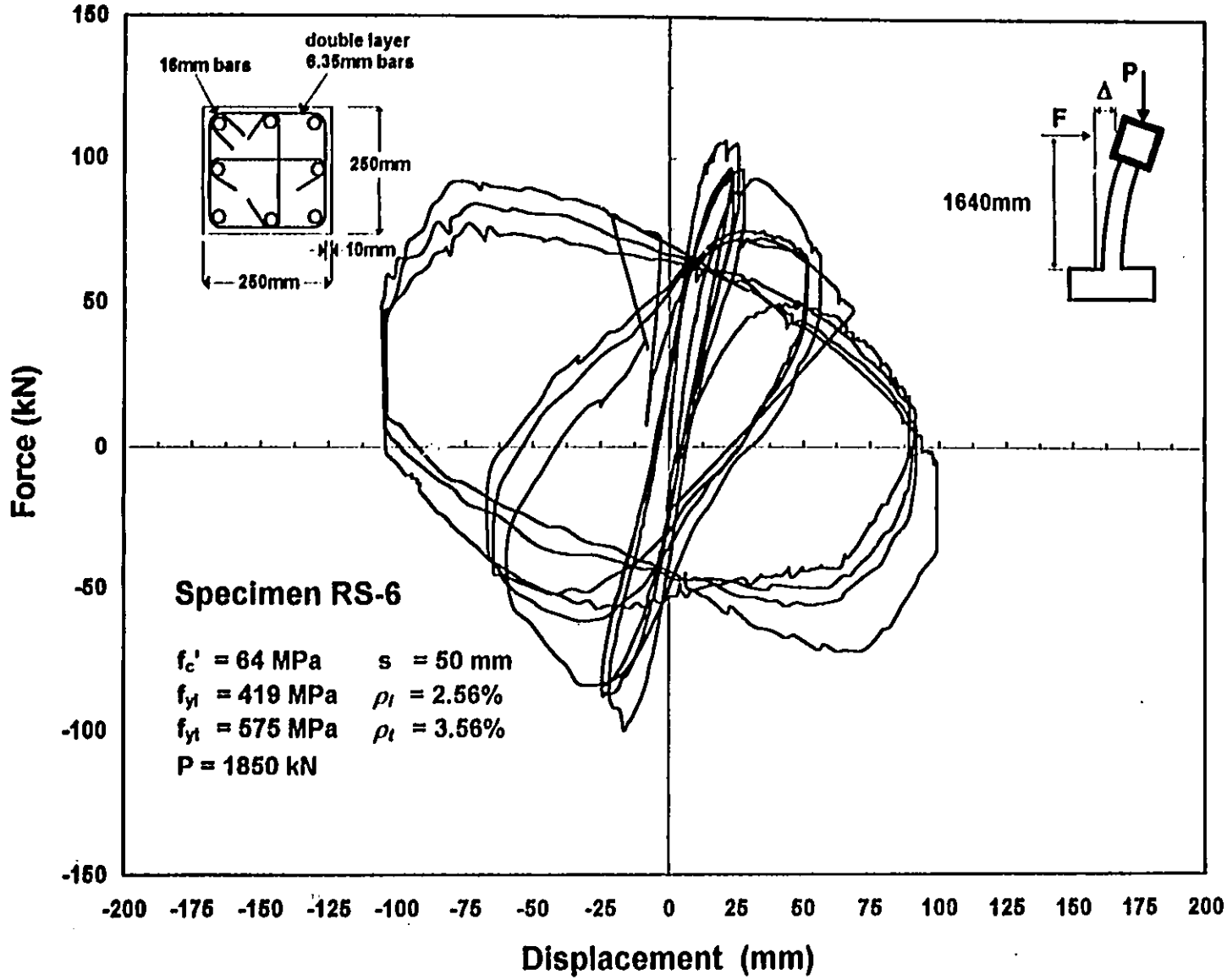

Fig. 49 Force - Displacement Relationship Including P-Δ Effect

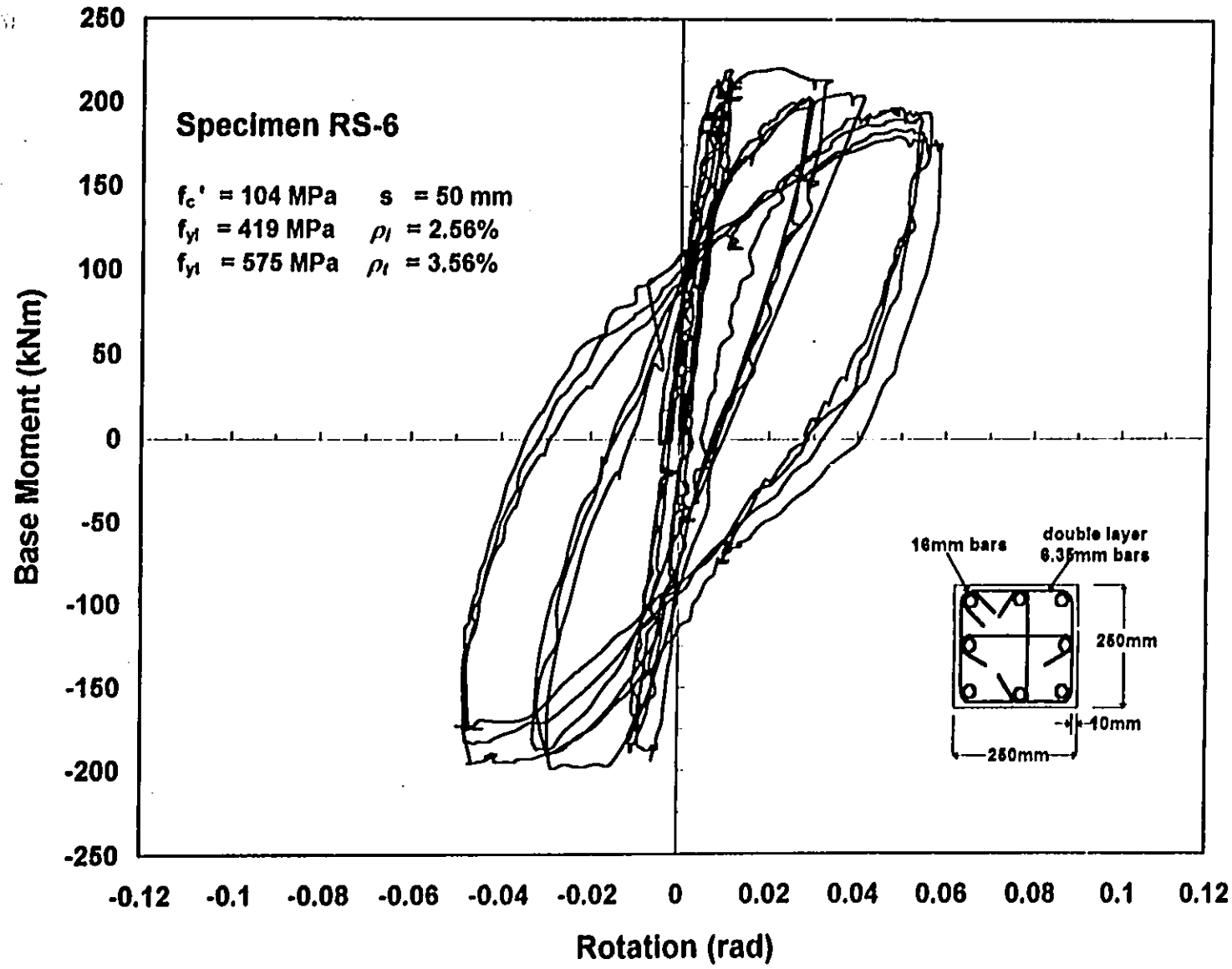

Fig. 50 Base Moment - Total Rotation Relationship in the Hinge Region

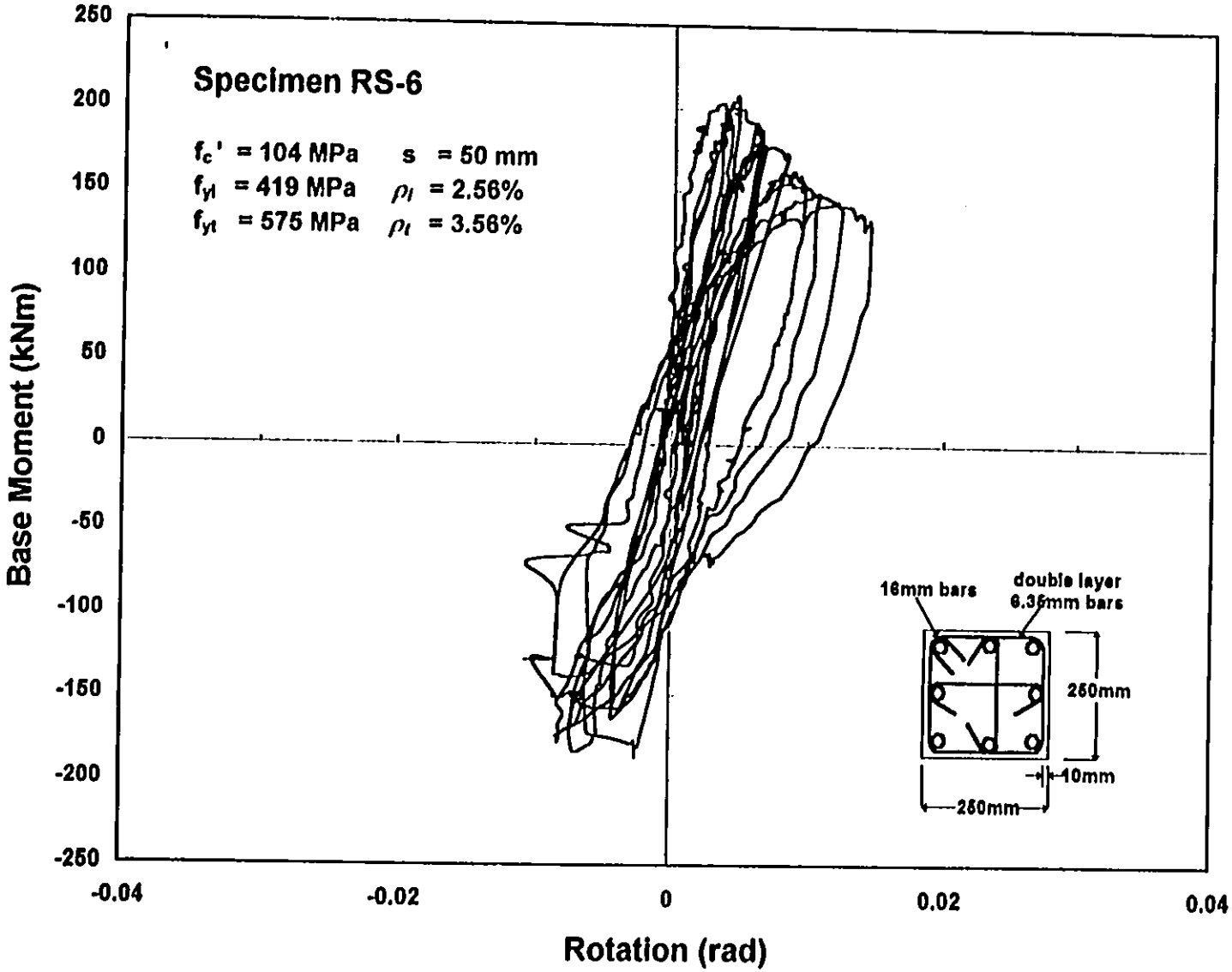

Fig. 51 Moment - Slip Rotation Relationship

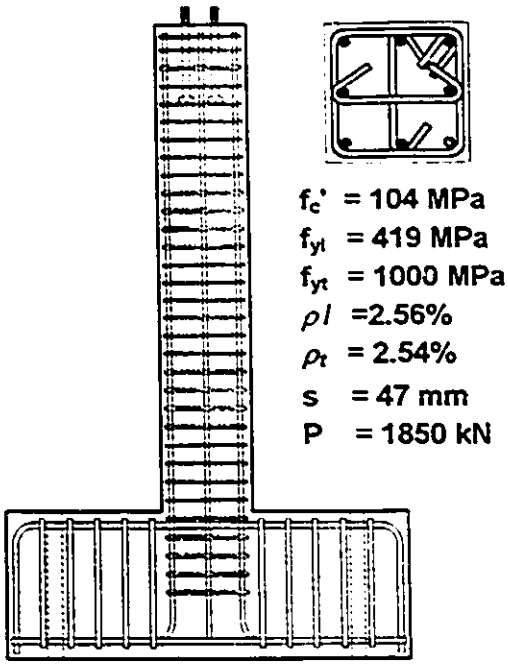

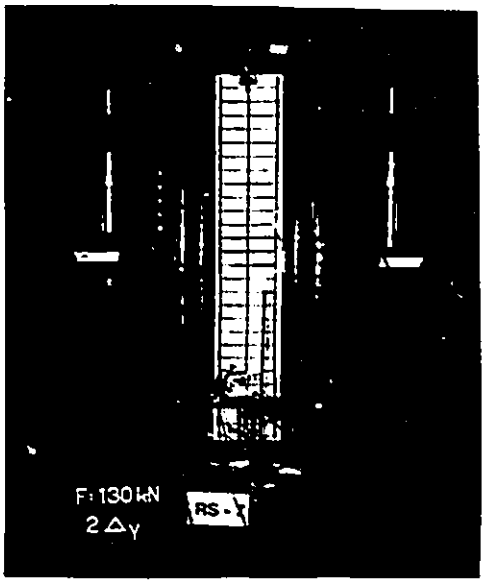

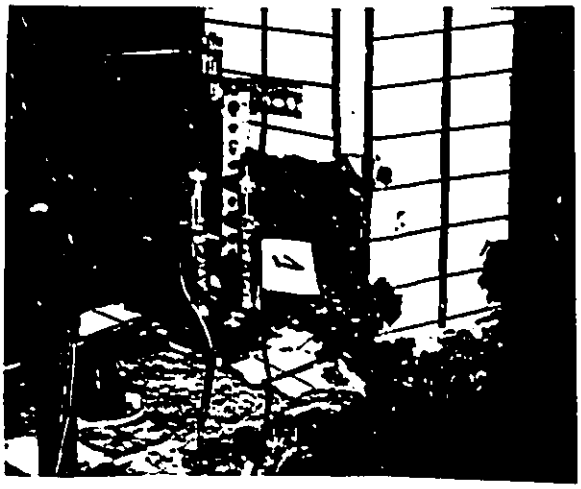

b) 1 Δy **c) 4 Δy**

Fig. 52 Extent of Damage at Different Load Stages Specimen RS-7

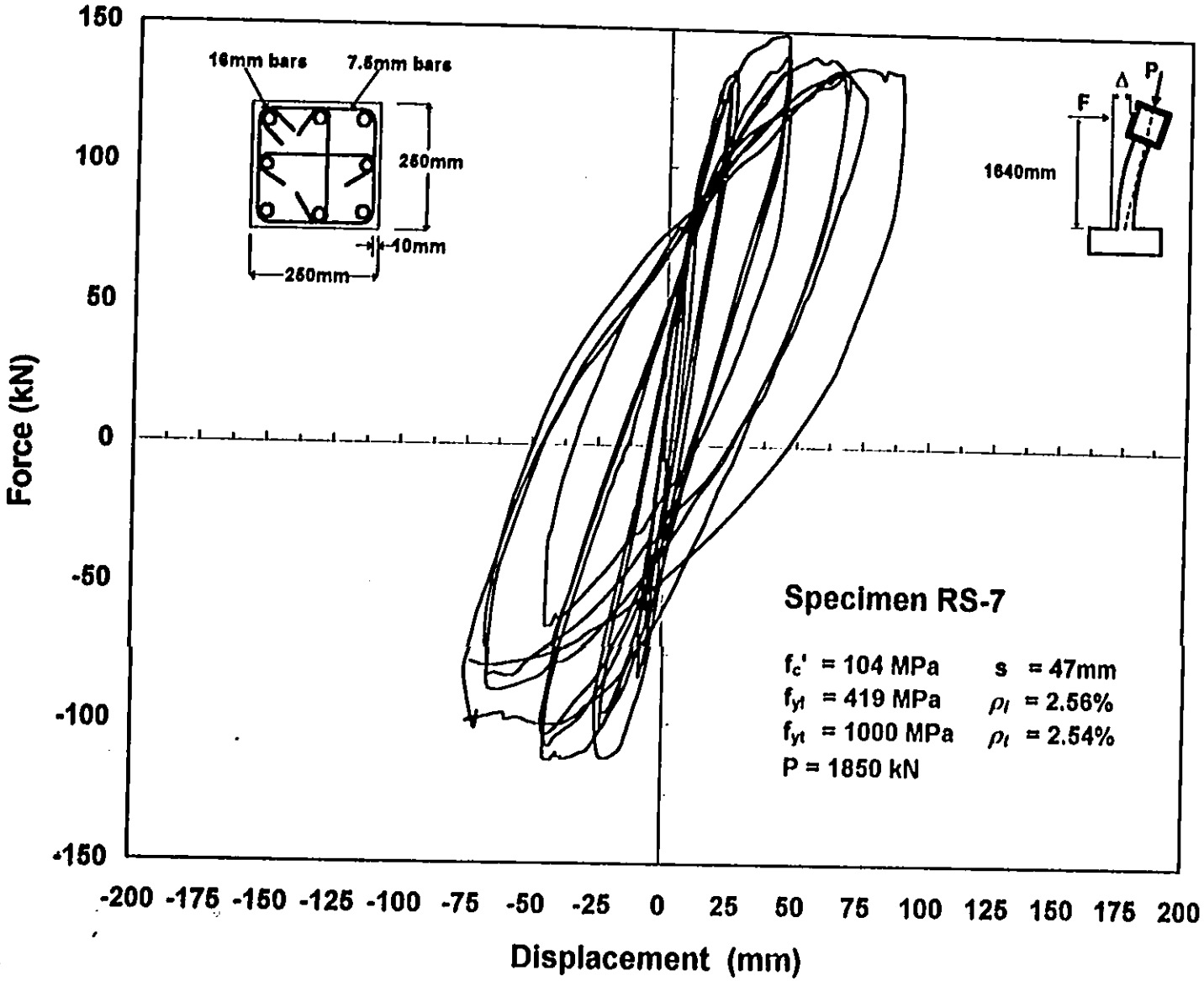

Fig. 53 Force - Displacement Relationship
Excluding PΔ Effect

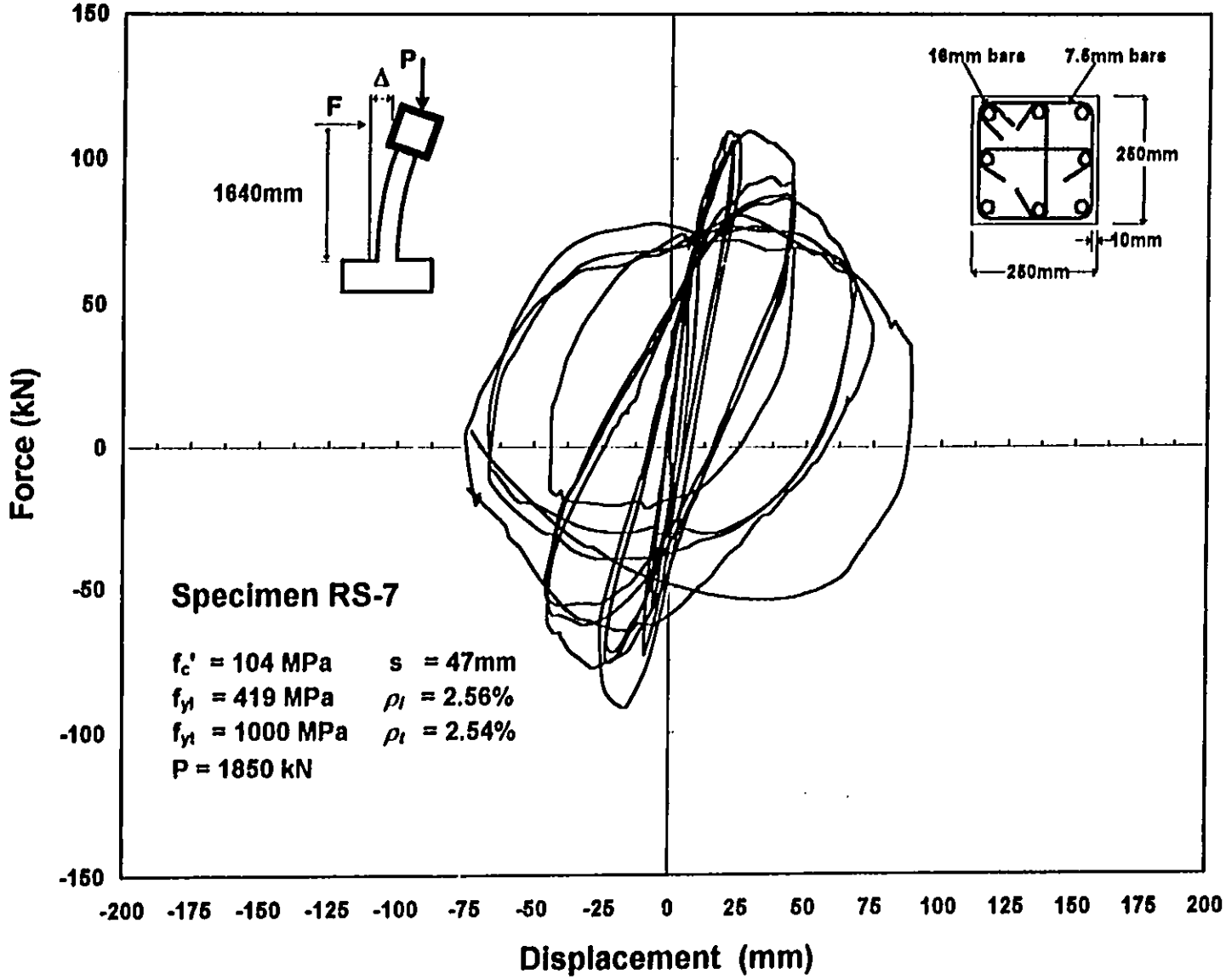

Fig. 54 Force - Displacement Relationship Including PΔ Effect

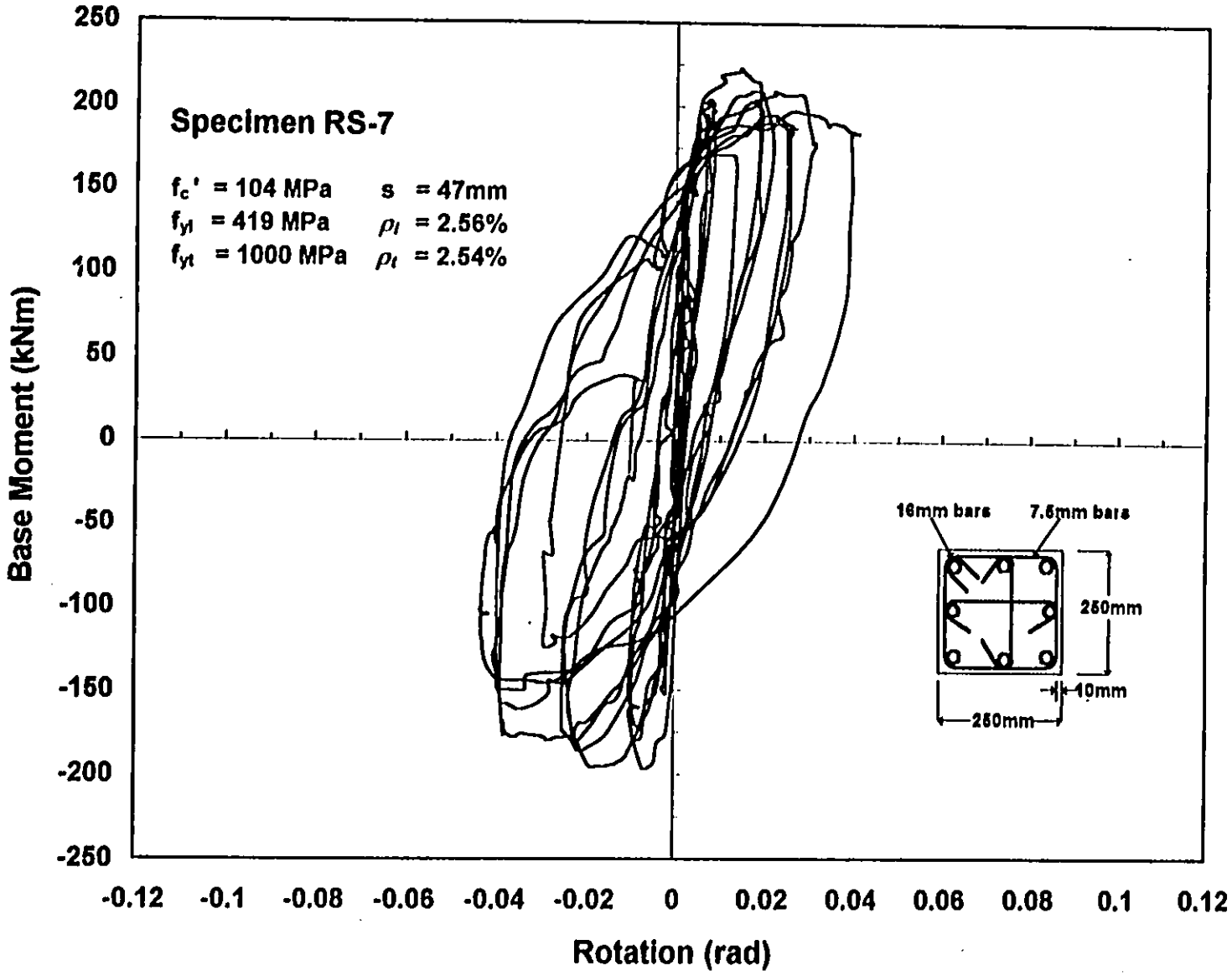

Fig. 55 Base Moment - Total Rotation Relationship in the Hinge Region

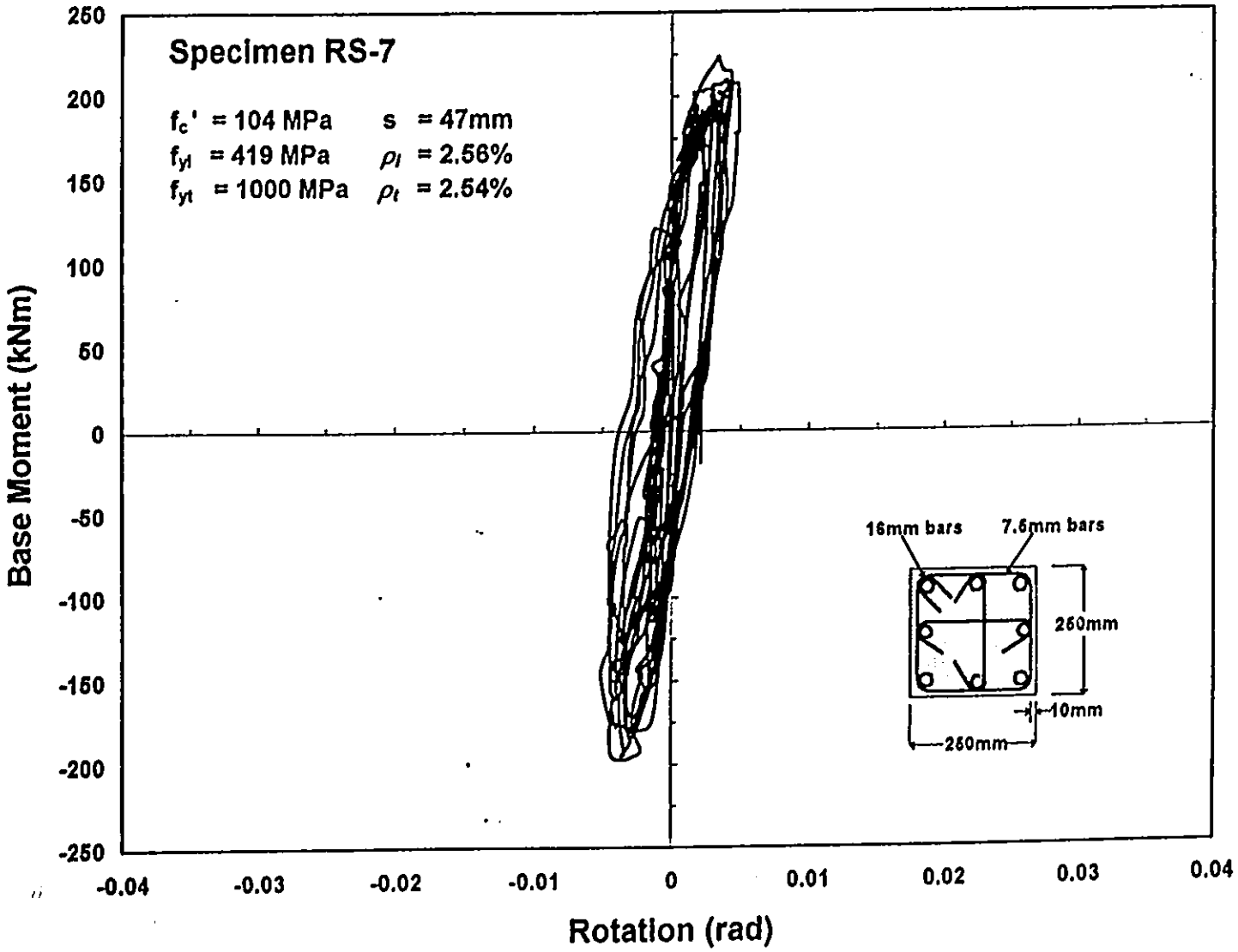

Fig. 56 Base Moment - Slip Rotation Relationship

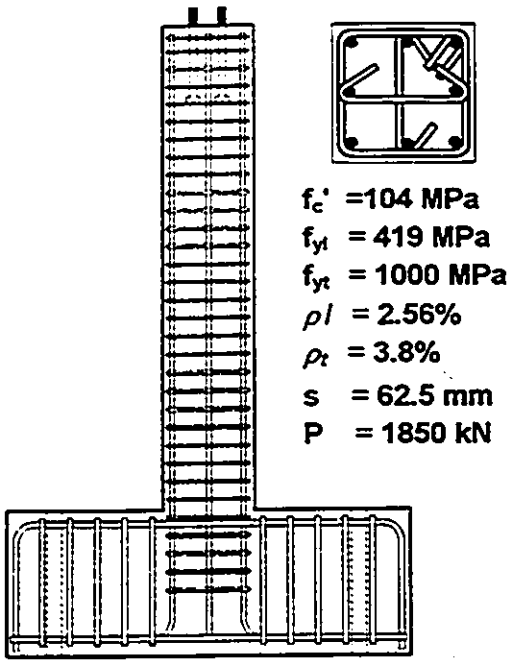

a) 1 Δy

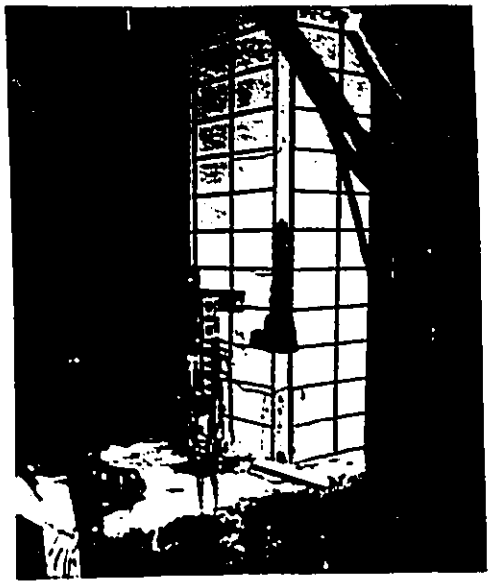

b) 2 Δy

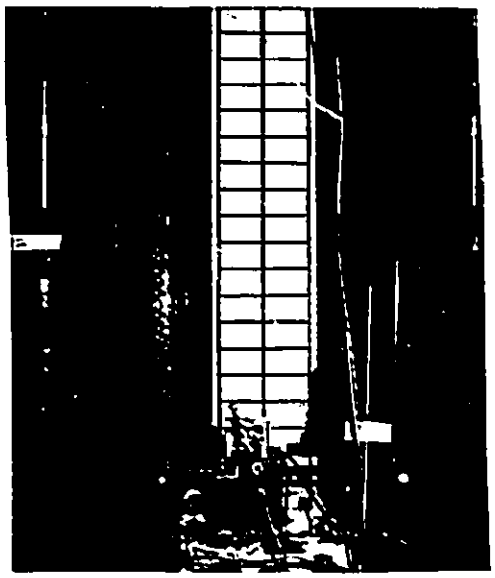

c) 3 Δy

Fig. 57 Extent of Damage at Different Load Stages Specimen RS-8

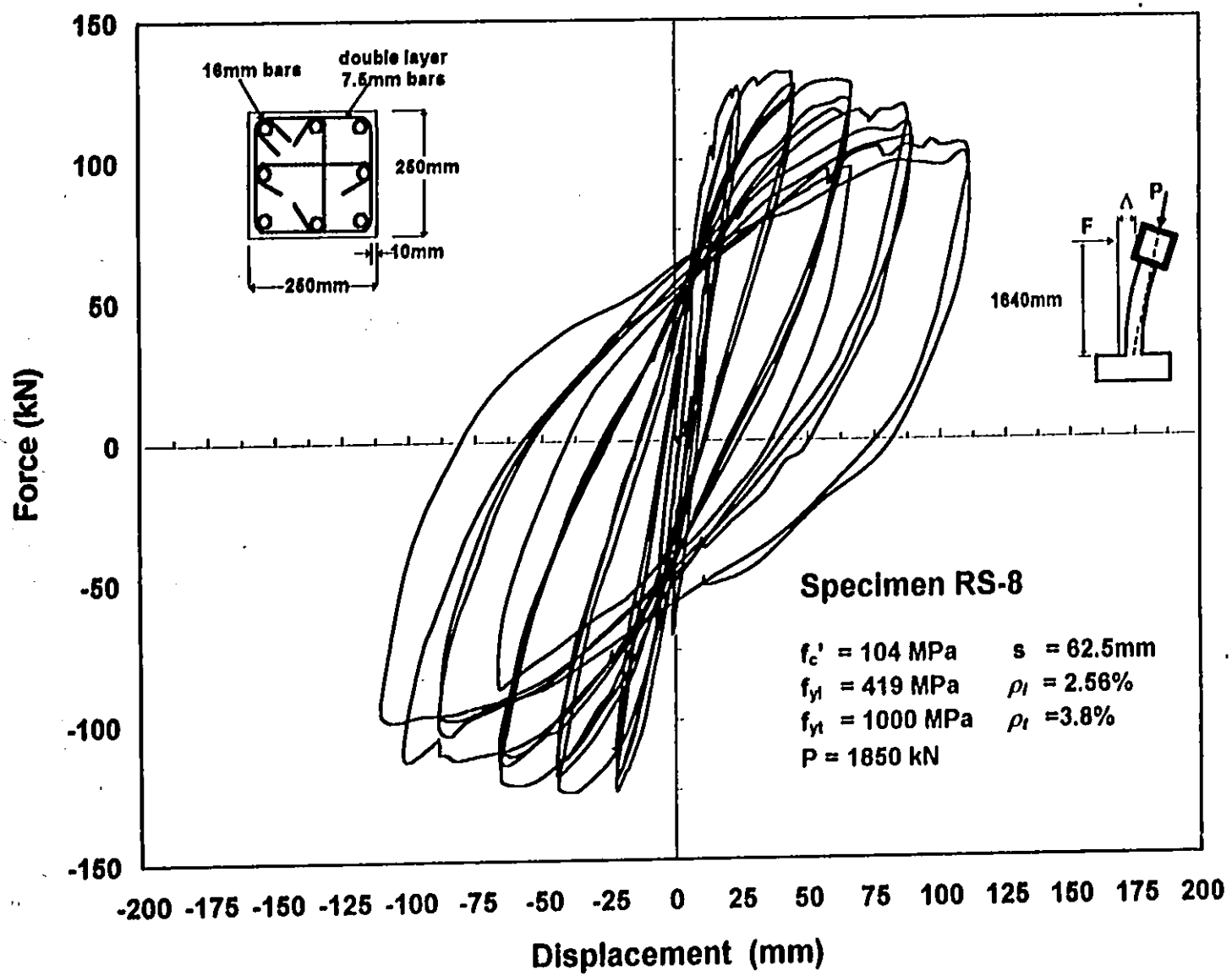

Fig. 58 Force - Displacement Relationship Excluding PΔ Effect

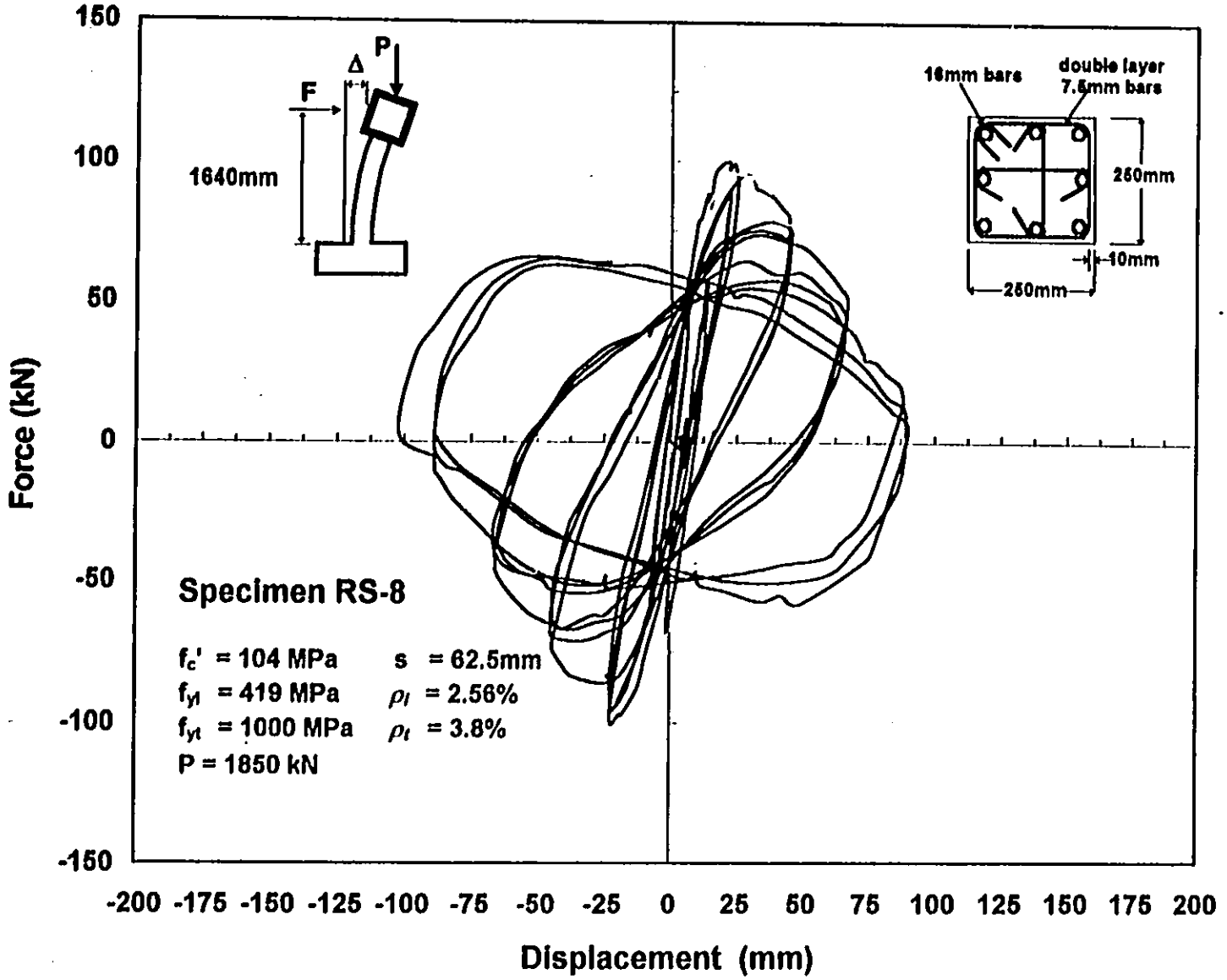

Fig. 59 Force - Displacement Relationship Including P-Δ Effect

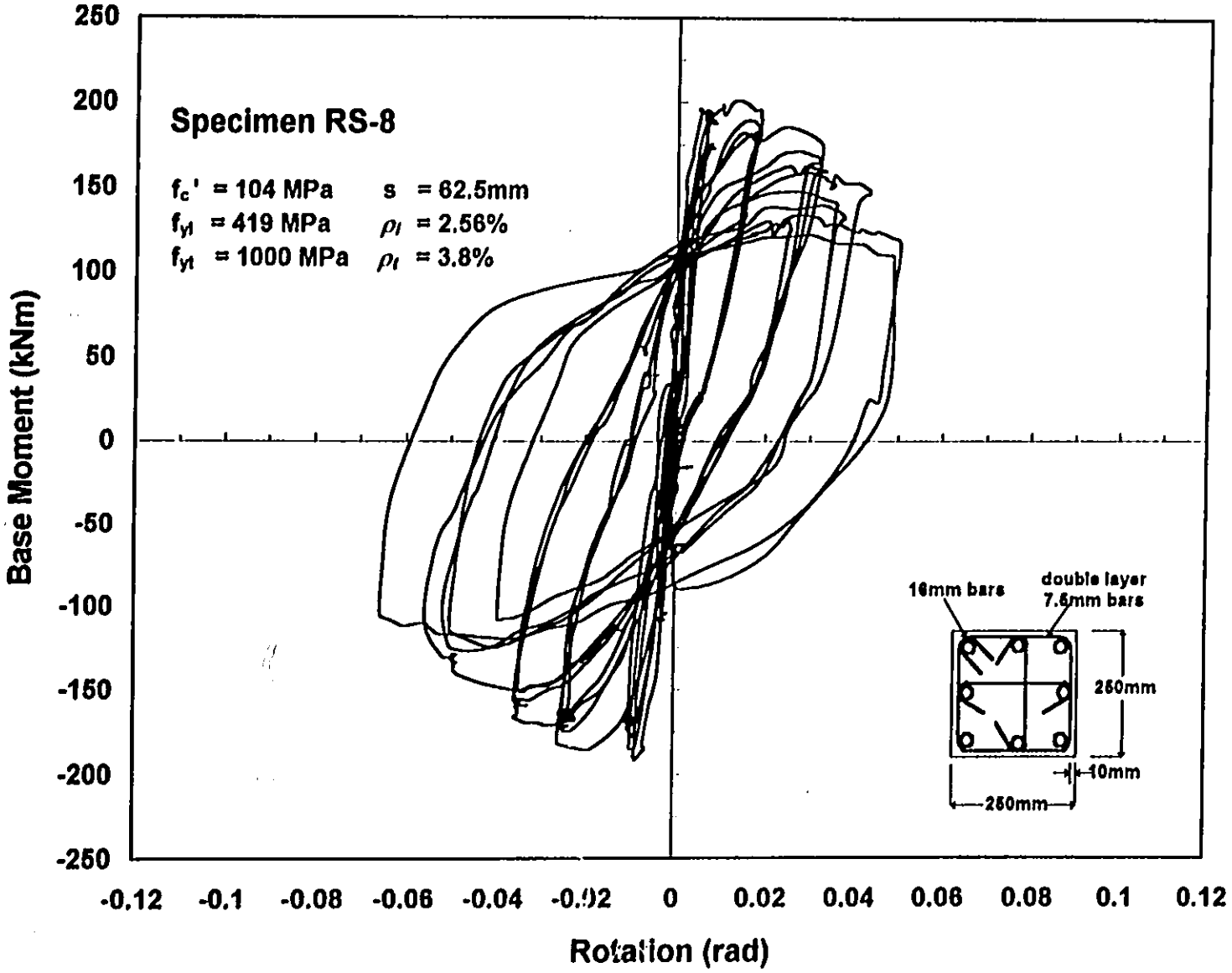

Fig. 60 Base Moment - Total Rotation Relationship in the Hinge Region

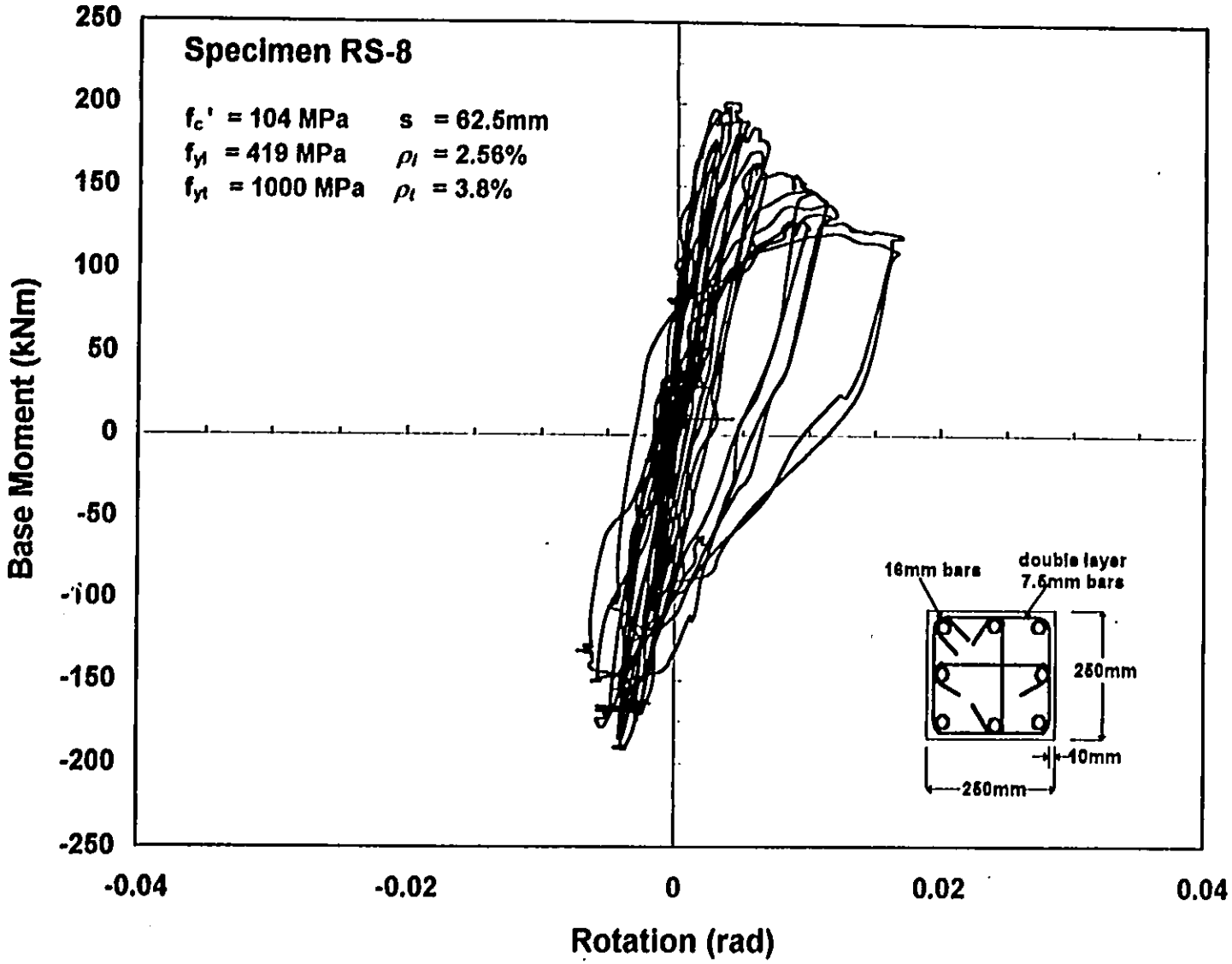

Fig. 61 Base Moment - Slip Rotation Relationship

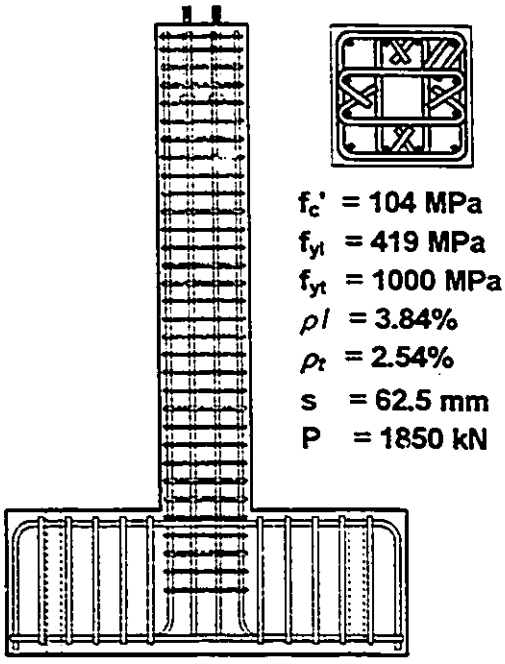

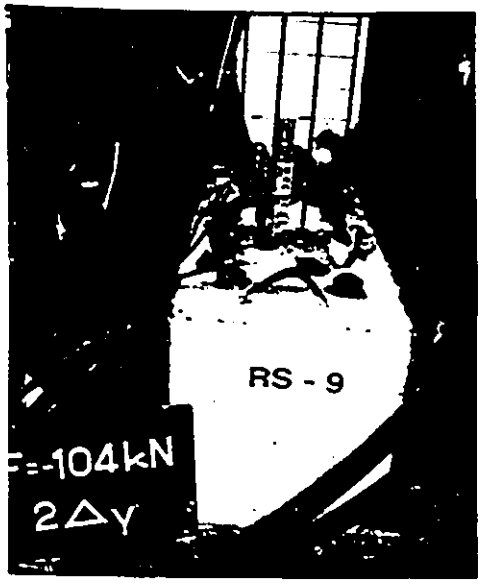

a) 2 Δy

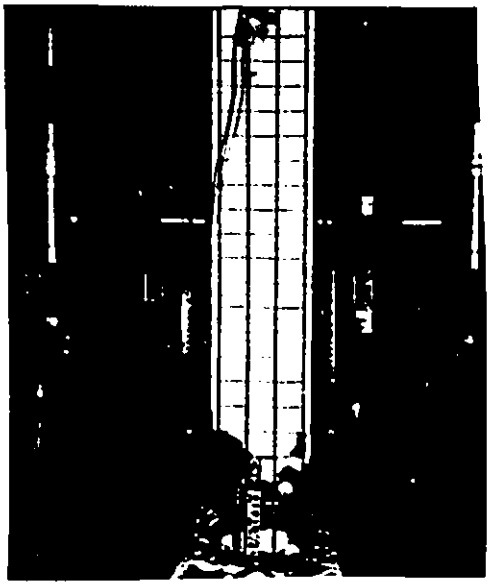

b) 3 Δy

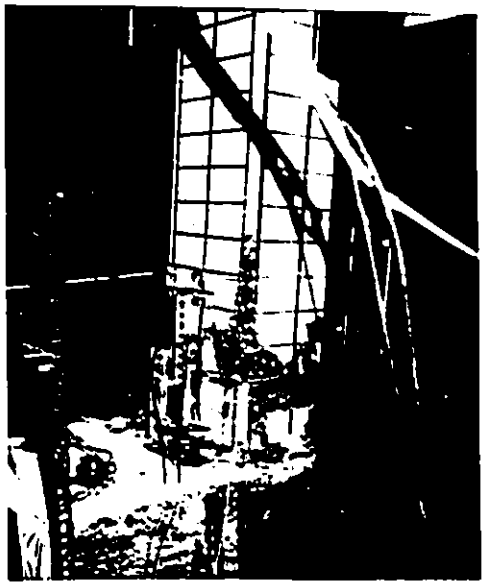

c) 4 Δy

Fig. 62 Extent of Damage at Different Load Stages Specimen RS-9

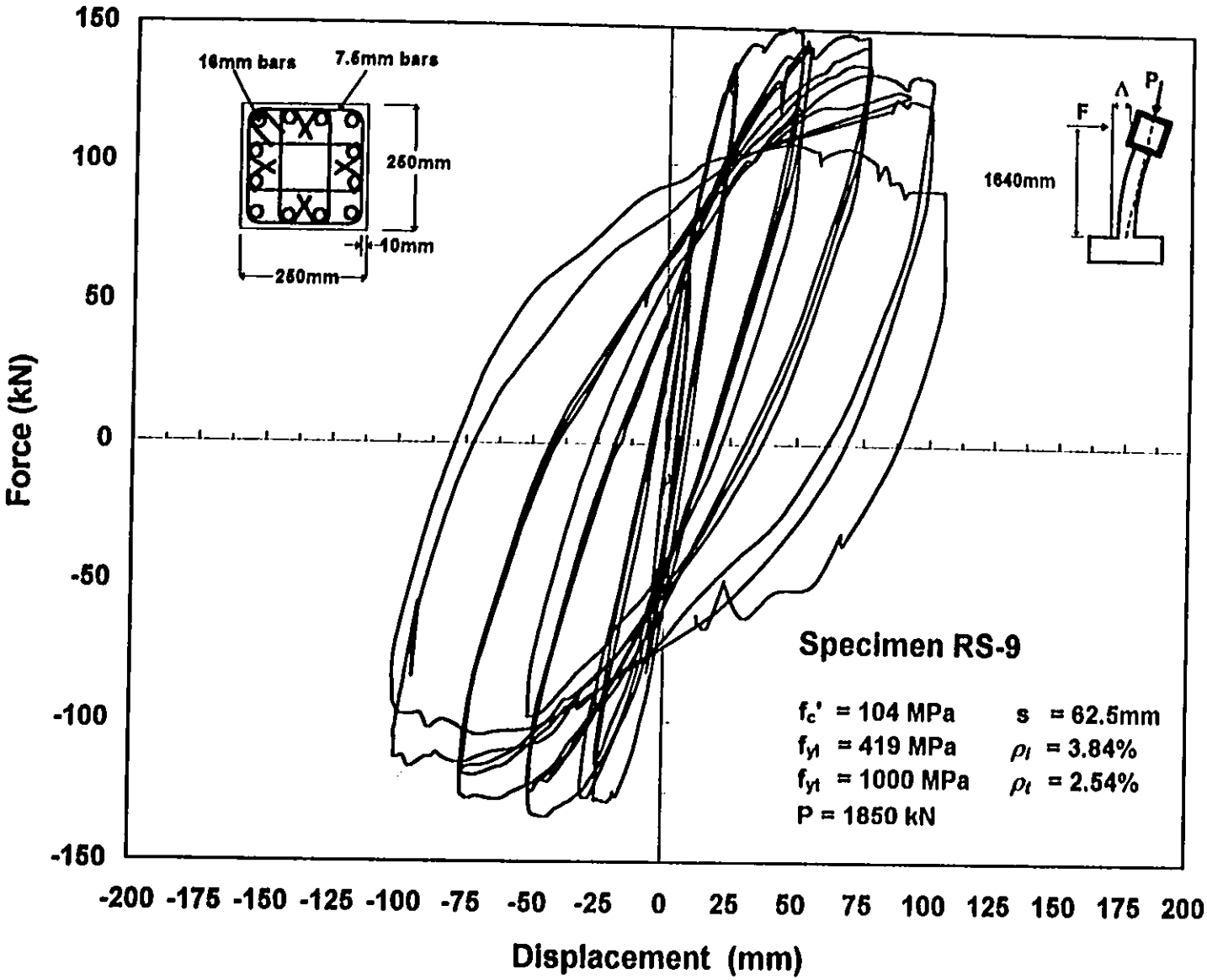

Fig. 63 Force - Displacement Relationship Excluding PΔ Effect

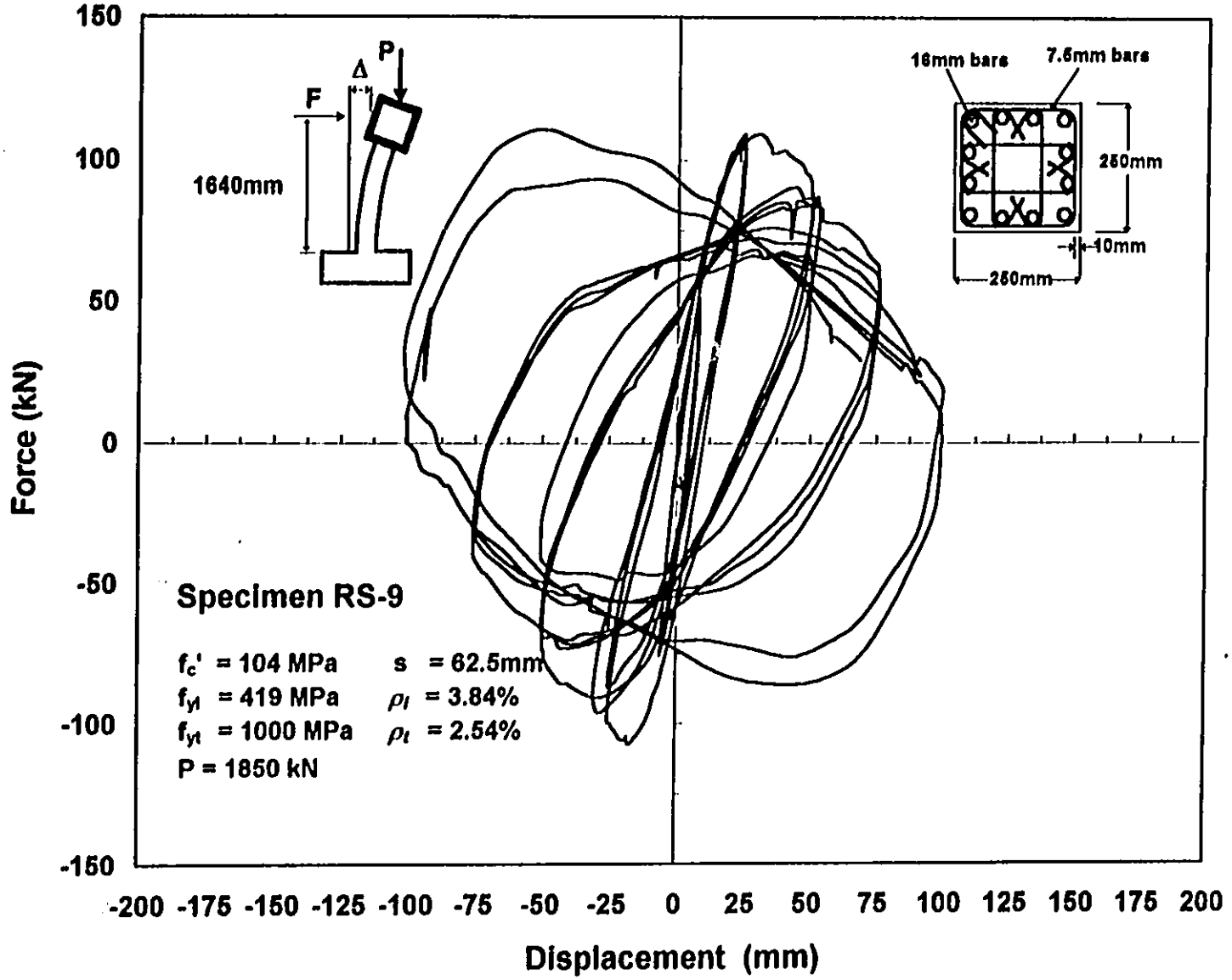

Fig. 64 Force - Displacement Relationship Including PΔ Effect

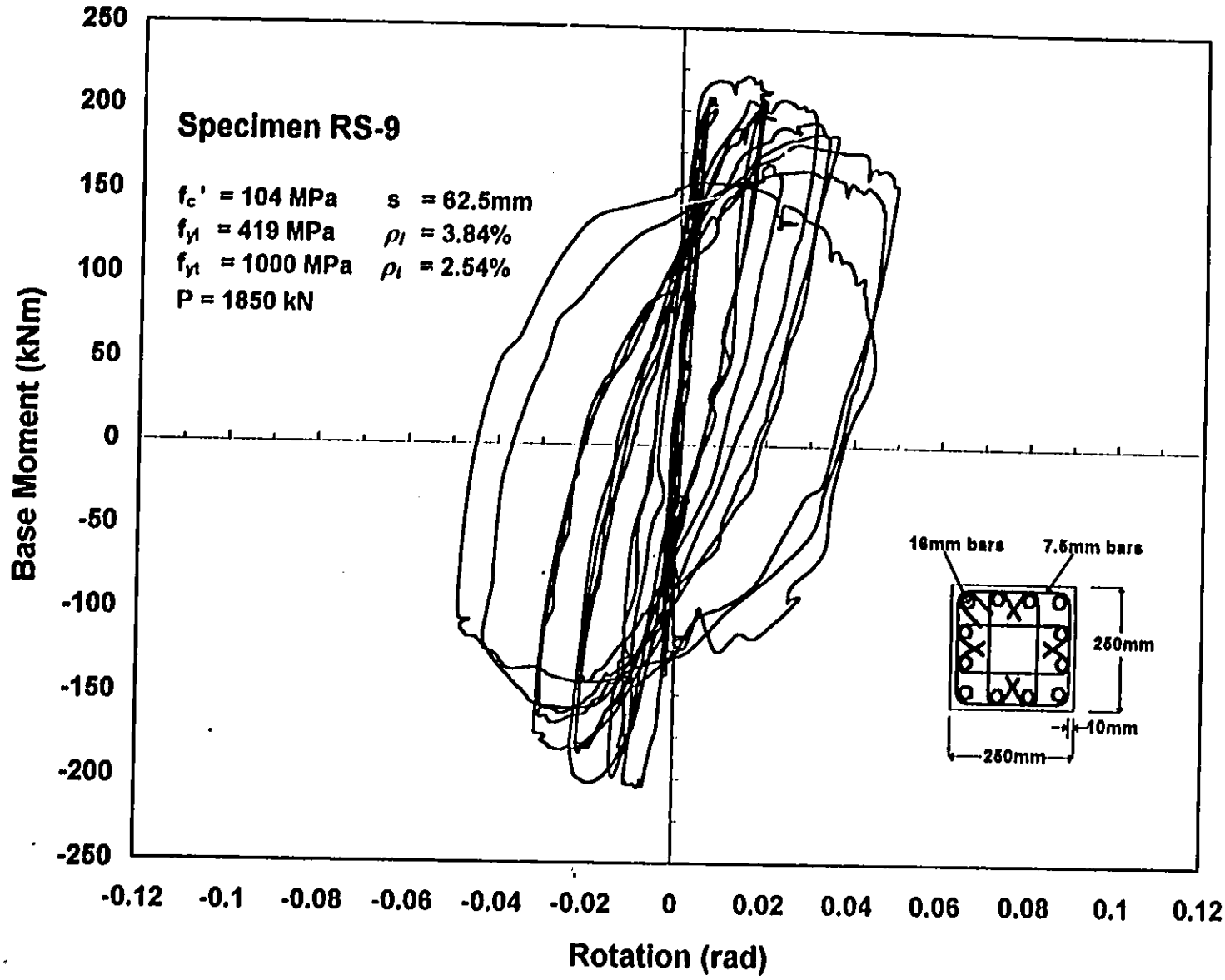

Fig. 65 Base Moment - Total Rotation Relationship in the Hinge Region

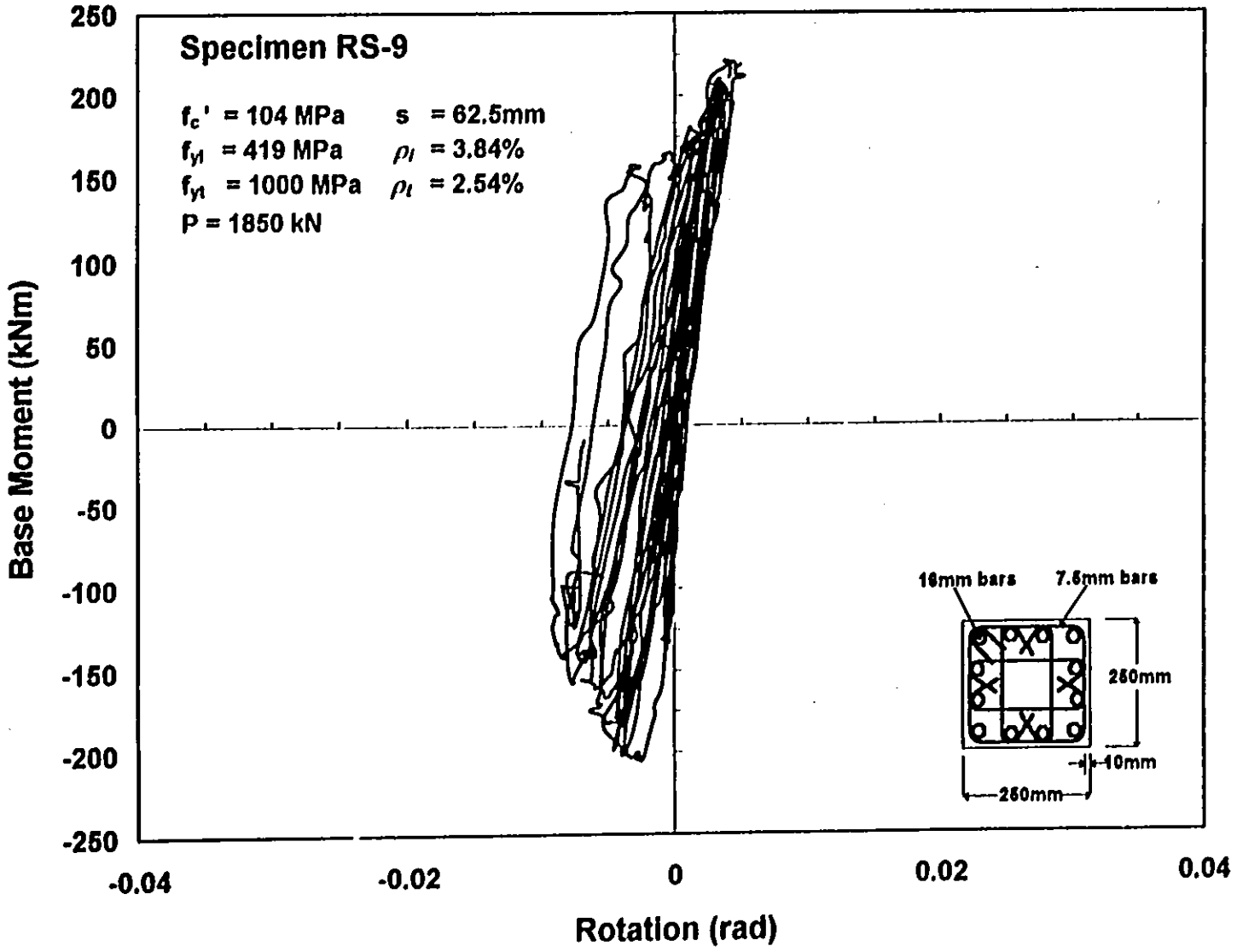

Fig. 66 Base Moment - Slip Rotation Relationship

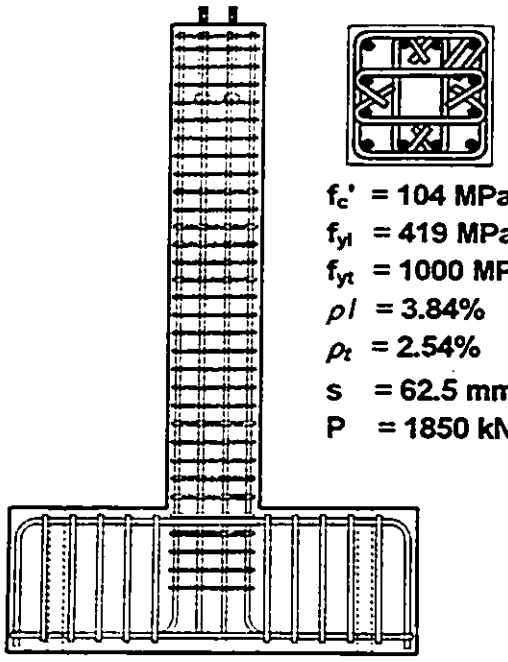

f_c' = 104 MPa
f_{yl} = 419 MPa
f_{yt} = 1000 MPa
ρl = 3.84%
ρ_t = 2.54%
s = 62.5 mm
P = 1850 kN

a) 2 Δy

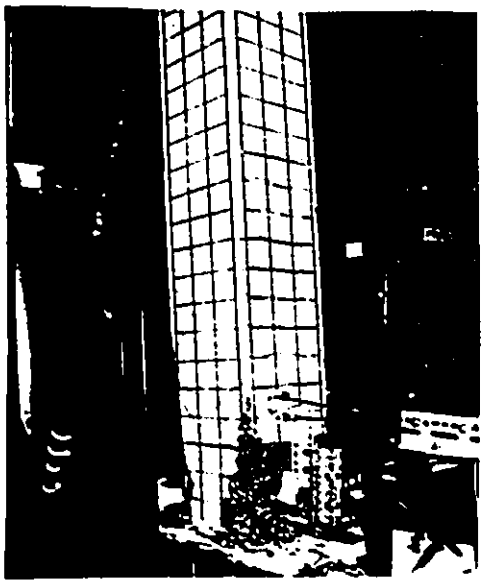

b) 3 Δy

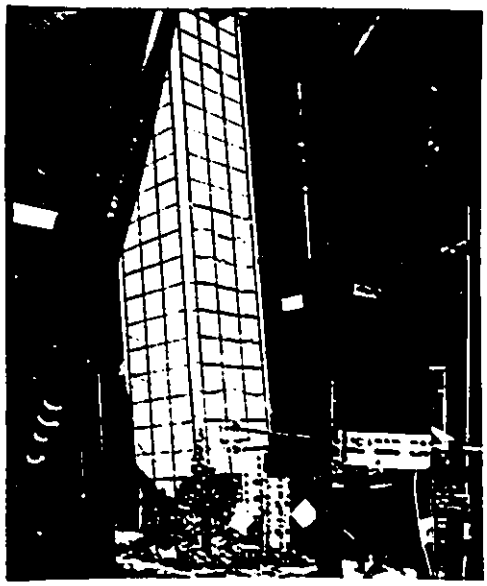

c) 6 Δy

Fig. 67 Extent of Damage at Different Load Stages Specimen RS-10

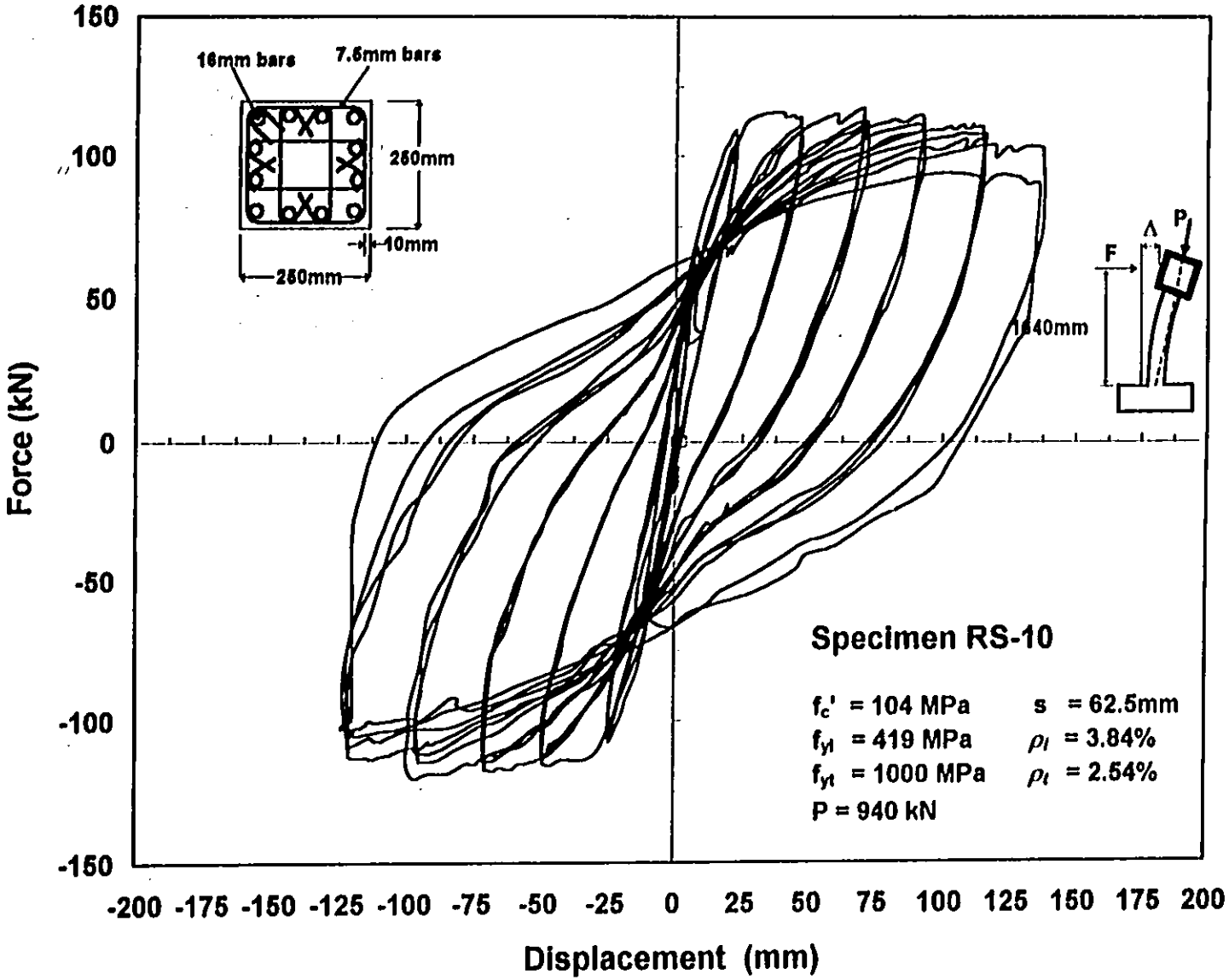

Fig. 68 Force - Displacement Relationship
Excluding PΔ Effect

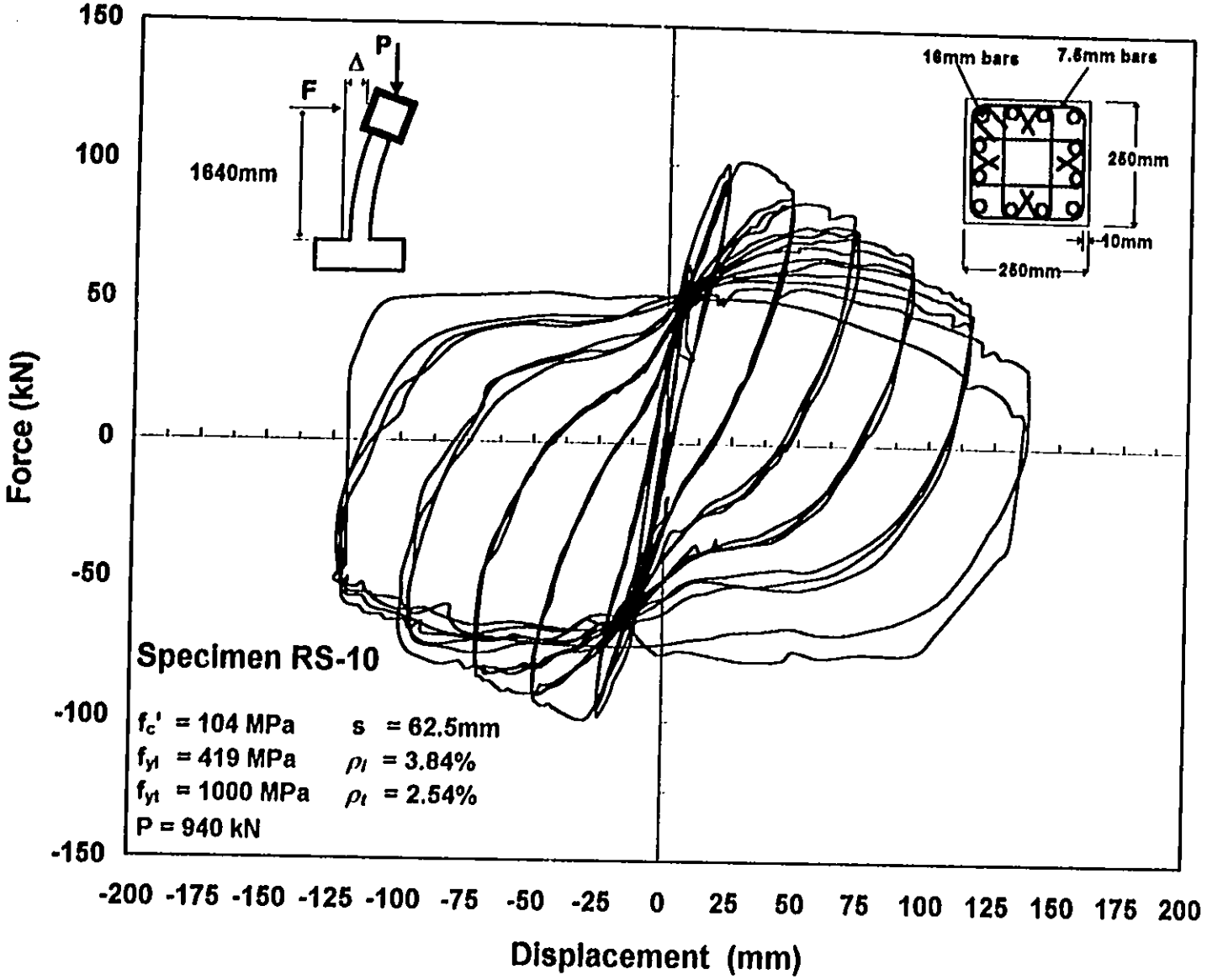

Fig. 69 Force - Displacement Relationship Including PΔ Effect

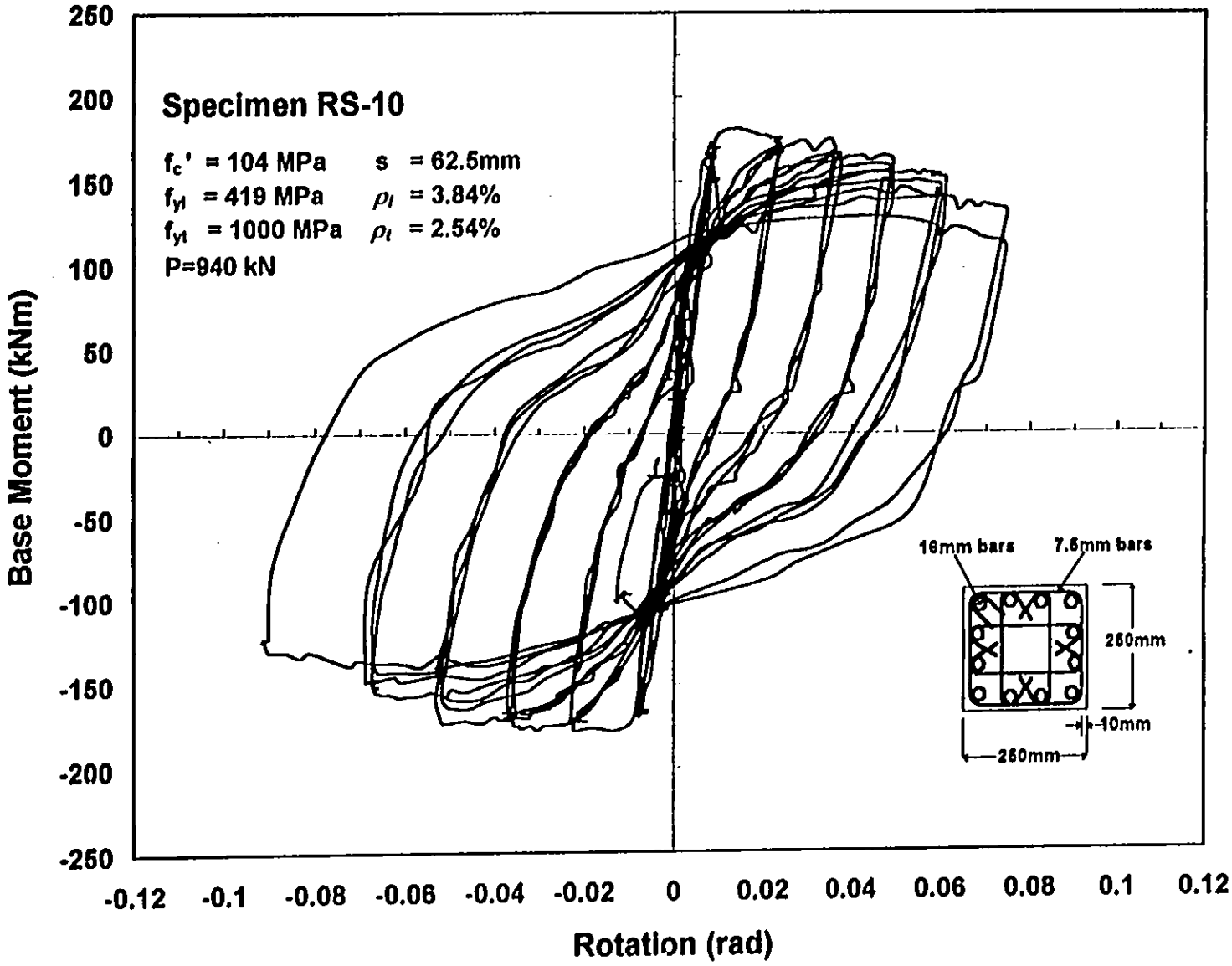

Fig. 70 Base Moment - Total Rotation Relationship in the Hinge Region

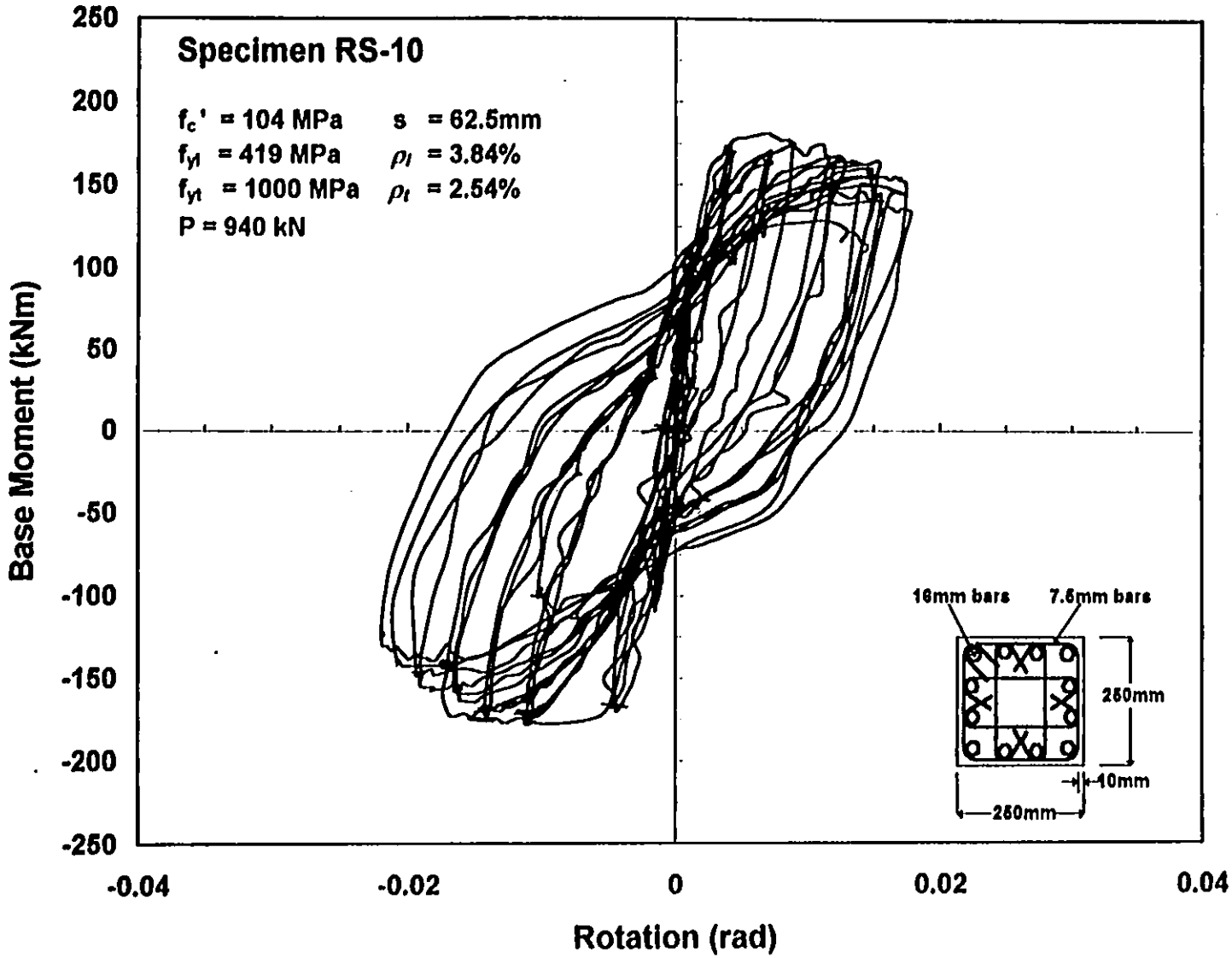

Fig. 71 Base Moment - Slip Rotation Relationship

Chapter 4

Analysis of Test Data

4.1 General

The results of column tests are analysed and discussed in this chapter. The analysis of test data includes investigation of test parameters, as well as comparisons of experimental and analytical force-displacement relationships. The effects of test parameters and comparisons with analytical results are presented in the following sections.

4.2 Effects of Test Parameters

The effects of test parameters were investigated by comparing force-displacement hysteretic relationships obtained by testing companion columns with different test parameters. The envelopes (backbone curves) of these relationships were normalized relative to their peak loads to show differences in column deformability in the inelastic range. The effects of the following parameters were investigated experimentally by testing 10 full-size columns:

a) Concrete strength.

b) Volumetric ratio of transverse reinforcement.

c) Yield strength of transverse reinforcement.

d) Spacing of tie steel.

e) Arrangement of lateral reinforcement.

f) Level of axial compression.

4.2.1 Effect of Concrete Strength

Two different strengths of concrete (64 MPa and 104 MPa) were considered in the experimental program, both within the high-strength range. Column RS-1 with 64 MPa concrete was identical to RS-9 with 104 MPa concrete, except for concrete strength. Both columns were confined with 12-bar arrangement and grade 1000 MPa high-strength reinforcement. The columns were subjected to 28% of their concentric capacities as constant axial compression. While both columns showed ductile characteristics, Column RS-9 with 104 MPa concrete started developing faster rate of strength decay beyond 4 % lateral drift, as compared to RS-1 with 64 MPa concrete which showed virtually no strength degradation until after 6 % lateral drift. The comparison of the normalized envelopes is shown in Fig. 72 and indicates that higher deformability is obtained in the lower strength concrete column.

4.2.2 Effect of Volumetric Ratio of Transverse Reinforcement

The effect of volumetric ratio of transverse reinforcement was investigated by testing two 104 MPa concrete columns with 8-bar arrangement and 1000 MPa lateral steel. Column RS-5 with ρ_s of 1.9 % and RS-8 with ρ_s of 3.8 % were identical in all respects except for the volumetric ratio ρ_s. The normalized

envelopes of force-displacement relationships are compared in Fig. 73. The results indicate a steady strength decay in RS-5 immediately after the peak load with a sudden failure at approximately 4 % lateral drift. Column RS-8, on the other hand, showed almost constant strength up to approximately 3.5 % lateral drift, followed by a slow and gradual strength decay. The importance of the volumetric ratio of transverse reinforcement on deformability of high-strength concrete columns becomes evident in this figure. However, the volumetric ratio requirement for confinement of HSC columns may be a function of the grade of lateral reinforcement. This relationship between the volumetric ratio and grade is discussed in Section 4.2.3.

4.2.3 Effect of Yield Strength of Transverse Reinforcement

The lateral pressure provided by confinement reinforcement is directly related to the magnitude of tensile force that can be developed in transverse reinforcement. This force is a function of the amount (as expressed by volumetric ratio) and yield strength of lateral steel. Higher grade transverse reinforcement is expected to develop a higher tensile force and higher lateral pressure. However, if lateral expansion of high-strength concrete is not high enough to activate higher grade of reinforcement, then the increase in lateral pressure and hence the potential improvement in concrete confinement may be limited.

The effectiveness of high-strength lateral reinforcement was investigated by testing

high-strength concrete columns with three grades of transverse reinforcement. The steel grades included were 420 MPa, 575 MPa and 1000 MPa. Columns RS-1 and RS-2 both had 64 MPa concrete and 2.54% volumetric ratio of transverse reinforcement. RS-1 was confined with 1000 MPa steel with 63 mm tie spacing

and RS-2 was confined with 575 MPa steel with 45 mm tie spacing. The normalized envelopes are shown in Fig. 74. The results indicate approximately the same deformability even though Column RS-1 had wider spacing of ties. This is attributed to the higher grade transverse reinforcement used in RS-1. Similar comparison can be made between Columns RS-6 and RS-8, both with 104 MPa concrete but confined with different grades of lateral reinforcement. The comparison is shown in Fig. 75 and indicates improved deformability in RS-8 with 1000 MPa lateral reinforcement even with increased tie spacing.

4.2.4 Effect of Tie Spacing

Specimens RS-3 and RS-4 were designed to investigate the effect of spacing of transverse reinforcement on deformability of high strength concrete columns. These columns had 104 MPa concrete and 419 MPa transverse reinforcement, with 100 mm ties spacing in RS-3 and 50 mm spacing in RS-4. The normalized envelopes of force-displacement relationships for the two columns are compared in Fig. 76. The results clearly demonstrate the importance of tie spacing on column confinement. Specimen RS-4 with a smaller spacing developed 5 % lateral drift at 20 % strength decay, as compared to RS-3 with twice the tie spacing which could only sustain 3.5 % drift at the same strength level. The effect of tie spacing can also be seen in Figs. 74 and 75 where Columns RS-1 and RS-2, and Columns RS-6 and RS-8 are compared to demonstrate the effect of transverse steel grade. In these comparisons each of the companion column had a different tie spacing and the effects of increased tie spacing was compensated by the increase in yield strength of transverse reinforcement. It may be concluded form these comparisons that the current maximum spacing requirement of h/4 for normal-strength concrete columns may also be used for HSC columns.

4.2.5 Effect of Tie Arrangement

The lateral confinement pressure generated by transverse reinforcement becomes more efficient if laterally supported longitudinal reinforcement is distributed along the perimeter of the section. Therefore, tie arrangements that consist of closely spaced lateral reinforcement, not only in the vertical plane but also in the horizontal plane, would improve the efficiency of lateral pressure and the resulting column deformability. The effect of tie arrangement was shown to be very significant on normal-strength concrete columns.

Two different arrangements of lateral reinforcement were used in this research program, consisting of either an 8-bar or a 12-bar arrangement. Columns RS-7 and RS-9 were companion specimens with identical properties except the arrangement and spacing of lateral reinforcement. Both columns had 104 MPa concrete and 1000 MPa transverse reinforcement. Figure 77 illustrates the comparison of normalized envelope curves for force-displacement hysteretic relationships. The comparison indicates that Column RS-9 with 12-bar arrangement and 63 mm tie spacing showed better ductility characteristics than RS-7 with 8-bar arrangement and 47 mm tie spacing. The results indicate than the improvement in tie arrangement from 8-bar to 12-bar was more than sufficient to offset the detrimental effects of 34 % increase in tie spacing.

4.2.6 Effect of Axial Compression

The columns tested in this investigation were subjected to a constant level of axial compression, simulating service gravity loads, while also subjected to inelastic lateral displacement reversals, simulating the effects of seismic loading. All

columns, with the exception RS-10, were initially loaded to 28% of their concentric load capacity, P_0. Column RS-10 was subjected to half as much axial compression, which was equal to 14 % of P_0. The effect of axial compression can be evaluated by comparing force-deformation characteristics of columns RS-10 and RS-9. The envelopes of force-displacement relationships for these two columns are shown in Fig. 78. The comparison indicates that RS-9 with axial compression of $28\%P_0$ showed rapid strength degradation beyond a lateral drift ratio of approximately 2%, while specimen RS-10 with $14\%P_0$ was able to sustain 5% lateral drift at 20% strength decay. It may be concluded that the effect of axial compression is to reduce column deformability within the inelastic range.

4.3 Analytical Research

The test data collected on HSC columns were verified against analytically generated column behaviour. This was done to assess the applicability of recently proposed material models, and analysis procedures commonly used for normal-strength concrete columns. The analytical work involved computation of inelastic force-displacement relationships for the columns tested, and computation of column strength using recently suggested stress distributions for HSC.

4.3.1 Computation of Force-Displacement Relationship

Force-displacement relationship for each column was analytically computed to be compared with the envelope of experimentally recorded hysteretic relationship. The analytical computations were conducted for monotonically increasing lateral load and constant axial compression. The monotonic curves were assumed to be representative of envelope (backbone) curves for hysteresis loops. This is generally

believed to be the case for normal-strength concrete columns [17], [18] and was assumed to also apply to HSC columns because of the absence of experimental data on HSC.

Analytical force-displacement relationships were constructed starting from sectional analysis. Moment-curvature relationships for column sections were first established through plane section analyses. Plane sections before bending were assumed to remain plane after bending in conducting these analyses. Material stress-strain relationships were used to relate strains and stresses across the section depth. Internal stresses obtained in this manner were used to establish internal forces, bending moments and curvatures corresponding to selected strain profiles. Confined concrete stress-strain model for high-strength concrete, recently developed by Razvi and Saatcioglu [19] was used to model the compression concrete. Experimentally obtained stress-strain relationships were used for reinforcing steel with strain hardening.

The confinement model employed is an extension of the model developed earlier by Saatcioglu and Razvi [20] for normal-strength concrete. The model is based on equivalent uniform pressure generated by confinement reinforcement. It incorporates the effects of the amount, grade, spacing and arrangement of transverse reinforcement. Different bar arrangements are considered through confinement pressures shown in Fig. 79 (a). The stress-strain model is illustrated in Fig. 79 (b).

The sectional analysis can be used to establish distribution of curvatures along column height. Integration of curvatures along the height results in member rotation, and the moment of the area under the curvature diagram results in lateral displacement caused by flexure. This procedure is based on well accepted

principles of strain compatibility and equilibrium, and should be applicable to analysis of HSC column if appropriate material models are utilized. One difficulty that may arise in the analysis is the computation of displacements during the descending branch of force-displacement relationship, beyond the maximum strength point. As column resistance drops in this region, plastification of the hinging region progresses while the applied moment decreases. This requires a more detailed consideration of curvatures within the plastic hinge region. An iterative procedure was developed by Razvi [21] to account for the localization of plastic hinge with increasing plastification and curvatures during degradation of strength. This is illustrated in Fig. 80. The procedure was adopted in this thesis, and was used in generating the force-displacement relationships.

Reinforced concrete members in flexure develop additional inelastic deformations due to yield penetration into the adjoining member. This deformation is usually referred to as "anchorage slip" and may not necessarily result in slippage or bond failure of anchored reinforcement. The penetration of yielding into the column footing, which is near the column critical section, results in extension of reinforcement in the footing. This produces additional column displacement that is not accounted for in flexural analysis. A procedure was developed by Alsiwat and Saatcioglu [22] to calculate deformations resulting from anchorage slip. Figure 81 illustrates the distribution of strains and stresses in embedded reinforcement based on the proposed procedure. This procedure was, however, developed for normal-strength concrete members. The application of the procedure to HSC columns is questionable because of the potentially different bond stress characteristics between the steel and concrete. However, the anchorage slip becomes small under high axial compression. The columns analysed in this research program are subjected to relatively high axial compression. Therefore, any error that may be introduced to anchorage slip calculations because of

potential differences in bond stress between normal-strength and high-strength concretes is believed to be very small. Therefore, the procedure developed by Alsiwat and Saatcioglu was adopted in this thesis and used in calculating horizontal column displacement in the inelastic range.

A computer software was used to employ the aforementioned analysis to HSC columns. The analytically obtained force-displacement relationships are compared with those recorded experimentally in Figs. 82 through 91. The comparisons are made for horizontal displacements at 1320 mm from the column footing interface where the concrete column ends and the loading beams starts, although this height is not the same as the height of the inflection point. The analytical results show good correlations with experimental data indicating that the procedure employed, with the analytical models adopted, can be used to compute inelastic displacements of HSC columns.

4.3.2 Computation of Column Strength

Computation of column strength is important for design purposes. Currently there is lack of experimental data on strength of HSC columns to provide insight into possible modifications that may be introduced to conventional procedures used for normal-strength concrete. The limited research conducted on concentrically tested HSC columns showed reduced column capacity due to premature spalling of cover concrete. Although this raised some concerns over the use of HSC in columns, the behaviour of cover concrete under strain gradient could be different that that under concentric compression. Therefore more research was needed under bending to establish column strength under combined bending and axial compression. A number of stress blocks were proposed in recent years to calculate column capacity for design purposes. These stress blocks were not intended to reflect the

effect of concrete confinement since strength enhancement in concrete due to confinement is ignored in current design practice.

Column capacities obtained in the experimental part of this research program are compared in this section with strengths obtained analytically using four different stress blocks and a confined concrete model, proposed by different researchers. The comparisons are tabulated in Table 4. The results indicate that all analytical predictions provide reasonably good estimates of recorded column capacities. The stress blocks without the effects of confinement produce conservative estimates, while the confined concrete model produces either closer or slightly higher values than those recorded experimentally.

Table 4 - Maximum Horizontal Forces (kN)

Specimen No.	Experimental Results	ACI STATE OF THE ART [26]		NEW ZELAND Bing,Park, Tanaka [25]	CSA A23.3-94 [23]	Ibrahim/ MacGregor [24]	Razvi/ Saatcioglu [19]
		Triangle	Rectangle				
1	125/129	84	82	99	116	117	125
2	125/118	84	82	99	116	117	120
3	124/133	102	101	100	111	115	125
4	109/136	102	101	100	111	115	127
5	128/126	102	101	100	111	115	129
6	136/123	102	101	100	111	115	130
7	150/114	102	101	100	111	115	134
8	132/126	102	101	100	111	115	145
9	150/134	113	111	127	118	120	146
10	117/120	105	104	111	96	96	125

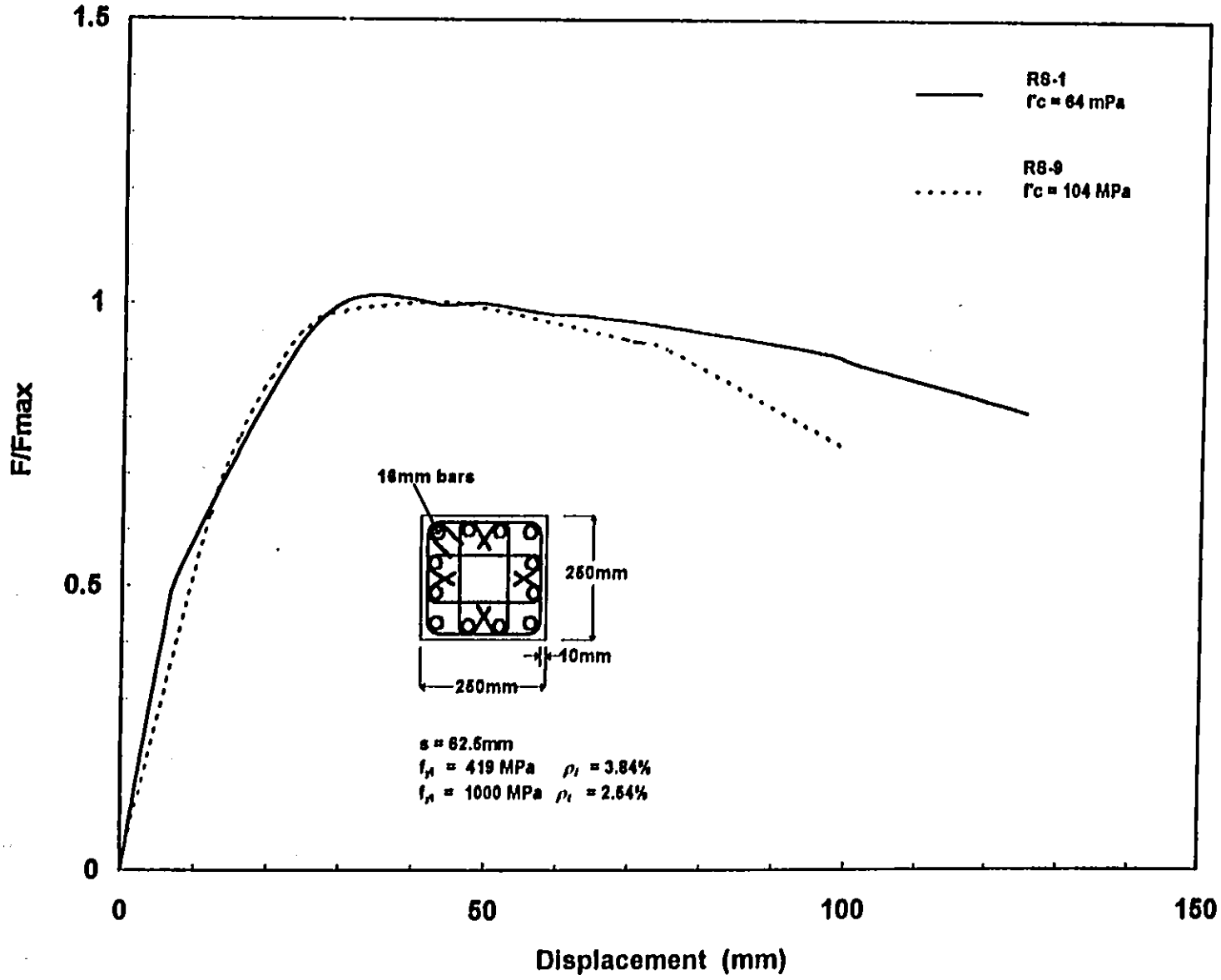

Fig. 72 Normalized Force - Displacement Relationship Envelopes Excluding PΔ Effect (Specimens RS-1 and RS-9)

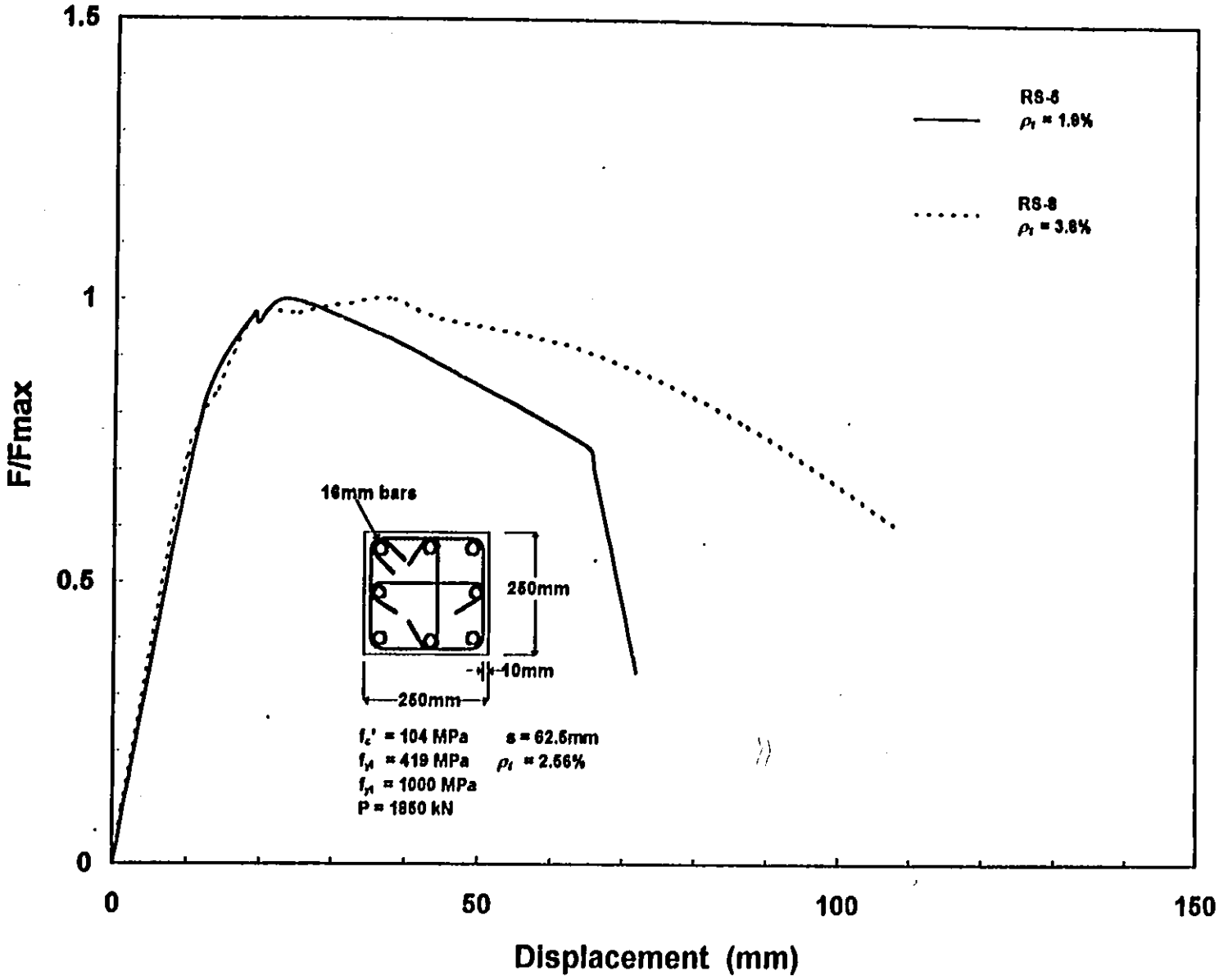

Fig. 73 Normalized Force - Displacement Relationship Envelopes Excluding PΔ Effect (Specimens RS-5 and RS-8)

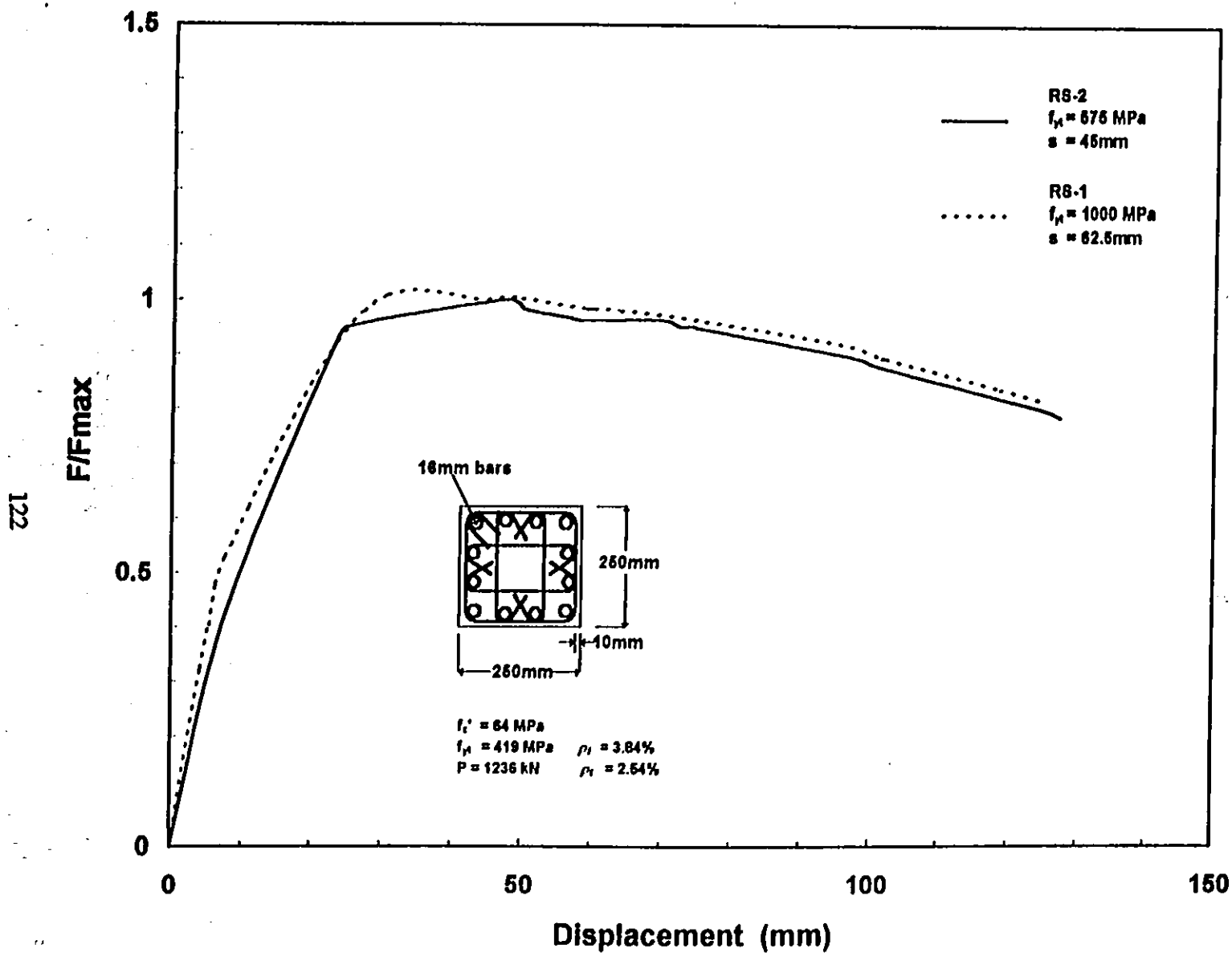

Fig. 74 Normalized Force - Displacement Relationship Envelopes Excluding PΔ Effect (Specimens RS-1 and RS-2)

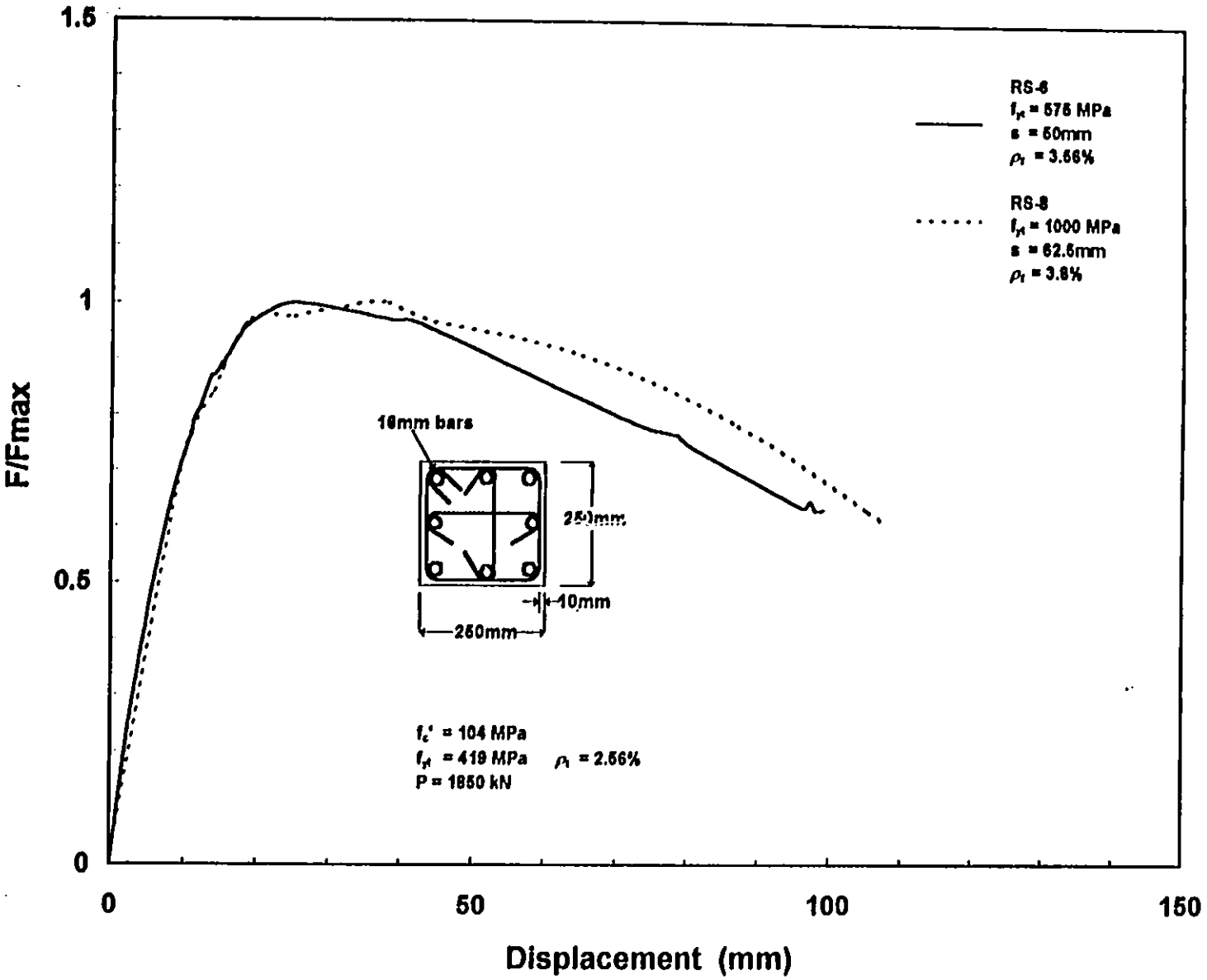

Fig. 75 Normalized Force - Displacement Relationship Envelopes Excluding PΔ Effect (Specimens RS-6 and RS-8)

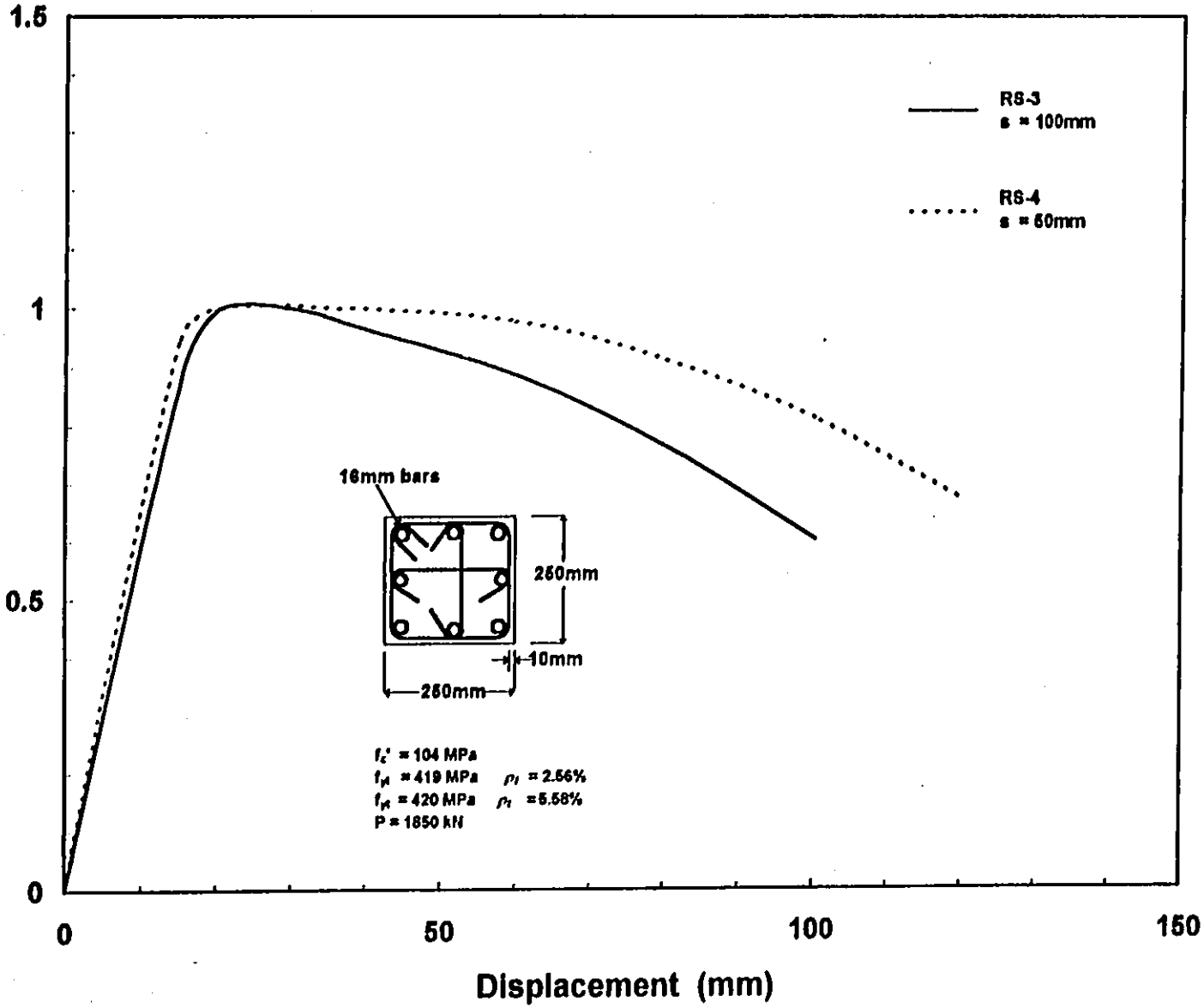

Fig. 76 Normalized Force - Displacement Relationship Envelopes Excluding PΔ Effect (Specimens RS-3 and RS-4)

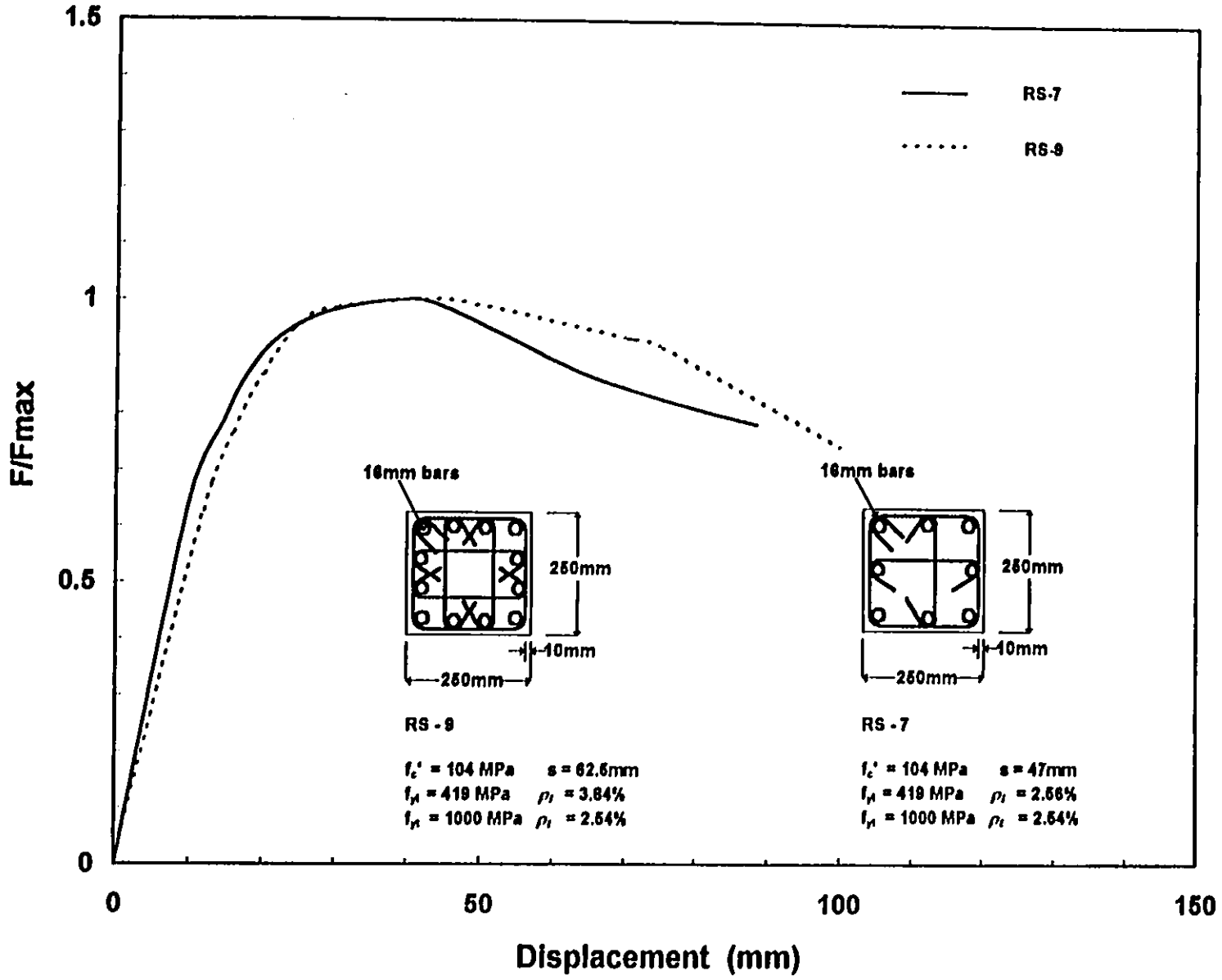

Fig. 77 Normalized Force - Displacement Relationship Envelopes Excluding PΔ Effect (Specimen RS-7 and RS-9)

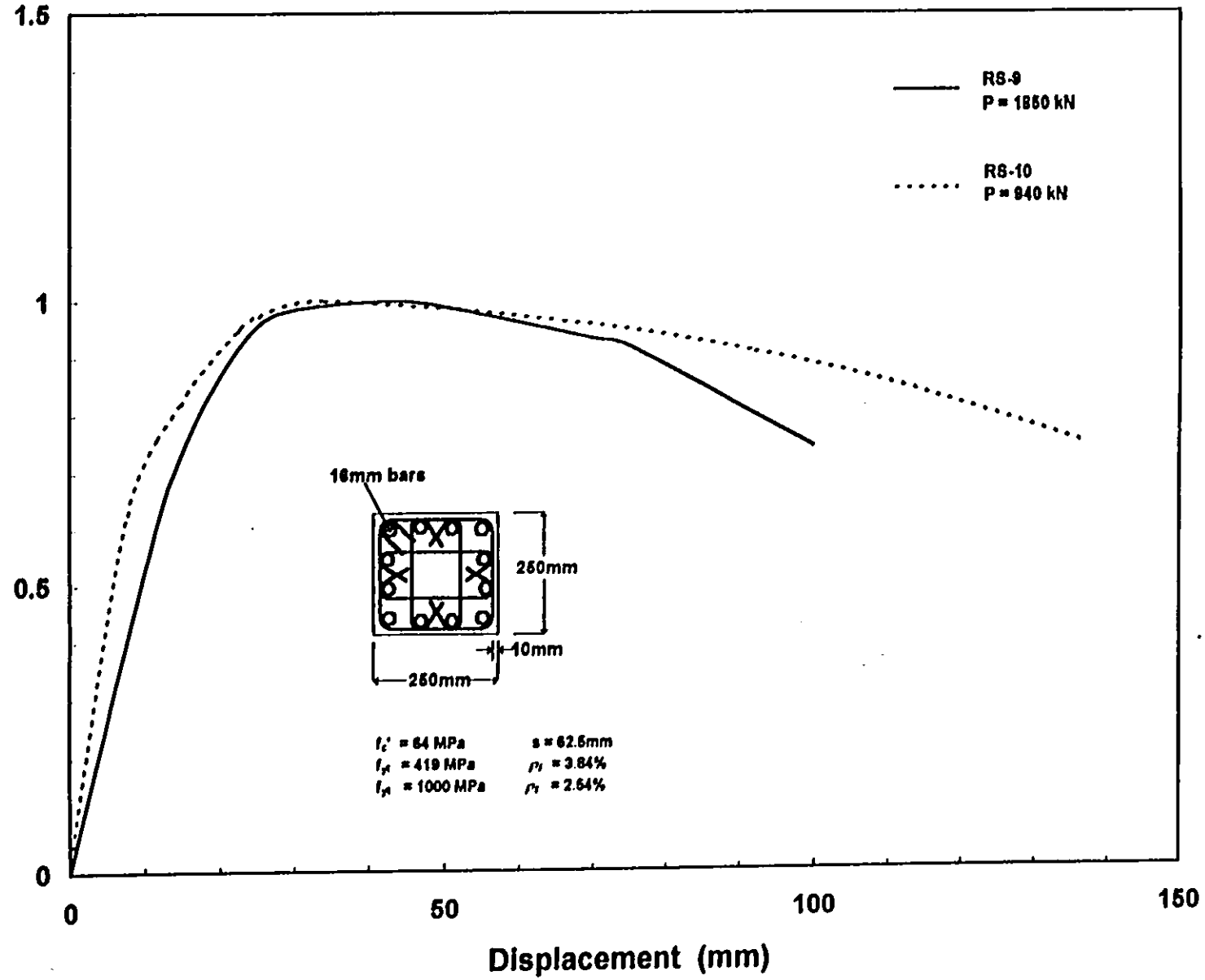

Fig. 78 Normalized Force - Displacement Relationship Envelopes Excluding PΔ Effect (Specimens RS-9 and RS-10)

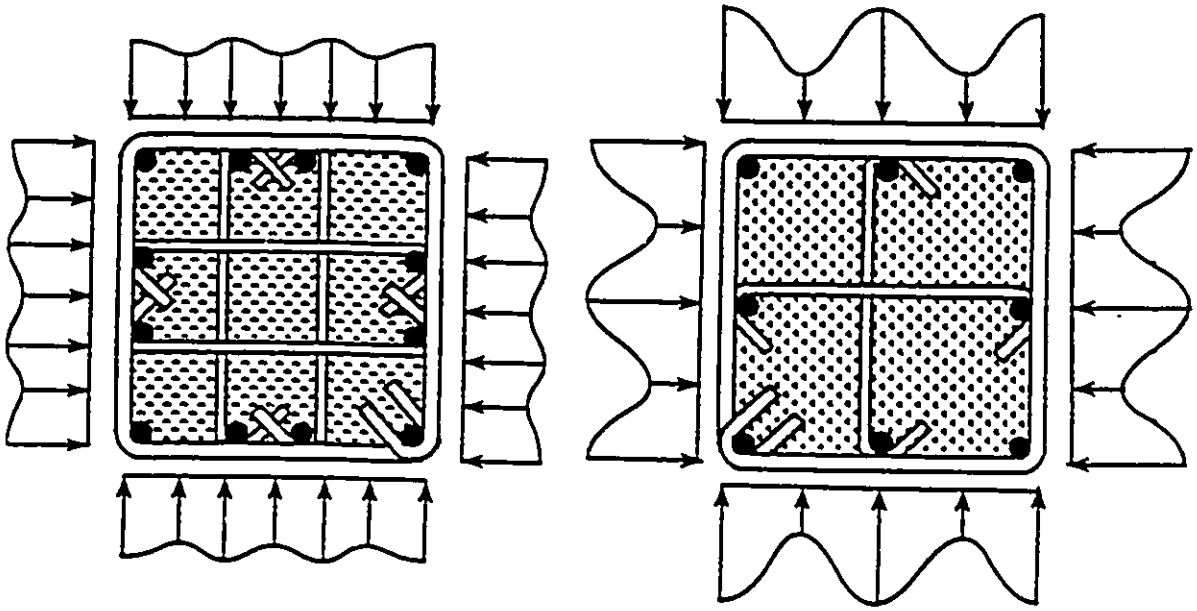

Fig. 79 (a) Pressure Distribution Resulting from Different Reinforcement Arrangement [21]

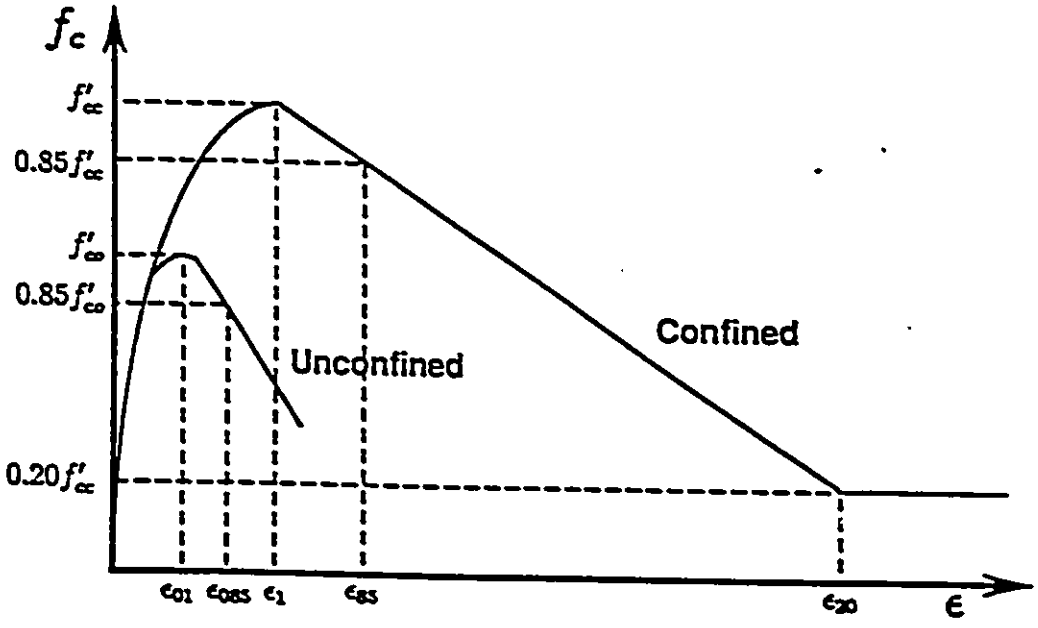

Fig. 79 (b) Stress Strain Relationship for Confined Concrete [21]

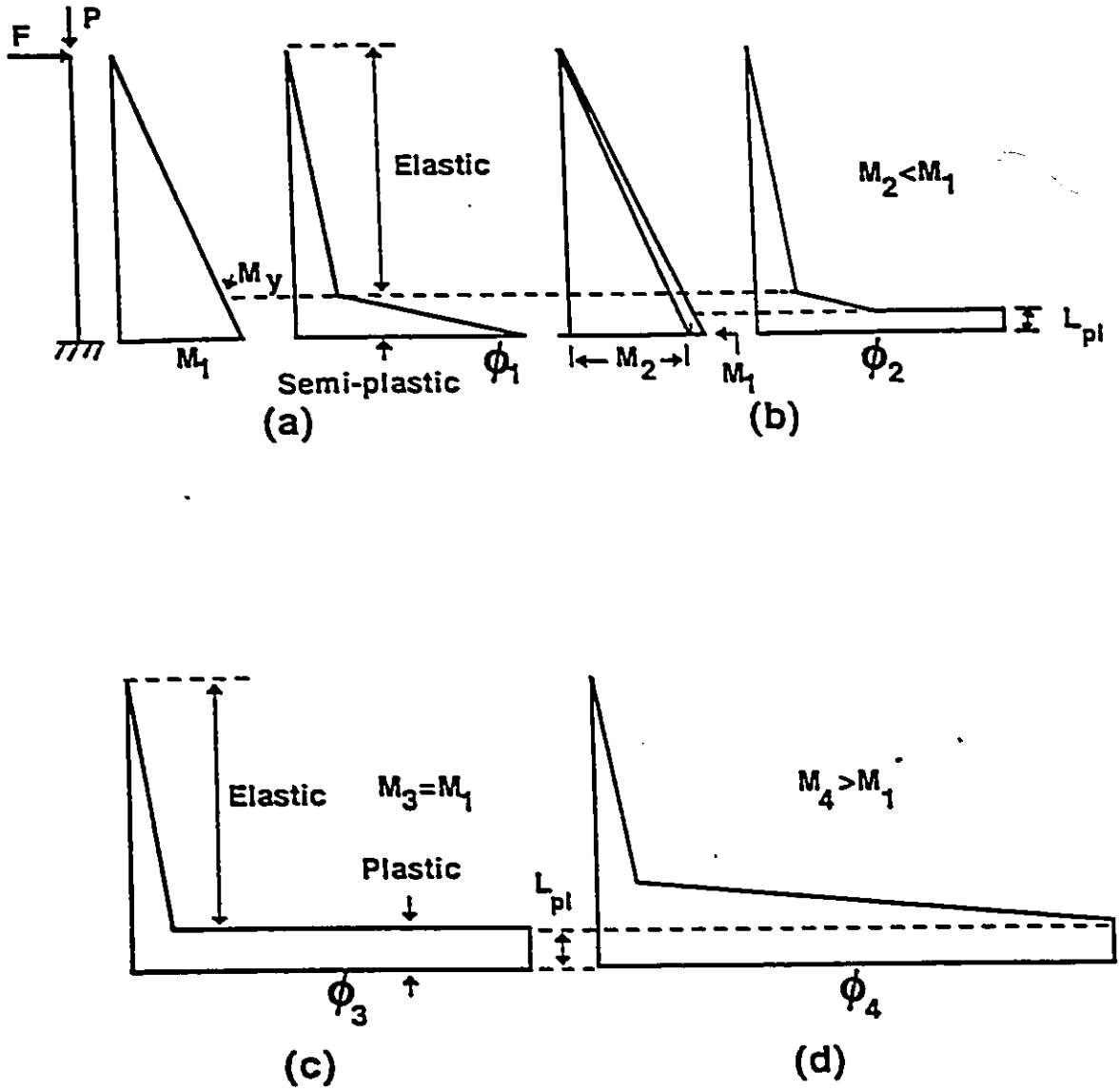

Fig. 80 Progressing of a Plastic Hinge [21]

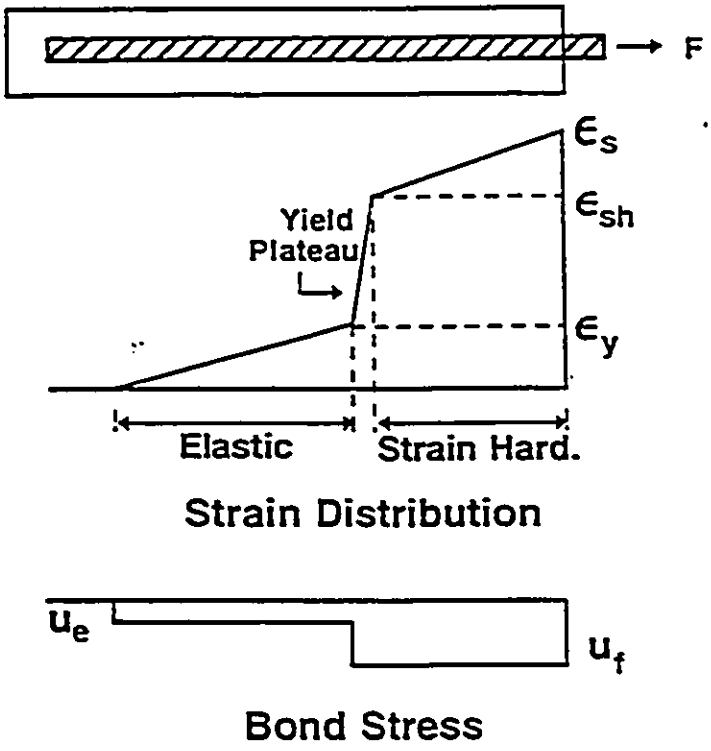

Fig. 81 Strain and Bond Stress in Anchored Reinforcement [22]

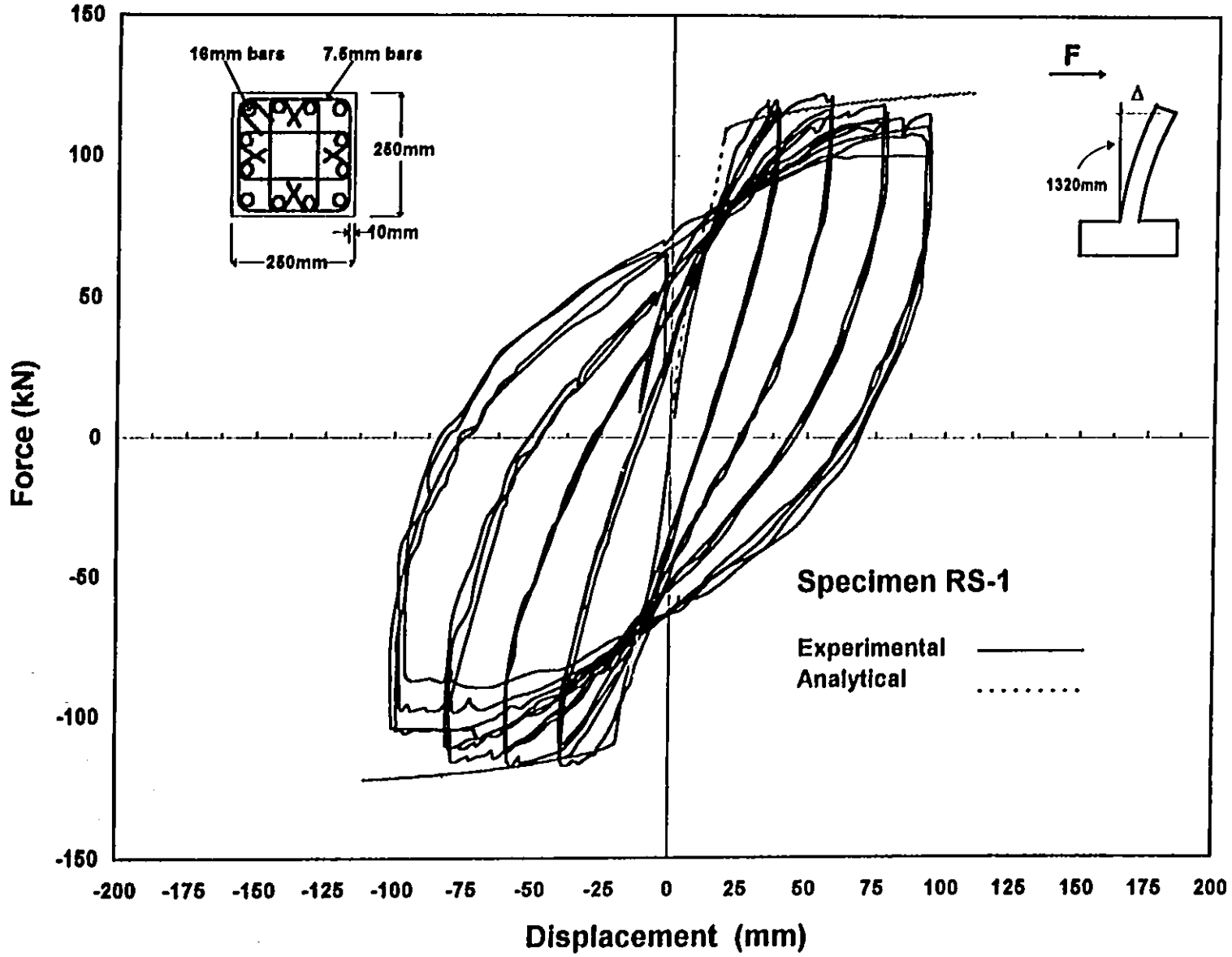

Fig. 82 Analytical and Experimental Force - Column Tip Displacement Relationships
Excluding P-Δ Effect

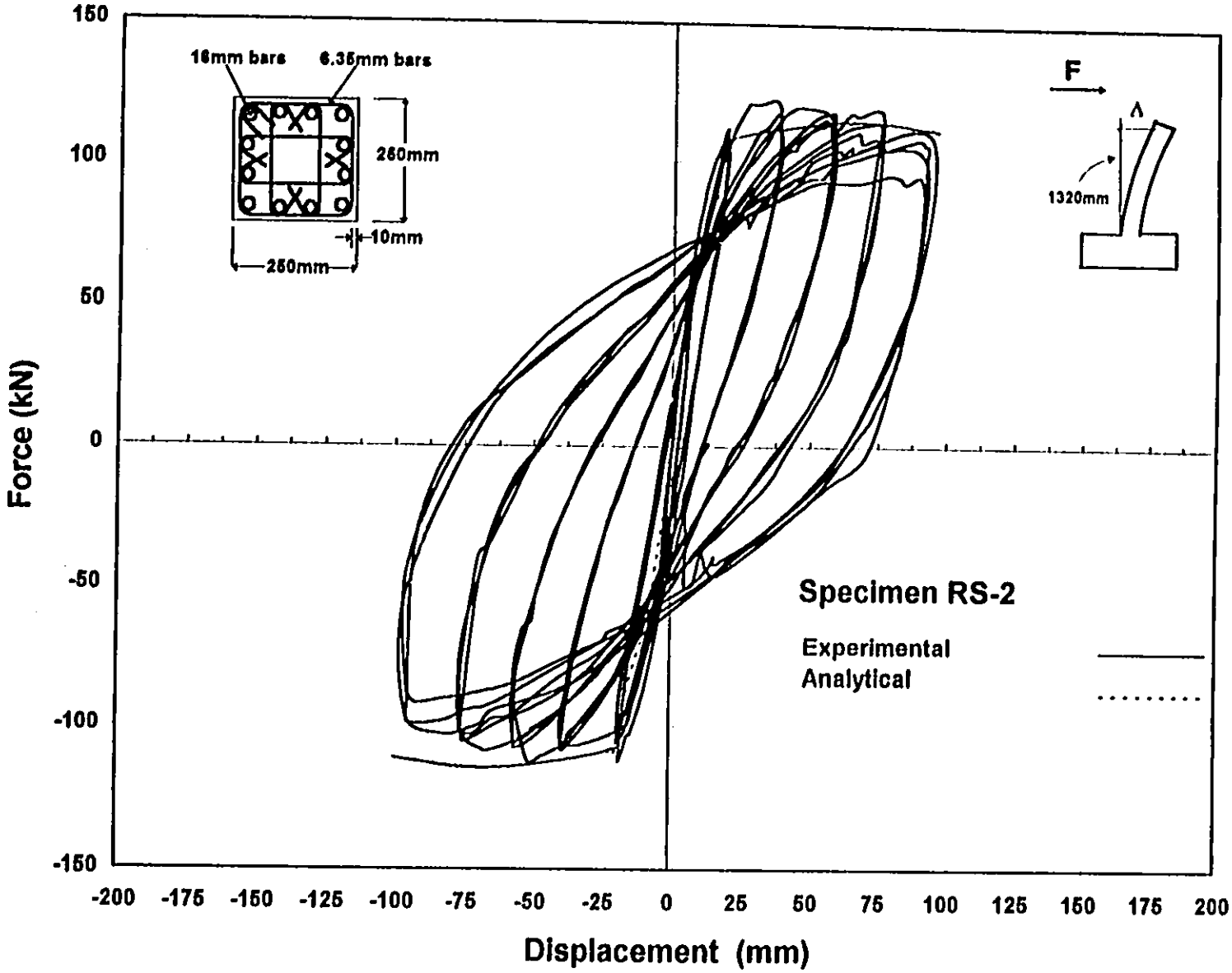

Fig. 83 Analytical and Experimental Force - Column Tip Displacement Relationships Excluding P-Δ Effect

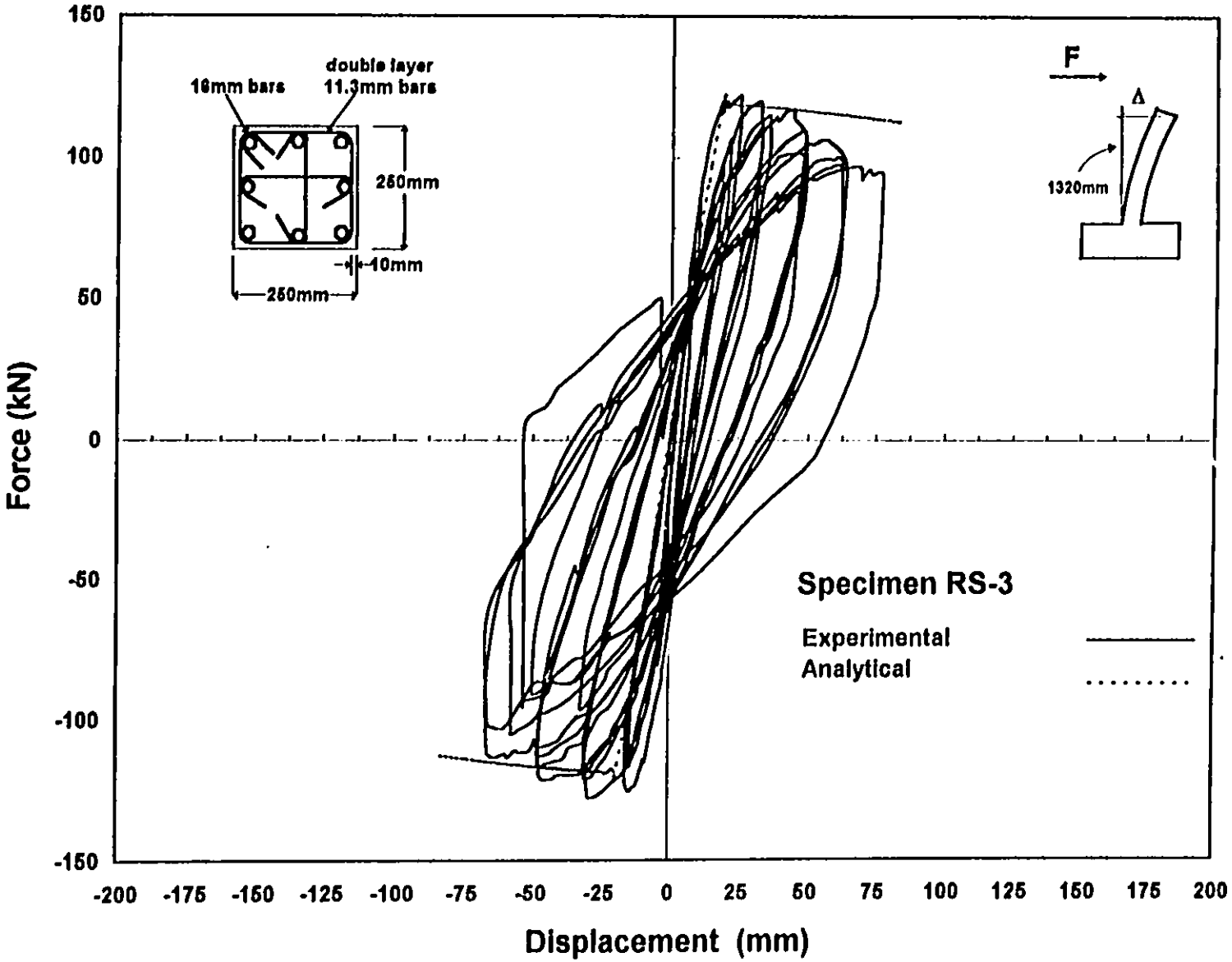

Fig. 84 Analytical and Experimental Force - Column Tip Displacement Relationships
Excluding P-Δ Effect

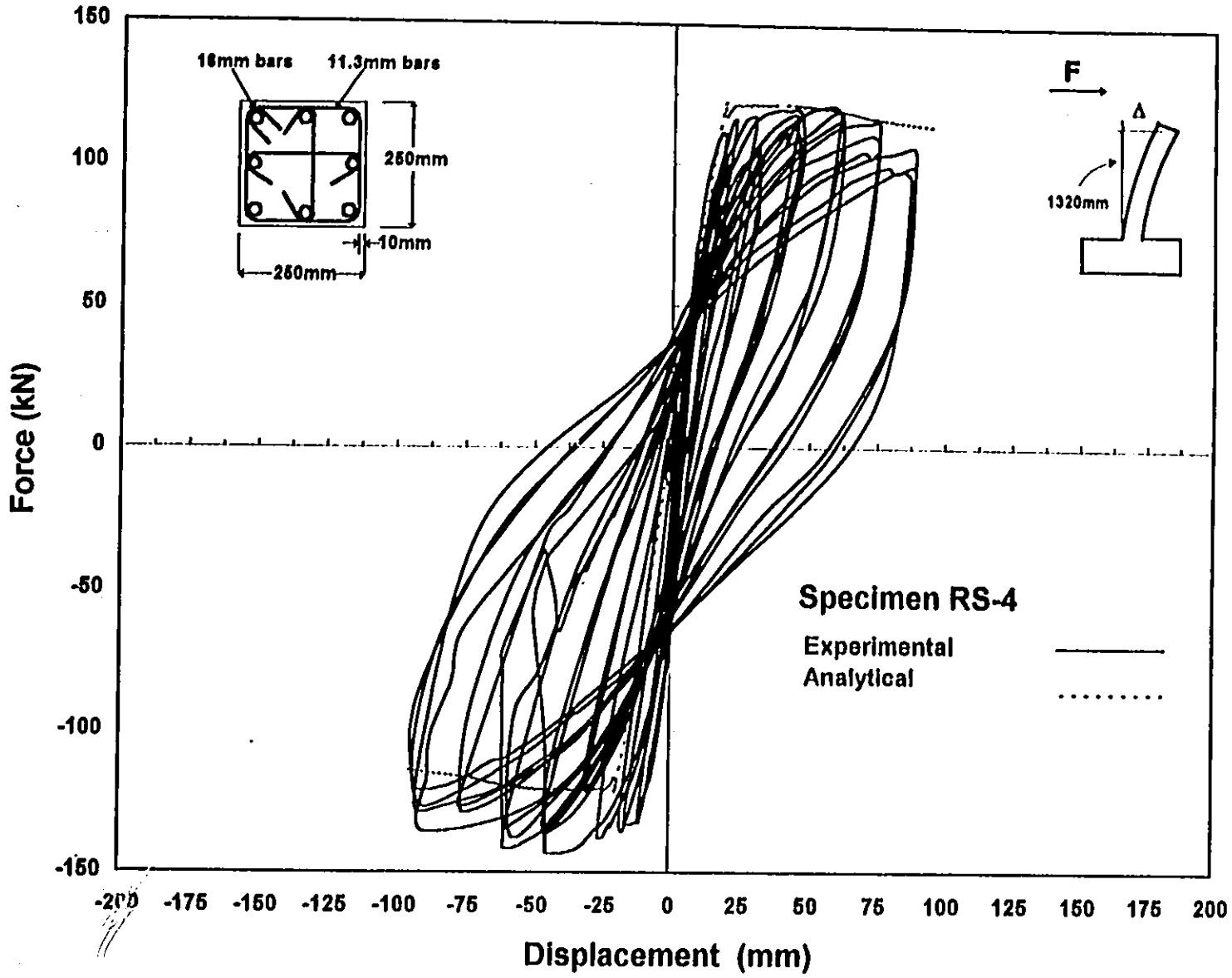

Fig. 85 Analytical and Experimental Force - Column Tip Displacement Relationships Excluding P-Δ Effect

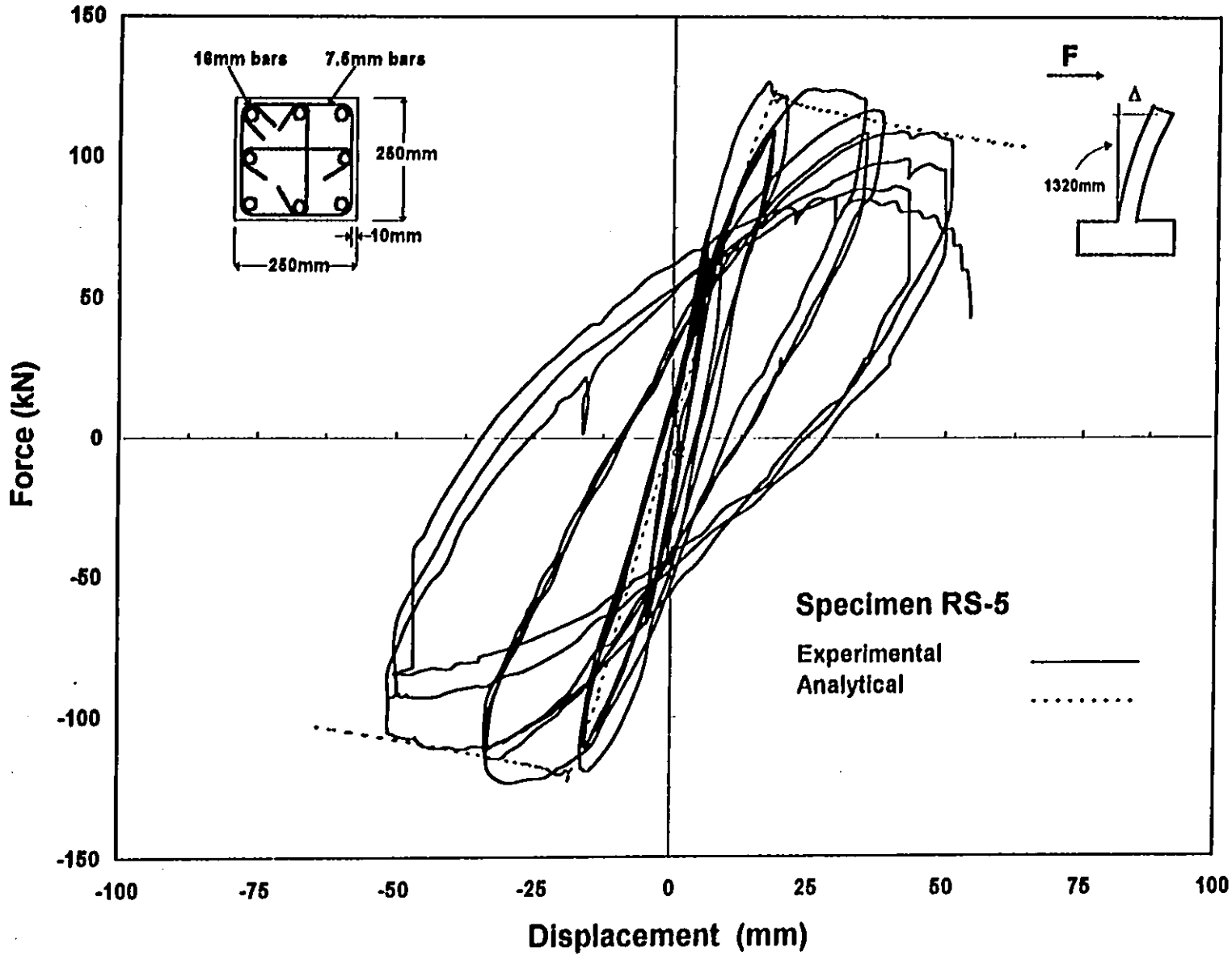

Fig. 86 Analytical and Experimental Force - Column Tip Displacement Relationship
Excluding P-Δ Effect

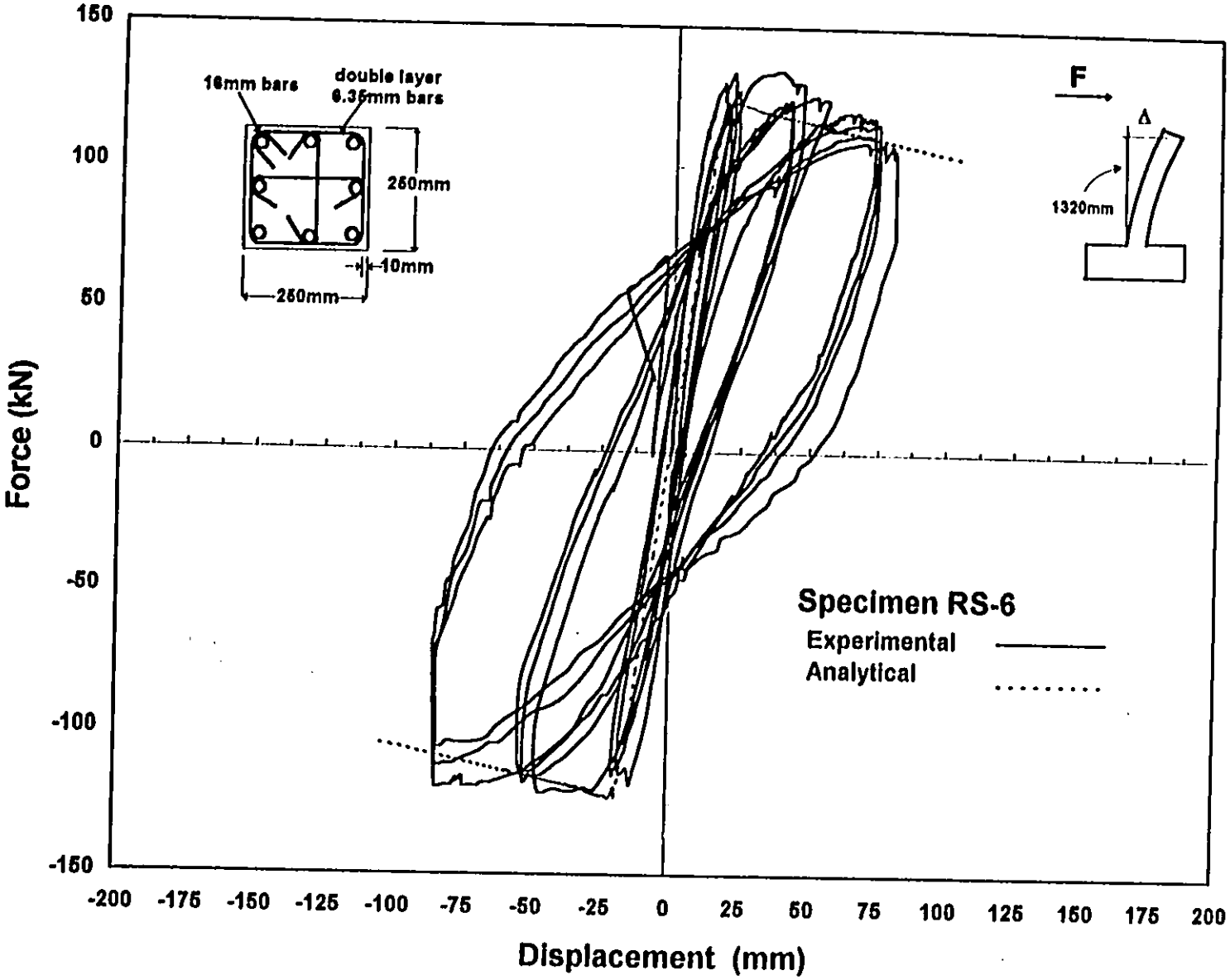

Fig. 87 Analytical and Experimental Force - Column Tip Displacement Relationship
Excluding P-Δ Effect

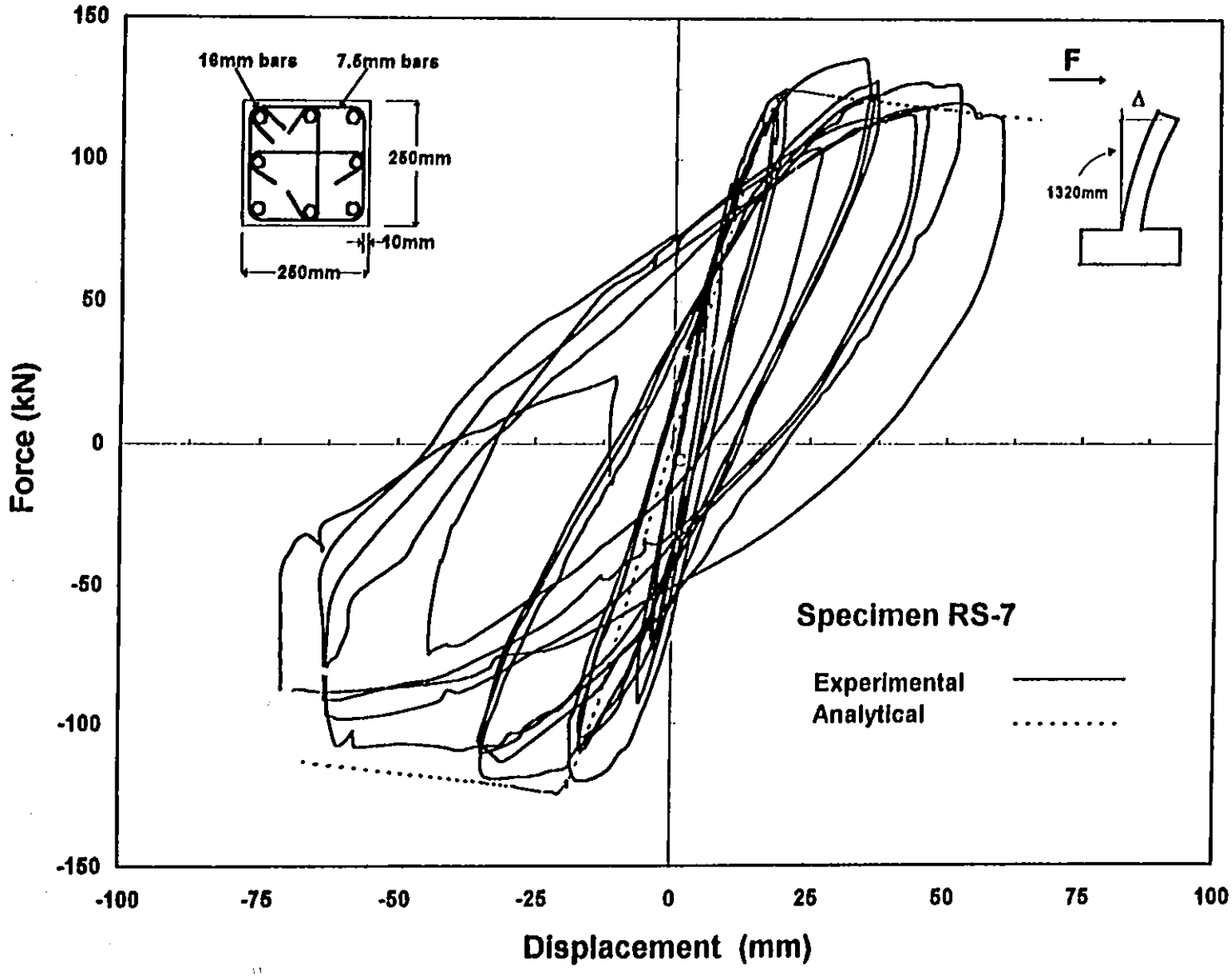

Fig. 88 Analytical and Experimental Force - Column Tip Displacement Relationship Excluding P-Δ Effect

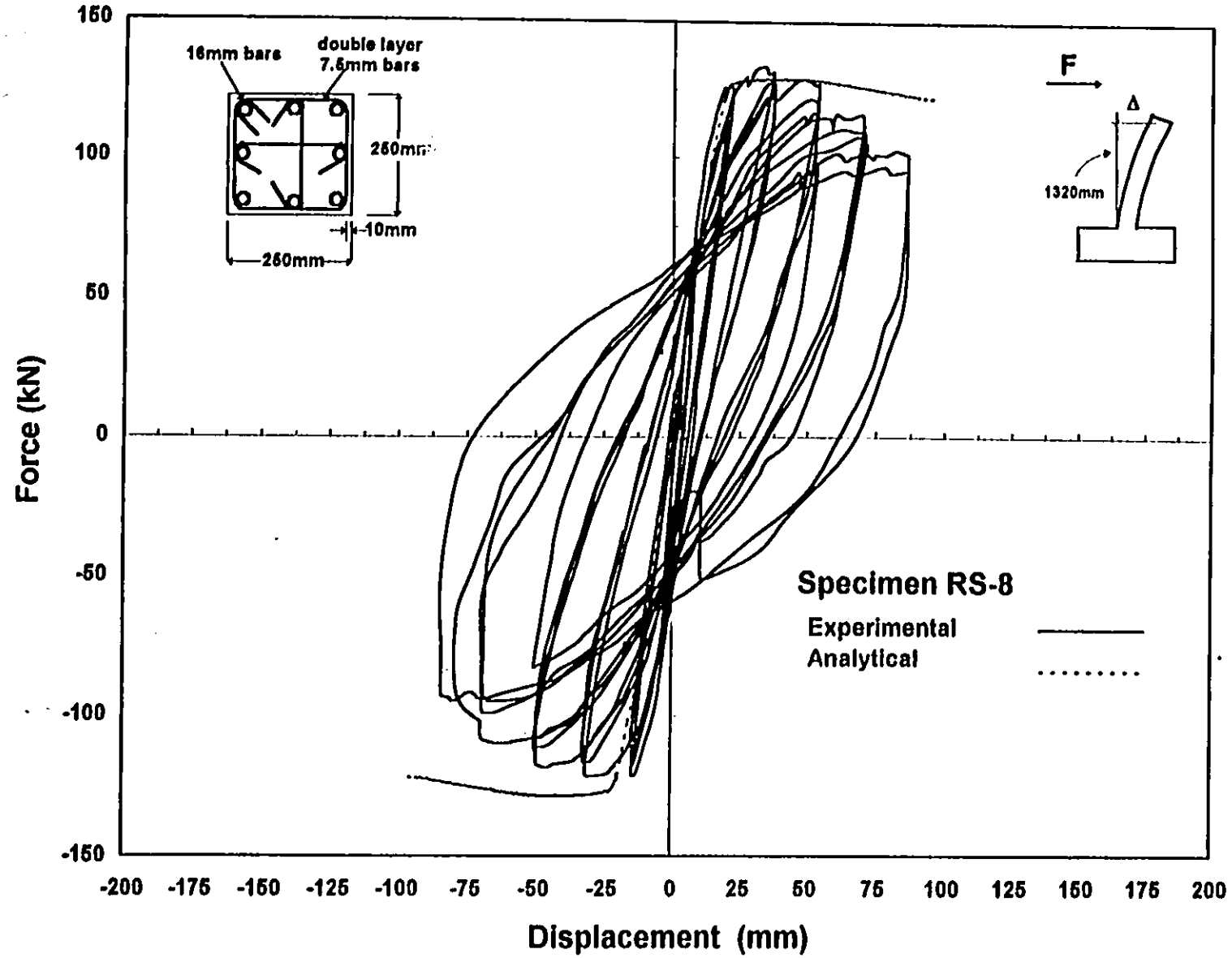

Fig. 89 Analytical And Experimental Force - Column Tip Displacement Relationship Excluding P-Δ Effect

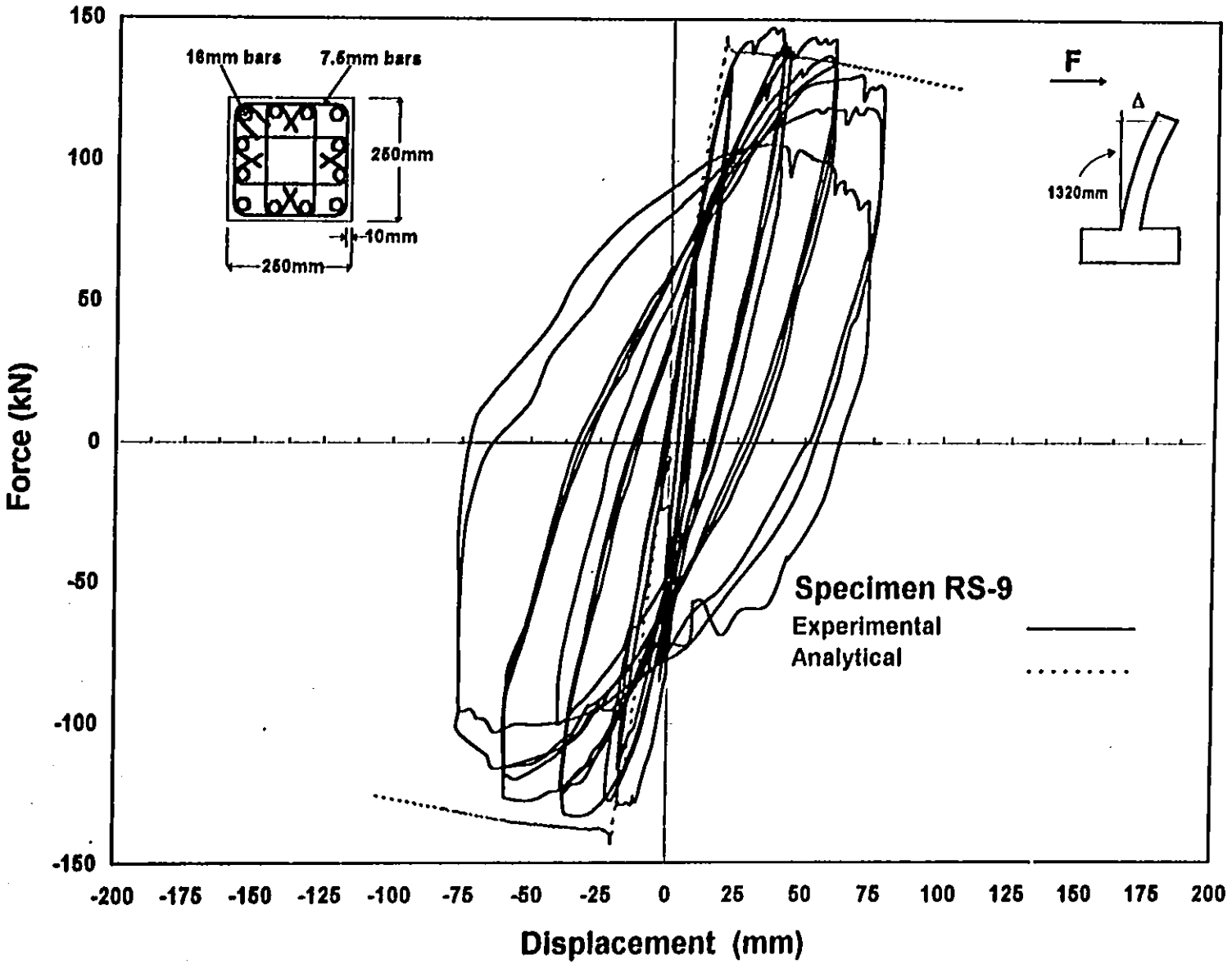

Fig. 90 Analytical and Experimental Force - Column Tip Displacement Relationships Excluding P-Δ Effect

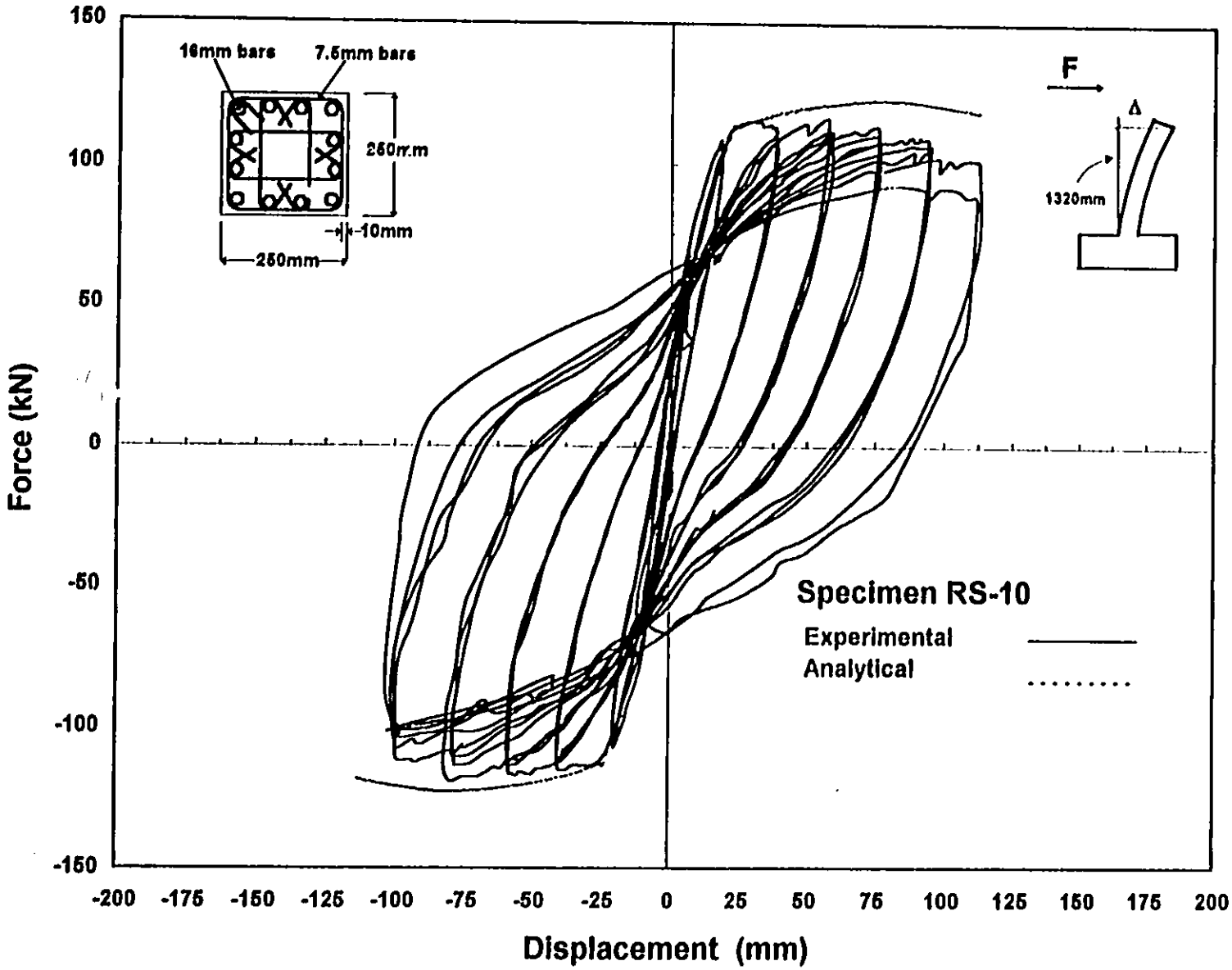

Fig. 91 Analytical and Experimental Force - Column Tip Displacement Relationships
Excluding P-Δ Effect

Chapter 5

Summary and Conclusions

5.1 Summary

Strength and deformability of square HSC columns were investigated experimentally. A total of 10 full-scale columns were tested under constant axial compression and lateral deformation reversals. The columns were confined with different confinement reinforcement to study the effects of confinement parameters on behaviour of HSC columns. The parameters considered include concrete strength; volumetric ratio, spacing, strength, and arrangement of transverse reinforcement; and axial compression. The recorded test data consisted of inelastic force-displacement and moment rotation hysteretic relationships at selected points along column height, as well as strain profiles in longitudinal and transverse reinforcement.

Inelastic analyses of columns were conducted starting from sectional behaviour. Plane section analysis was conducted for each column to establish moment-

curvature relationship based on a confined concrete model. Column rotations and displacements were then computed using the curvature distribution along column height and a model that simulates the plastification of column hinging region. The analytical results were compared with experimentally recorded force-displacement relationships.

5.2 Conclusions

The following conclusions can be drawn from the experimental and analytical investigations reported in this thesis.

- High-strength concrete columns with concrete strengths of up to 100 MPa can be designed to perform in a ductile manner under simulated seismic loading. However, the volumetric ratio of confinement steel required for HSC is higher than that commonly used for conventional-strength concrete columns.

- Deformability of HSC columns decreases with increasing concrete strength. A 104 MPa concrete column tested in this investigation developed approximately 4% lateral drift prior to rapid degradation of strength, as compared to a companion column with 64 MPa concrete which showed no strength degradation until after 6% lateral drift.

- The volumetric ratio of transverse reinforcement is an important parameter that provides confinement to the core concrete and stability to the longitudinal column reinforcement. The 104 MPa columns tested in this investigation showed reasonably ductile behaviour, with little or no strength degradation up to 4% lateral drift when the volumetric ratio was 2.5% and higher. The column with 1.9% volumetric ratio showed strength degradation immediately after the

peak load, exhibiting brittle response.

- The grade of lateral reinforcement has an effect on confinement of HSC columns. Columns with higher grade lateral reinforcement were able to sustain similar inelastic deformations as those with lower grade steel, with increased tie spacing. The results further indicate that the increase in strength of lateral reinforcement also makes up for some reduction in the volumetric ratio of transverse reinforcement. The strain gauge data indicate that although increased tensile stresses were developed in high-strength transverse reinforcement, the level of stress was not high enough to suggest yielding of steel. The column tested under low axial compression did not develop higher stresses in transverse reinforcement than that corresponding to the yield strength of ordinary grade steel. This observation, coupled with earlier observations made on concentrically loaded columns may suggest that the effectiveness of higher-grade lateral reinforcement depends on the level of axial compression on a column.

- The spacing of tie reinforcement plays a major role in confinement of HSC columns. The column with approximately h/2 tie spacing, reflecting the maximum spacing for shear reinforcement, could only develop 3.5% lateral drift as compared to a companion column with approximately h/4 tie spacing that developed 5% lateral drift. It appears that the current maximum tie spacing limitation of h/4 for confinement of ordinary-strength concrete columns may also be appropriate for HSC columns.

- Well distributed and laterally supported longitudinal reinforcement provide superior confinement characteristics in HSC columns. Comparisons of companion columns indicate that the maximum spacing requirement may be

relaxed in HSC columns with closely spaced and laterally supported longitudinal reinforcement.

- The effect of axial compression is to reduce ductility in HSC columns. This suggests that the confinement steel requirements must be more stringent for heavily compressed columns.

- The analysis techniques commonly used for normal-strength concrete columns can also be used for HSC columns. Force-displacement relationships obtained from inelastic flexural analysis agree well with those recorded experimentally. It is important, however, to utilize proper material models for HSC and reinforcing steel. The confinement model developed recently by Razvi and Saatcioglu [16], based on HSC column tests under concentric compression, provide good estimates of column response under strain gradient.

- The rectangular stress block commonly used for normal-strength concrete columns can not be used for strength calculations of HSC columns. The stress-strain relationship of HSC shows almost linear ascending branch, as compared to parabolic distribution of lower strength concretes. Therefore, it may be more appropriate to use a triangular stress block or a rectangular stress block with an equivalent area for HSC columns. The test data indicates good correlations with recently suggested stress blocks for HSC.

APPENDIX A
STRAIN GAUGE DATA

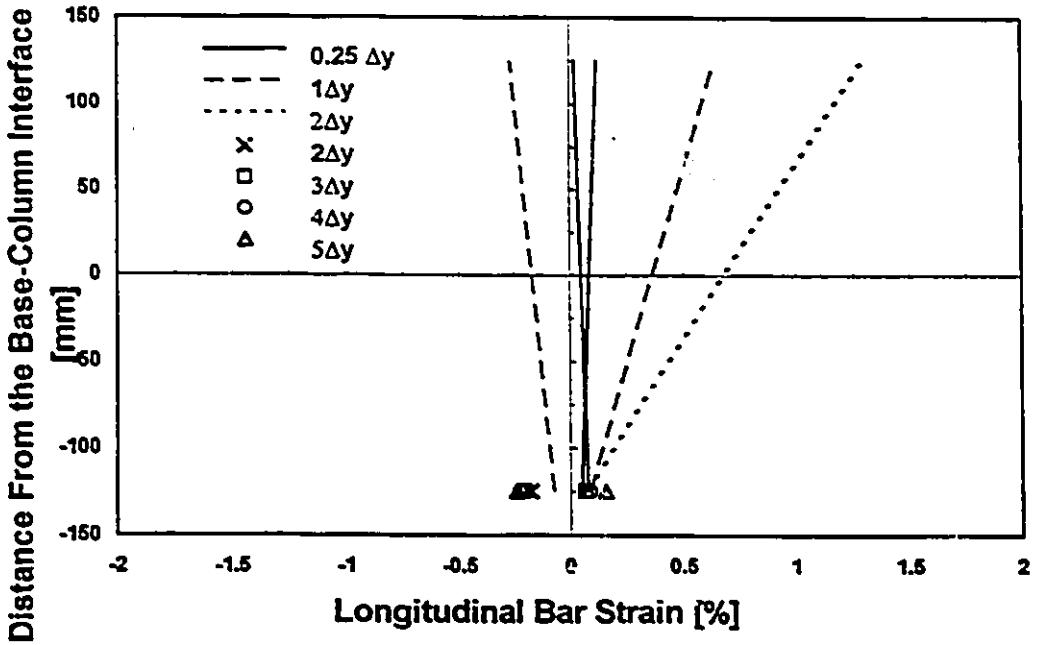

a) Three Straingage Bar

Fig. A.1 Longitudinal Bar Strains Measured in Specimen RS-1 - tension; +compression

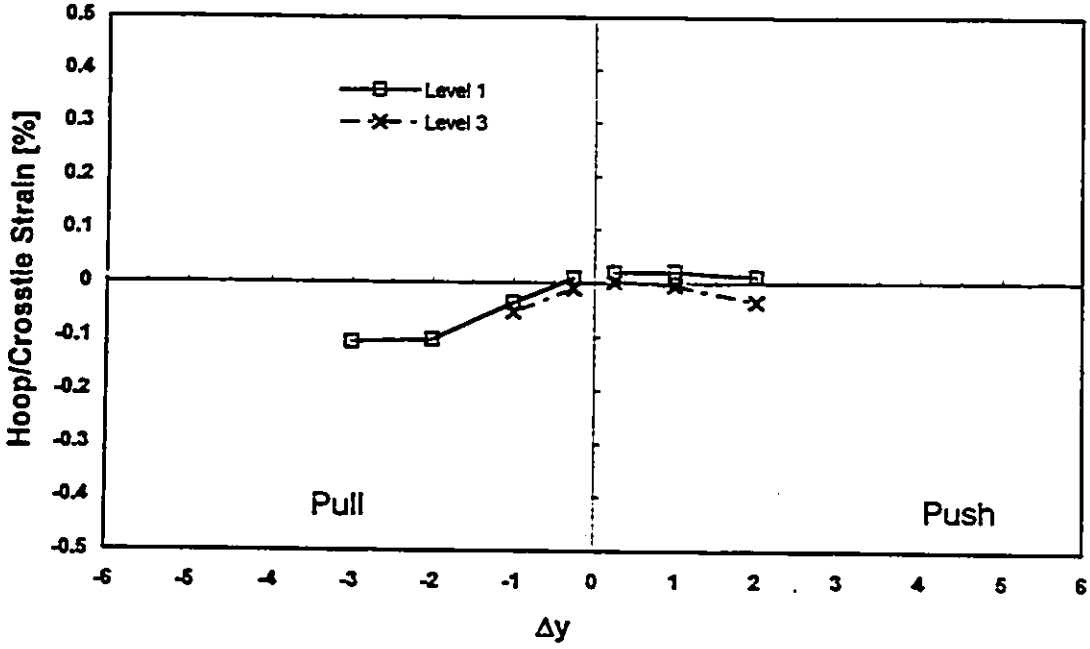

a) Strains at S1

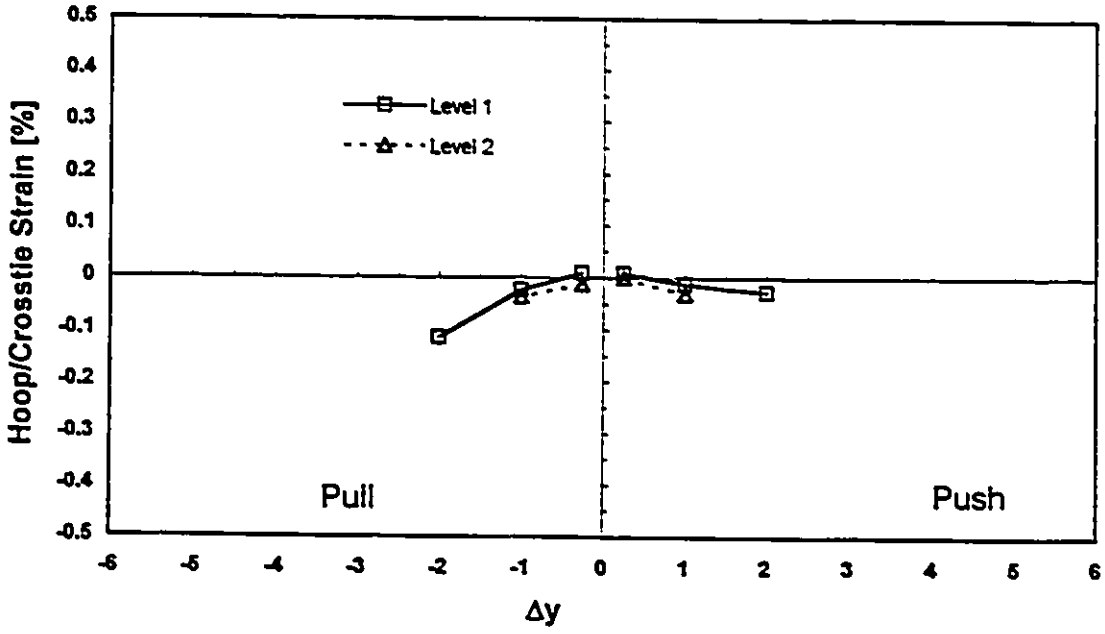

b) Strains at S2

Fig. A.2 Transverse Reinforcement Strains Measured in Specimen RS-1 (negative - in tension)

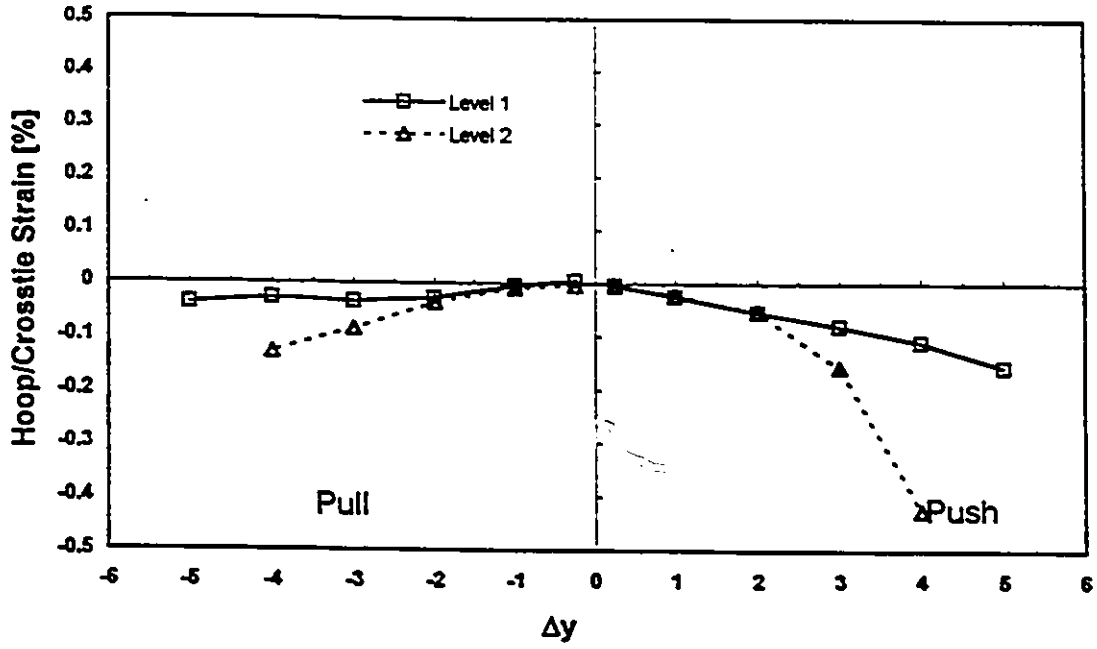

a) Strains at S3

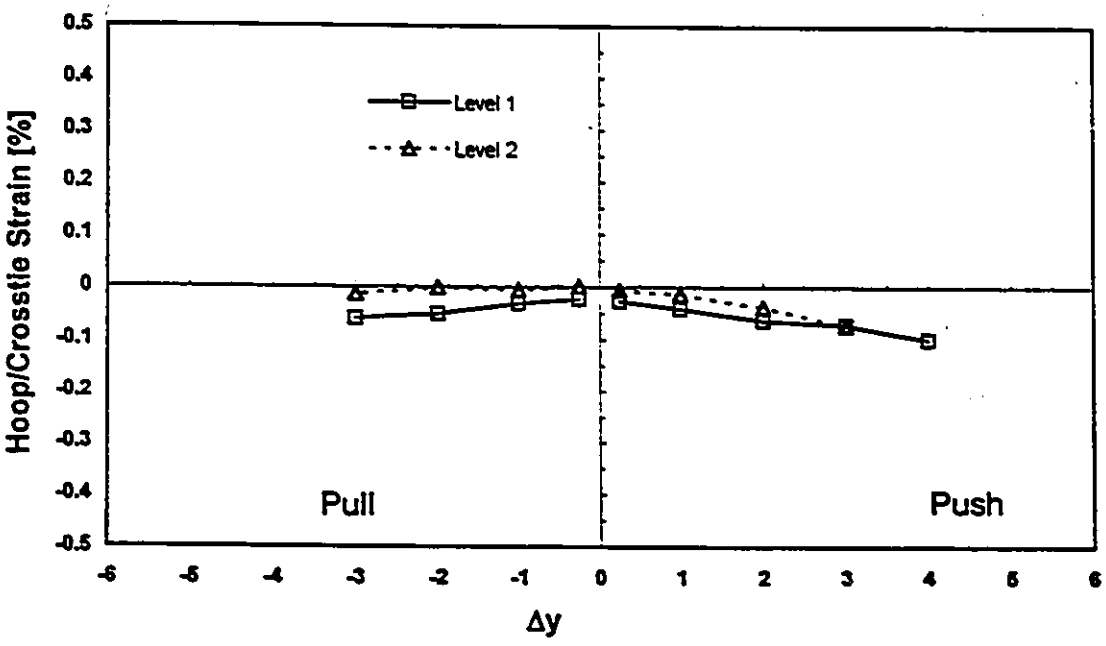

b) Strains at S4

Fig. A.2 Transverse Reinforcement Strains Measured in Specimen RS-1 - Continued (negative - in tension)

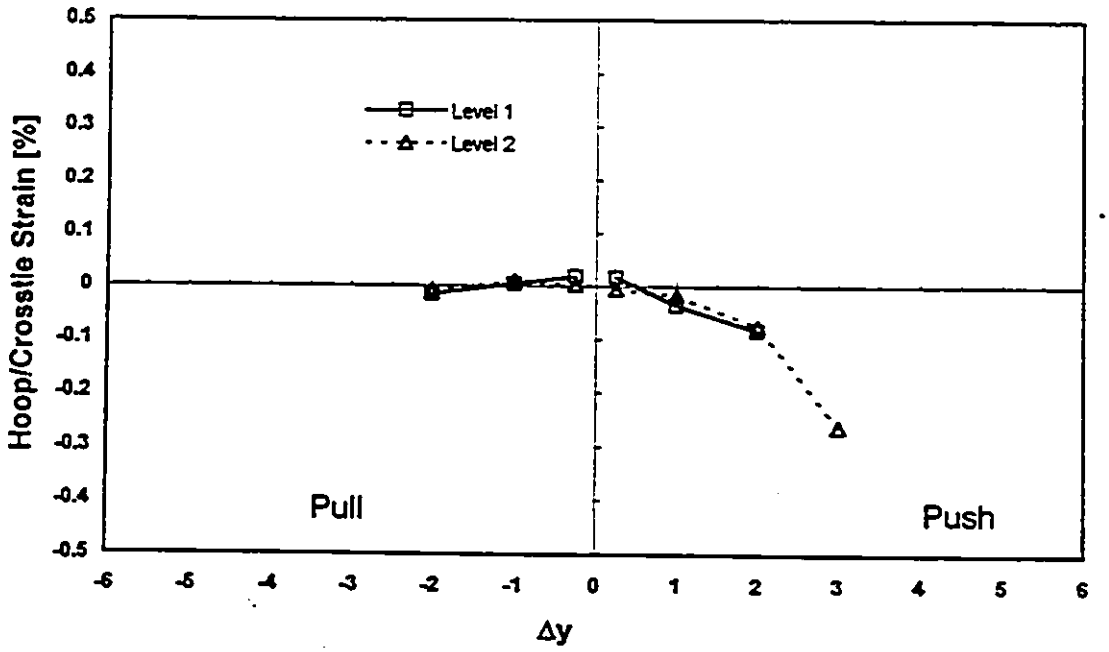

a) Strains at S5

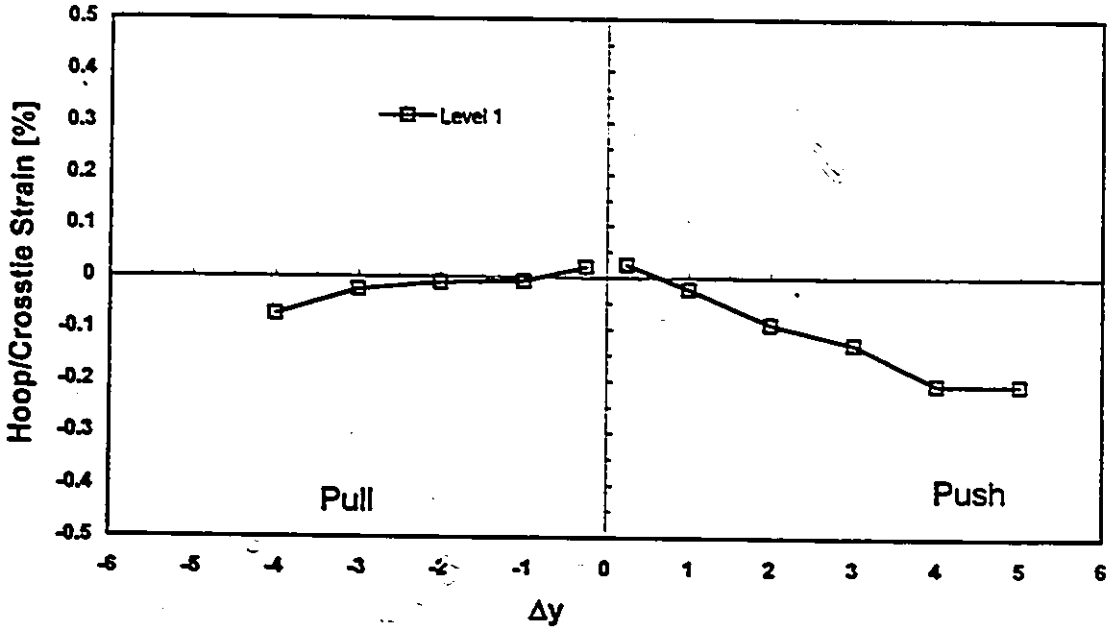

b) Strains at S6

Fig. A.2 Transverse Reinforcement Strains Measured in Specimen RS-1 - Continued (negative - in tension)

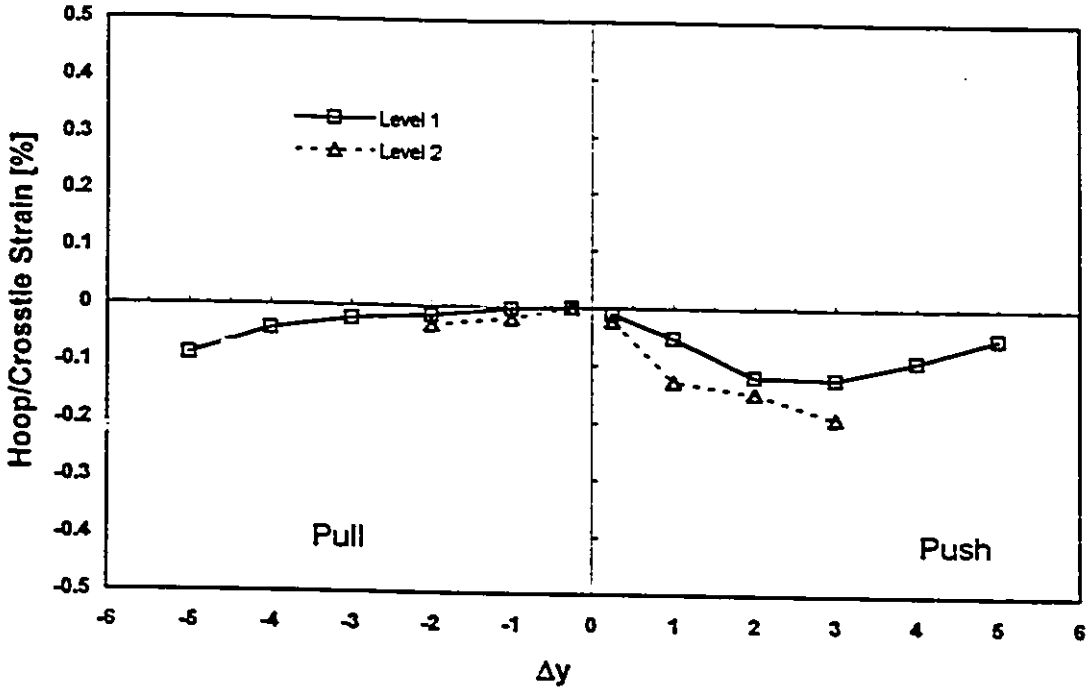

a) Strains at S7

Fig. A.2 Transverse Reinforcement Strains Measured in Specimen RS-1 - Continued (negative - in tension)

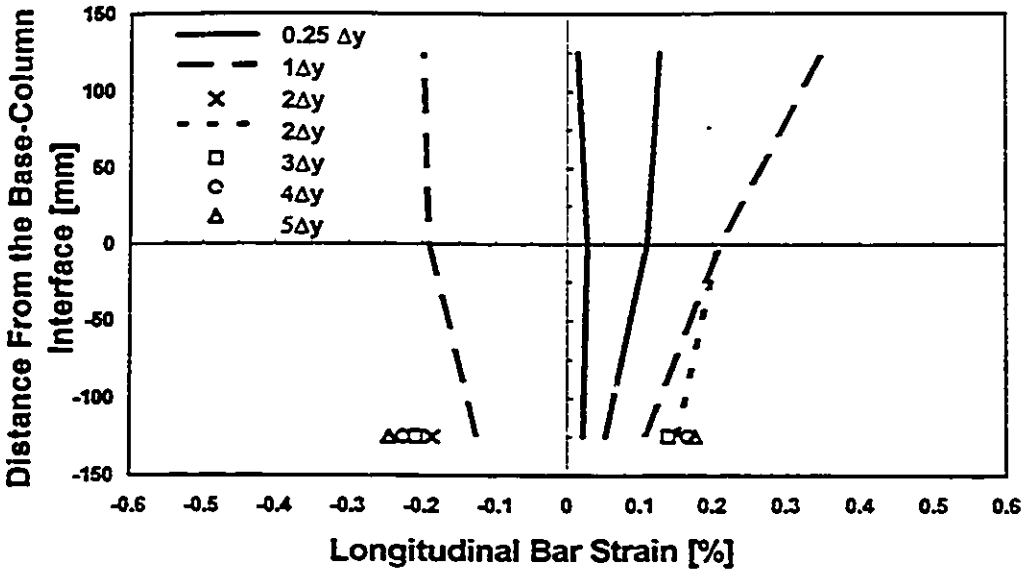

a) Three Straingage Bar

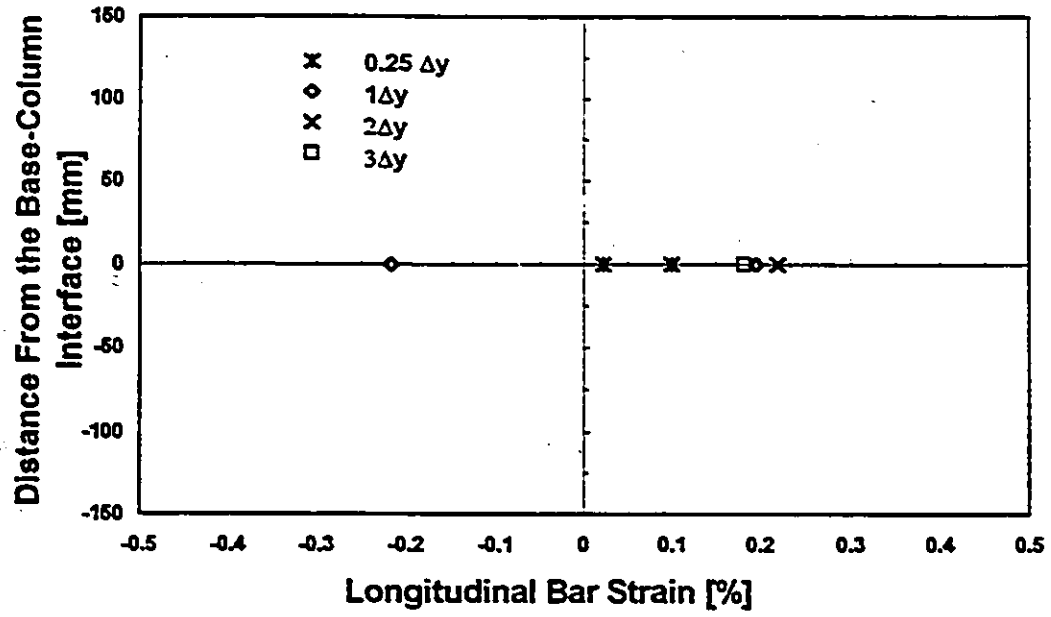

b) One Straingage Bar

Fig. A.3 Longitudinal Bar Strains Measured in Specimen RS-2 - tension; +compression

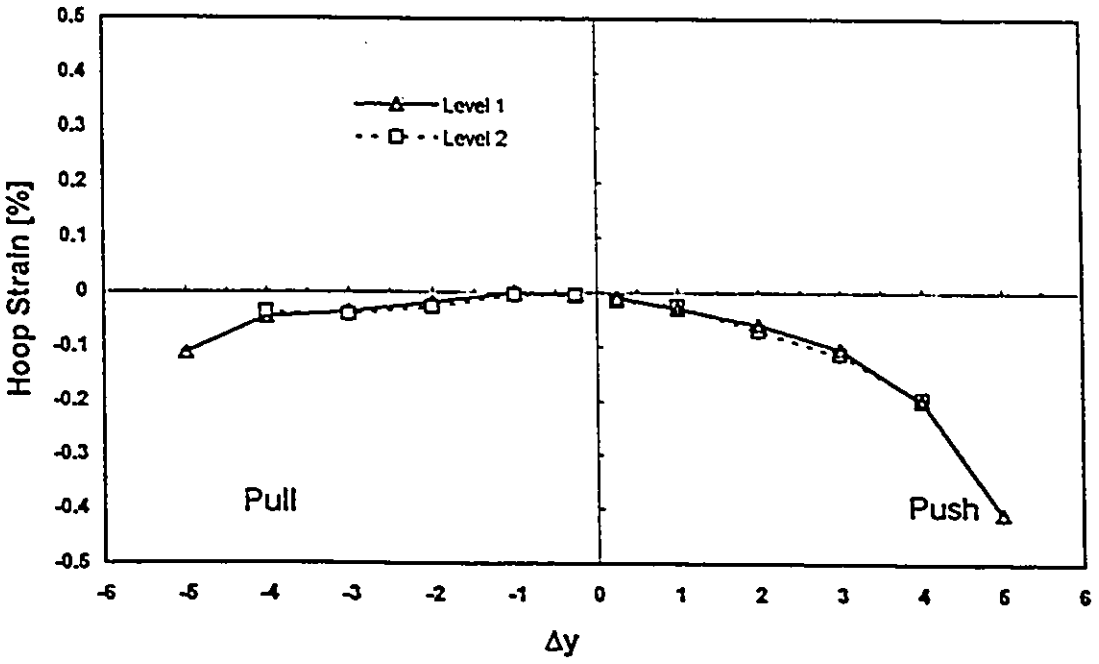

a) Strains at S3

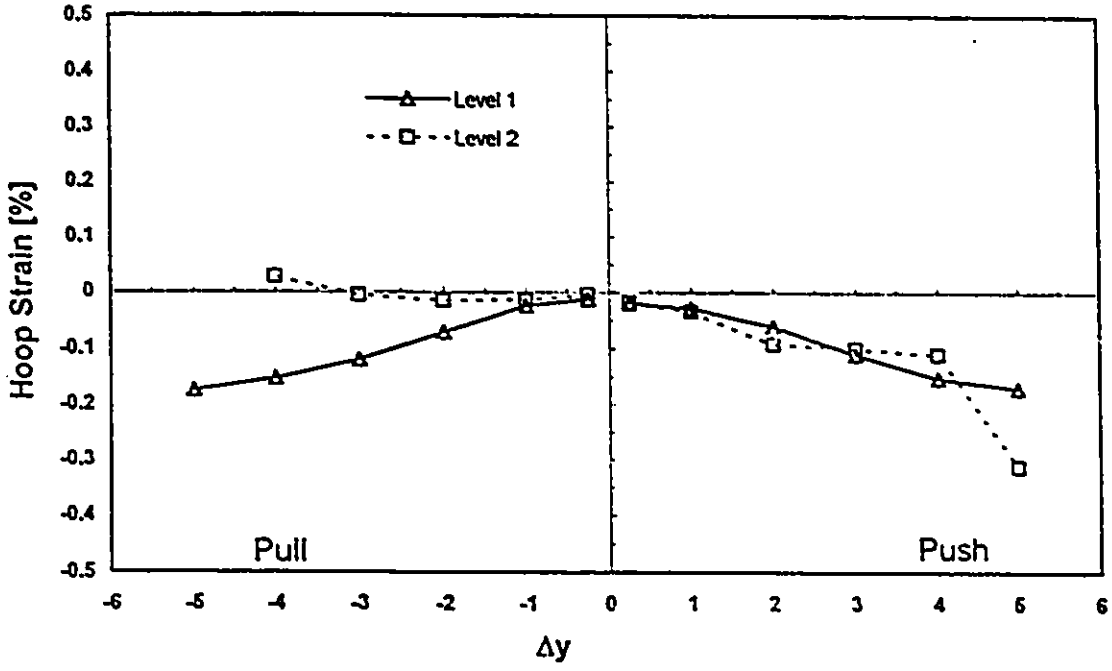

b) Strains at S4

Fig. A.4 Transverse Reinforcement Strains Measured in Specimen RS-2 - Continued (negative - in tension)

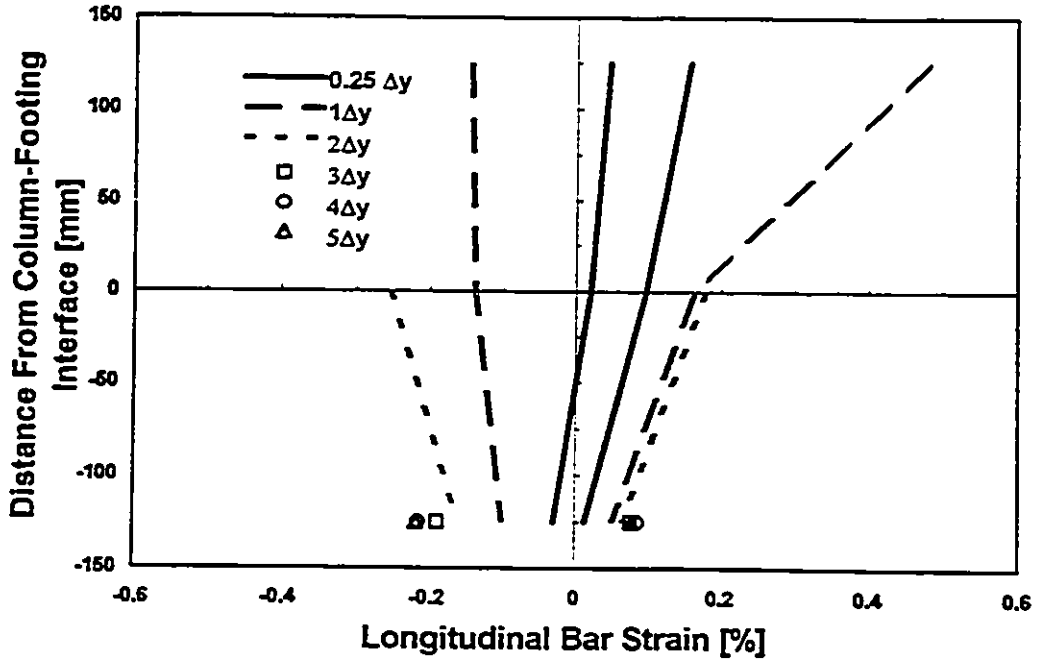

a) Three-Gauge Bar

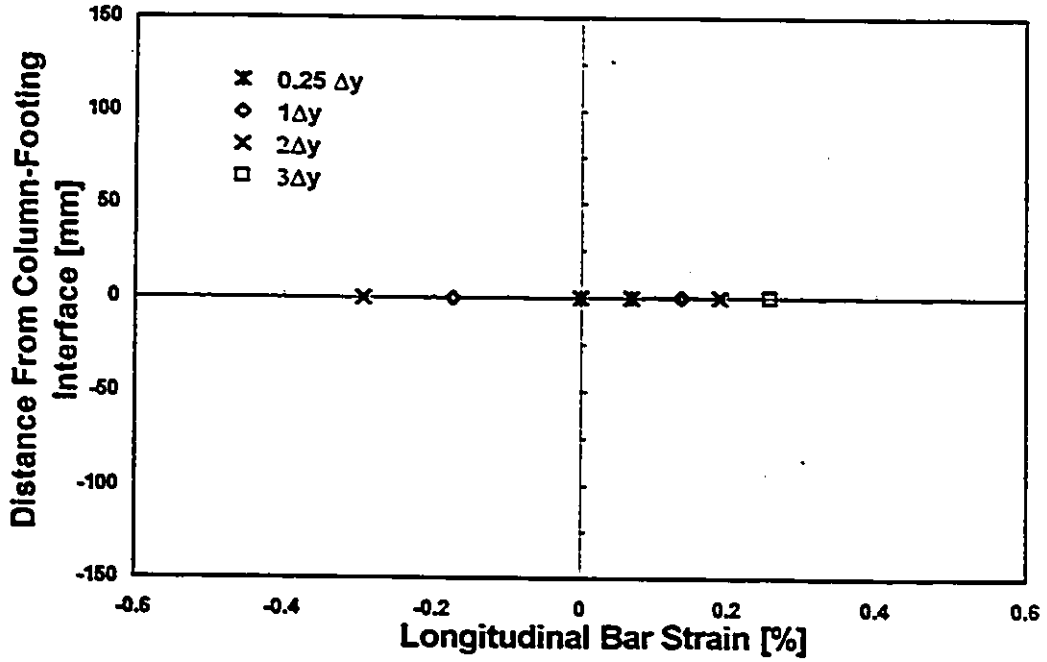

b) Single-Gauge Bar

Fig. A.5 Longitudinal Bar Strains Measured in Specimen RS-3 - tension; +compression

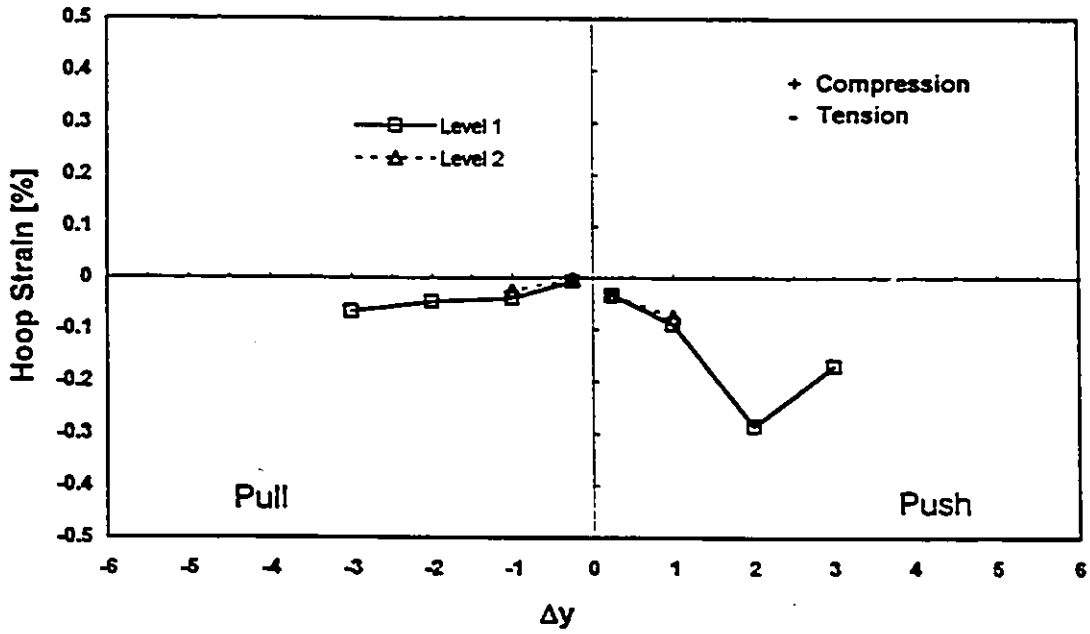

a) Strains at S1

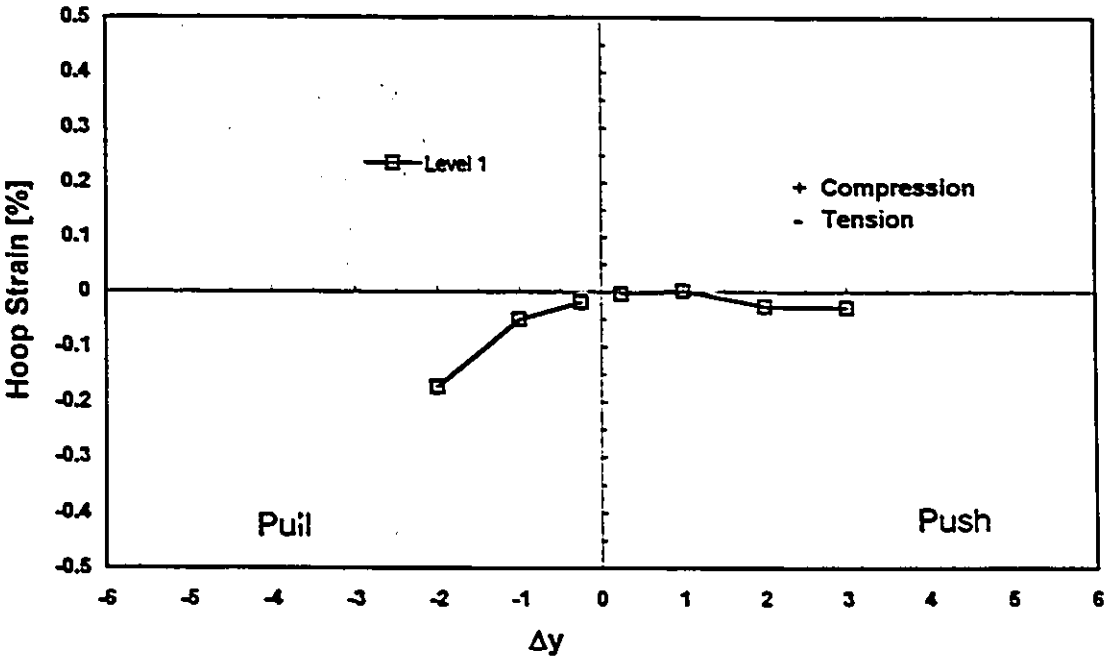

b) Strains at S3

Fig. A.6 Transverse Reinforcement Strains Measured in Specimen RS-3 (negative - in tension)

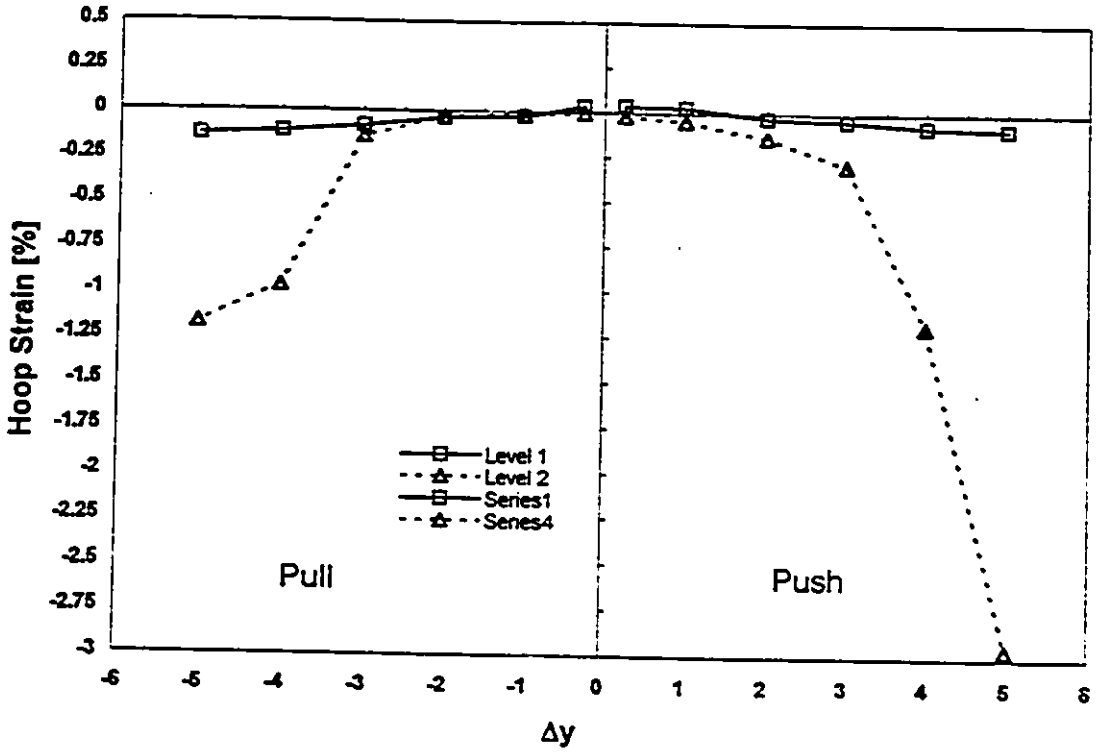

a) Strains at S4

Fig. A.6 Transverse Reinforcement Strains Measured in Specimen RS-3 - Continued (negative - in tension)

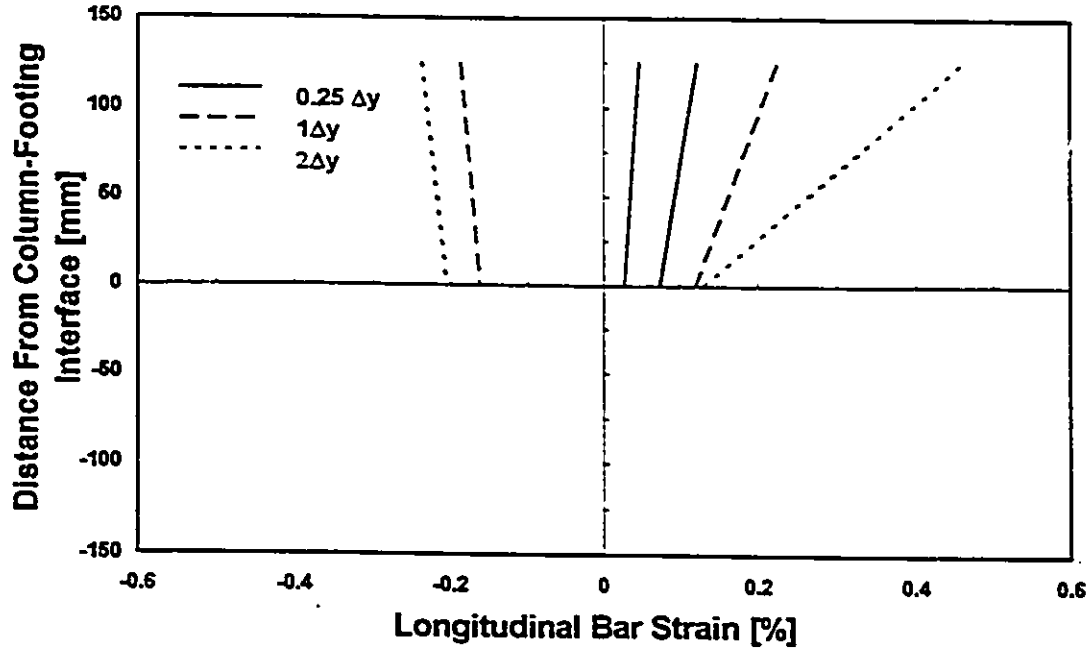

a) Three-Gauge Bar

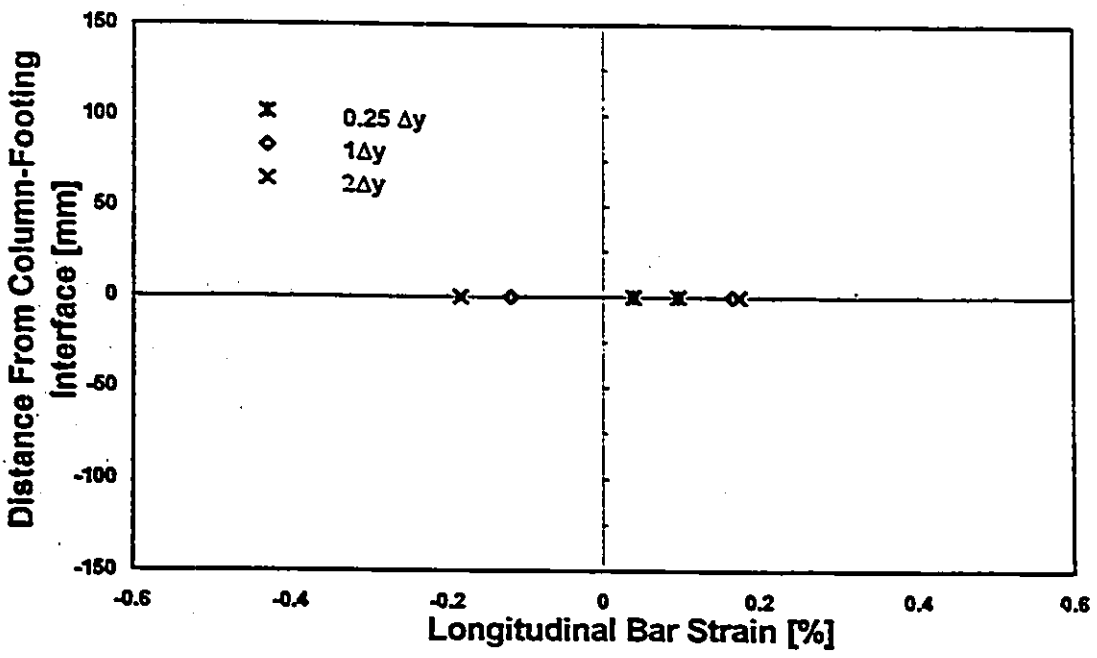

b) Single-Gauge Bar

Fig. 7 Longitudinal Bar Strains Measured in Specimen RS-4 - tension; + compression

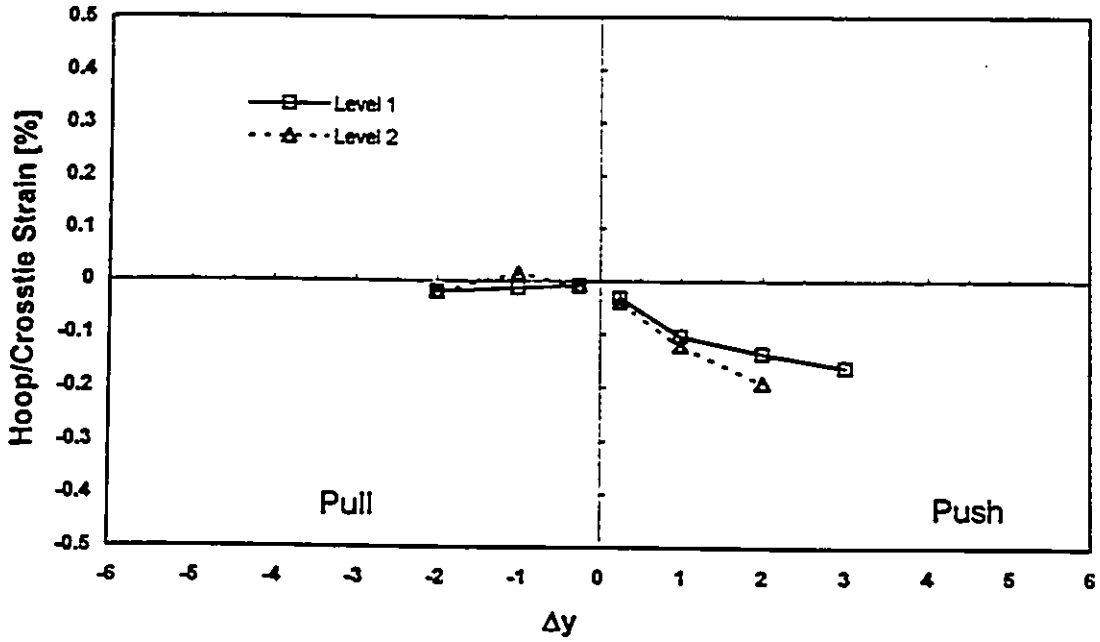

a) Strains at S1

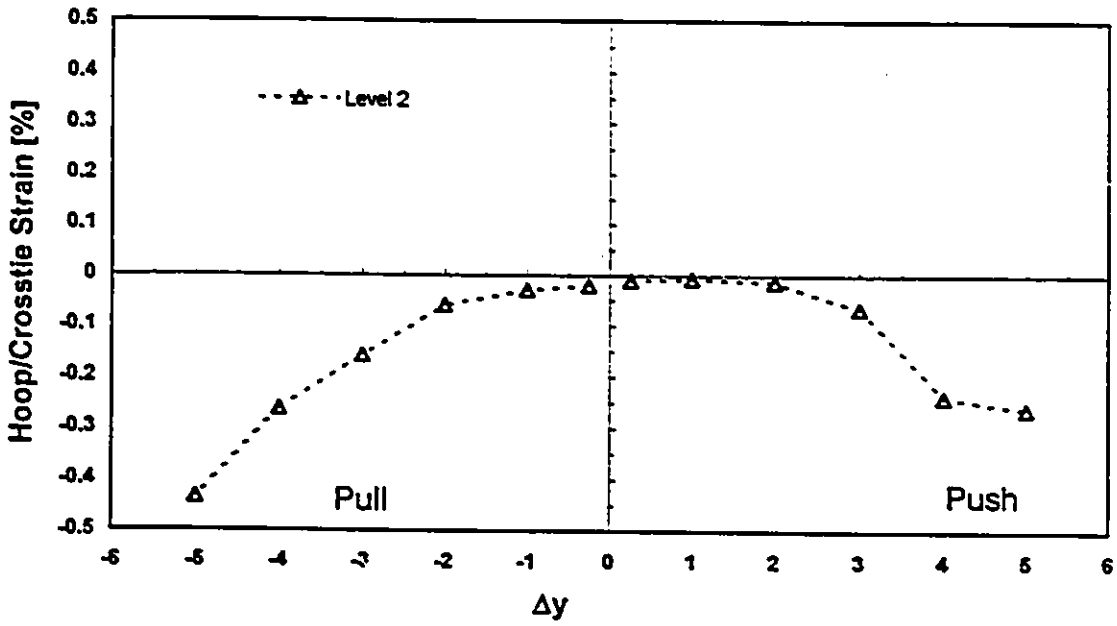

b) Strains at S2

Fig. A.8 Transverse Reinforcement Strains Measured in Specimen RS-4 (negative - in tension)

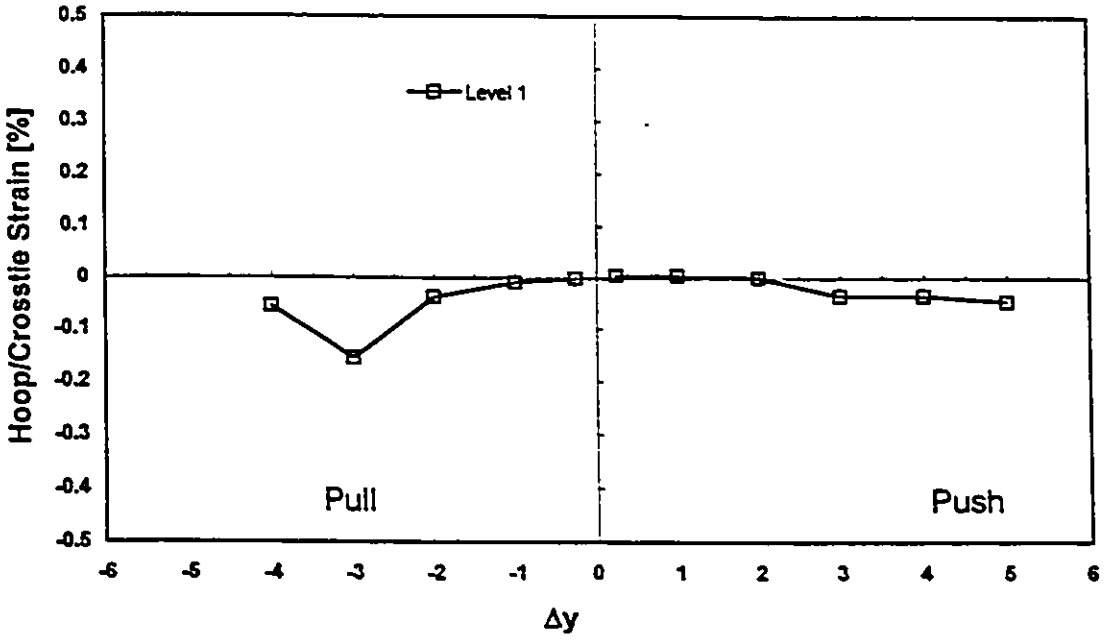

a) Strains at S3

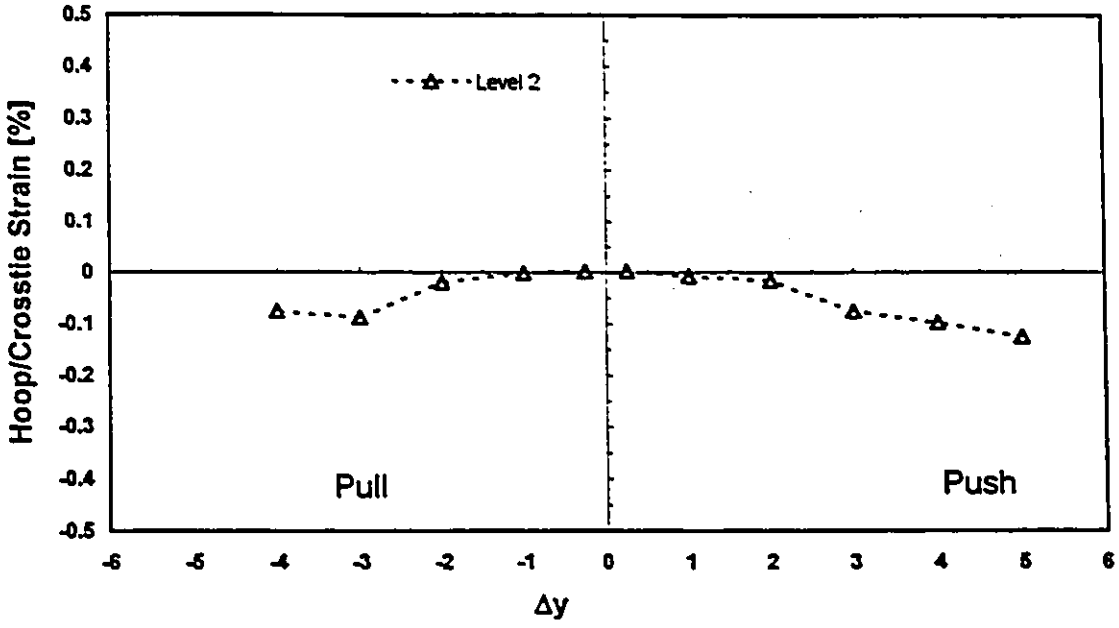

b) Strains at S4

Fig. A.8 Transverse Reinforcement Strains Measured in Specimen RS-4 - Continued (negative - in tension)

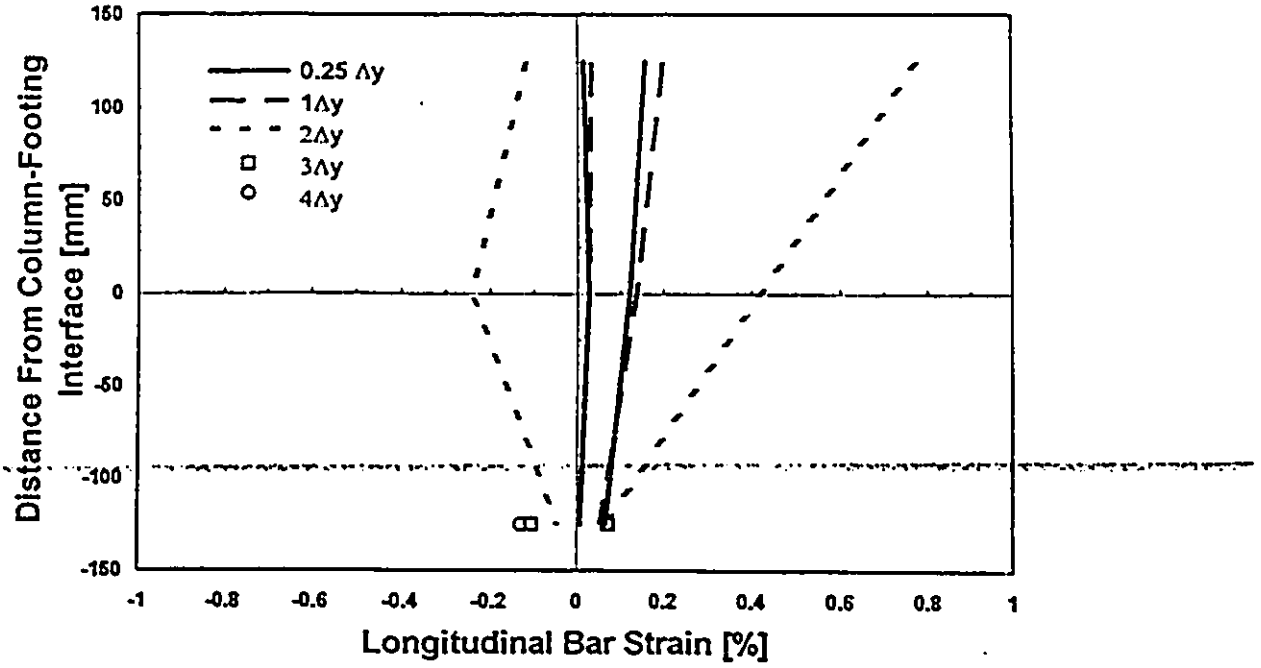

a) Three-Gauge Bar

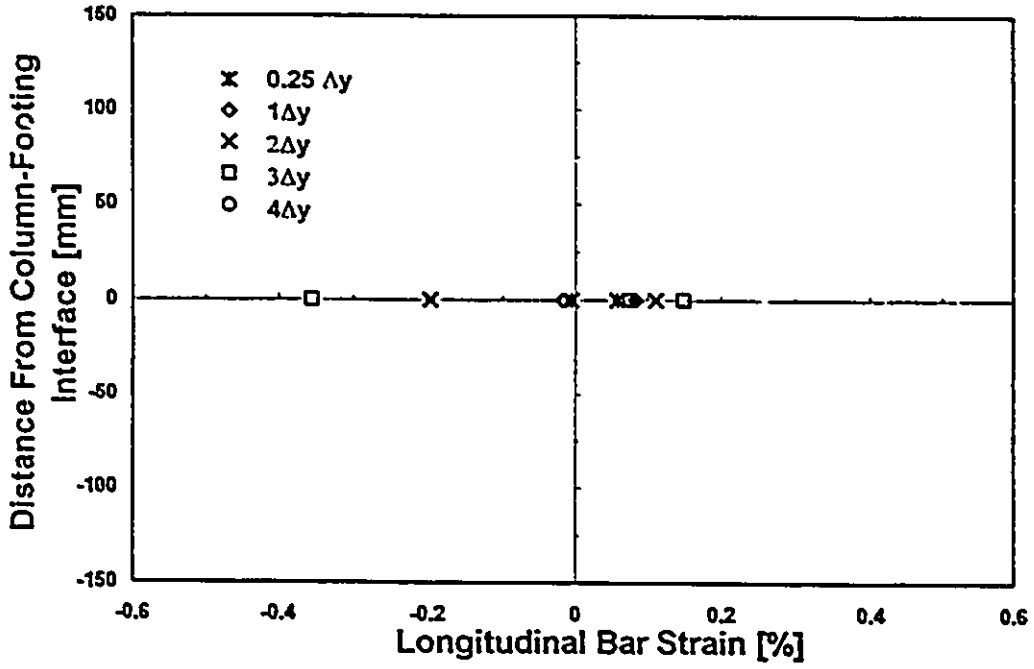

b) Single-Gauge Bar

Fig. A.9 Longitudinal Bar Strains Measured in Specimen RS-5 - tension; + compression

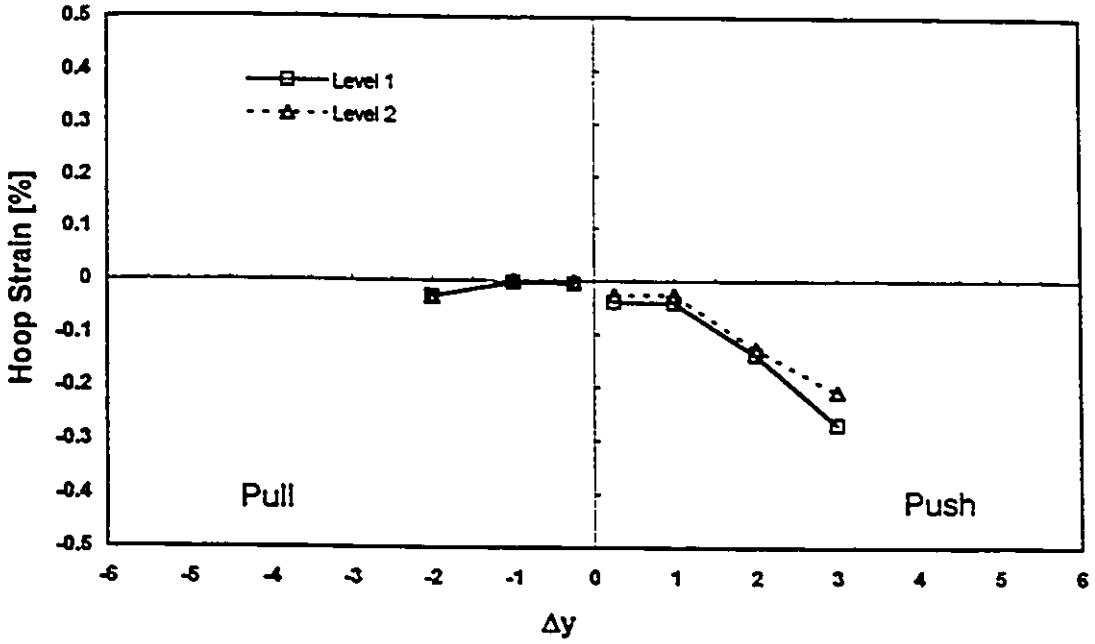

a) Strains at S1

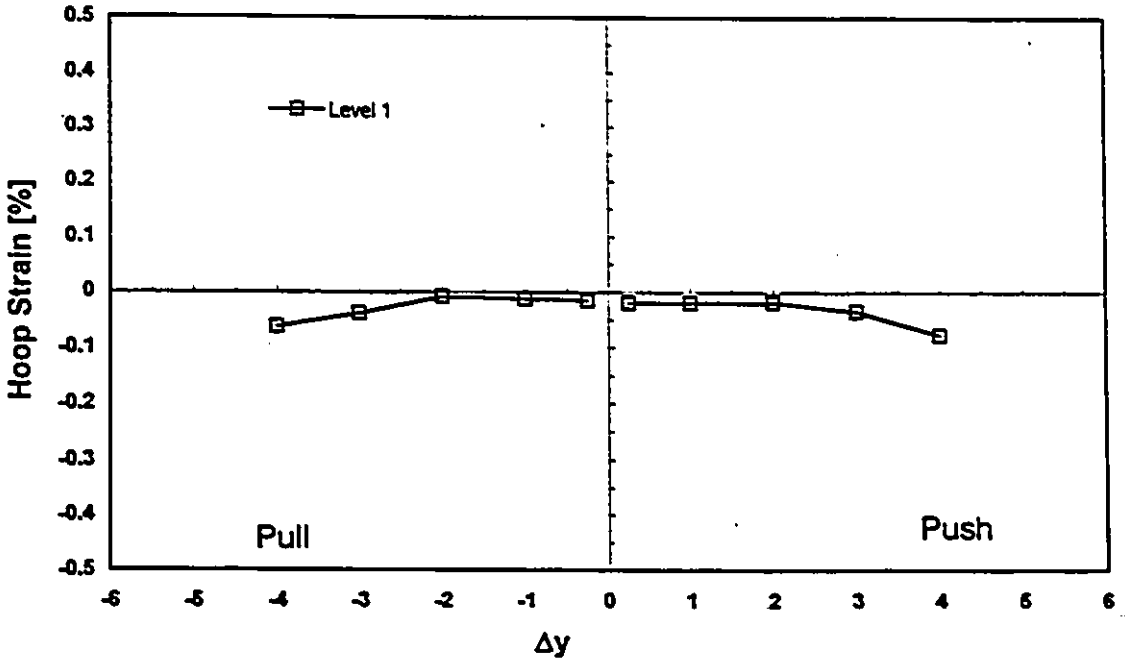

b) Strains at S3

Fig. A.10 Transverse Reinforcement Strains Measured in Specimen RS-5 (negative - in tension)

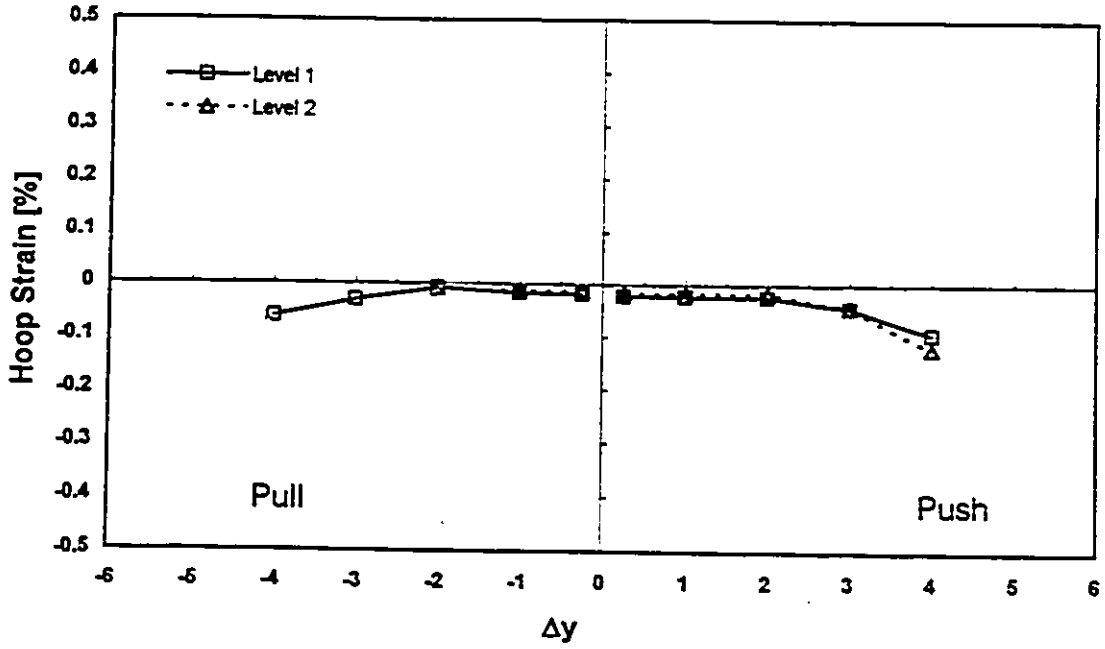

a) Strains at S4

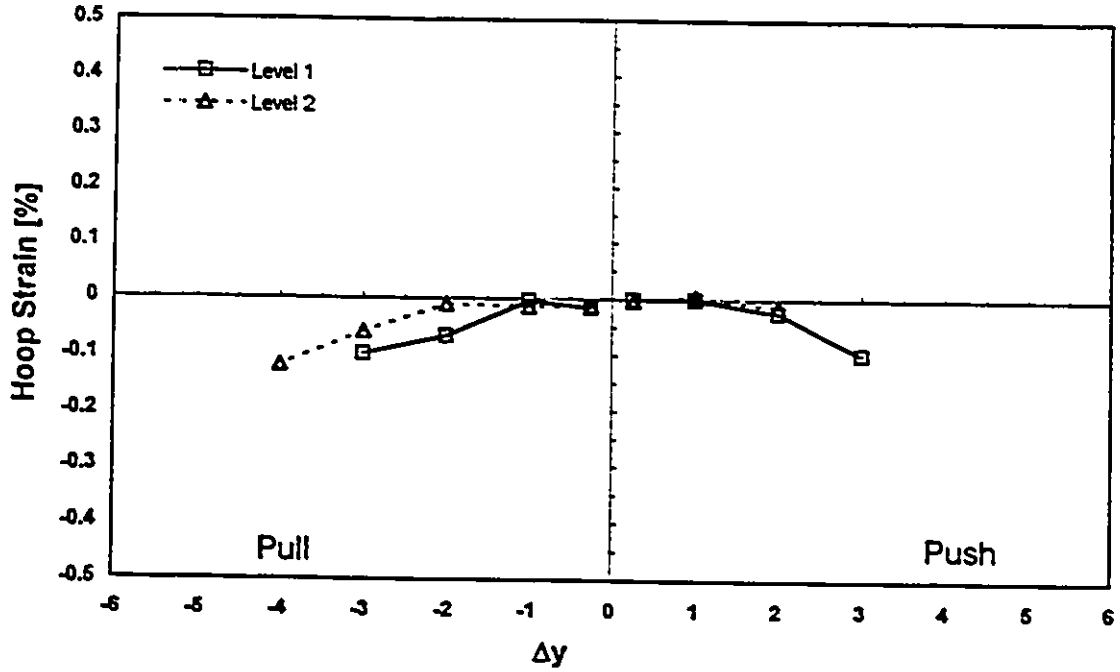

b) Strains at S5

Fig. A.10 Transverse Reinforcement Strains Measured in Specimen RS-5 - Continued (negative - in tension)

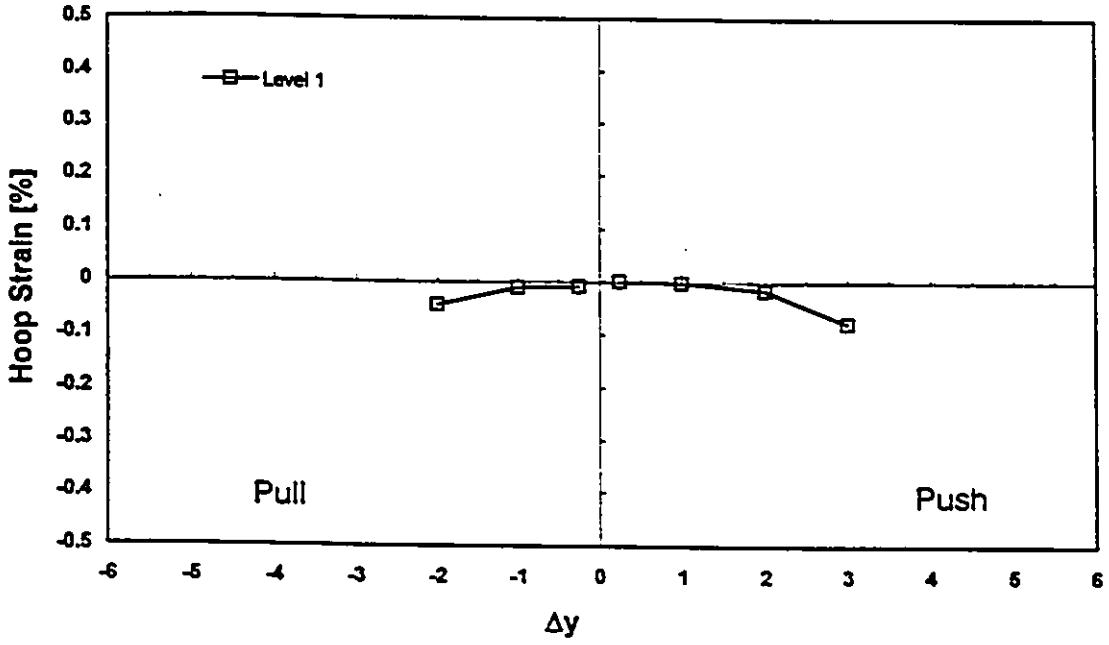

a) Strains at S6

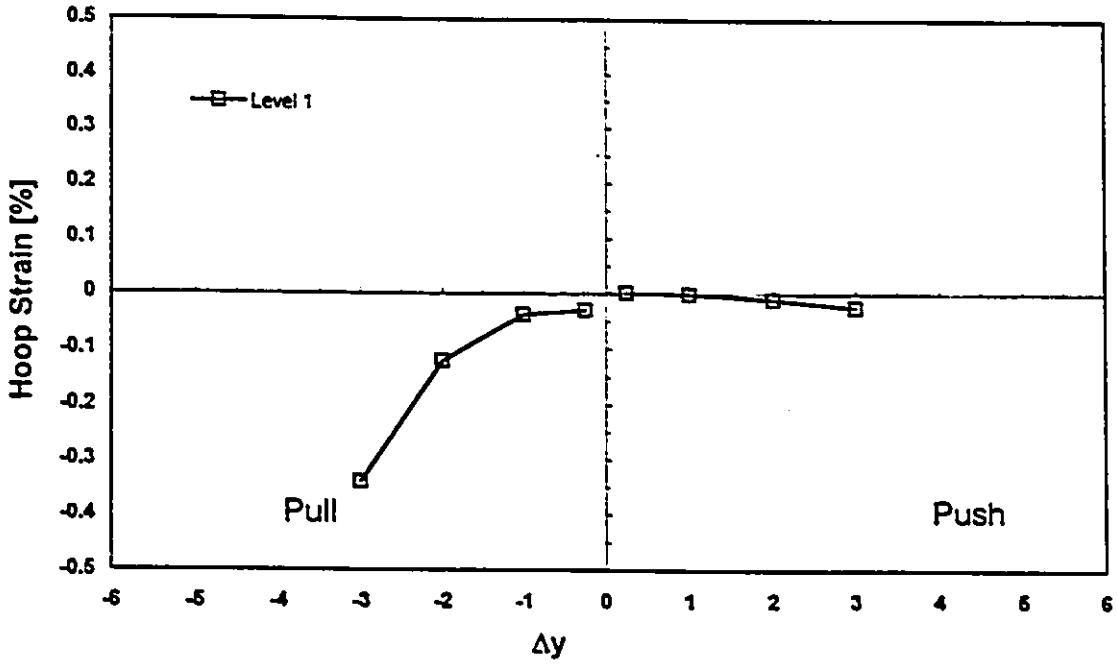

b) Strains at S7

Fig. A.10 Transverse Reinforcement Strains Measured in Specimen RS-5 - Continued (negative - in tension)

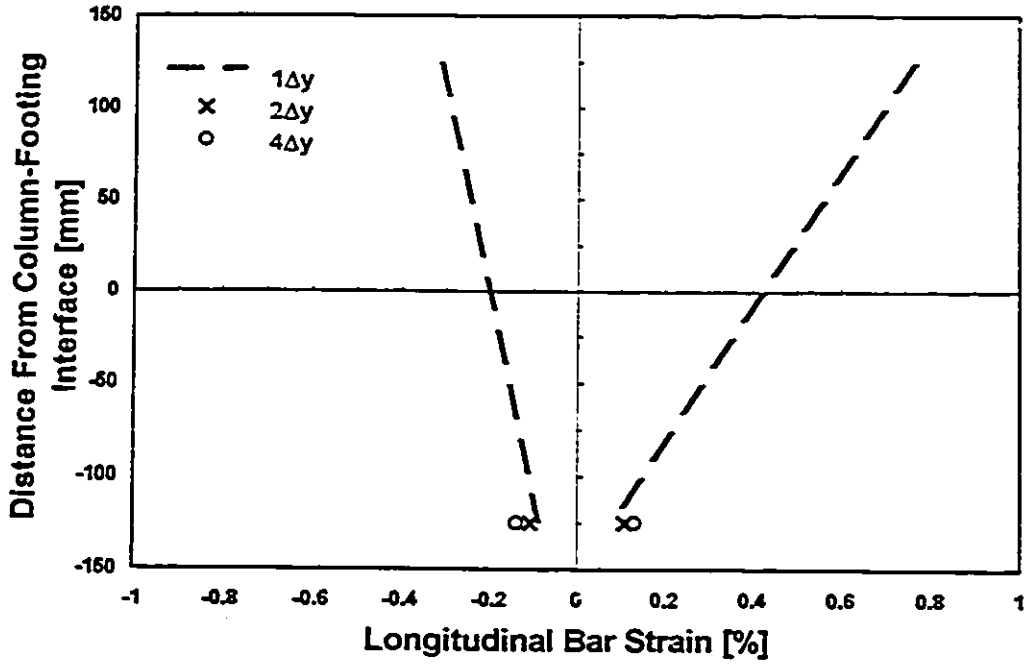

a) Three-Gauge Bar

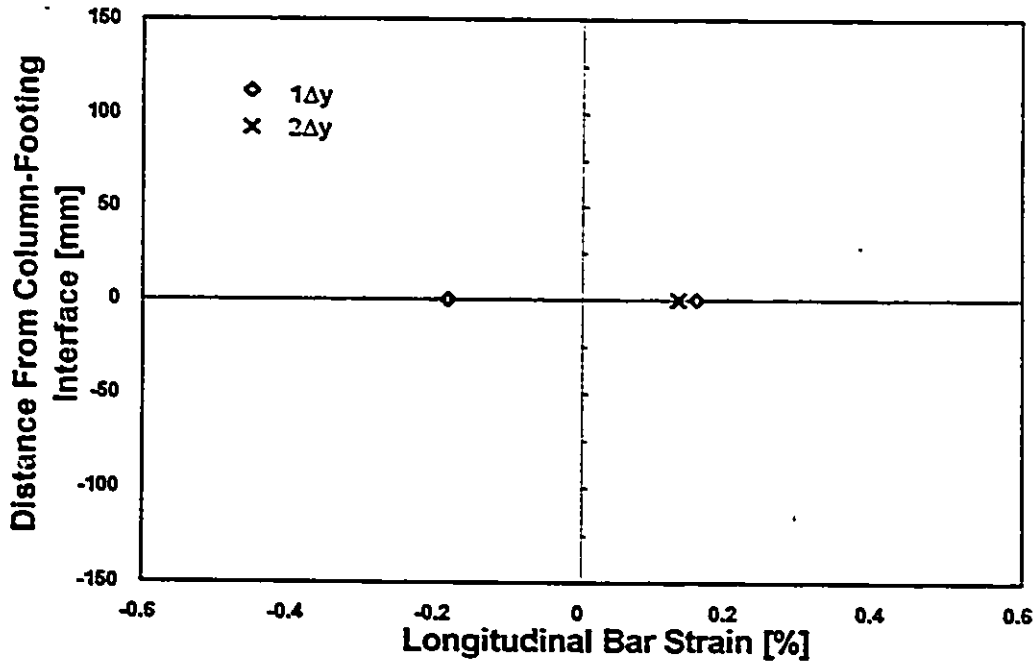

b) Single-Gauge Bar

Fig. A.11 Longitudinal Bar Strains Measured in Specimen RS-6 - tension; + compression

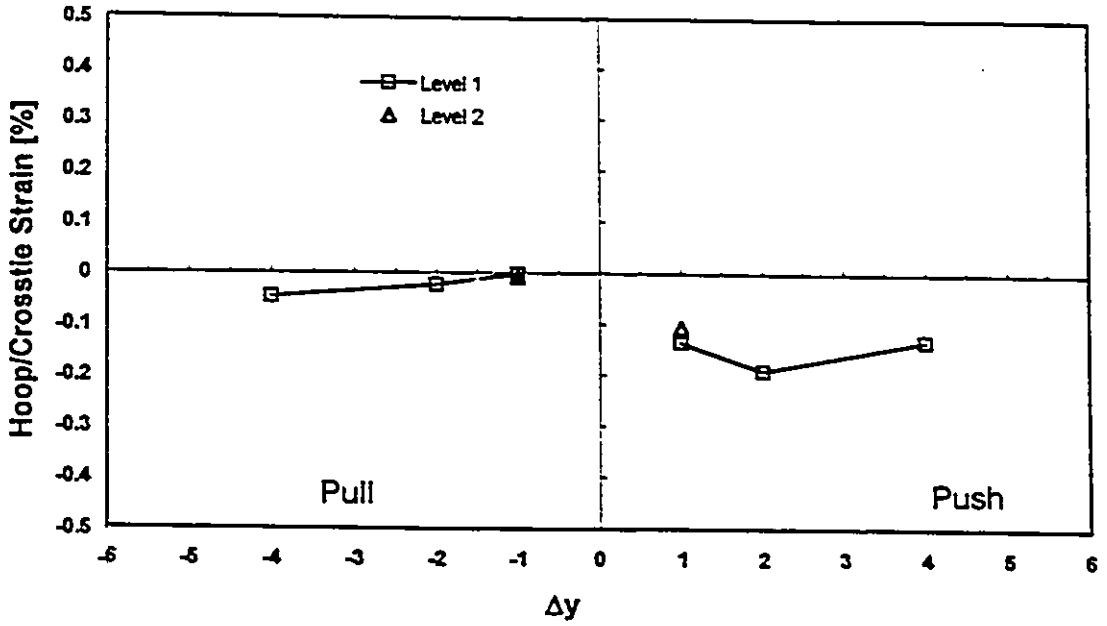

a) Strains at S1

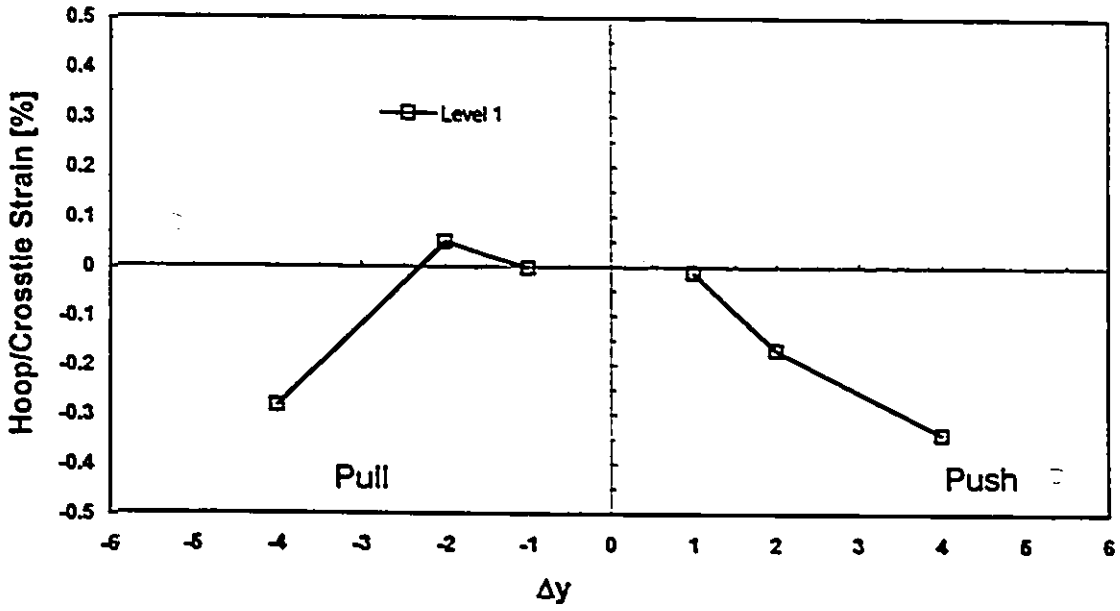

b) Strains at S3

Fig. A.12 Transverse Reinforcement Strains Measured in Specimen RS-6 (negative - in tension)

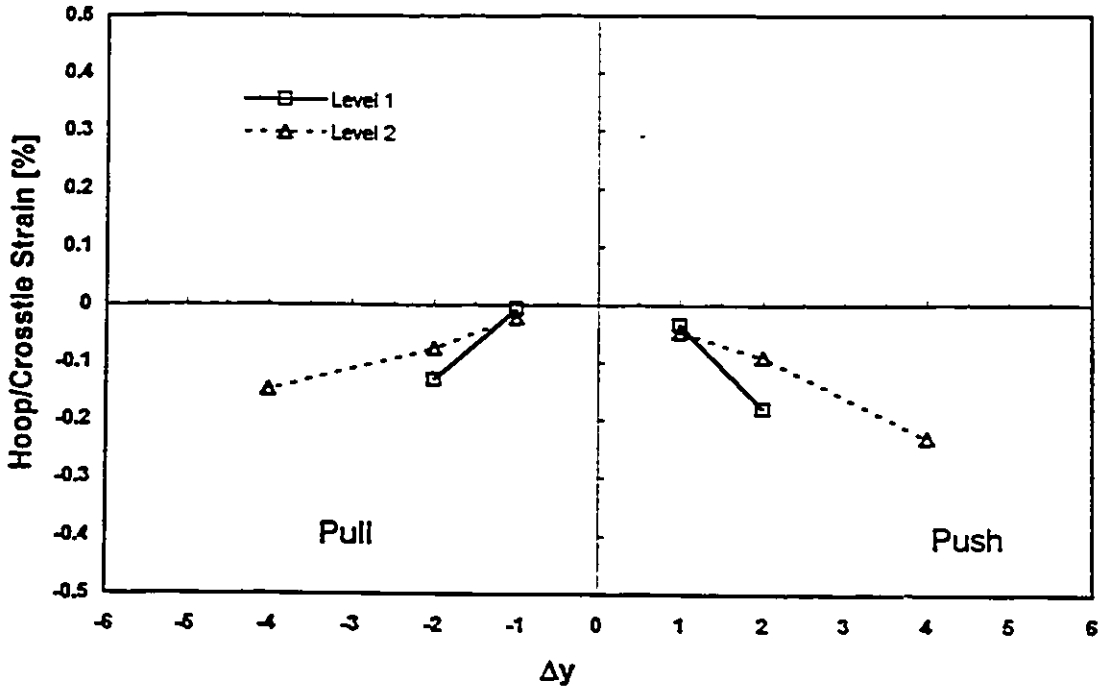

a) Strains at S4

Fig. A.12 Transverse Reinforcement Strains Measured in Specimen RS-6 - Continued (negative - in tension)

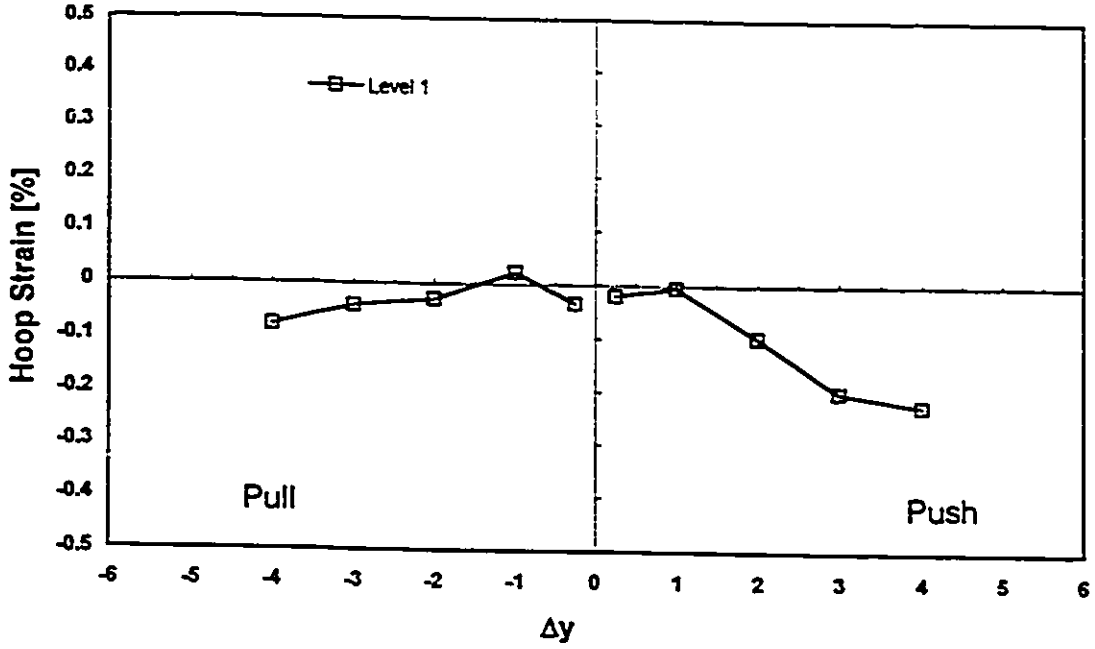

a) Strains at S1

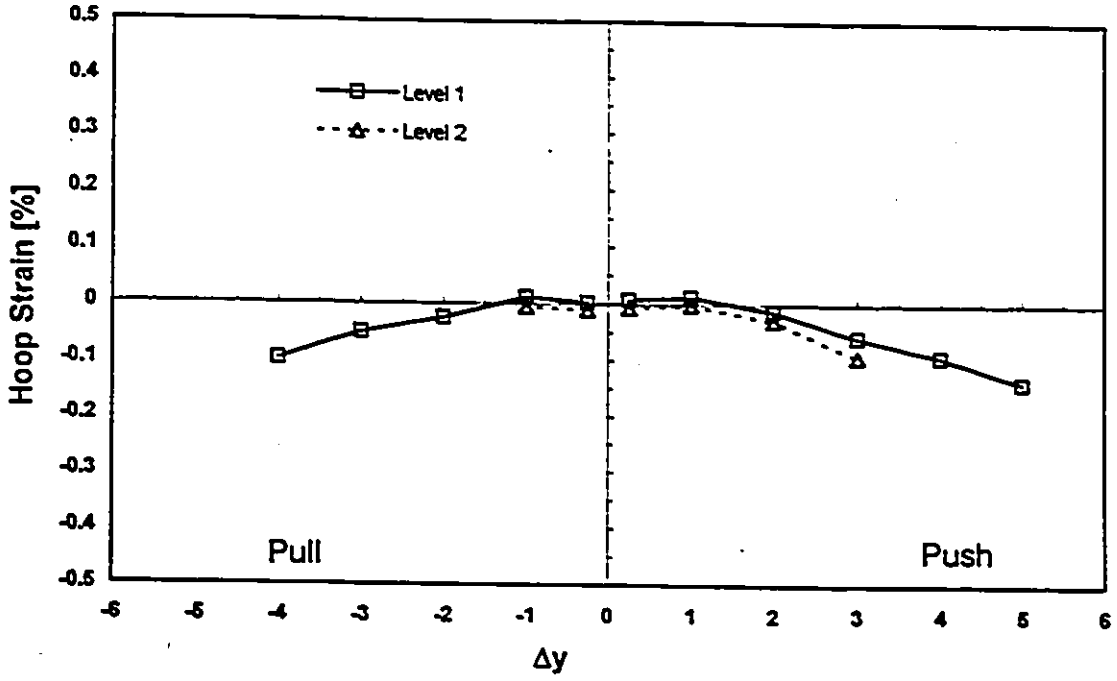

b) Strains at S2

Fig. A.13 Transverse Reinforcement Strains Measured in Specimen RS-7 (negative - in tension)

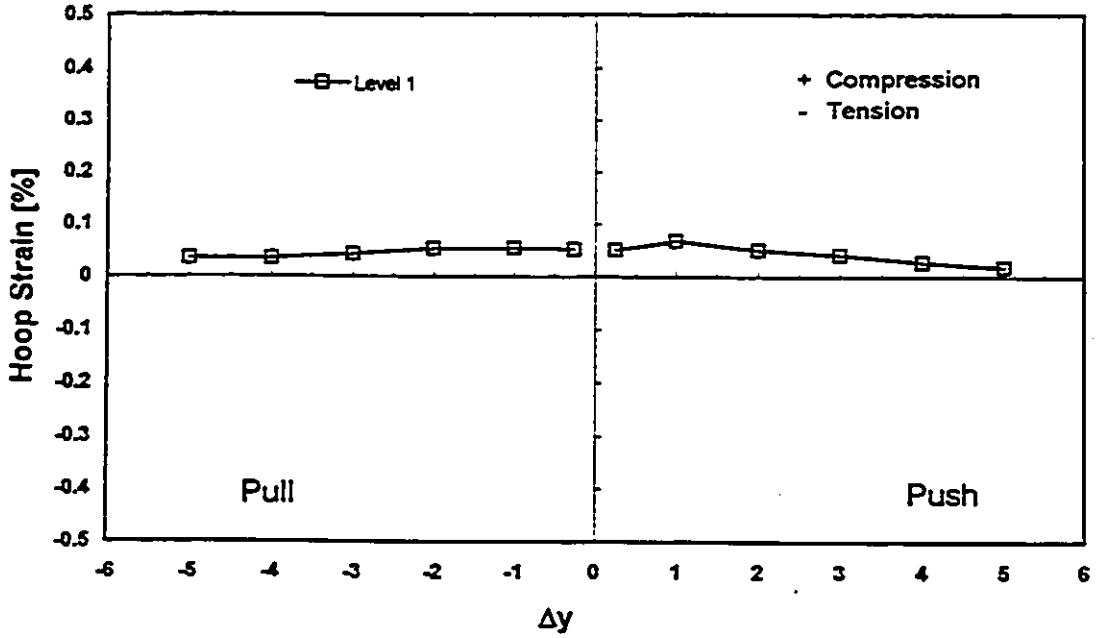

a) Strains at S3

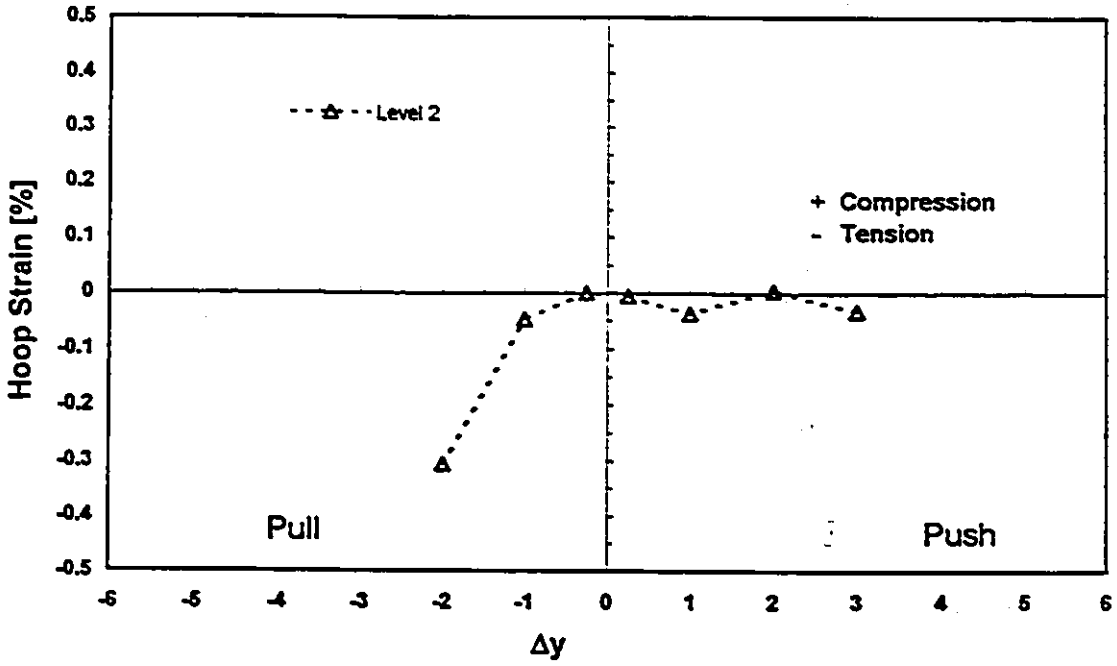

b) Strains at S4

Fig. A.13 Transverse Reinforcement Strains Measured in Specimen RS-7 - Continued (negative - in tension)

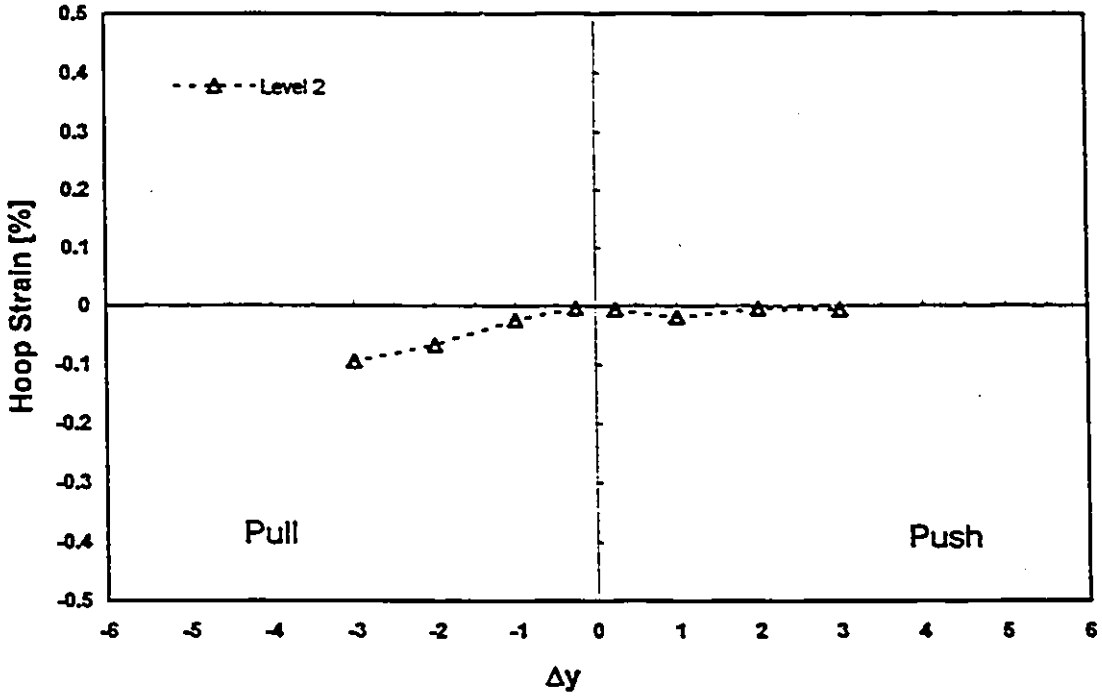

a) Strains at S5

Fig. A.13 Transverse Reinforcement Strains Measured in Specimen RS-7 - Continued (negative - in tension)

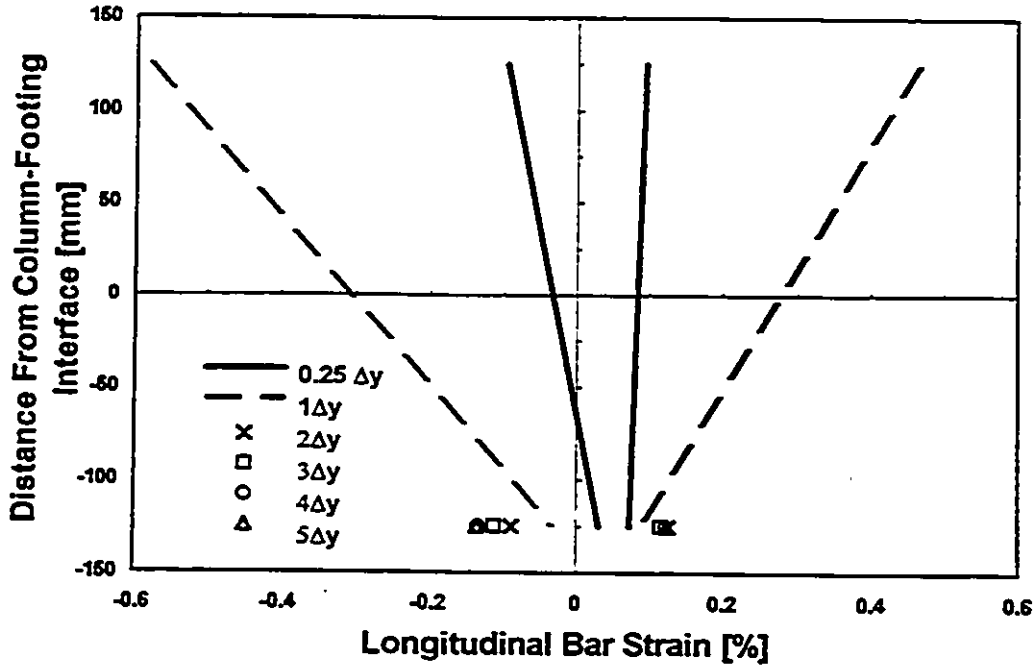

a) Three-Gauge Bar

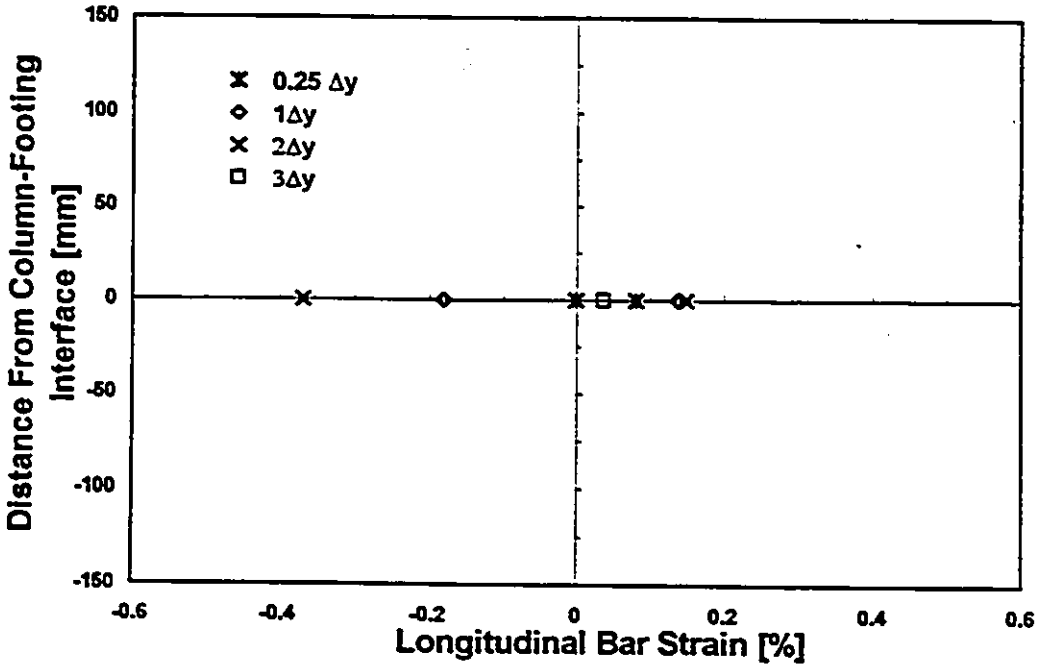

b) Single-Gauge Bar

Fig. A.14 Longitudinal Bar Strains Measured in Specimen RS-8 - tension; +compression

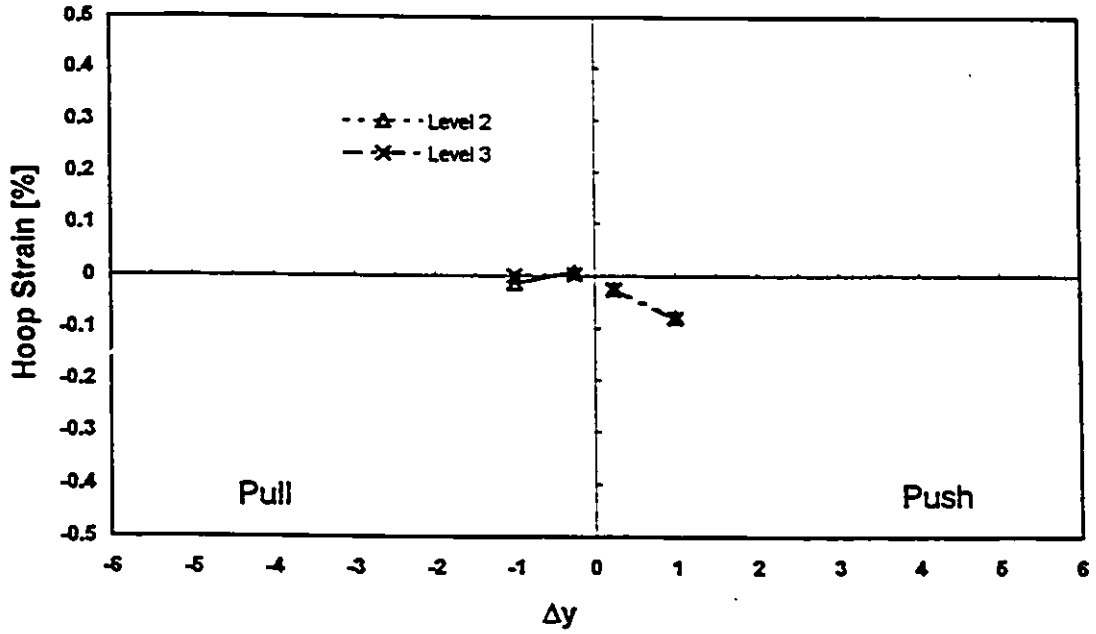

a) Strains at S1

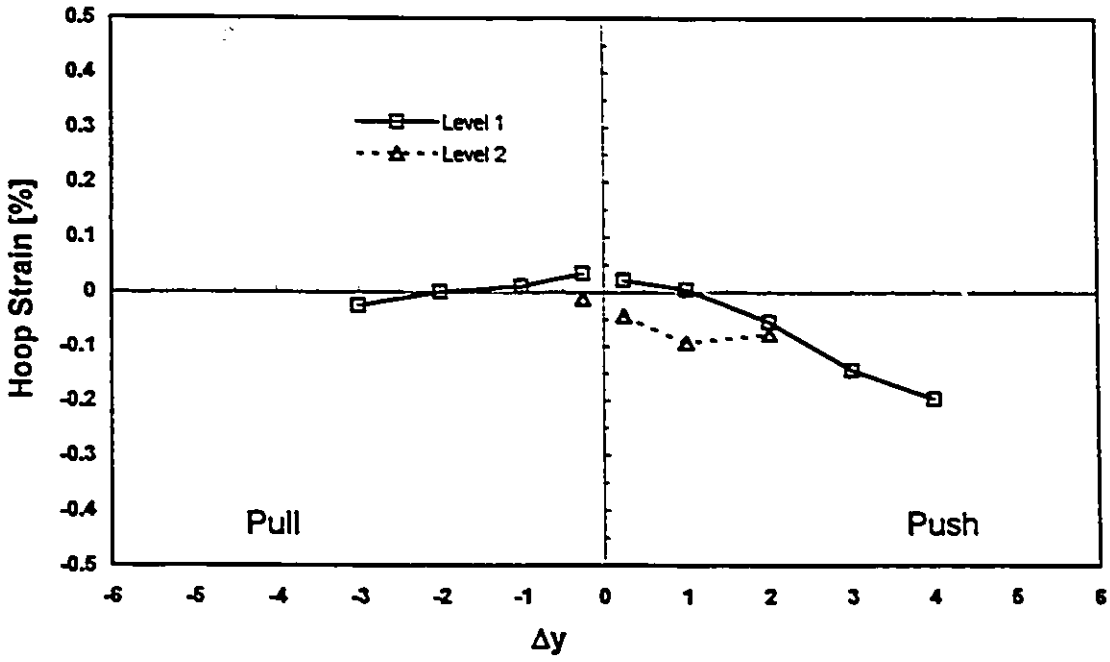

b) Strains at S2

Fig. A.15 Transverse Reinforcement Strains Measured in Specimen RS-8 (negative - in tension)

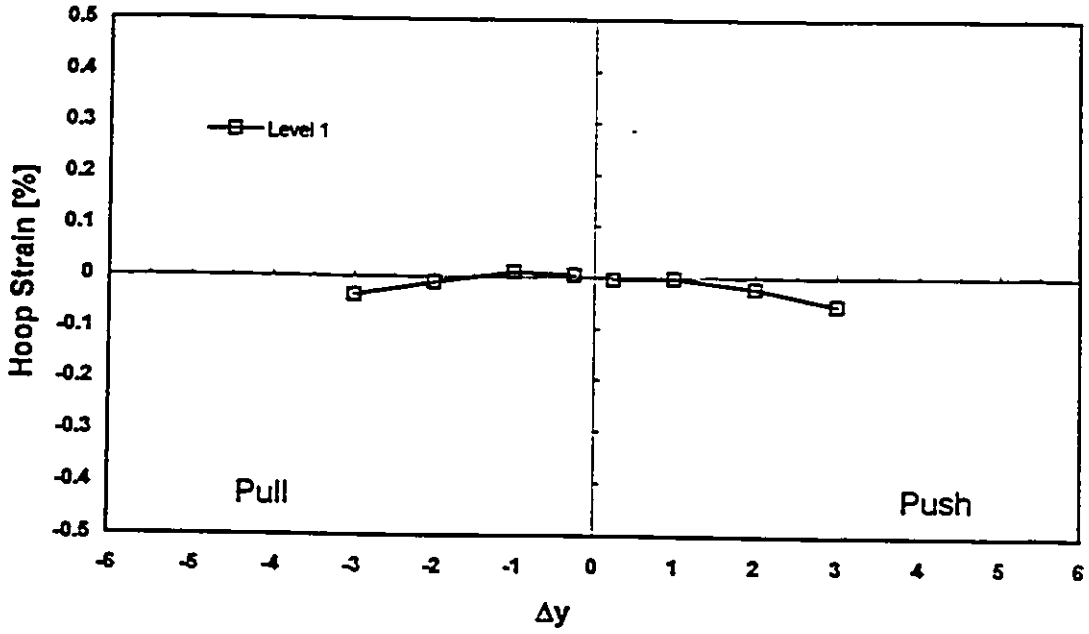

a) Strains at S3

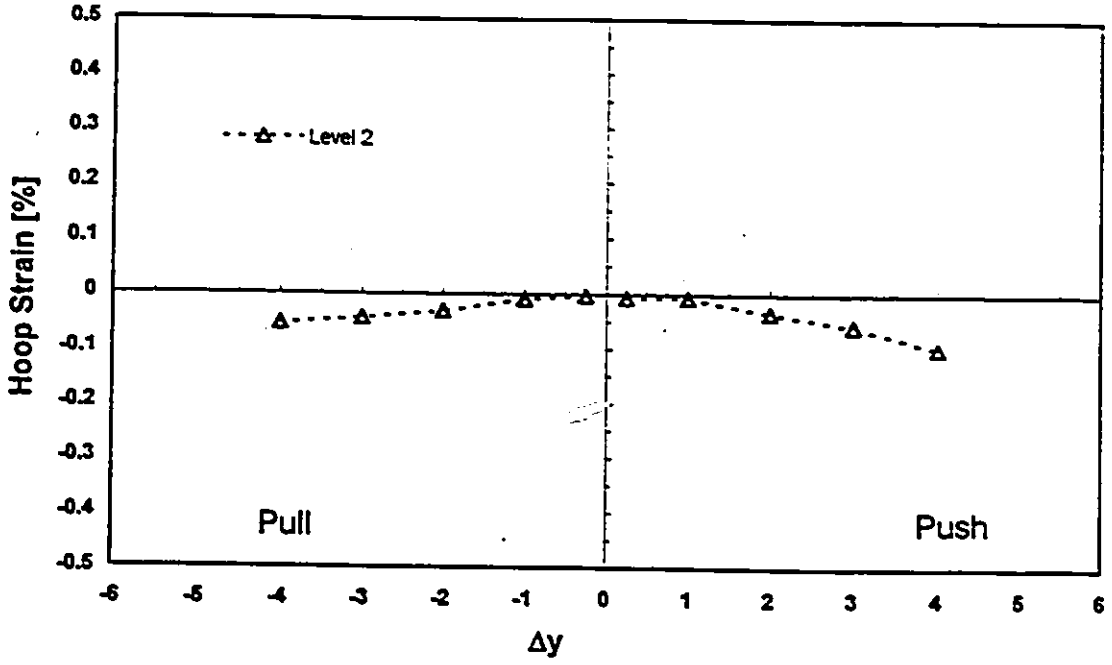

b) Strains at S4

Fig. A.15 Transverse Reinforcement Strains Measured in Specimen RS-8 - Continued (negative - in tension)

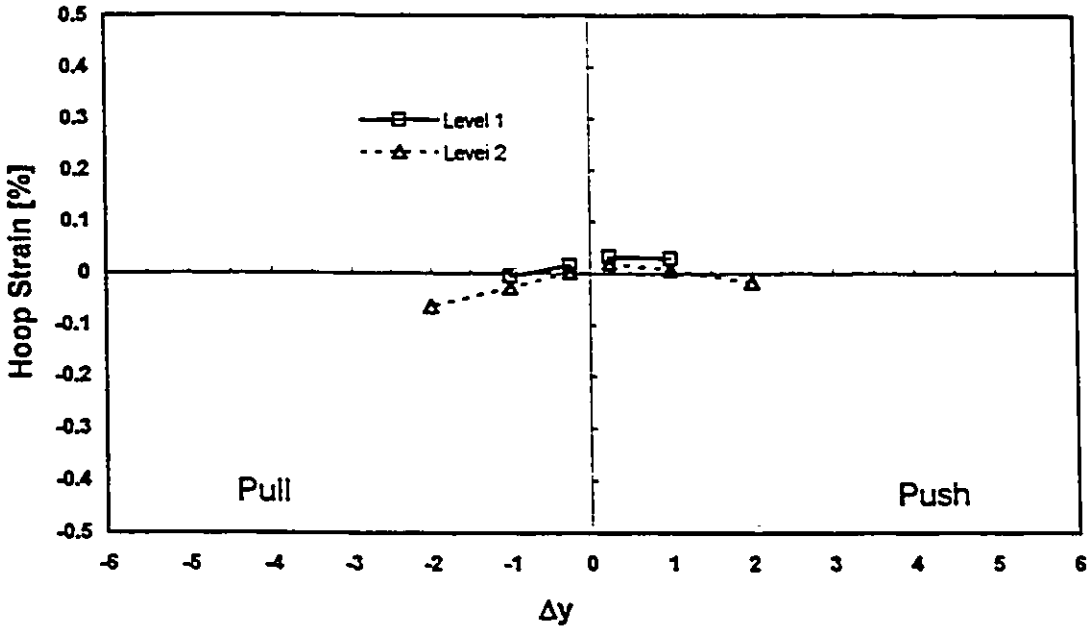

a) Strains at S5

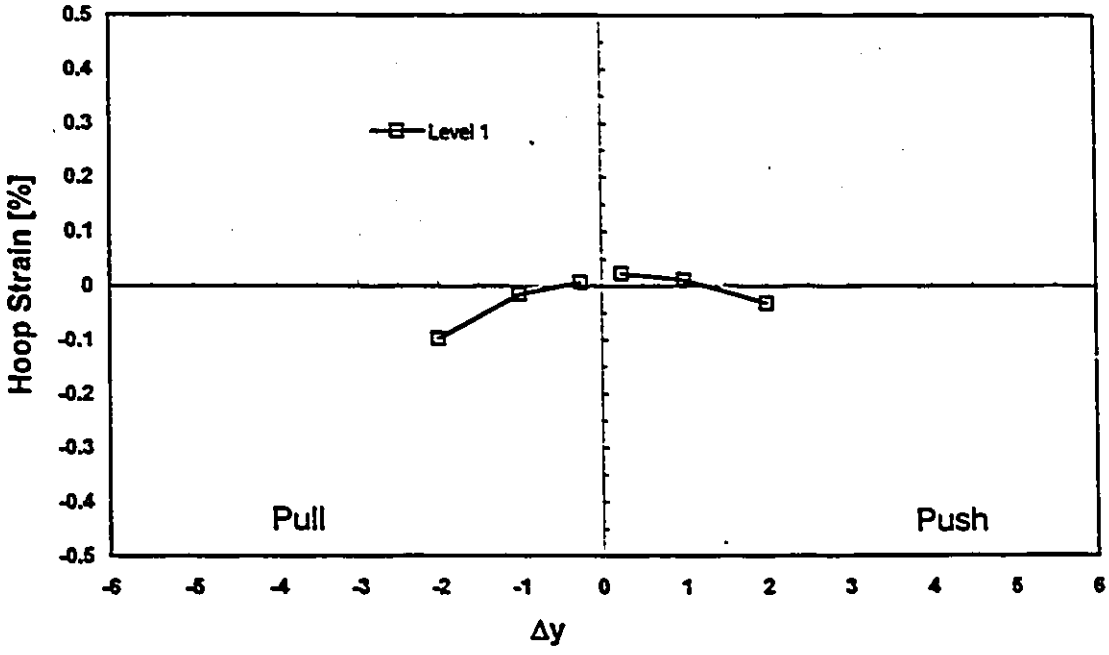

b) Strains at S6

Fig. A.15 Transverse Reinforcement Strains Measured in Specimen RS-8 - Continued (negative - in tension)

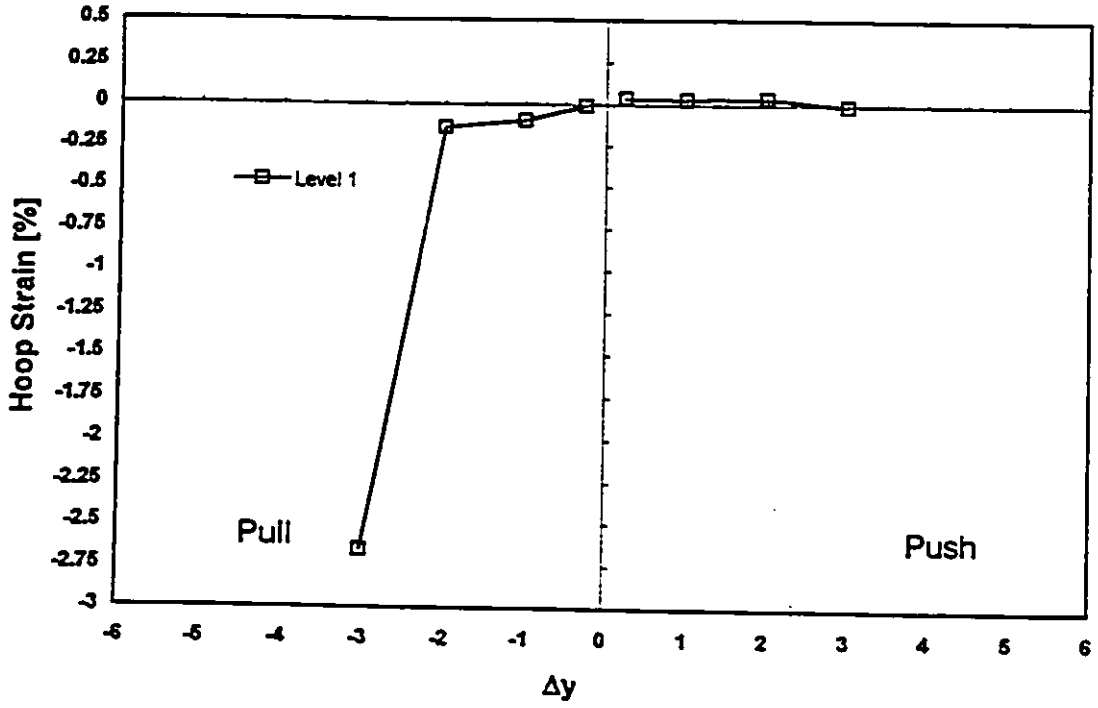

a) Strains at S7

Fig. A.15 Transverse Reinforcement Strains Measured in Specimen RS-8 - Continued (negative - in tension)

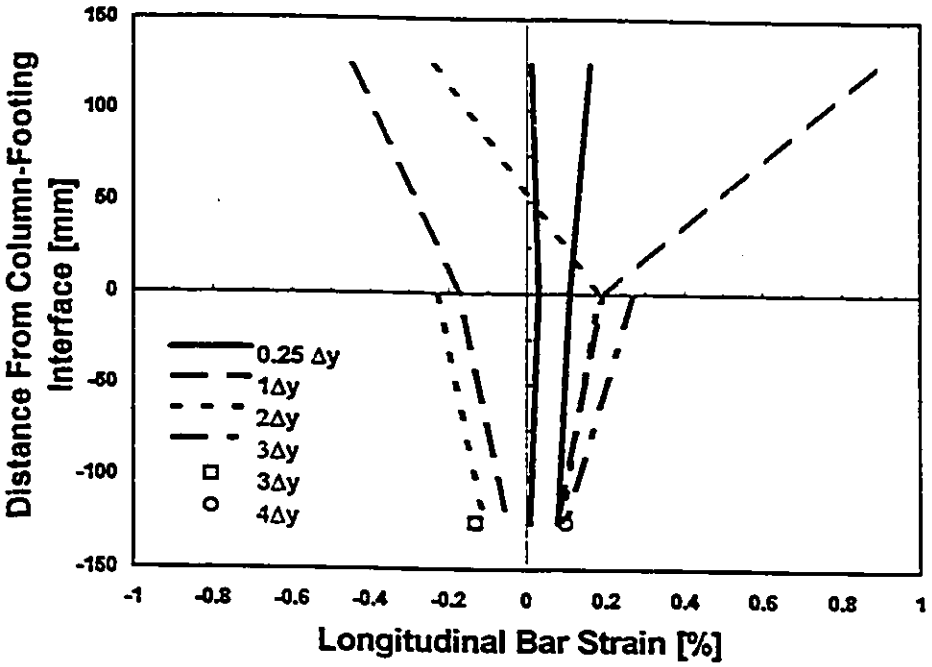

a) Three-Gauge Bar

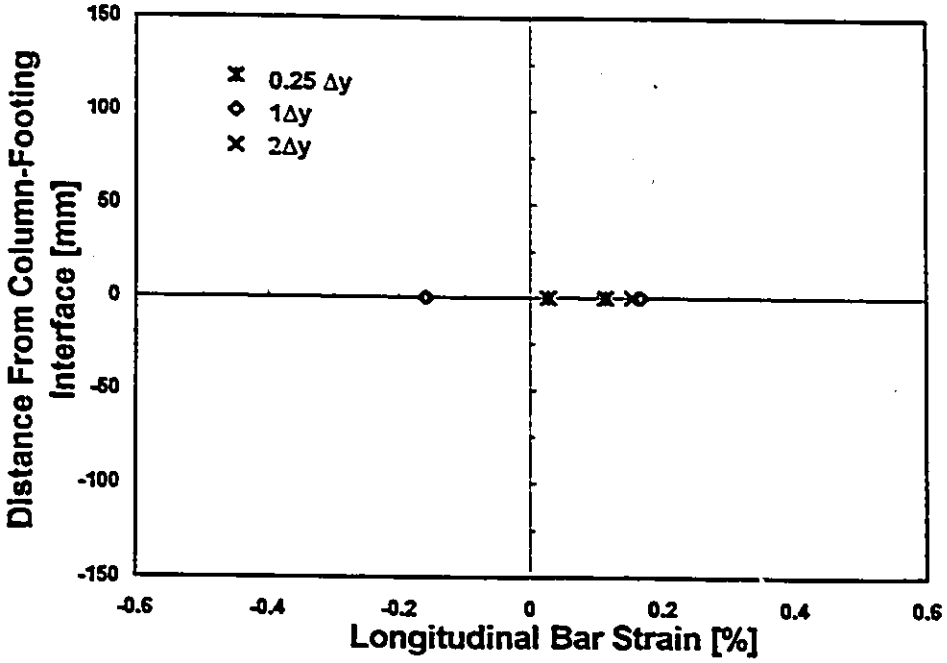

b) Single-Gauge Bar

Fig. A.16 Longitudinal Bar Strains Measured in Specimen RS-9 - tension; +compression

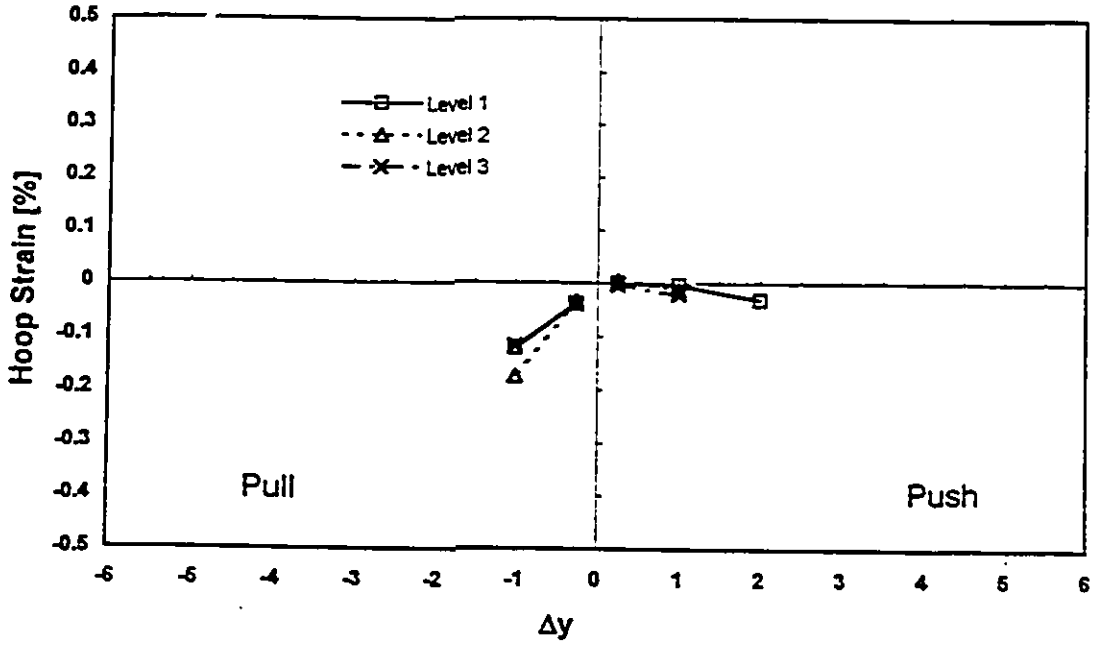

a) Strains at S1

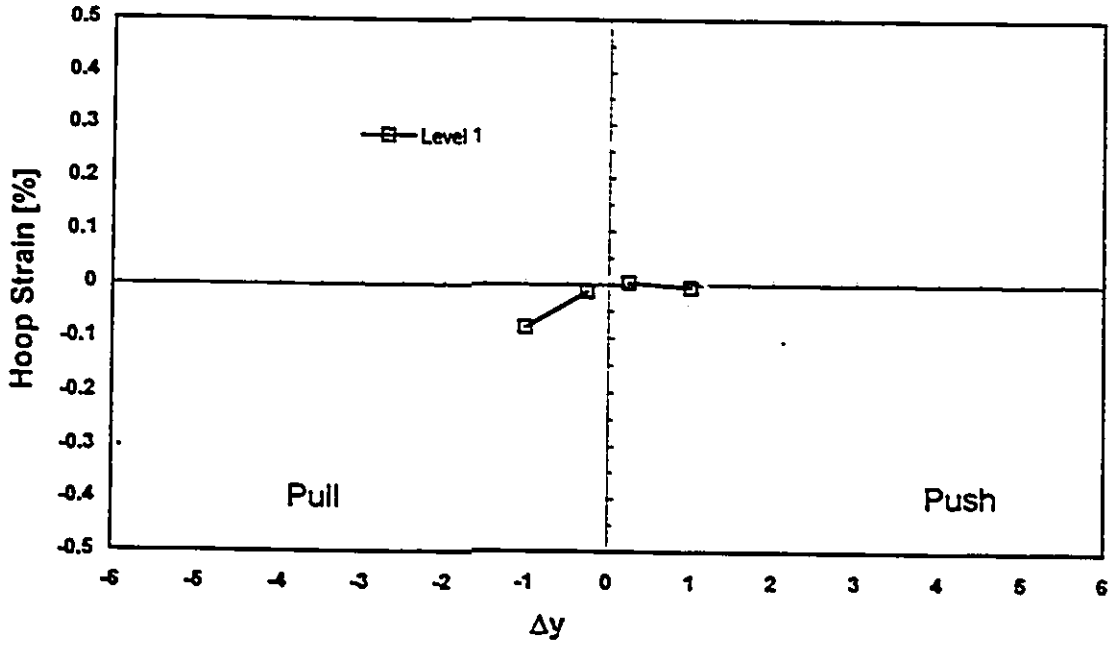

b) Strains at S2

Fig. A.17 Transverse Reinforcement Strains Measured in Specimen RS-9 (negative - in tension)

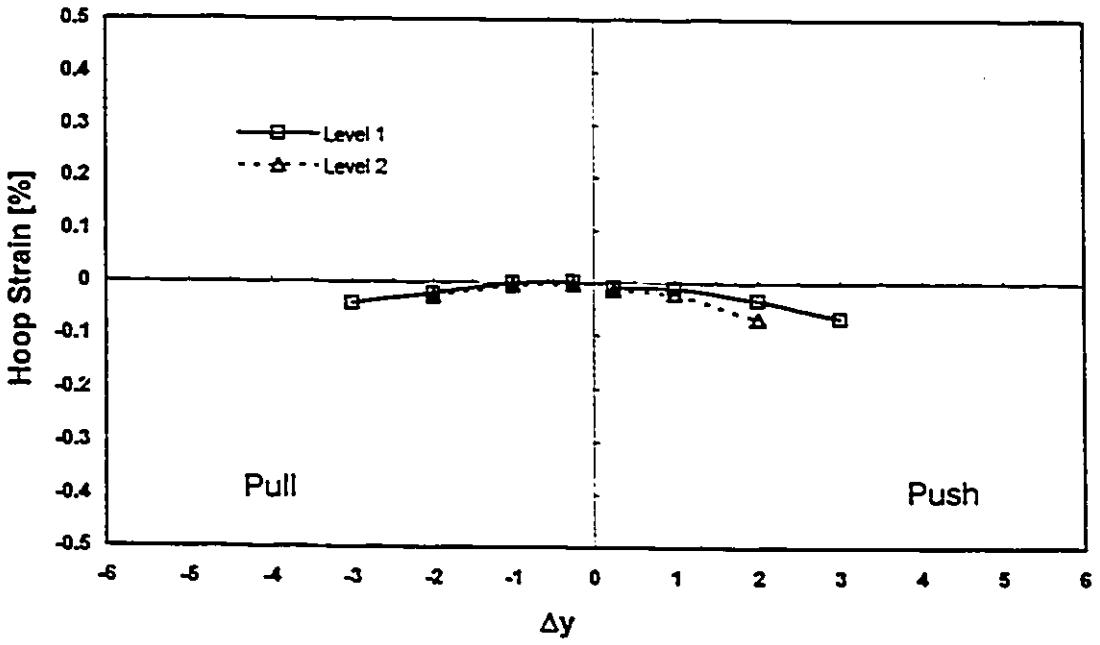

a) Strains at S3

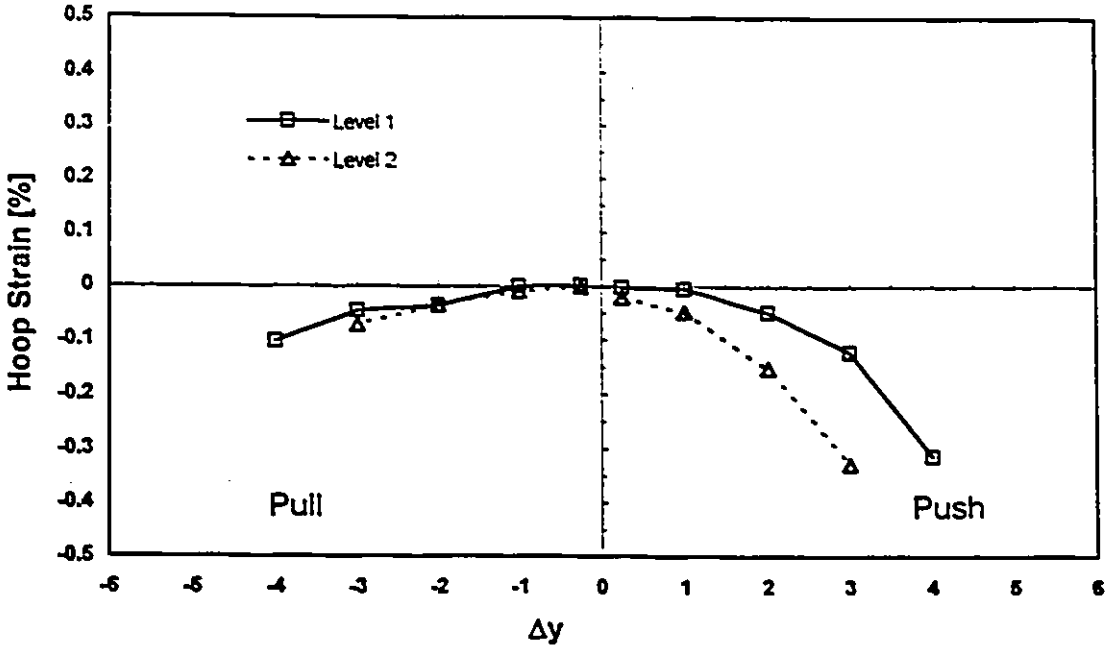

b) Strains at S4

Fig. 17 Transverse Reinforcement Strains Measured in Specimen RS-9 - Continued (negative - in tension)

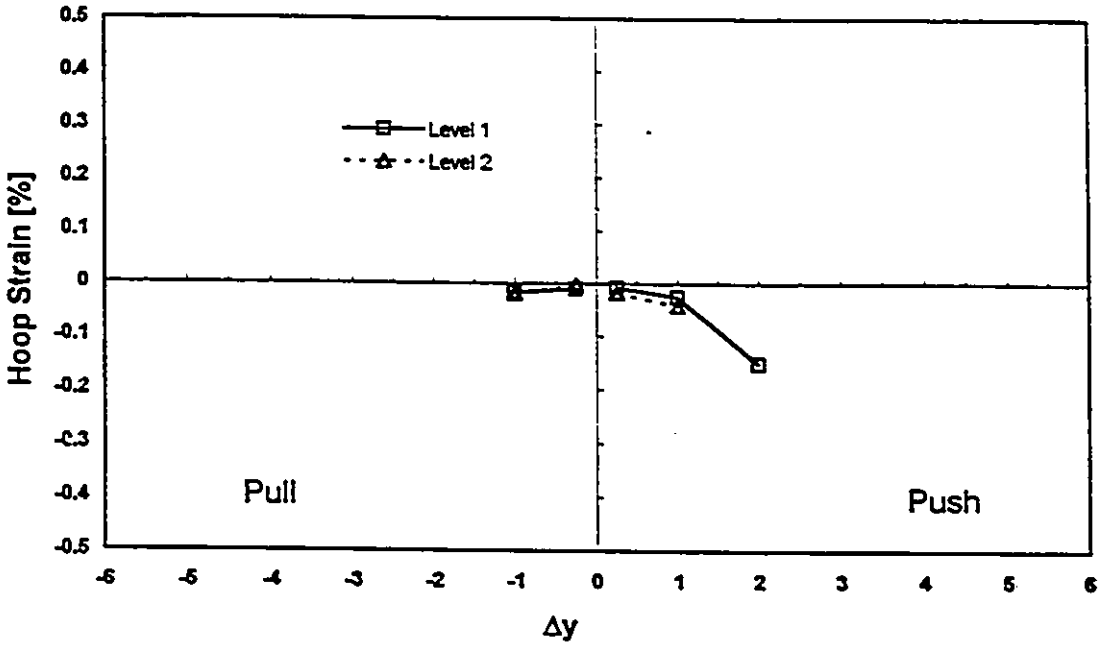

a) Strains at S5

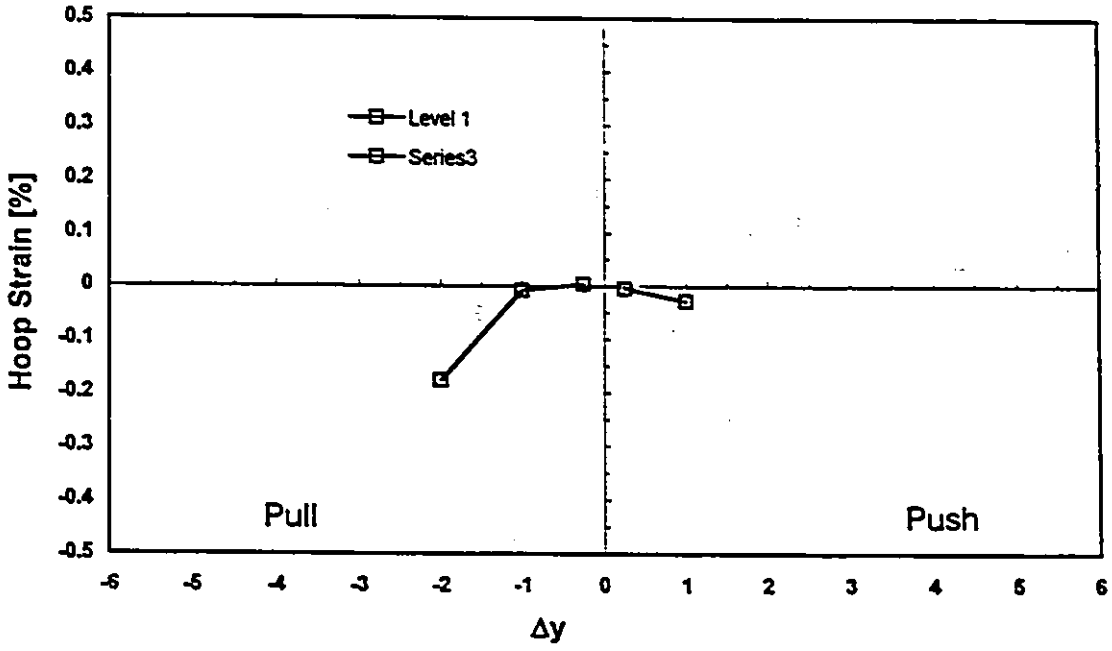

b) Strains at S6

Fig. A.17 Transverse Reinforcement Strains Measured in Specimen RS-9 - Continued (negative - in tension)

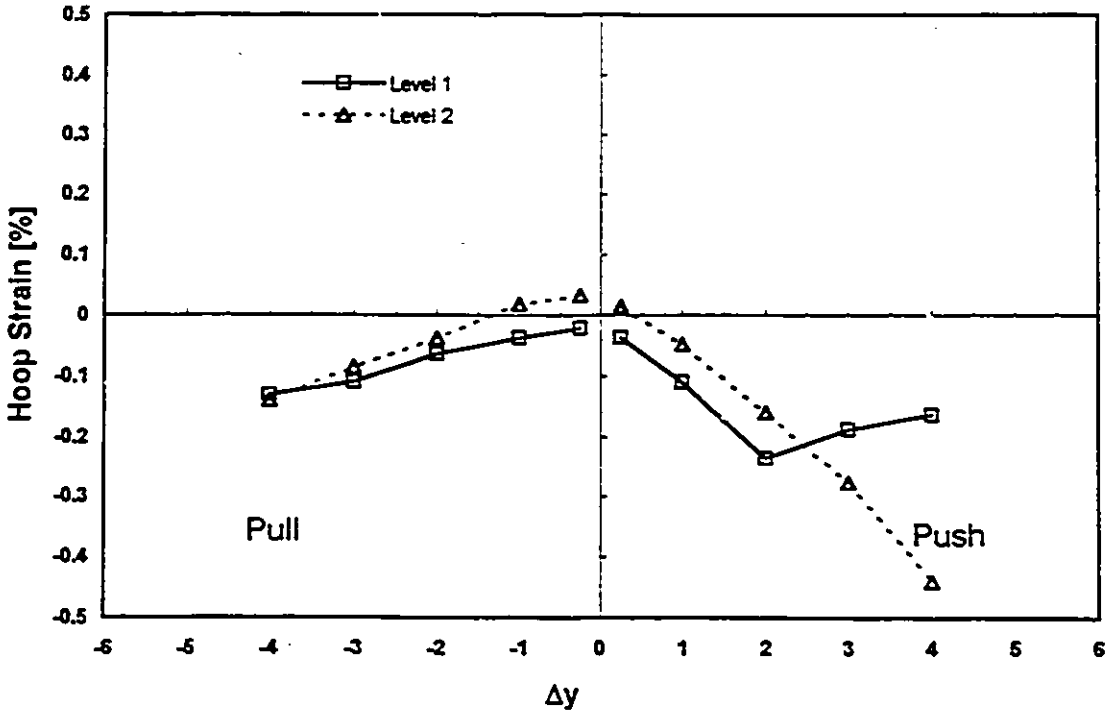

a) Strains at S7

Fig. A.17 Transverse Reinforcement Strains Measured in Specimen RS-9 - Continued (negative - in tension)

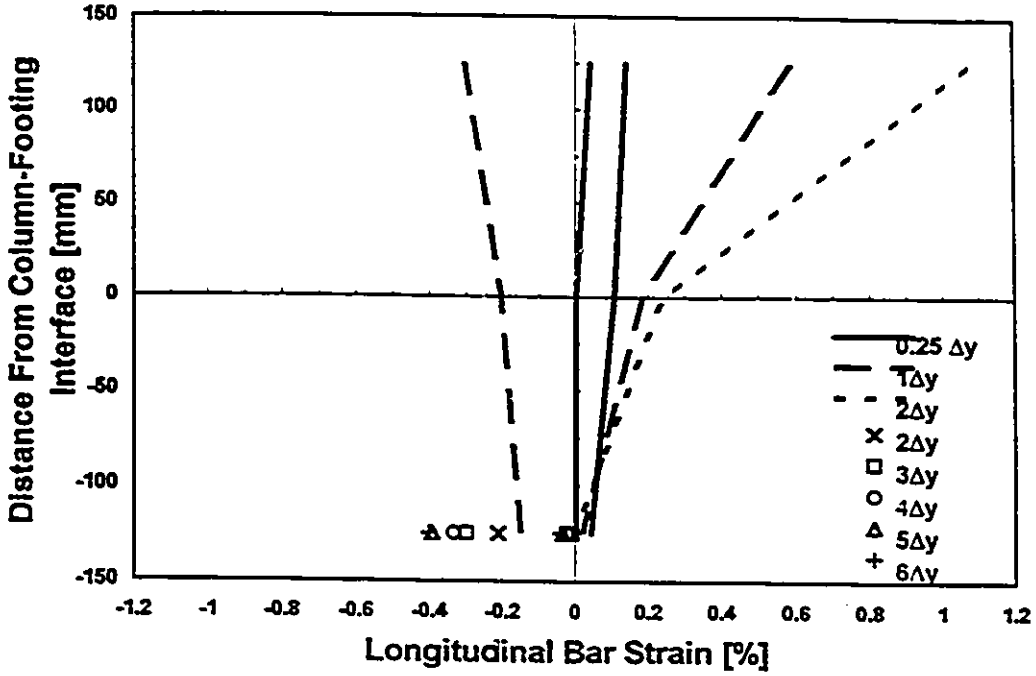

a) Three-Gauge Bar

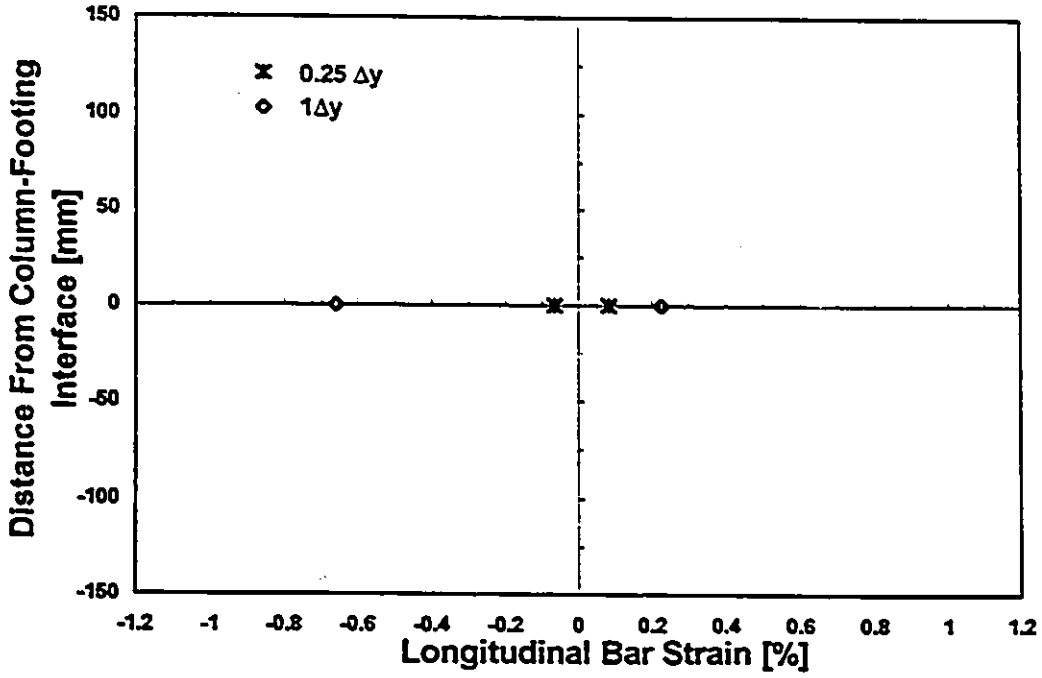

b) Single-Gauge Bar

Fig. A.18 Longitudinal Bar Strains Measured in Specimen RS-10 - tension; +compression

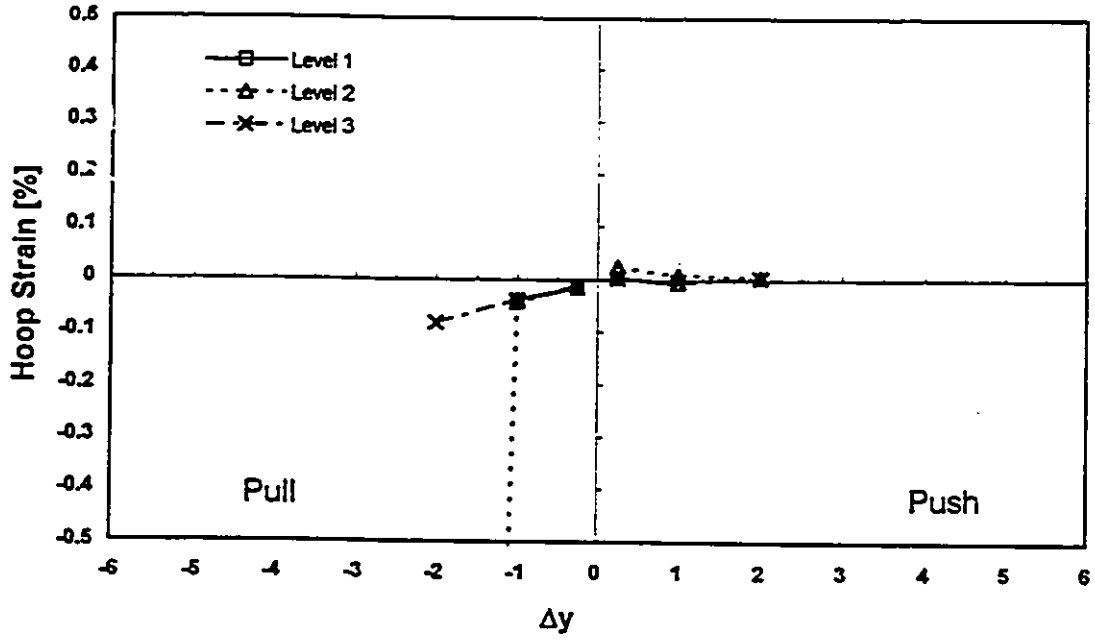

a) Strains at S1

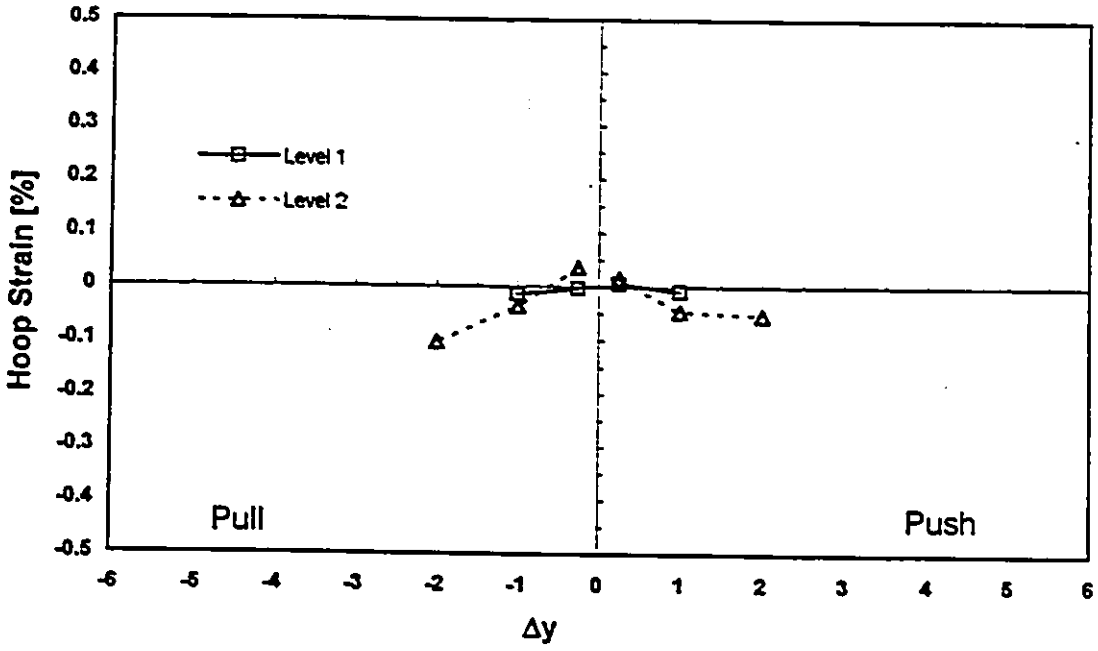

b) Strains at S2

Fig. A.19 Transverse Reinforcement Strains Measured in Specimen RS-1C (negative - in tension)

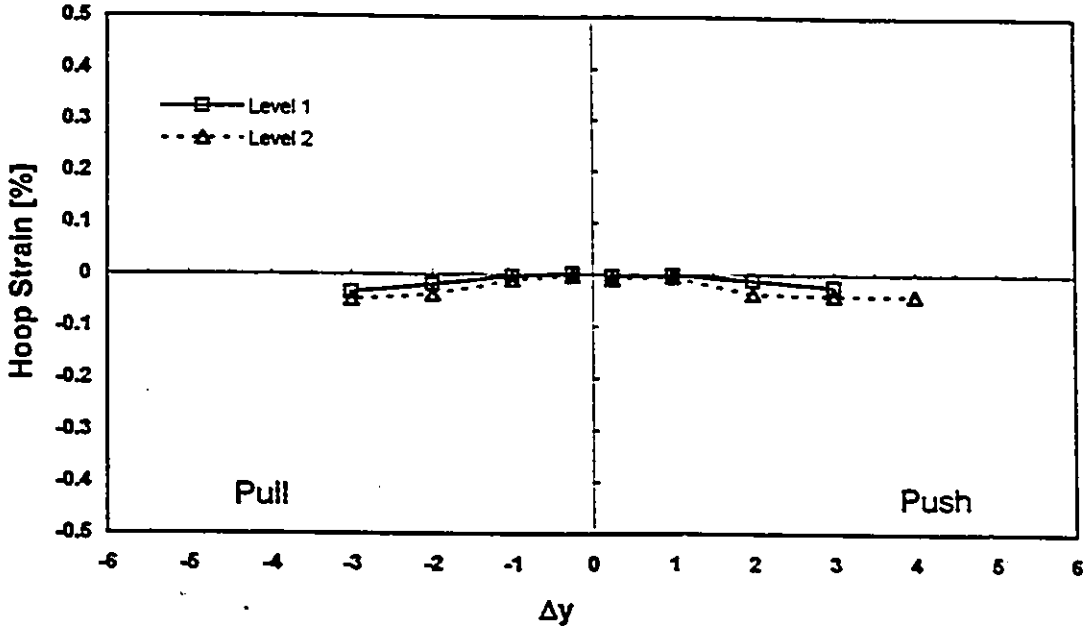

a) Strains at S3

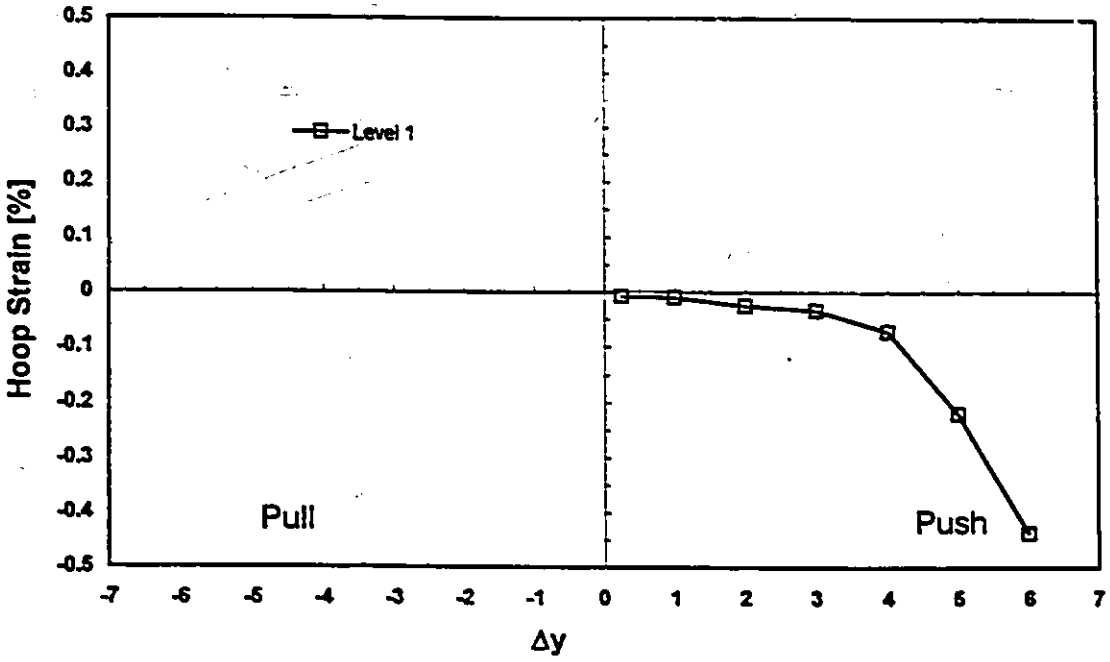

b) Strains at S4

Fig. A.19 Transverse Reinforcement Strains Measured in Specimen RS-10 - Continued (negative - in tension)

Bibliography

[1] Thomsen, J.H, and Wallace, J.W., *Lateral Load Behaviour of Reinforced Concrete Columns Constructed Using High-Strengths Materials,* ACI Structural Journal, Vol. 91, No. 5, Sept. - Oct. 1994 pp. 605-615

[2] Azizinami, A., Baum Kuska, S. S., Brungardt, P., Hatfield, E. *Seismic Behaviour of Square High-Strength Concrete Columns* ACI Structural Journal, V.91, No.3, May-June 1994.

[3] Sakai,Y., Otani, S. *Ductility of Columns Under Flexural Compression,* First Meeting of the Tri-Lateral Project on the Use of High Strength Concrete, Kyoto, Japan, May 19-21, 1993.

[4] Bing, L., Park, R., Tanaka, H. *Effect of Confinement on the Behaviour of High Strength Concrete Columns Under Seismic Loading Pacific Conference on Earthquake Engineering*, New Zealand, 20-23 November 1991.

[5] Kato, D. *Ductility of Members with Shear and Flexure*, First Meeting of the Tri-Lateral Project on the Use of High Strength Concrete, Kyoto,

Japan, May 19-21, 1993.

[6] Kuramoto, H., Minami K., *Experiments on the Shear Strength of Ultra-High Strength Reinforced Concrete Columns Earthquake Engineering*, Tenth World Conference, 1992 Balkema, Rotterdam.

[7] Kabeyasawa, T., Shen, F.H., Rubiano, N.R. *Experimental Study on Behaviours of Ultra High Strength Reiforced Concrete Columns under Tri-Axial Forces* Transactions of the Japan Concrete Institute Vol. 13, 1991.

[8] Hibi, J., Mihara, Y., Otani, S., Aoyama, H. *Behaviour of Reinforced Concrete Columns Using High Strength Concrete After Flexural Yielding*, Transactions of the Japan Concrete Institute Vol. 13, 1991.

[9] Sakai, Y., Hibi, J., Otani, S., Aoyama, H. *Experimental Study on Flexural Behaviour of Reinforced Concrete Columns using High-Strength Concrete* Transactions of the Japan Concrete Institute Vol. 12, 1990.

[10] Kabeyasawa, T. Li, K.N., Huang, K. *Experimental Study on Strength and Deformability of Ultra-High Strength Reinforced Concrete Columns* Transactions of the Japan Concrete Institute Vol. 12, 1990.

[11] Muguruma, H., Watanabe, F., Komuro, T. *Applicability of High Strength Concrete to Reinforced Concrete Ductile Column.* Transactions of the Japan Concrete Institute Vol. 11, 1989.

[12] Chung, H., Hayashi, S., Kokusho, S. *Reinforced High Strength Concrete Columns Subjected to Axial Forces, Bending Moments and Shear Forces,* Transactions of the Japan Concrete Institute Vol. 2, 1980.

[13] Muguruma, H., Nishiyama, M., Watanabe, F., Tanaka, H. *Ductile Behaviur of High-Strength Concrete Columns Confined by High-Strength Transverse Reinforcement,* ACI International Conference on "Evaluation and Rehabilbitation of Concrete Structures and Innovations in Design" SP-128-54, Vol. 2, Hong Kong, December1991, pp. 887-891

[14] Watanabe, F., Muguruma, H., Matsutani, T., Sanda, D. *Utilization of High Strenght Concrete for Reinforced Concrete High-Rise Buildings in Seismic Area,* Proceedings Symposium in Stavangar, Norway, June 15-18, 1987, Tapir Publishers 1987.

[15] CSA, Design of Concrete Structures for Buildings (CAN3-A23.2-M84),Canadian Standards Association, Ontario, 1984

[16] ACI Committee 318, Building Code Requirements for Reinforced Concrete (ACI 318-89), American Concrete Institute, Detroit, 1992

[17] Saatcioglu, M., Salamat, A. H., and Razvi, S. *Confined Columns under Eccentric Loading,* Journal of Structural Engineering, ASCE, Vol. 121, No. 11, Nov. 1995, pp. 1547-1556.

[18] Fafitis, A., and Shah, S. P. *Predictions of Ultimate Behavior of Confined Concrete Columns Subjected to Large Deformations.* ACI Structures Journal, Vol. 82, No. 4, pp. 423-433.

[19] Razvi, S. and Saatcioglu, M. *Analytical Model for Confined High-Strength Concrete.* Research Report, Ottawa-Carleton Earthquake Engineering Research Centre, 1995.

[20] Saatcioglu, M. and Razvi, S. *Strength and Ductility of Confined Concrete,* Journal of Structural Engineering, ASCE, Vol. 118, No. 6, Nov. 1992, pp. 1590-1607.

[21] Razvi, S., *Confinement of Normal and High Strength Concrete Columns,* A Thesis Submitted to the Faculty of Graduate Studies and Research in a Partial Fulfilment of the Requirements for the Degree of Doctorate of Philosophy in Civil Engineering, Department of Civil Engineering, University of Ottawa, Canada, June 1995

[22] Alsiwat, J., Saatcioglu, M., *Reinforcement Anchorage Slip Under Monotonic Loading,* Journal of Structural Engineering, ASCE, Vol. 118, No. 9, 1992 pp. 2421-2438

[23] CAN3-A23.3-94 *Design of Concrete Structures for Buildings,* Canadian Standards Association, Rexdale, Ontario, 1994.

[24] Ibrahim, H., MacGregor, J.G., *Flexural Behaviour of High Strength*

Concrete Columns, Structural Engineering Report No. 196, University of Alberta, Edmonton, Alberta, March 1994.

[25] Bing, L., Park, R., Tanaka, H., *Effect of Confinement of High Strength Concrete Columns under Seismic Loading,* Pacific Conference on Earthquake Engineering, New Zealand, Nov. 1991.

[26] *High Strength Concrete Columns: State of the Art,* Prepared by the ACI-ASCE Committee 441 Subcommittee on Ultra High Strength Concrete, 1994.